HIGH-RESOLUTION ULTRASONIC

NON-DESTRUCTIVE TESTING

Stephen McLaren.

Thesis submitted for the degree of

Doctor of Philosophy.

The Department of Physics
City University
Northampton Square
London EC1V 0HB

October 1987

CONTENTS

ABSTRACT

The use of ultra-short pulse wideband ultrasonic transducers in Non-Destructive-Testing (NDT) has been investigated both theoretically and experimentally. It is demonstrated that the resolution of pulse-echo NDT is affected by diffraction effects which also complicate the interpretation of echo signals. These diffraction effects are interpreted in terms of the plane- and edge-wave model of transducer fields.

Improvements can be obtained by the use of non-uniformly excited transducers of two basic types: the first, the plane-wave-only (PWO) source, is more strongly excited at its centre than towards the rim, where the excitation is gradually reduced to zero in order to remove the edge wave. The second type, an edge-wave-only (EWO) source, is more strongly excited at its rim than in the centre, thereby effectively removing the plane wave.

Computer modelling of pressure waveforms in the field of PWO and EWO sources has been carried out using an extension to the impulse response method. Experimental point-pressure waveform measurements in the field of a prototype EWO transducer, made using a miniature ultrasonic probe, are in reasonable agreement with the calculated results.

Detailed calculations are made of the transmit-receive mode (pulse-echo) responses arising from solid targets of various size in a fluid medium interrogated by uniformly and non-uniformly excited sources. The theoretically predicted results are in good agreement with experimentally measured results obtained using a conventional transducer and an equivalent prototype EWO transducer. The effects of target size, field position and material on both the amplitude and shape of the echo responses are investigated. The structure of the responses is explained in terms of the plane and edge waves radiated by the source. Implications for the use of techniques to both size (Distance,Gain,Size curves) and characterise (ultrasonic spectroscopy) defects are examined. The applications of new, non-uniformly excited transducers in high-resolution NDT and ultrasonic imaging are evaluated.

ACKNOWLEDGEMENTS

I take this opportunity to sincerely thank Dr. J.P.Weight for all his advice,encouragement and help over the past three years. I also wish to acknowledge all the various members of the Ultrasonics Group with particular reference to Mr. C.Gatcombe and Mr. R.Brittain.

Financial support was provided by the Procurement Executive MOD (RAE Establishment).

Finally I wish to give special thanks to my parents Mr. and Mrs. A.W.J. McLaren for their constant encouragement and support throughout my entire education and to my wife Helen for her assistance and forbearance.

COPYRIGHT DECLARATION

I grant powers to the University Librarian to allow this thesis to be copied in whole or in part without further reference to me. This permission covers only single copies made for study purposes, subject to the normal conditions of acknowledgement.

LIST OF FIGURES & TABLES

TABLES

SYMBOLS

All symbols and abbreviations are normally defined where they first appear in the text. Standard abbreviations for units are used throughout and are not included here.

a	Source radius
c	Velocity of sound in a fluid
E	Output voltage from a conventional transducer used in transmit-receive (pulse-echo) mode
E_w	Output voltage from a non-uniformly excited transducer in pulse-echo mode
J_1	Bessel function of the first kind
k,K	Wavenumber, constant of proportionality
N	Outward normal to the surface S of a volume V
P	Sonic pressure
P_i	Pressure impulse response
P_o	Normalising pressure
Q	Field point
Q(r,t)	Scattering strength
S	Surface area
r	Distance
t	Time
V	Volume
v(t)	Source velocity motion
v	Velocity amplitude distribution (weighting profile)
Z	Distance co-ordinate, target range
y	Radial distance off axis

GREEK SYMBOLS

θ, γ	Angular co-ordinate
λ	Wavelength
ρ	Density
ϕ	Velocity potential
ϕ_i	Velocity potential impulse response
Ω	Included angle of equidistant arc

1. INTRODUCTION

The ultrasonic pulse-echo technique is widely used in the examination of materials and in particular the detection and location of flaws or defects. However it is no longer sufficient to merely locate flaws. Ultrasonic flaw characterisation, which refers to the determination of size, shape, orientation, composition etc., is becoming increasingly important in modern non-destructive evaluation (NDE). This is because with the advent of fracture mechanic calculations, a more definitive description of flaws by means of high-resolution non-destructive testing (NDT), can allow a better assessment to be made of the danger a particular flaw poses to the material or structure in which it is present.

A detailed knowledge and understanding of the interaction of ultrasound with real defects and targets is therefore of fundamental importance if currently-used defect characterisation techniques are to be reliably applied and more accurate alternative techniques or transducers developed. To this end the study of echo responses from solid planar targets of various size, shape and material composition interrogated with short pulses from conventional transducers (typical of those used in NDT) forms a major part of this thesis. This has been done both experimentally and theoretically using a finite-sized target model that allows accurate calculations (as confirmed by experiment) to be made for target and source geometries of finite dimensions in both the near and far field. Most previous work on modelling echo waveforms from targets of finite dimensions has been confined to the far field only. It should be pointed out that only aspects relating to the propagation of ultrasound from the transducer face and its subsequent scattering and reception in pulse-echo mode are considered and not the electro-mechanical transduction process and the generation of ultrasound.

For a conventional source, diffraction effects have been shown to impose limitations on lateral and range resolution as well as introducing complicated echo patterns especially in the near field. The use of non-uniformly excited sources offers a possible means of overcoming these limitations. An investigation of the radiated fields and echo responses obtained from such sources has therefore been carried out in order to assess their ability in high-resolution NDT applications in both the near and far field. Furthermore, a direct comparison of non-uniformly

excited sources with conventional uniformly excited sources is also made with a view to determining their potential as replacements for currently used conventional sources.

Although the emphasis on the findings and conclusions presented here has been directed towards NDT, they are equally applicable to other related fields such as seismic survey work, sonar and particularly medical diagnosis since the body can be treated as a first approximation as though it is a fluid.

Briefly, the material presented in this work is laid out as follows: Chapter 2 begins by briefly reviewing continuous-wave and transient radiation theory for propagation in fluids, as well as introducing the impulse response method for the calculation of pressure waveforms and transmit-receive mode responses for uniformly excited transducers and an extension which takes account of non-uniform excitation. The plane- and edge-wave model of the radiated field from a conventional piston source is introduced before considering a finite-sized target model that allows calculations to be made of echo responses from solid, planar targets of arbitrary size and field position, interrogated by either uniformly or non-uniformly excited sources.

Chapter 3 describes the various transducers and measuring systems used to obtain the experimental waveform measurements and ultrasonic images presented in this work.

Detailed calculations of pressure waveforms and transmit-receive mode (pulse-echo) responses from targets of various size in fluids are given in chapter 4. These are compared with experimental results obtained using typical wideband conventional transducers as well as equivalent non-uniformly excited transducers. Some preliminary field point waveform measurements in solids are also reported.

The theoretical results and the experimental calculations are discussed in chapter 5 with regard to their implications for high-resolution NDT and flaw characterisation.

A short chapter outlining proposed future work is included before the final concluding remarks in chapter 7.

2. THEORY

Much of the theoretical and experimental work presented in this thesis is associated with the propagation of ultrasound in a fluid medium and its interaction with solid targets of known properties immersed within it. The scattering of ultrasonic waves in a solid medium is generally more involved than for a fluid since shear as well as compression waves may be generated. Nevertheless a study of ultrasonic scattering in a fluid medium provides valuable insight into the nature of the ultrasonic waves scattered and reflected from target flaws that typically in NDT lie within a solid medium. Any extensions to the ideas and conclusions drawn from studies in a fluid medium to the case of solids will therefore be made in qualitative terms only and a more rigorous theoretical description left to future work.

Only a brief summary of the already well known continuous-wave (CW) theory for fluids is included since the trend in the recent development of pulse-echo testing has been to use wideband transducers which generate very short pulses of ultrasound. Such transducers were developed in an attempt to improve target resolution and are a pre-requisite of techniques which make use of frequency analysis in target characterisation. The interpretation of echoes obtained from these transducers requires an understanding of the structure of the transient field. Transient field theory (including the impulse response method which accurately predicts the propagation of ultrasound in a fluid) is therefore considered, followed by a discussion of the plane- and edge-wave structure of the radiated field and the associated diffraction effects. One way of overcoming the limitations imposed by these effects is the use of non-uniformly excited sources which offer the potential of improved high-resolution NDT over conventional (uniformly excited) sources. The various theoretical approaches used in the prediction and study of the fields radiated by such sources are therefore reviewed, before finally introducing the development of a mathematical model that allows accurate theoretical predictions to be made of echo waveforms from simple solid planar targets of various size and shape at any arbitrary field position, interrogated by either uniformly or non-uniformly excited sources.

2.1 Continuous-wave (steady-state) theory.

The most important aspect of a source emitting continuous sinusoidal waves into a fluid is the spatial dependance of the pressure field amplitude. In other words this is an acoustic diffraction pattern; a piston source in an infinite baffle may be considered to act as an aperture illuminated by a plane wave. In typical ultrasonic applications the wavelengths and source dimensions are such that both Fresnel (near field) and Fraunhofer (far field) diffraction phenomena, analagous to those in optics are observable. In CW propagation the far field is usually taken to begin at about $r_f = a^2/\lambda$, where a is the source radius and λ the wavelength.

The steady-state solutions for the field of a circular piston source undergoing sinusoidal oscillation in a fluid have appeared in numerous published studies. The Rayleigh surface integral [1] in particular forms the starting point for many of these investigations. Physically the Rayleigh integral is a statement of Huyghens' principle as expounded by Fresnel, which for a planar piston source means that every point on the piston surface may be considered as the source of an outgoing hemispherical wavelet. In general the Rayleigh integral can only be solved analytically in a few specific regions of the radiated field. These now well known analytic expressions (see Hunter [2] chapters 3 and 4) can be derived for the steady-state pressure variations at all points lying on axis and for the pressure variations across the beam (at a given range) in the far field of a circular piston source.

The pressure distribution along the axis of a circular source, as shown in Fig. 2.1.1., is characterised by a rapidly varying series of maxima and minima. The pressure variation across the beam in the far field has the form of the well known Fraunhofer diffraction pattern for a circular aperture. The pressure distribution across the beam (normalised by the on-axis value) is given by

$$\frac{P(\theta)}{P_o} = \frac{2J_1(ka\sin\theta)}{Ka\sin\theta} \qquad \ldots\ldots\ldots\ldots (1)$$

where a is the source radius, y the off-axis distance, z the field point range, $\theta = \tan^{-1}(y/z)$ and J_1 is a Bessel function of the first kind. Off axis, in the near field, analytic solutions are not available and a

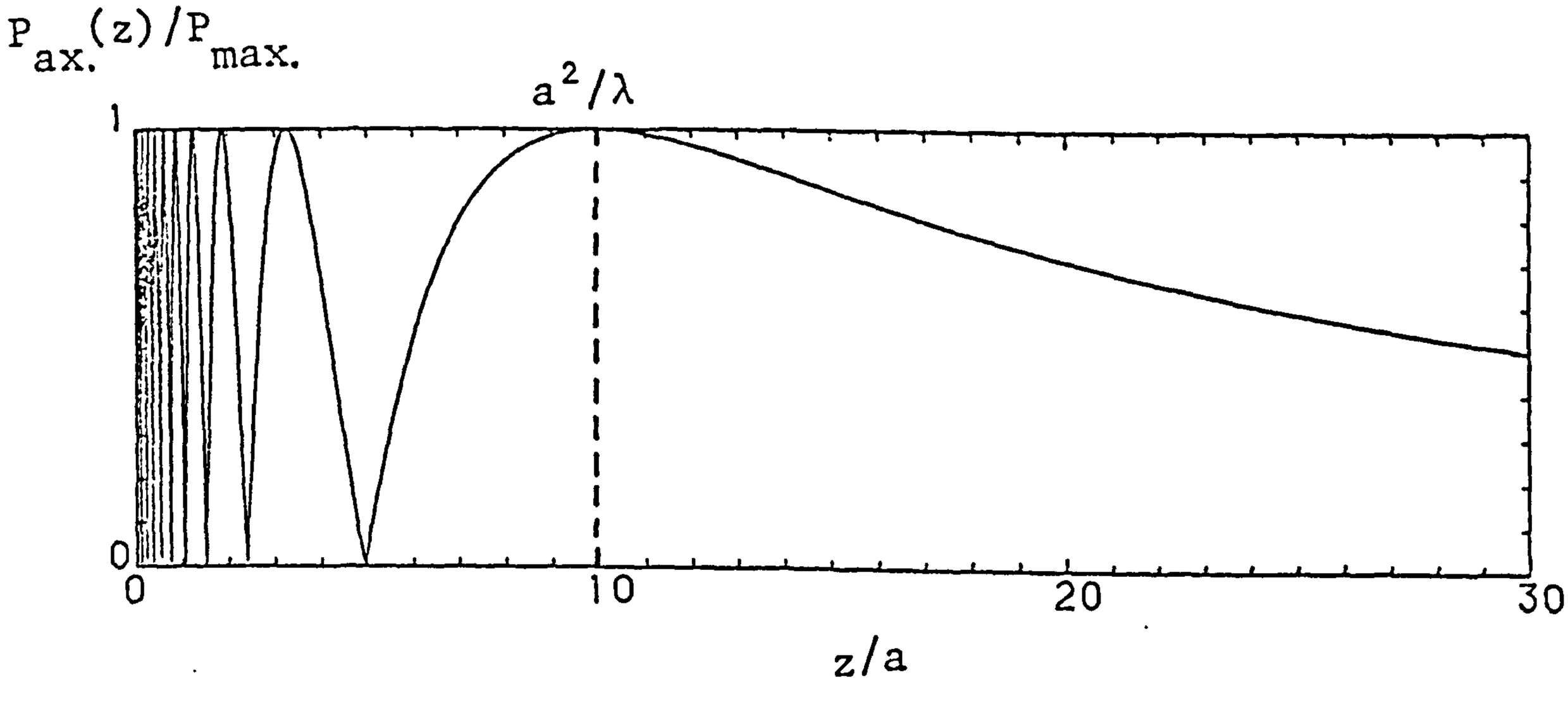

Fig 2.1.1 Variation in the steady-state axial pressure $P_{ax.}$ of a circular piston source of radius a as a function of range z. Plot of $P_{ax.}/P_{max.}$ (where the amplitude $P_{max.}$ is twice that of the plane wave emitted) versus z/a is for $a = 10\lambda$.

numerical evaluation of the Rayleigh integral must be made. Approximate series expansions of the integral have been used to calculate [3, 4] the near field pattern. More recently Zemanek [5] has published detailed computations for this region of the field using numerical integration techniques.

2.2 Transient radiation theory.

With transient (short pulse) excitation of transducers typically found in pulse-echo ultrasound systems, steady-state solùtions are no longer adequate in describing the field structure [6,7]. CW theory can only predict the amplitude of a pressure pulse containing several cycles of a sinusoidal wave during that fraction (if any) of the pulse for which steady-state conditions apply. Moreover with pulsed excitation of the source, temporal as well as spatial information concerning the pulsed wavefronts is of interest and accurate transient solutions are required. In theory such solutions can be obtained by expressing the pulsed field as a weighted superposition of single frequency, steady-state harmonic solutions but as mentioned in the previous section even these steady-state solutions are not available for the general field point. This method, known as harmonic synthesis, is described by Freedman [8] and Papadakis and Fowler [9].

A comprehensive review of transient radiation theory has been made by Harris [10] who has traced the various approaches to a few fundamental methods of analysis, principal among these being the solutions of Rayleigh [1], King [11] and Schoch [12]. It would appear that most calculations of transient piston fields [13-18] have been based on an impulse response (convolution integral) representation either directly or indirectly. The convolution integral approach, which has been developed notably by Stephanishen [18], introduces the concept of an impulse response (so called from the analagous temporal impulse response of linear circuit theory) which relates the acoustic field to the radiating source geometry. The impulse response is determined by solving analytically the Rayleigh surface integral for an impulsive motion of the source. The pressure at an arbitrary piston velocity can then be obtained by convolution of the impulse response with the source velocity. The calculations given later of pressure waveforms and transmit-receive mode echo responses make use of the impulse response method. This approach allows acoustic fields to be theoretically determined for either transient or CW piston motion and at an arbitrary field point in both the near and far field.

It is convenient here to clarify the meaning of near field when used in the context of short-pulse wideband ultrasound typically used in high-resolution NDT. The definition for the end of the near field in CW

propagation given in the previous section (i.e. $r_f = a^2/\lambda$) is no longer satisfactory since wideband pulses contain a range of frequencies and hence the choice of a value for the wavelength is somewhat arbitrary. Whenever the terms near and far field are used in this thesis it should be assumed that the value of wavelength used in the estimate of r_f corresponds to the centre frequency, or frequency of maximum output if the pulse spectrum is not symmetrical. It should however be remembered that the highest usable frequency in the pulse spectrum may extend much higher than this figure. For example,a typical velocity motion for the transducers(9.5mm radius aperture) used here is a single cycle of a 2MHz sinusoid (λ= 0.75 mm in water). By the definition just outlined above this corresponds to an estimate of r_f = 120 mm. However, there is usable energy in the pulse spectrum up to 2.5 times the centre frequency so that near-field effects can be extended up to 300 mm in water or about 75 mm in metals. For a centre frequency of 6 MHz, which is more representative of that used in practice, a factor of three can be placed on the above figures. Much high-resolution NDT will therefore inevitably fall within the near-field region. It should be further noted that the near field of a non-uniformly excited source will be defined in terms of the near-field region of a corresponding uniformly excited source.

2.3 The plane- and edge-wave model of diffraction.

The similarity between continuous-wave acoustic fields and optical diffraction patterns has already been mentioned. In 1802 Young [19] suggested a simple theory to qualitatively explain optical diffraction phenomena. He proposed that the observed light field in front of an opaque obstacle (e.g. a knife edge) or an aperture in an opaque screen, resulted from interference between the direct plane wave and a wave emanating from the boundary (or edge). This has come to be known as the plane-and edge-wave model of diffraction. Schoch [12] was the first to apply this model to acoustics when he was able to show that his integral expression for the field of a source undergoing CW motion could be mathematically decomposed into a geometrical wave and a boundary diffraction wave. This model has also been used to explain the way in which short pulses of sound propagate from a piston source, Kaspar'yants [20], Kozina and Makarov [21] and Tupholme [22] being amongst the first to do so.

It has been shown [6] that a good physical understanding of the structure of the acoustic field radiated from a circular source in a fluid medium is provided by the concept of a plane wave which travels in the geometric region directly in front of the source together with a toroidal edge wave of opposite phase originating from the source periphery. In the shadow region, outside the geometric region, only the edge wave is present. Interestingly, the portions of the edge wave directed into the shadow region are of opposite phase to those portions directed into the geometric region. Furthermore the directivity of the edge wave does not have a uniform amplitude with direction of propagation. The directivity of the edge wave exactly compensates for the spreading nature of the wavefront, with the result that its axial amplitude remains constant with range. This characteristic illustrates that the edge wave is not simply a wave from the edge of the source but that it arises, as does the plane wave, from the summation of all the Huyghens' wavelets from the whole surface of the source.

Previous experimental studies concerned with obtaining field point pressure waveforms [23-28] and stroboscopic schlieren visualisations [6, 29, 30] of transient and CW fields in fluids, have demonstrated that the plane- and edge-wave components are not just mathematical artefacts. The edge waves have been shown to actually exist and can be time resolved

from the direct plane wave given suitable experimental conditions. The investigations referred to above have also been able to show the detailed structure of the edge wave.

The variations in the pressure waveform with field-point position in a fluid and the form of the corresponding pressure-amplitude beam profile for a uniformly excited source, are a result of diffraction effects caused by the interaction of the plane wave and the edge wave. As later illustrated in chapter 4 and discussed in chapter 5, these diffraction effects impose limitations on important transducer characteristics such as range and lateral resolution.

2.4 The impulse response (I-R) method.

Rayleigh's equation for arbitrary motion of a source radiating into a fluid expresses the velocity potential at a point as the sum of contributions from all the elementary Huyghens' sources that make up the source surface. This gives

$$\phi(r,t) = 1/2\pi \iint_s \frac{V_n(t-r/c)}{r}\, ds \qquad \text{.....(2)}$$

where (see Fig. 2.4.1) ϕ is the velocity potential, v_n is the normal velocity of the piston, r is the distance from the field point to the surface element ds and c is the velocity of sound in the fluid.

The pressure in a fluid of density ρ_o is given by

$$P(r,t) = \rho_o \frac{\partial \phi}{\partial t} \qquad \text{.....(3)}$$

If the piston velocity v is uniform over the piston surface then

$$v(t-r/c) = v(t) * \delta(t-r/c) \qquad \text{.....(4)}$$

where * denotes, as usual, convolution. Thus the velocity potential is

$$\phi(r,t) = V(t) * \phi_i(r,t) \qquad \text{.....(5)}$$

and the impulse response is therefore

$$\phi_i(r,t) = \iint_s \frac{\delta(t-r/c)ds}{2\pi r} \qquad \text{.....(6)}$$

After a velocity impulse has been applied to a piston at t = 0, the field at a point Q is made up of contributions from all points on the piston surface a distance ct from Q; these points, equidistant from Q, lie on a circular arc centered at the projection of Q on the source (z = o) plane (see Fig. 2.4.1). By a simple change of variable [17, 18] a very simple result is obtained for the solution to eq. (5), namely that the velocity potential for an impulsive motion of a source is proportional to the

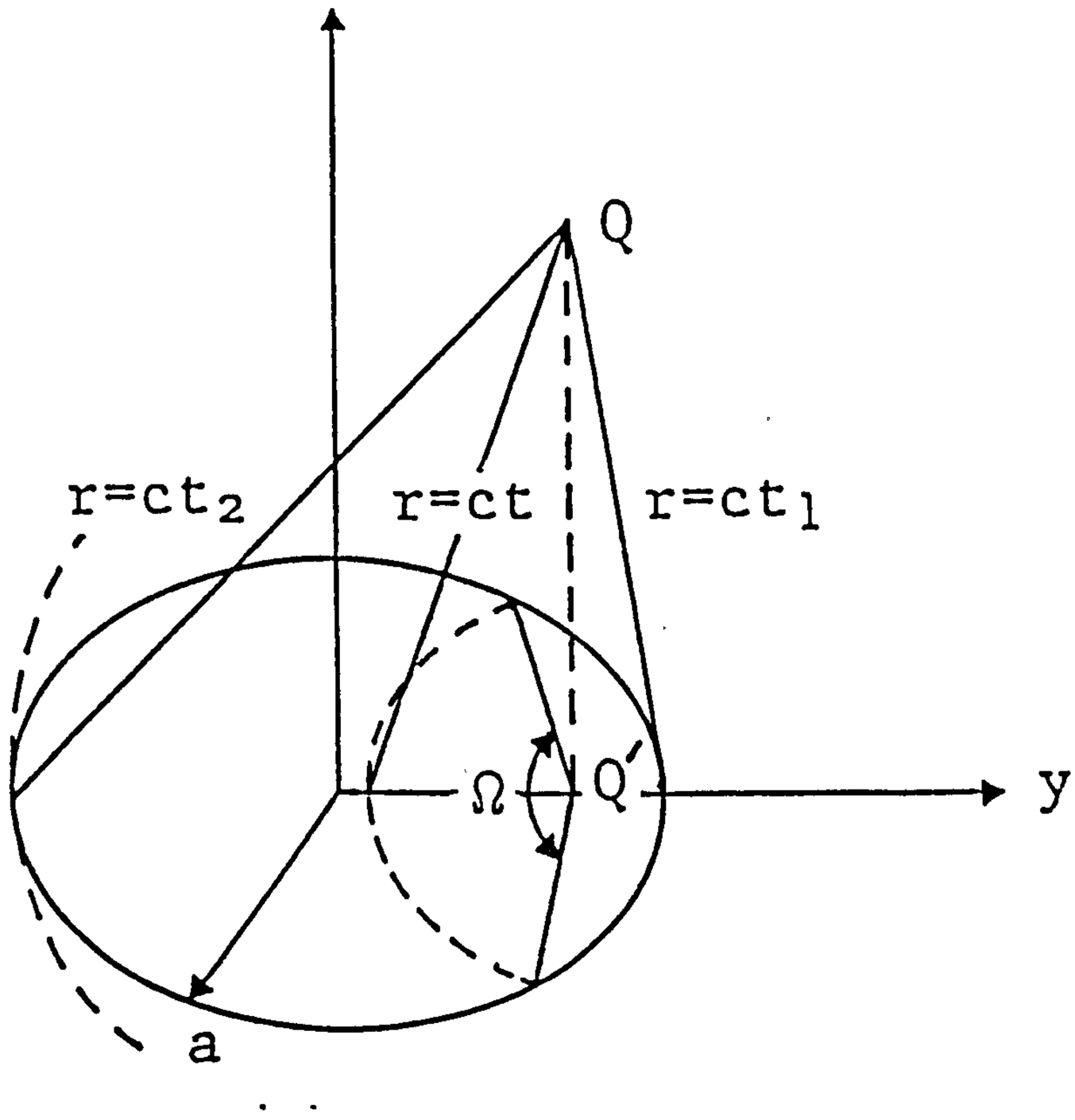

Fig 2.4.1 Geometry of the equidistant arcs on the source surface used in determining the velocity potential impulse response function. Q′ is the perpendicular projection of the general field point Q.

length of equidistant arc included on the source surface. Expressed mathematically this is

$$\phi_i(r,t) = c\Omega(ct)/2\pi \qquad \text{if } r_1 < ct < r_2 \qquad \text{.....(7)}$$

and $\phi_i(r,t) = 0$ elsewhere, where Ω is the full angle of the included equidistant arc. For the case of a circular source analytic expressions for Ω (ct) have been given by a number of authors [17, 18, 31]. Those tabulated by Robinson et al [17] are summarised in Appendix 1. The pressure impulse response may then be obtained directly or by numerical differentiation and convolved with the source velocity motion; the convolution being conveniently perfomed by computer.

It should be noted that the above solution is valid in all parts of the field, is applicable to arbitrary piston shapes and can also be used for arbitrary velocity driving functions. However, the above relationships assume that the field intensities are such that non-linear effects are negligible and that the source acts as a rigid piston.

2.4.1 Extension of the impulse response method to calculate pulse-echo waveforms from an idealised point-like target in a fluid.

By invoking the principle of reciprocity the impulse response method has been extended to allow calculations to be made of the transmit-receive mode responses of a uniformly excited source interrogating a point-like target. If the source is considered to function as a receiving transducer which is uniformly pressure sensitive, its output voltage E(t), when used in transmit-receive mode, on reception of the echo from an idealised point reflector is given by [23]

$$E(t) = -\frac{K\rho_o}{2c_o} v(t) * \frac{\partial \phi_i}{\partial t} * \frac{\partial \phi_i}{\partial t} \qquad \text{.....(8)}$$

where K is a constant.

The above result is obtained by making the simplifying assumptions that the incident wave is locally plane and that the target has a reflection coefficient of -1. The double convolution of eq. (7) means that pulse-echo waveforms and beam profiles are quite different to those obtained for the field point pressures.

2.4.2 Graphical solution to the impulse response approach.

The impulse response method can be conveniently described with the aid of simple graphical constructions which also serve to illustrate the plane- and edge-wave structure of the radiated field. Graphical solutions close to a source undergoing single cycle sinusoidal motion are shown for three different field positions;

(a) On axis;
(b) off-axis, but within the geometrical beam ; and
(c) outside the geometrical beam.

Figure 2.4.2 shows the on-axis graphical solution for a circular piston source. The area on the piston surface represents equidistant arcs at successive (arbitrary) time intervals. If at first the source is considered to undergo an impulsive velocity motion, the velocity potential ϕ_i at a field point Q(Q' is the projection of Q on the piston surface) jumps to a constant value at t_1. This is the time at which the contribution from the nearest point of the piston (in this case the piston centre) reaches Q. Between t_1 and t_2 the equidistant arcs remain complete circles and therefore Q_1 remains constant. At t_2 the contribution from the furthest point on the piston (ie. from the edge) arrives at Q and ϕ_i abruptly falls to zero. Thus ϕ_i has the "top-hat" form shown in Fig. 2.4.2(a). The corresponding pressure is proportional to the time differential of ϕ_i and therefore consists of two equal and opposite delta functions separated by the time difference between waves arriving from the near point of the source and those arriving from the furthest point, the edge. For an arbitrary piston motion this double pulse is retained. These two pulses result from Young's direct plane wave and diffracted edge wave. On axis, the edge-wave contributions arrive similtaneously to give an inverted replica of the earlier arriving plane wave. At greater ranges on axis, the time separation between the plane- and edge-wave pulses decrease until they eventually overlap producing the effect of differentiation in the far field [6, 17].

Off axis, but inside the geometrical projection of the source (see Fig. 2.4.2(b)) the velocity potential again jumps to a constant value at t_1 and remains constant until time t_2, the time of arrival of contributions from the nearest edge. After t_2 the equidistant arcs are no longer complete and ϕ_i decreases reaching zero at t_3 which corresponds to the transit time from the far edge. Differentiating to obtain P_i

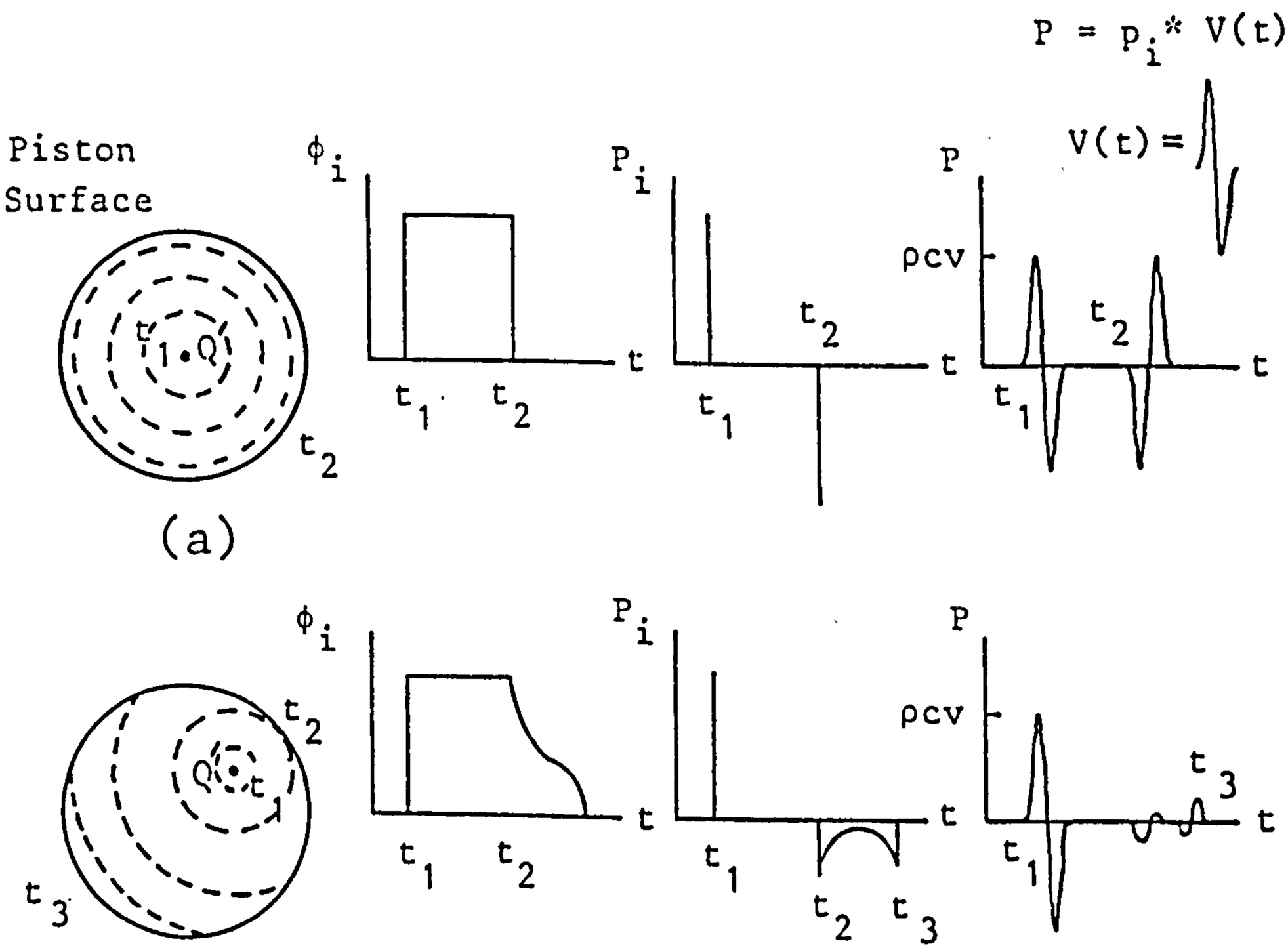

Fig 2.4.2 Graphical calculation of the pressure waveforms from a circular piston source: (a) on axis, (b) in the geometric beam region, and (c) outside the geometric beam region.

yields a delta function followed by two time "smeared" and inverted pulses. For a single cycle sinusoidal excitation the pressure waveform then consists of a sine wave pulse followed by two smaller, distorted and inverted replicas of this pulse. The first pulse represents the plane wave and the two trailing pulses are edge waves from the nearer and further portions of the source rim.

Outside the geometrical beam (Fig. 2.4.2.(c)) the equidistant arcs are never complete. ϕ_i rises slowly to a maximum value which is less than for points within the geometrical beam before reaching zero again at time t_3. The pressure waveform now consists of two edge wave pulses only. Note however that the first edge wave, directed into the shadow region, is the same polarity as the plane wave and of opposite polarity to the second edge wave directed into the geometric region.

2.5 Non-uniformly excited sources.

Although the uniformly excited rigid planar piston has been the subject of longstanding theoretical interest, it has also been recognised that modelling the surface vibration amplitude in terms of a non-uniform velocity amplitude distribution (weighting profile) was of practical importance. Specifically, it was realized that non-uniformly excited sources could have certain properties and beam characteristics which would offer advantages over conventional, uniformly-excited sources in applications requiring high-resolution target characterisation.

2.5.1 Continuous-Wave theory.

In earlier studies [32, 37] the Rayleigh and King integrals have been used to study the affect of various source distributions on the axial and far-field CW pressure fields of non-uniformly excited sources. The form of the piston motion has usually been assumed to be axisymmetric, i.e. a function of the radial distance from the centre. Several analytic functions (see section II B of reference [10]) have been used to represent the axisymmetric vibration amplitude. All have a maximum amplitude at the piston centre and decrease monotonically with distance off axis. In particular the simply-supported radiator and clamped (at the source edge) radiator have been used to describe the surface motion of such transducers.

More recently a general solution, valid at all field points, was obtained by Greenspan [38] who generalised the King integral to account for a non-uniform vibration amplitude. Evaluation of the result yielded analytic expressions for the impulse response of a circular piston for certain specific analytic amplitude distributions. Using similar approaches to Greenspan, several authors [39-41] have also subsequently investigated the radiated CW fields from various forms of axisymmetric, non-uniformly excited transducer both in the near and far field.

These studies revealed that when the amplitude distribution across a source emitting CW decreases in a monotonic manner from the centre to the edge, the field pattern becomes smoother and broader in comparison with a uniformly vibrating piston source. The well known large pressure fluctuations (maxima and minima) in the near field are smoothed out and the sidelobe maxima are significantly reduced with this type of non-uniformly excited source.

The aim with CW operation is to produce a uniform pressure amplitude throughout the field. Von Haselberg and Krautkramer [42] have shown that a good approximation to such a field is provided by a source with a non-uniform velocity distribution which is Gaussian as a function of radius. Several practical transducers [43-46] have been constructed using modified electrode designs which produce a Gaussian (or quasi-Gaussian) radial electric field and thereby induce a similar amplitude distribution in the velocity motion of the source. This technique, whereby the motion of the source is made non-uniform over its surface, is known as shading or apodisation. The term apodisation is taken from the analagous technique employed in optics [47] which is used to suppress diffraction sidelobe maxima.

It has previously been noted [6,38] that a major disadvantage of such a source is that in general both its sensitivity and its lateral resolution are reduced compared with a uniformly excited source of the same aperture. Resulting from the asymptotic way in which the Gaussian approaches zero on each side of the central maximum, any practical approximation to such a weighting profile cannot be truncated too much without re-introducing near-field fluctuations. Therefore only the central regions of the source can be excited to any great extent thereby reducing the collimation of the beam and its sensitivity with range. Furthermore, as the length of the near field is effectively reduced,the consequent beam-spreading can spoil the lateral resolution. Theoretically and experimentally a number of investigators [39, 40, 48-51] have attempted to reach compromise solutions using various weighting (velocity amplitude) distributions to overcome this drawback.

It has also been noted [40, 41, 52, 53] that by shading a transducer in the opposite sense to that explained above, i.e. by exciting the edges of the source more strongly than the centre, it is possible to produce a narrow pencil-beam centered on axis. The simplest way of realising such a device is a simple ring (or annular) transducer which can maintain a high degree of focusing and hence high lateral resolution, over a large depth of field. One major disadvantage of an annular source is the formation of large sidelobes straight ahead of the rim. This effect is highly undesirable because it can lead to the appearance of false or spurious signals. Burckhardt et al [53] have attempted to reduce these sidelobes by sequentially switching segments of

an annular transducer. Kondrat'ev and Karpel'son [52] have also tried to overcome this limitation by smoothly varying the velocity distribution of the source from zero at the centre to a maximum at the rim.

2.5.2 Pulsed (transient) radiation theory.

Greenspan [38] was the first to present an approach for evaluating transient pressure fields from non-uniformly excited sources. As mentioned earlier Greenspan generalised the King integral to account for sinusoidal excitation of a circular piston having an axisymmetric velocity amplitude distribution. Then, in an analysis of the transient case, he obtained an expression for the velocity potential impulse response by taking the inverse Laplace transform of his solution. Evaluation of the result allowed analytic expressions to be obtained for certain analytic source velocity distributions. Velocity potential impulse responses, plotted in a similar manner to Stephanishen [18] and Robinson et al [17], were presented for simply-supported, clamped and Gaussian radiators. These expressions can be convolved with the piston velocity waveform to obtain the transient pressure field. This method of determining the radiated field from non-uniformly excited sources relies on cylindrical symmetry and is therefore limited to the case of circular pistons. Furthermore, it is only for certain specific analytic vibration amplitude distributions that the exact solutions reduce to closed form expressions. In general the evaluation of the impulse response for a non-uniformly excited source must be performed numerically.

More recently Harris [54] has developed an extension of the convolution integral approach to obtain a general impulse response function for arbitrarily shaped pistons with arbitrary, non-uniform velocity amplitude distributions. The transient pressure fields are evaluated as before by convolution of this function with the source velocity function. This approach is also extended to account for the effect of a finite receiver on the form of the measured transient field. For a point receiver the impulsive velocity potential for a circular non-uniformly excited source is given by

$$\phi_i(r,t) = \frac{c}{\pi} \int_0^{\theta(ct)} V_\sigma(ct,\theta)\,d\theta \qquad \text{.....(9)}$$

where $v_e(ct,\theta)$ is the axisymmetric velocity distribution. Note that the source distribution is written in terms of the observer based co-ordinates ct(or R) as shown in Fig. 2.5.1 and not as a function of the distance off axis y as in section 2.4. As illustrated in section 2.4.2 the magnitude of the impulse response for a uniformly vibrating source at some time t is proportional to the angle $\Omega(ct)$. The more of the piston source located a distance ct from the point Q at time t the greater the impulse response function at that time. The interpretation of eq. (9) for a non-uniformly excited source is similar but now the contribution at time t is weighted by the distribution function $v_e(ct,\theta)$. Thus the magnitude of the impulse response depends not only on the length of the circular arc but also on the piston velocity amplitude along that arc.

In general, eq. (9) must be evaluated numerically. Harris has calculated the pressure impulse response for both point and finite-sized receivers and for various analytic weighting profiles including simply-supported, clamped, Fermi, Bessel and Gaussian. The corresponding transient pressure waveforms are also presented for two piston velocity waveforms - a Gaussian pulse and a Gaussian modulated sinusoidal burst.

Independently of Harris both Stephanishen [55] and Tjotta and Tjotta [56] have also generalised the impulse response method to the case of a source with a non-uniform velocity distribution obtaining results equivalent to eq. (9). Tjotta and Tjotta studied the affect of amplitude shading and rigidity at the source edge, on the near and far fields of pulsed radiators. In this particular paper the emphasis was placed on pointing out general properties and to obtain analytical rather than numerical results. By expressing the velocity distribution in terms of a set of radially symmetric eigenfunctions, Stephanishen expressed the pressure as a sum of convolution integrals involving generalized impulse responses which are dependent on the eigenfunctions and time dependent velocities. In general the solution must be evaluated numerically. However, Stephanishen was able to derive series expressions for the generalized impulse response corresponding to a special case of interest, the spatial velocity distribution described by a Bessel function of the first kind and zero order. On axis, transient pressure waveforms in the near field of such a radiator were also presented.

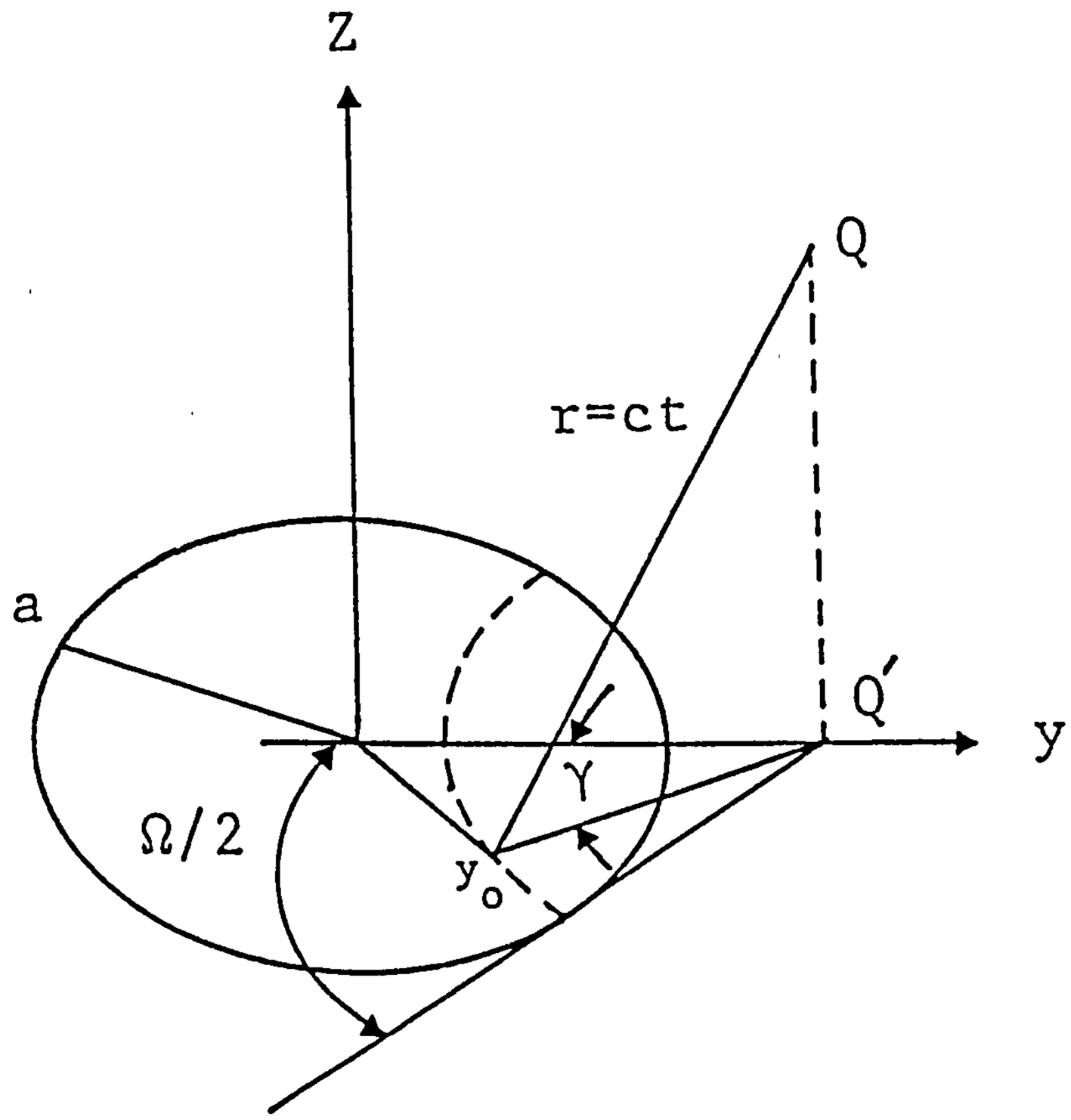

Fig 2.5.1 Circular piston geometry for evaluation of the velocity potential impulse response function at a general field point Q in the field of a source with a non-uniform velocity amplitude distribution.

In all the preceding publications the general conclusions were the same. When the vibration amplitude is not uniform, with a reduced amplitude at the edge, the pressure waveform on axis no longer displays the separate plane- and edge-wave structure discussed previously. The plane wave becomes distorted and the edge wave is reduced in size. The time delay beween the two pulses is also shortened, indicating a reduction in the effective radius of the radiator and the corresponding near-field length. Between the initial and final portions of the pulse, which are loosely identified with plane-and edge-wave components, lies an intermediate non-zero pressure region. Harris [54] has attributed the pressure in this region of time to a "membrane" component wave which owes its existence to the presence of a non-uniform vibration amplitude.

Further extensions of the impulse response method [57, 58] have also been made to investigate acoustic fields from non-planar, curved sources with a non-uniform amplitude distribution. This has been carried out with a view to obtaining good lateral resolution over a large range.

In all the work presented here transient pressure fields radiated by a planar piston having an arbitrary axisymmetric velocity distribution are calculated using the impulse response method along with the principle of superposition. The pressure at an arbitrary point in the field of an axisymmetrically weighted source is then considered to be due to the sum of the pressures from a collection of concentric sources of different radius, each of which undergoes uniform in-phase motion of arbitrary amplitude. For example, the field from an annular transducer may be simply described by the subtraction of the field of one source from another of the same amplitude but larger radius. This is illustrated in Fig. 2.5.2(a). Similarly a source excited more strongly in the centre than at the edge may be synthesized by the addition of successive plane pistons of varying radius, see Fig. 2.5.2(b). This approach was originally proposed by Weight [6, 59] and has been used by Gatcombe [60] to theoretically investigate the fields radiated from non-uniformly excited sources.

The pressure due to each source is given by

$$P(r,t,y) = v(t,y) * P_i(r,t,y) \qquad \ldots\ldots\ldots\ldots (10)$$

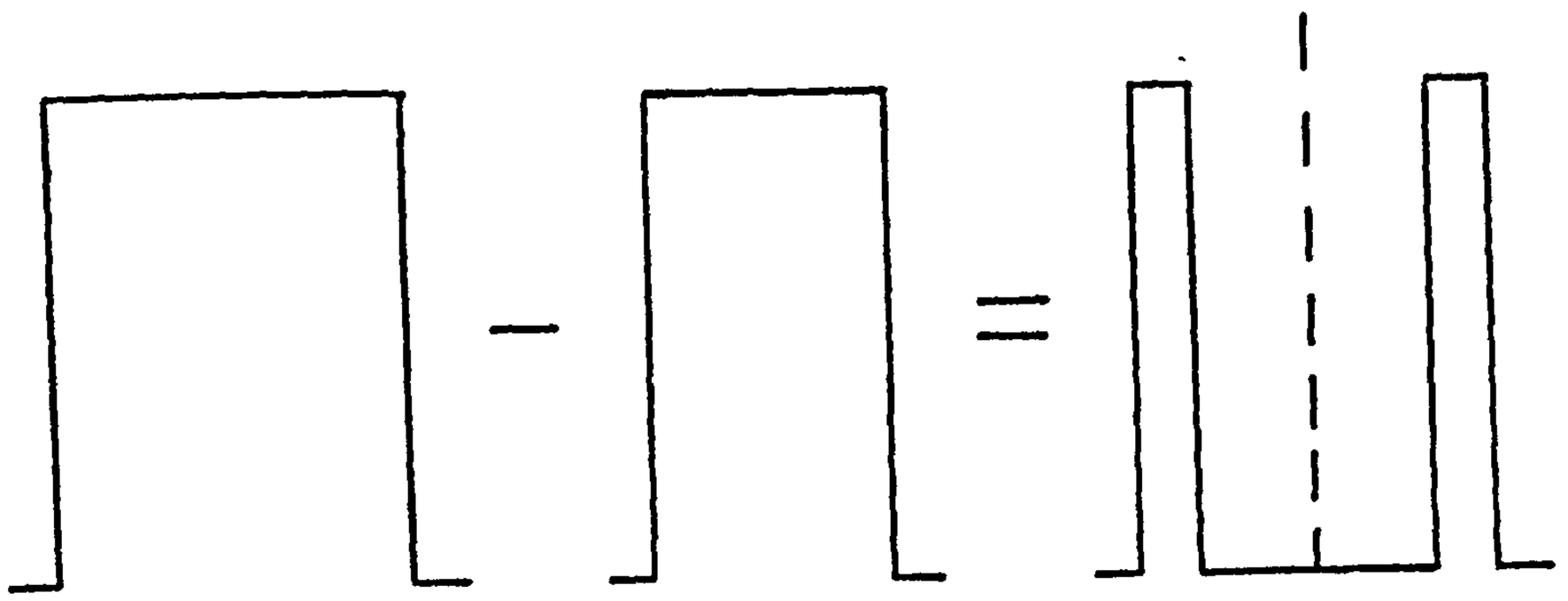

(a)

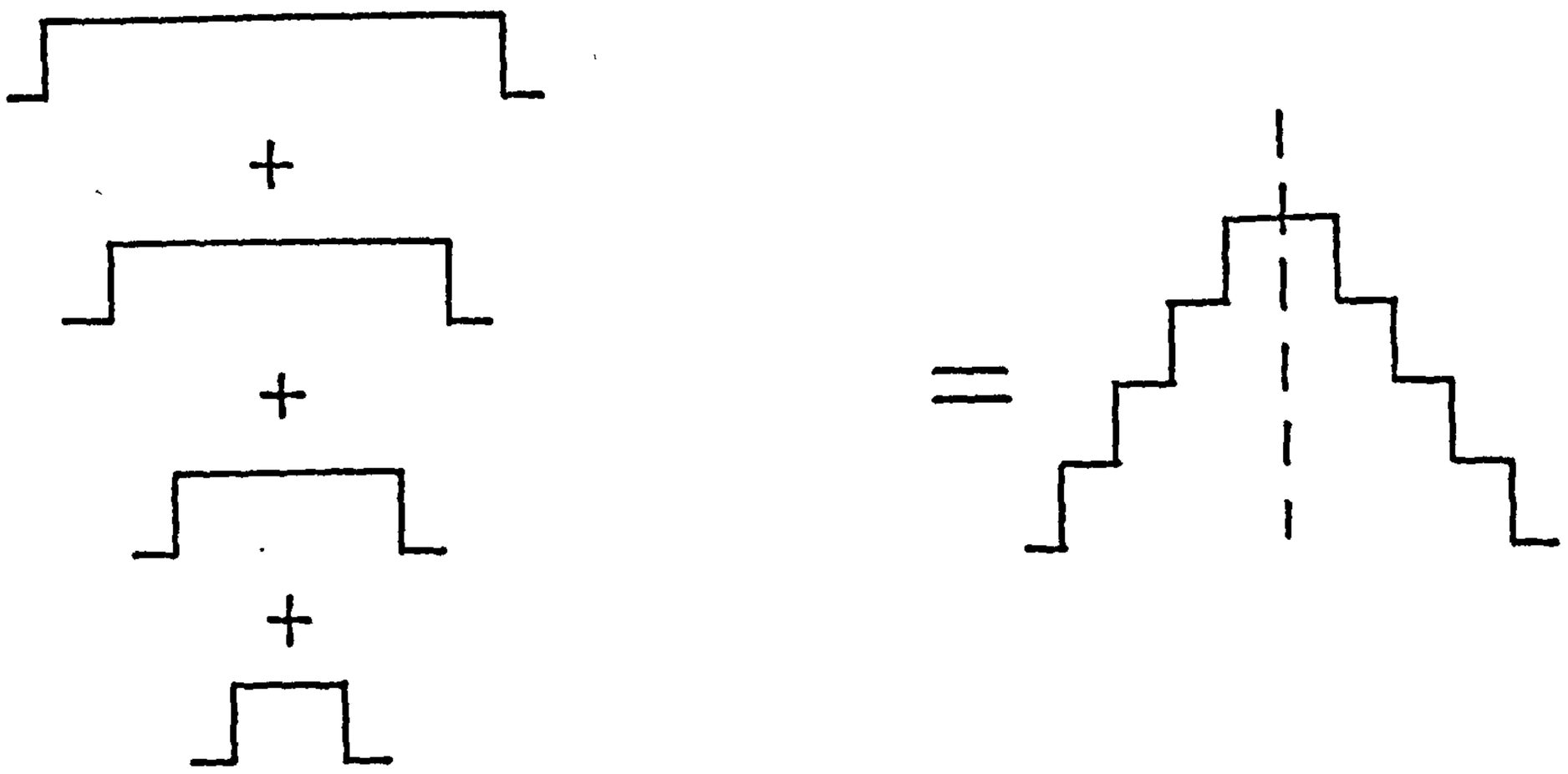

(b)

Fig 2.5.2 Schematic diagram illustrating how a non-uniformly excited source may be represented as a collection of plane piston contributions: (a) an annulus, subtraction of one plane piston field from another; and (b) an increase in amplitude with radius, synthesized by the addition of plane piston fields.

where $P_i(r,t,y)$ is the impulse pressure response of a piston of radius a and the source velocity v(t,y) is now a function of radial displacement y. The pressure due to a weighted source of radius a is then

$$P_w(r,t) = \int_0^a P(r,t,y)dy \qquad \text{.....(11)}$$

Calculations of pressure waveforms are made by numerical integration of the above expression. In a similar manner the transmit-receive mode response of a non-uniformly excited source interrogating a small target can also be determined by making use of eq. (8). The electrical output, E_w, from the source on receiving the reflection from a point-like target is thus given by

$$E_w(r,t) = -\frac{kv(t)}{2\rho c} * \int_0^a P_i(r,t,y) * P_i(r,t,y)dy \qquad \text{.....(12)}$$

2.5.2.1 Non-uniformly excited plane-wave-only (PWO) and edge-wave-only (EWO) sources.

Although with transient excitation of uniformly excited sources the radiated field is inherently more uniform than for the CW case [28], there are still significant variations in pulse shape throughout the field due to diffraction effects. The application of ultrasonic spectroscopy techniques [61, 62] to characterise defects within engineering components and welds is complicated by such diffraction effects. These effects, which introduce strong modulation into echo spectra (see later, section 4.3.1) and therefore tend to mask any modulation due to defect characteristics [59], are caused by the interaction of plane and edge waves. In wideband NDT applications the major aim is to produce simple pulse shapes throughout the field so as to allow an easier interpretation of echo signals to be made. An obvious way of eliminating the diffraction effects is to remove either the plane wave or the edge wave.

In order to obtain a constant pulse shape at all field points and uniform beam shape, all that is seemingly required is to remove the edge wave by exciting the source at the centre and not at all at the edge. However, it is the interaction between the plane and edge waves from a uniformly excited source that gives the beam its directivity. The wavefront from a transducer which has been shaded to produce no edge

waves would spread out with range. This results in the loss of sensitivity and increased beam spreading, both of which are undesirable. The computer modelling of Weight [6] and Gatcombe [60] has shown that a suitable weighting function which minimizes these disadvantages must have a smooth transition from a constant velocity region at the centre to zero at the edge, see Fig. 2.5.3. For the transition, cosinusoidal and Gaussian forms [60] appear to offer the best compromise, giving simple pulse shapes but retaining much of the directivity of a uniformly excited source. Weight [59] has termed this type of source a plane-wave-only (PWO) transducer.

By exciting a source in the opposite sense to a PWO source, i.e. more strongly towards its rim, it is possible to shade-out the plane wave. This produces a source which effectively radiates edge waves alone (an EWO tranducer). High lateral resolution will be obtained with this type of source because at every point on axis the edge-wave contributions from all portions of the rim add up in phase giving a large amplitude at all axial ranges. Off axis the edge waves arrive at different times and the response is much reduced. It should be pointed out that it is impossible to realise an "ideal" EWO transducer which radiates solely edge waves with the same characteristics as those radiated by a uniformly excited source (see section 2.3, the plane- and edge-wave model). This is because the edge wave from a uniformly excited source arises from the summation of all the Huyghens' wavelets distributed over the surface of the source. Attempting to eliminate the plane wave by exciting a source only at the rim results in some of the desirable characteristics of the ideal edge wave, such as the constant amplitude on axis, being lost. An infinitesimally small ring source would in fact radiate a uniform toroidal wave the amplitude of which falls-off with range z as $1/\sqrt{z}$. Therefore in practice only an approximation to an ideal EWO transducer can ever be constructed.

A simple ring source is an obvious way of attempting to produce a practical version of an EWO tranducer. However, if the ring width is a few wavelengths (centre frequency) wide, then both plane and edge waves are emitted. This leads to drawbacks including the formation of large responses in directions straight ahead of the source rim and large variations in sensitivity with range. As for the PWO source a weighting profile with a smooth transition from maximum excitation at the rim to zero at the centre must be chosen so as to maximize the overall on-axis

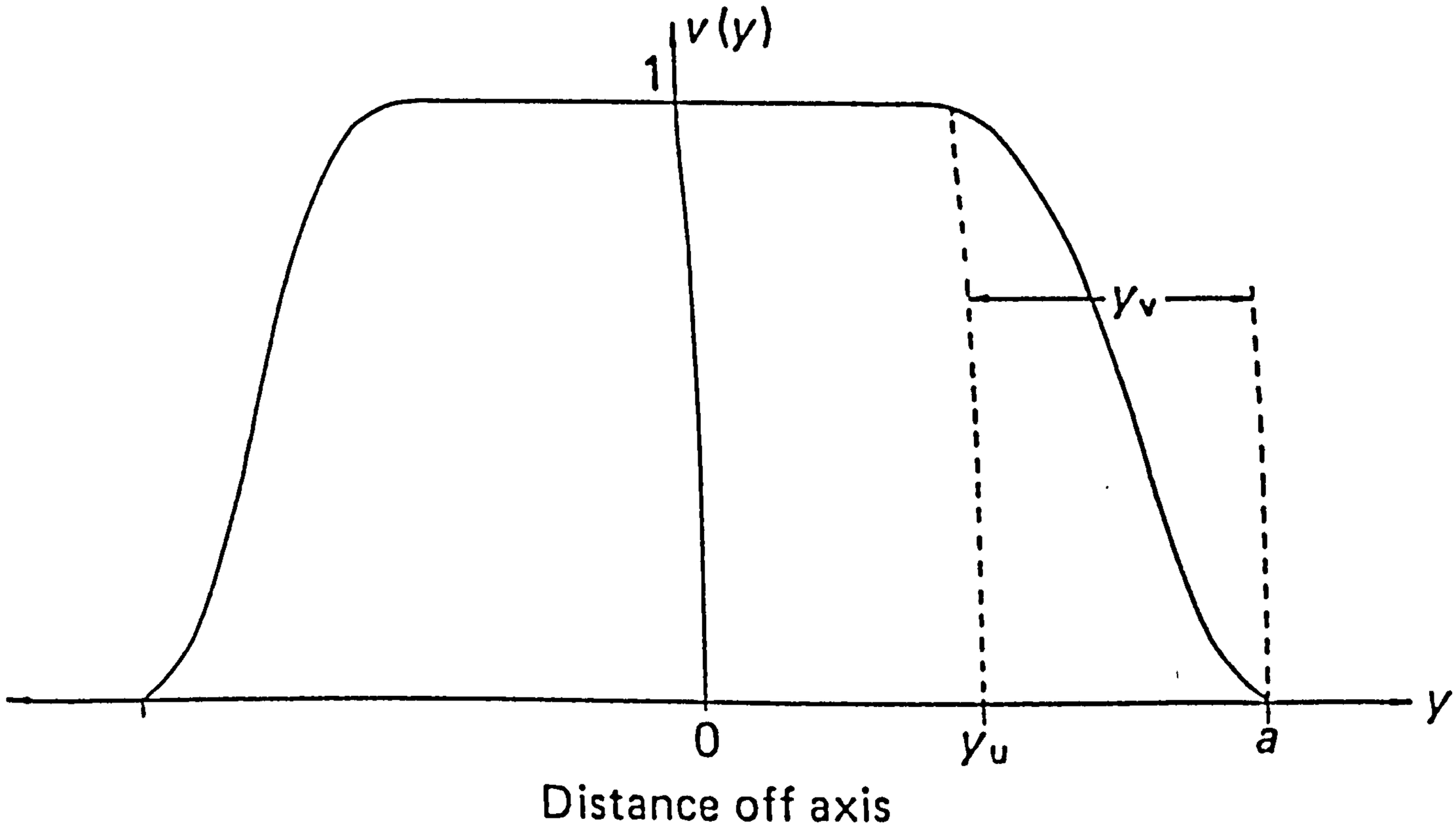

Fig 2.5.3 Velocity weighting function for a plane-wave-only source: $v(y) = 1,\ 0<y\leqslant y_u;\ v(y) = 1/2[1+\cos\pi/y_v(y-y_u)],\ y_u\leqslant y<a.$

sensitivity with range, whilst minimizing any unwanted rsponse straight ahead of the source rim. There is generally a trade-off between these two conflicting factors to obtain the optimum spatial and temporal field characteristics.

EWO transducers have already been constructed {59,63] within the Ultrasonics Group at the City University. The various characteristics of such transducers are evaluated in chapter 4 and subsequently discussed in chapter 5.

The treatment adopted so far in this section has been confined to propagation in fluids. It has been shown by Weight [64] that even a normally-coupled compression-wave transducer can radiate shear-wave components in a solid. This shear wave arises from the compresssion edge wave which propagates from the rim of the transducer and partially mode converts into a shear edge wave. In a similar manner an EWO transducer will also radiate shear edge waves which can again complicate NDT target and defect characterisation. In practice the shear wave echoes from defects are often well separated in time from the compression wave signals. However, the diffraction effects in the radiated field remain more complicated than in fluids since the amount of edge wave mode conversion which takes place is a function of angle and hence range. Theoretical modelling of non-uniformly excited transducers radiating into solids is left to further work and only experimental measurements will be included here (section 4.8). Since shear edge waves result from mode conversion of edge waves, a PWO source which radiates no edge waves will not generate any shear-wave components when normally-coupled to a solid. Such a device would therefore produce simple pulse shapes even when coupled to a solid.

2.5.3 Relationship between time-of-flight and range for an EWO source

For a uniformly excited or PWO source there is a linear relationship between the time of flight of the plane-wave echo pulse from a target (defect) and the range of the target from the plane of the source. In contrast, for a EWO source the arrival time of a pulse at a given axial point is directly proportional to the distance of that point from the of the source, see Figure 2.5.4. Thus echoes from equally-spaced axial targets will not appear equally spaced on a time-series display (e.g. an oscilloscope) which has a linear time base.

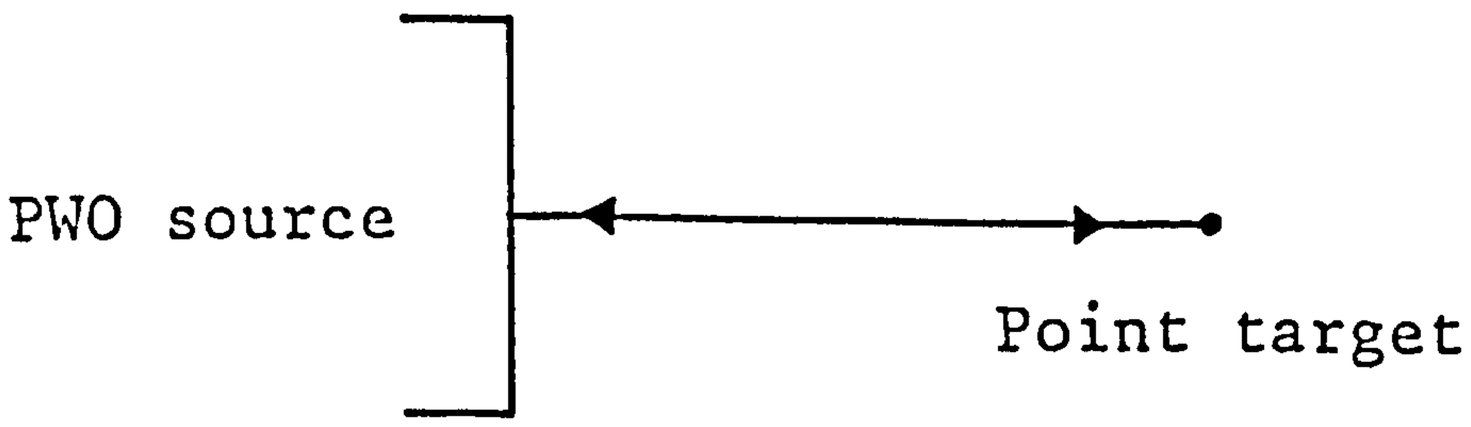

(a)

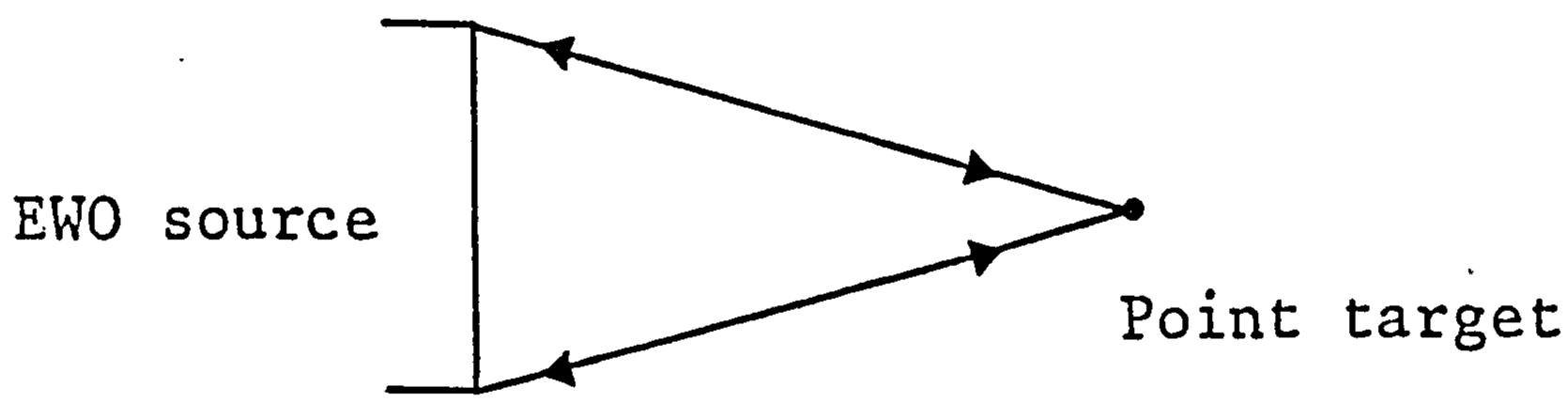

(b)

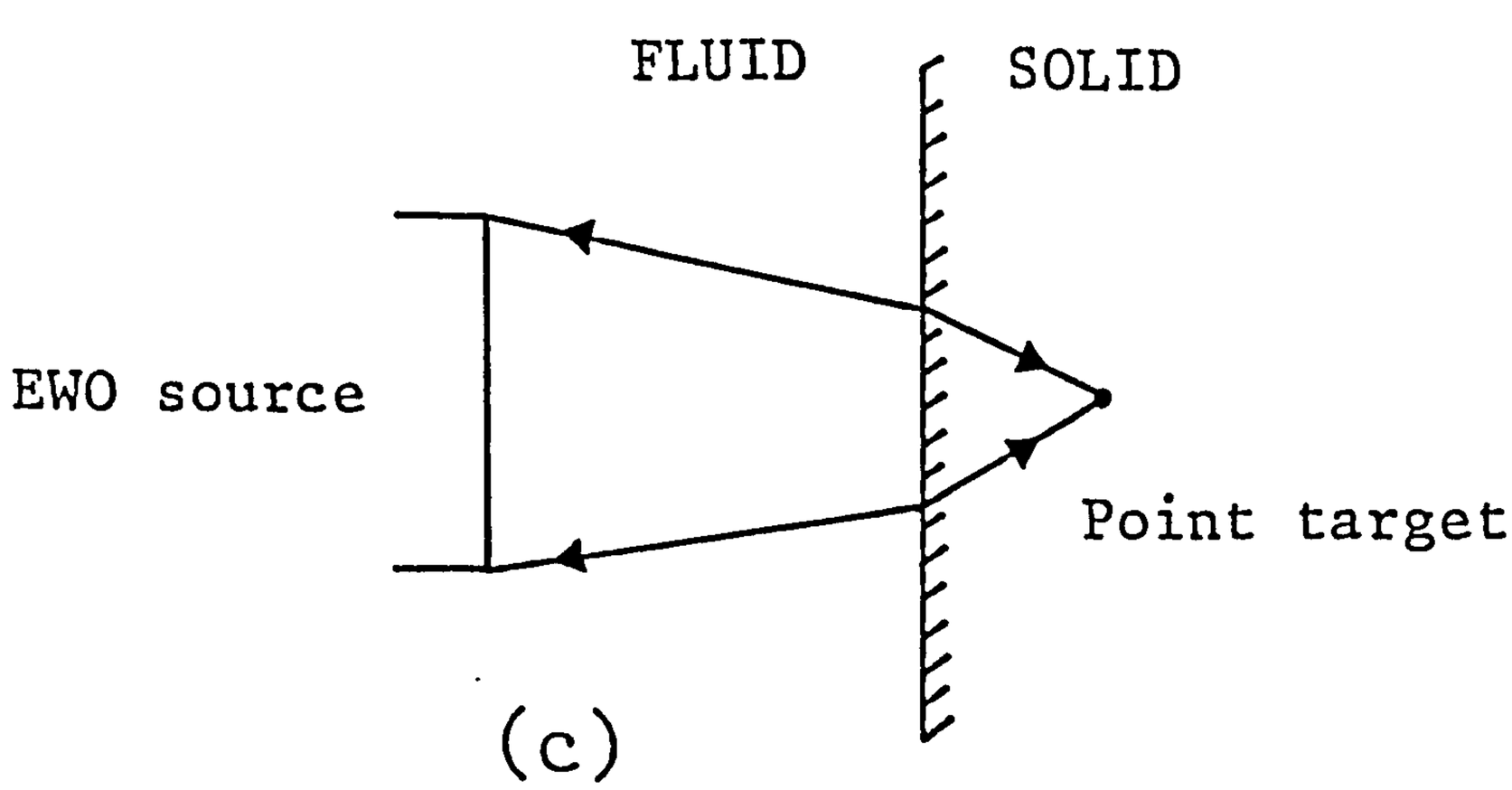

(c)

Fig 2.5.4 Schematic diagram illustrating the relationship between target range and echo time-of-flight for various configurations of non-uniformly excited sources: (a) a PWO source and (b) an EWO source interrogating a point target in a fluid; and (c) an EWO source interrogating a point target across a fluid/solid interface.

For the case of a uniform propagating medium, simple trigonometry (see Fig. 2.5.4(b)) allows the error in indicated target range x(t) to be calculated. In a similar manner the required shaping of the time base waveform to give a display showing equally-spaced targets at equal intervals can also be easily calculated. For the case of a water-coupled EWO source interrogating targets in a solid, such calculations cannot be carried out using closed-form expressions. The problem (see Fig. 2.5.4.(c)) is analogous to that of calculating the actual depth from the apparent depth of an object viewed from a medium of different refractive index to that containing the object. In this case closed form expressions may only be obtained by making small angle approximations. For typical immersion testing applications these approximations can lead to significant errors. In B-scan images of test blocks using an EWO transducer and water coupling shown in later results, the positional error in target depths is determined using an iterative technique formulated by Gatcombe [60]. This method uses as a first guess the small angle approximation to determine the actual ray path traversed from the source periphery to the target via refraction at the liquid/solid boundary. The algorithm converges quickly allowing the positional error in depth to be calculated. Correction curves can thus be easily generated by calculating the positional error at a number of target depths. A number of such curves are given in section 4.9.3.

2.6 Transmit-receive mode responses from finite-sized targets in a fluid medium.

Earlier studies [65,69] of the echo responses from finite-sized targets are not valid throughout the entire radiated field. Based on the assumption that the wavefronts incident on flaws or scattering obstacles are uniformly plane over the whole flaw surface, they are valid only at ranges well into the far field of the source. Other attempts to obtain simple expressions for scattering due to finite-sized targets make use of the wave equation for an inhomogeneous medium [70,71]. The scatterer or target is then represented as an inhomogeneity or fluctuation in the density and velocity of the fluid medium in the region of the scattering volume. Ueda and Ichikawa [72] have used this latter approach, obtaining a general expression for the echo waveform from a weakly scattering, finite-sized target by expressing the scattering medium in terms of a discrete model. Prior to the work of Ueda and Ichikawa, pulse-echo waveforms from isotropic reflectors in a fluid medium have only been predicted at an arbitrary field point for the case of an idealized point-like target [6,23].

In this section the theoretical approach used by Ueda and Ichikawa to predict echo responses from weakly scattering, axial, circular planar targets of finite dimensions is briefly reviewed. An extension of their model is also introduced which allows calculations to be made of the echo responses from normally-aligned targets of simple geometry (other than circular) lying at arbitrary field positions, both on and off axis. A further extension of the model to the case of strong scatterers is also presented.

2.6.1. Transmit-receive mode responses for a weakly scattering volume.

The wave equation for an inhomogeneous medium [70,71] provides the starting point for the analysis of echoes reflected from weakly scattering volumes. In this analysis it is assumed that the scattering volume V is embedded in a uniform fluid medium of density ρ_o and sound velocity C_o as shown in Fig. 2.6.1. The scatterer is then represented by fluctuations $\Delta\rho$ and Δc in the density and velocity respectively of the fluid medium in the region of the scattering volume. If it can be assumed that these fluctuations are small, such that $\Delta c \ll C_o$ and $\Delta\rho \ll \rho_o$,

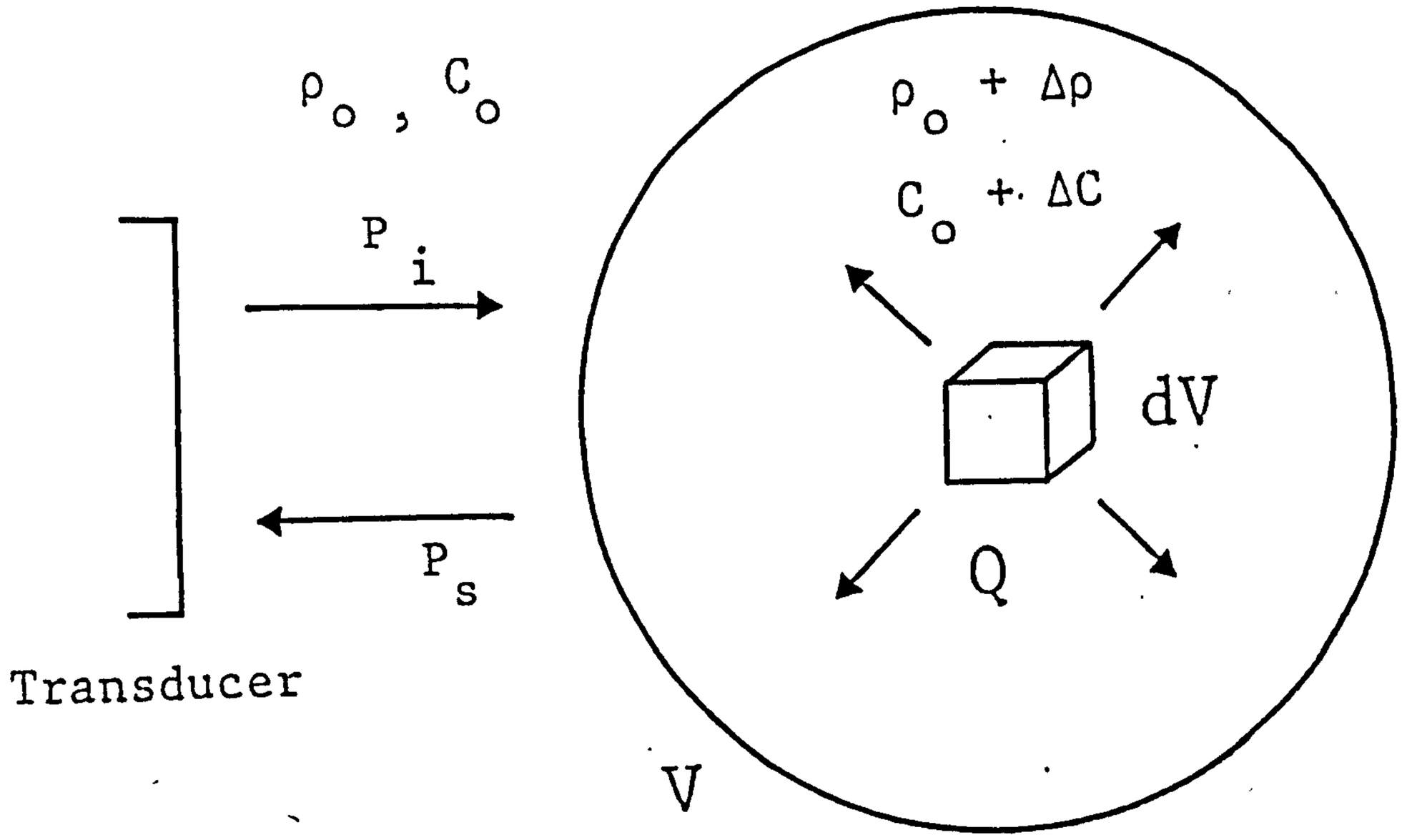

Fig 2.6.1 Geometry of the ultrasonic scattering from an inhomogeneous medium.

the wave equation can be expressed as

$$\left(\frac{1}{c_o^2}\right)\left(\frac{\partial^2 P}{\partial t^2}\right) - \nabla^2 P = \frac{2\Delta c}{c_o^3}\left(\frac{\partial^2 P}{\partial t^2}\right) - \left(\frac{1}{\rho_o}\right)\nabla(\Delta\rho).\nabla P \qquad \text{.....(13)}$$

where P is the sound pressure. If it is also assumed that the scattered wave $P_s(r,t)$ from the volume V is very much smaller than the incident $P_i(r,t)$ and that no multiple scattering takes place, then the scattered wave pressure is given by

$$P_s(r,t) = \int_V \frac{Q(r,t - r/c_o)}{4\pi r} dv \qquad \text{.....(14)}$$

where dV is a volume element and Q(r,t) is the scattering strength of the inhomogeneous medium which is as follows

$$Q(r,t) = \frac{2\Delta c}{c_o^3}\left(\frac{\partial^2 P_i(r,t)}{\partial t^2}\right) - \left(\frac{1}{\rho_o}\right)\nabla(\Delta\rho).\nabla P_i(r,t) \qquad \text{.....(15)}$$

The first term of eq. (15) represents the contribution to the scattered wave from the velocity fluctuation and the second term the contribution from the density fluctuation. Integrating these contributions over the source surface gives the echo voltage signals from the source for the density and the velocity fluctuations.

By expressing the scattering medium in terms of a discrete model (where the medium is represented by a number of small cubes of uniform density and sound velocity) Ueda and Ichikawa were able to show that at ranges larger than one source radius the echo signals from density and velocity fluctuations are identical; Stacey [73] has since shown that the same result can be obtained in the continuum without recourse to a discrete model. The echo response can then be expressed in terms of a single fluctuation in the specific acoustic impedance of the medium $\Delta(\rho c)$. Their expression for the output voltage E(t) from a source, which is uniformly pressure sensitive and used in transmit-receive mode response, on receiving the echo from a weak scatterering, arbitrarily shaped reflector is as follows

$$E(t) = \rho_o V(t) * \frac{\Delta(\rho c)}{2\rho_o c_o} \int_s \frac{\partial \phi_i}{\partial t}(t,y,z) * N.\nabla\phi_i(t,y,z)ds \qquad \text{.....(16)}$$

where ds is a surface element on the scattering volume, N is the outer normal to that surface, v(t) is the source velocity function and $\phi_i(t,y,z)$ is the velocity potential impulse response at a field point as

described in section 2.4. The term $\Delta(\rho c)$ represents the fluctuation of the specific acoustic impedance of the fluid medium due to the presence of the scatterer and $\Delta(\rho c)/\rho_o c_o$ is given by

$$\frac{\Delta(\rho c)}{\rho_o c_o} = \frac{\Delta\rho}{\rho_o} + \frac{\Delta c}{c_o} \qquad \text{.....(17)}$$

In general the solution to eq. (16) requires the evaluation of a double integral over the scattering surface. In some instances however, the geometry of the scatterer is such that the double integration reduces to a single line integral. Ueda and Ichikawa have examined such a case for a circular piston source and a flat-ended cylindrical rod having faces parallel and both being centered on axis as shown in Fig. 2.6.2 (see section 2.6.2).

It should be noted at this point, that implicit in the derivation of eq. (16) is the assumption that both the medium of propagation and the scattering medium are fluids. Even so, Ueda and Ichikawa have used this expression to predict the form of echo responses from weakly-scattering solid targets in fluid media. Thus the effect of mode conversion at the solid/fluid interface is not taken into account. However, results presented in chapter 4, which are awaiting publication [74], clearly show that the effect of mode conversion can be neglected and hence confirm that the mathematical model eq. (16) may also be used to accurately predict echo responses from solid targets in fluid media.

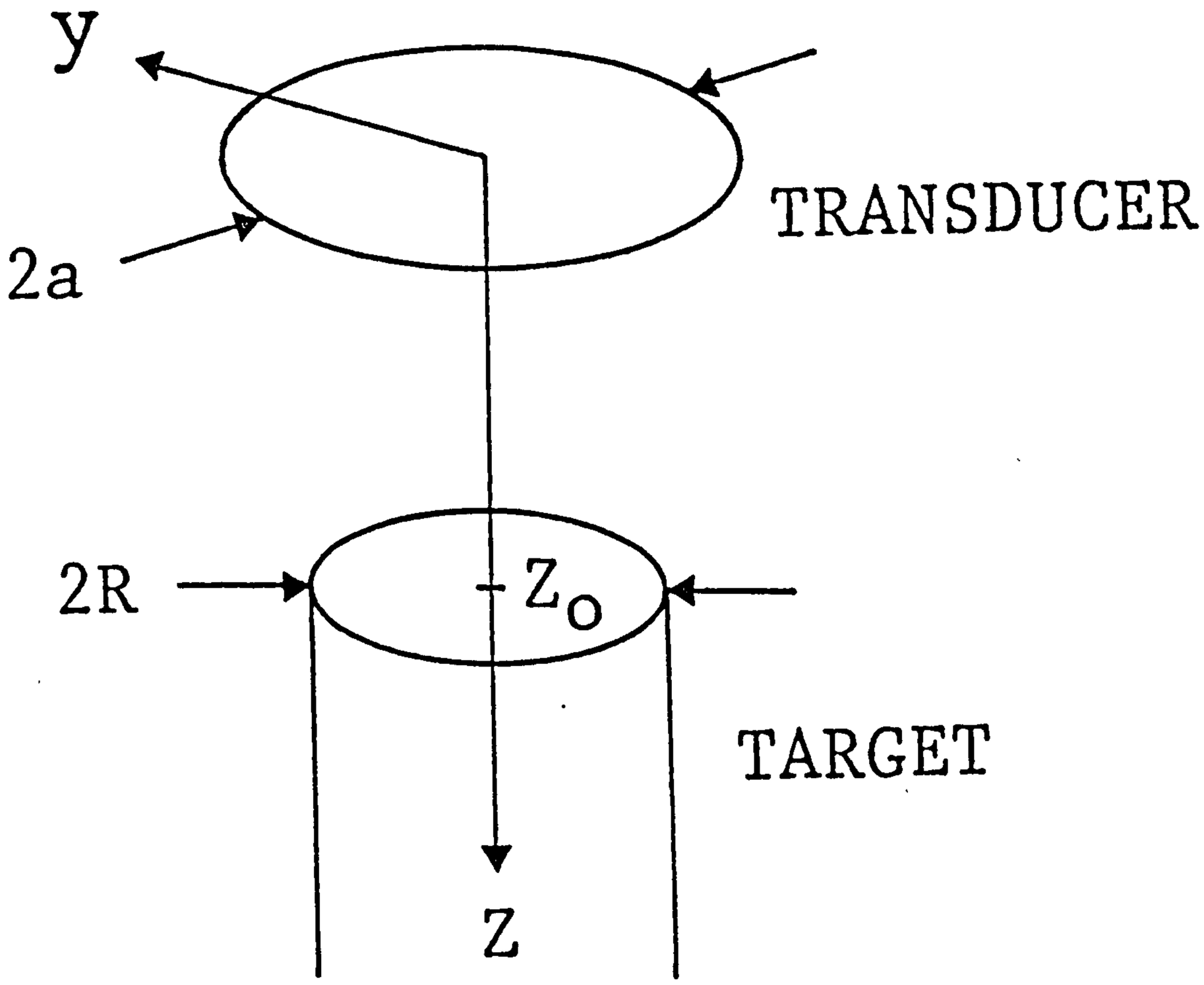

Fig 2.6.2 Geometry for determining the transmit-receive mode response for a circular transducer interrogating an axial, normally-aligned, flat-ended cylindrical target centered at co-ordinates $0,Z_o$.

2.6.2 Transmit-receive mode responses from the perfectly smooth, normally-aligned, circular flat-end of a cylindrical target centred on axis.

The pulse-echo output from a source of finite dimensions interrogating the scatterer shown in Fig. 2.6.2 (which is assumed to be isotropic) is found from eq. (16).

$$E(t) = \rho_o V(t) * \frac{\Delta(\rho c)}{2\rho_o c_o}\left[\int_{s_u} \frac{\partial \phi_i}{\partial t} * \frac{\partial \phi_i}{\partial z}\, ds + \int_{s_s} \frac{\partial \phi_i}{\partial t} * \frac{\partial \phi_i}{\partial y}\, ds\right] \quad \ldots\ldots\ldots\ldots (18)$$

where the first integral gives the contribution from the upper surface of the target and the second integral is the contribution from its sides. For the case of normal incidence considered here only the contribution from the upper surface is significant.

As a result of the circular symmetry of the radiated field from a circular source, the velocity impulse response at all points on a circular arc on the scattering surface that are equidistant from the source centre are identical. The surface integral in eq. (18) may therefore be transformed into a line integral expression by treating the upper surface of the reflector as a sum of circular segments ds - all points on a segment being equidistant from the source centre. When the target is on axis the circular arcs are complete and ds is

$$dS = 2\pi y dy \quad \ldots\ldots\ldots\ldots (19)$$

By also making the substitution $Z = c_o t$ the echo signal from a normally-aligned, flat-ended, cylindrical target is therefore

$$E(t) = \frac{\rho_o}{2} v(t) * \frac{\Delta(\rho c)}{\rho_o c_o} \int_0^R \frac{\partial \phi_i}{\partial t} * \frac{\partial \phi_i}{\partial t}\, 2\pi y dy \quad \ldots\ldots\ldots\ldots (20)$$

As can be seen, the double convolution within the integral in eq. (20) is of similar form to that for the transmit-receive mode response of a point target given in eq. (8) in section 2.4.1. The recognition of this similarity allows a simple physical interpretation to be made; namely, that as might be anticipated, the echo waveform from the surface of a finite-sized target can be thought of as the sum of contributions from all the elementary point targets that make up its surface.

Ueda and Ichikawa's model (eq. 20) predicts that targets of identical size but with different acoustic properties (i.e. velocity and

density), will give rise to echo responses with identical pulse shape but different amplitudes. The relative magnitude of the echo amplitudes is equal to the ratio of the constant terms in eq. (20) which is

$$\frac{\Delta(\rho c)_1}{\Delta(\rho c)_2} = \frac{\rho_0 \Delta c_1 + c_0 \Delta \rho_1}{\rho_0 \Delta c_2 + c_0 \Delta \rho_2} \qquad \text{.....(21)}$$

where $\Delta(\rho c)_1$ is the fluctuation in the specific acoustic impedance due to one target and $\Delta(\rho c)_2$ is the corresponding value for the second target. As mentioned previously the model has been derived for the case of weak scatterers. In this case there is no problem in using the definition of Δc and $\Delta \rho$ given by eq. (17). However, as will be shown later the model accurately predicts the shape of the echo waveform from strong scatterers and with simple modification can determine with reasonable accuracy the relative amplitudes of echo waveforms from strong scattering targets of differing acoustic properties.

With strong scatterers the corresponding fluctuations in sound velocity and density can no longer be considered small and it is preferable to use an alternative form suggested by Stacey [73]

$$\Delta c = \tfrac{1}{2} c_0 \left(1 - \frac{c_0^2}{c^2}\right) \qquad \text{.....(22)}$$

$$\Delta \rho = \rho_0 \ln\left(\frac{\rho}{\rho_0}\right) \qquad \text{.....(23)}$$

However, as demonstrated in section 4.6.2, even the above relationships in eqs. (22) and (23) cannot accurately predict echo amplitude ratios from targets with acoustic properties which result in large differences in sound velocity and density from those of the propagating medium. The experimental evidence presented later clearly shows that in this case a more precise estimate of the relative amplitude of echoes is given by simply taking the ratio of the target reflection coefficients for normally incident plane waves. Indeed, it is interesting to note that where the fluctuations in velocity and density are small it can be shown that the ratio of the conventional pressure coefficients reduces to eq. (21).

The mathematical model described by eq.(20) is valid only for planar circular targets on axis. Here a straightforward extension of this model is presented which allows theoretical waveforms to be calculated for planar circular target both on and off axis. Using this same method, echo waveforms from simple planar target shapes other than circular can be easily calculated.

2.6.3 Transmit-receive mode responses from flat-ended, cylindrical targets off axis.

When integrating over off-axis target surfaces, some or all of the equidistant circular ring segments are incomplete and ds in eq. (20) is then given by

$$dS = \theta(y)ydy \qquad \text{.....(24)}$$

where $\theta(y)$ is the angle of equidistant arc included on the target surface. The angle of equidistant arc is found by the law of cosines

$$\theta(y) = 2\cos^{-1}\left[\frac{y^2 + y_{off}^2 - R^2}{2yy_{off}}\right] \qquad \text{.....(25)}$$

where the axes and other variables are defined in Fig. 2.6.3.

It is therefore proposed that a general finite-sized target model for weak and strong scattering, normally-aligned, flat-ended, cylindrical targets both on and off axis should be given by

$$E(t) = \frac{\rho_o}{2} v(t) * \left[\frac{\rho_1 c_1 - \rho_o c_o}{\rho_1 c_1 + \rho_o c_o}\right] \int_0^{R+y_{off}} \frac{\partial \phi_i}{\partial t} * \frac{\partial \phi_i}{\partial t} \theta(y)ydy \qquad \text{.....(26)}$$

where the term $\Delta(\rho c)/\rho_o c_o$ is replaced by the pressure reflection coefficient. Note that when none of the target surface falls on the axis, the lower limit of the integral in eq. (26) becomes y_{off}-R. Transmit-receive mode responses from targets of simple geometry (e.g. rectangles, triangles etc) can be obtained by deriving from basic geometric considerations simple analytic expressions similiar to that in eq. (25) for the angle of equidistant arc on the target surface.

When the upper surface of a target is not normally-aligned to the source axis the solution of the surface integral does not reduce to a single line integral and requires the numerical evaluation of a double integral (see eq. (16)). Modelling of such target geometries is left to future work. It should in fact be possible to theoretically calculate echo waveforms from any arbitrary reflector or scatterer using this method.

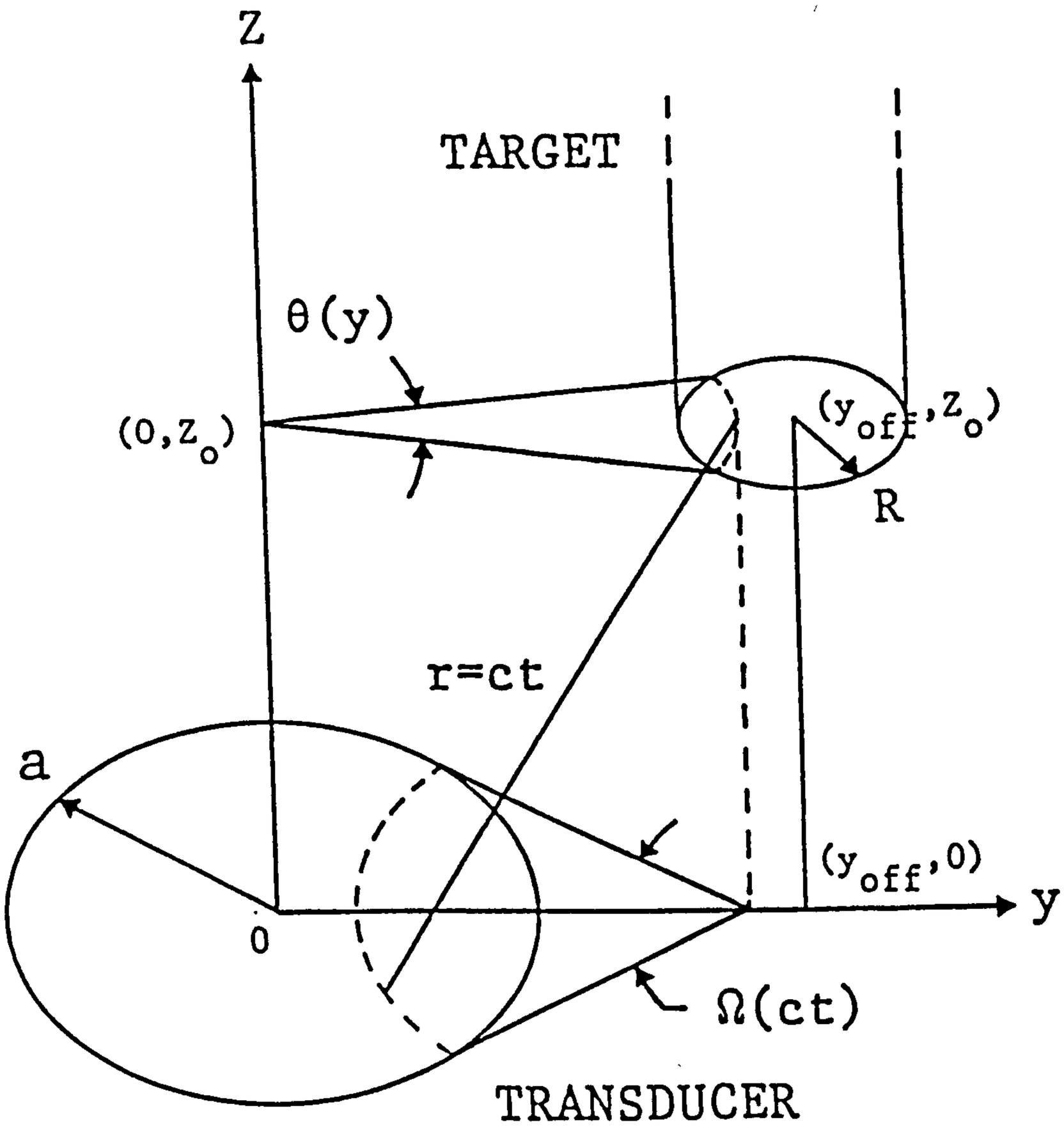

Fig 2.6.3 Geometry for determining the transmit-receive mode response for a circular transducer of radius a, interrogating a circular target of radius R. The target, with its face parallel to the transducer, is centered at co-ordinates Y_{off}, Z_o.

3. EXPERIMENTAL APPARATUS.

Essentially the measurements taken fall into two basic categories:-

(a) Measurements of pressure and transmit-receive mode response waveforms from both conventional (uniformly excited) and non-uniformly excited sources radiating into a fluid medium; for the transmit-receive mode case the corresponding lateral beam profiles have also been measured. Some preliminary pressure waveform measurements in solids were also carried out using a non-uniformly excited EWO transducer; and

(b) B-scan images of various test targets in both liquids and solids using uniformly and non-uniformly excited sources.

Most of the instrumentation used has been fully described elsewhere [75] and a brief description only is given here.

3.1 Excitation and receiving system.

The measuring system consisted of a conventional wideband excitation and receiving electronics system together with an automatic scanning water tank which provided positional accuracy of ±0.1mm, angular accuracy of ±0.1° and allowed movement in three orthogonal directions, Fig. 3.1.1 shows a block diagram of the measuring system.

The excitation source is a thyristor pulse generator which applies a unidirectional pulse to a wideband transmitting transducer. The width and rise time of this pulse can be adjusted so as to obtain single cycle ultrasonic pulses of varying shape and frequency content. When making pressure measurements the receiving system consists of a miniature receiving transducer and head amplifier which are directly connected to a main amplifier and a gated amplifier; in transmit-receive mode the transmitting transducer is directly connected to the receiving amplifiers. The gate is activated by a delayed pulse which is synchronized with the signal to be gated. The range and width of this gate is adjustable so as to include as little or as much of the received signal as desired. The gated signals could subsequently be fed to a number of analytical or recording devices including:-

(a) An analogue oscilloscope. Using a scope camera, waveforms could be photographed directly from the screen;

(b) a digital oscilloscope. This was used to capture and digitize waveforms for subsequent computer modelling;

(c) a Metrotek MD 702 gated peak detector which was used to make transverse beam profiles by detecting the amplitude of the pulsed waveforms. The detector gave a dynamic range of 40 dB and included the option of half or full-wave detection; and

(d) a digital scan converter. This piece of equipment is described in section 3.4.

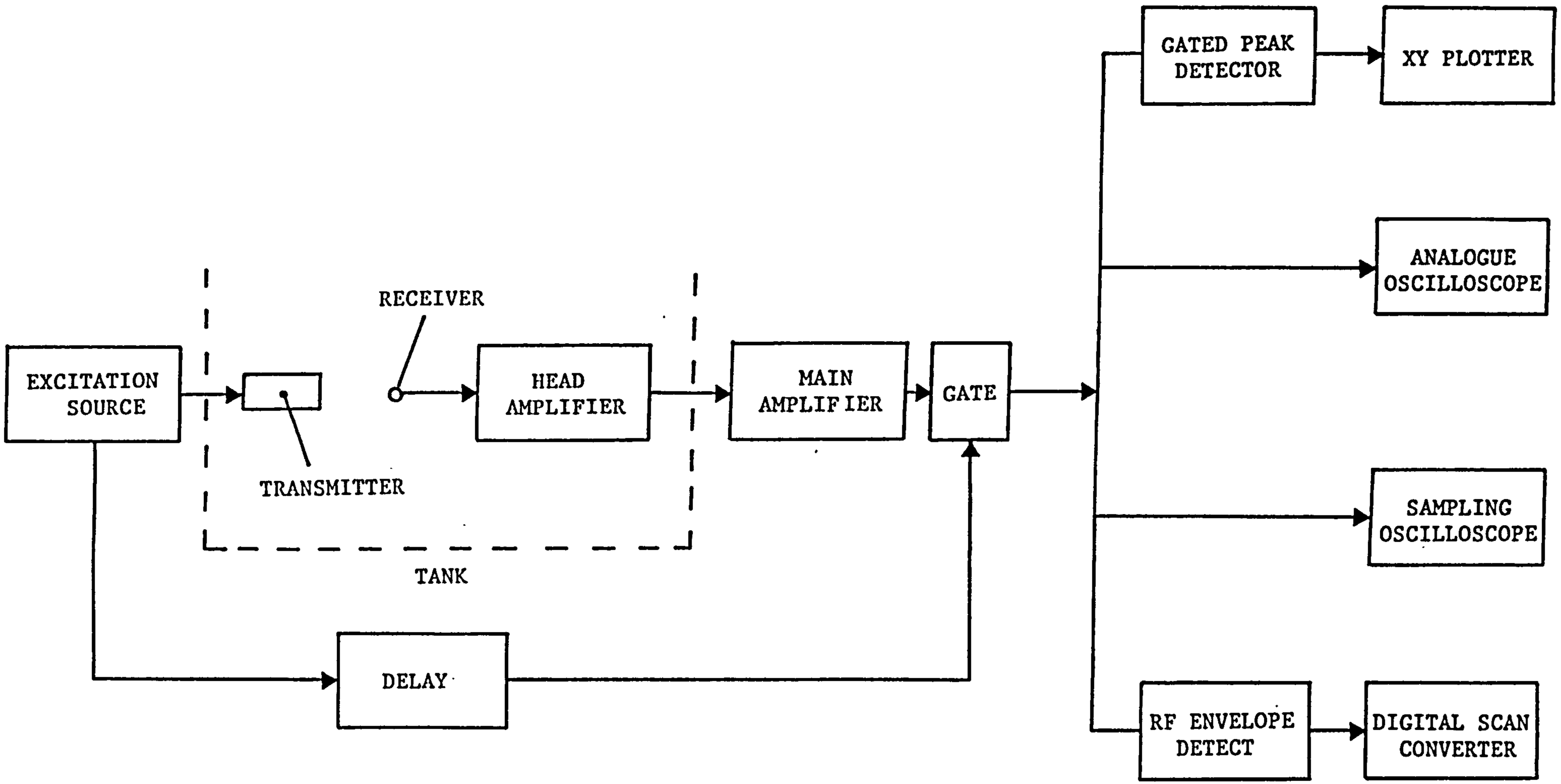

Fig 3.1.1 Block diagram of excitation and receiving system.

3.2 Transmitting transducers.

The transmitting transducers studied included:

(a) A conventional uniformly excited Panametrics (V3289) transducer with a 9.5mm radius aperture. These commercially-available transducers are manufactured from heavily-damped discs of lead metaniobate (PMN) with 10MHz half-wavelength thickness. Earlier work [2,27,29,32] has shown that these transducers are well modelled by assuming ideal piston behaviour; and

(b) a conventional Panametrics transducer (V3289) as above, modified into a prototype edge-wave-only transducer. An approximation to the required form of non-uniform excitation was made by simply removing the front face electrode and replacing it with an annular electrode 0.5mm in width at the rim of the active element. When the electrodes are excited, field fringing effects arise between the large back face and the small front face annular electrode. On the disc element this results in a velocity amplitude distribution which has an approximately Gaussian fall-off from a maximum at its rim to zero at its centre. The transducer was designed to be used with water coupling and in order to prevent water providing an earth electrode a glass slide was used as an insulating layer. The front face of the glass slide was coated with a conducting layer of paint, electrically connected to the earth electrode to provide a screen against Radio Frequency interference. This prototype device is further described in reference [76] which also gives details of alternative methods of construction.

3.3 Miniature receiving probe.

The small receiving probes used to make field-point pressure measurements are improved versions of specially-constructed devices first constructed within the Ultrasonics Group at the City University [6] which are now fabricated from PMN. These probes have a typical diameter of 0.2mm and are usable in the frequency range 0.5-8HMz. Such a frequency response ensures that the output waveform from the probe is an accurate representation of the impinging ultrasonic waves used here. At a frequency of 2MHz, their sensitivity to an incoming wave at 45° incidence is not more than 3dB down on that of a normally incident wave.

3.4 B-scan imaging system.

The process of converting acoustic echo information into a visual B-scan image was carried out using the imaging system illustrated schematically in Fig. 3.4.1.

The digital scan converter, a Hughes ANARAM 80 with a microprocessor-controlled image memory, accepts X and Y positional data and converts it into locations within a random access memory consisting of a 512x512 4-bit word matrix. The signal to the X input is a D.C. voltage level representing the lateral position of the transducer whilst a voltage ramp at the Y-input synchronized with the pulse-echo signal provides the information on the echo time-of-flight and hence the echo depth. At the same instant as the positional information is being processed the rectified envelope of the RF return echo signal (video mode), which is passed to the Z-input, is digitized at a rate of 12.6 MHz. Every sample is assigned to one of sixteen grey scale levels and this value placed into the relevant element of the memory matrix as determined by the positional data. Each element within the memory corresponds to a picture element or pixel in the final displayed image. The output from the scan converter conforms to the standard 625 line 50 Hz television format and can therefore be fed directly to a TV display monitor for direct viewing, video recording and photography.

Various pre-programmed pre-processing functions are selectable. Thus the grey scale levels can be allocated to ultrasonic echo data in a manner which favours or enhances those portions of the echo amplitude variation having the greatest significance. For example, by choosing a pre-processing function which assigns most of the sixteen grey scale levels to the stronger echoes the unwanted detail in the weaker signals may be removed. Conversely another selection could assign the majority of grey scale levels to the weak echoes and retain only gross distinctions between strong signals. The disadvantage of pre-processing is that it alters the B-scan image as it is "written" into the memory. Therefore if an inappropriate choice is made the scan must be repeated. More useful are the post-processing functions which are similar to the pre-processing functions except that they are carried out after the image has been stored in digital form and therefore effects only the displayed image and not the originally stored data.

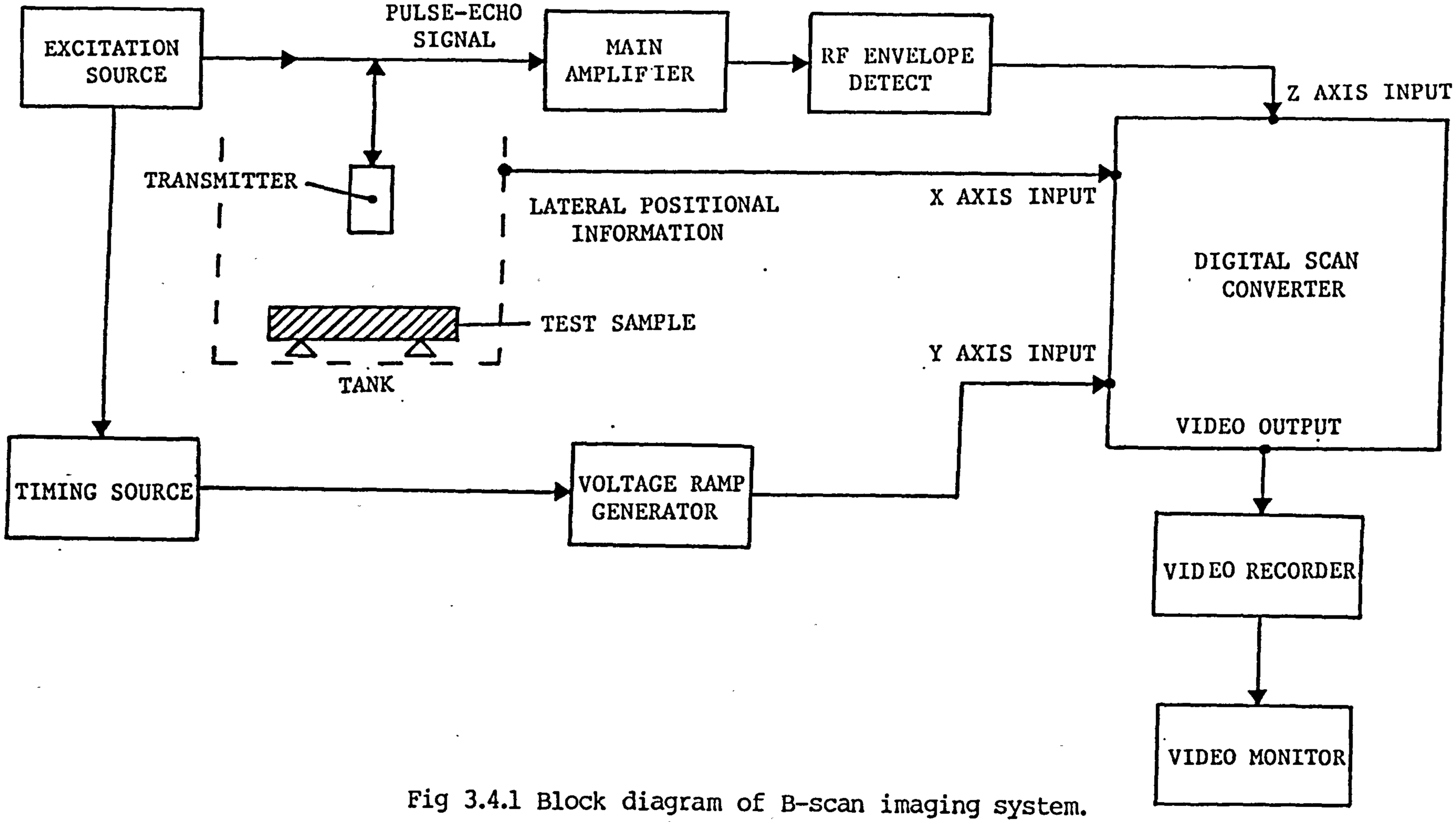

Fig 3.4.1 Block diagram of B-scan imaging system.

4. RESULTS

In this section both calculated and experimental results are given. Detailed calculations of pulsed pressure waveforms and transmit-receive mode responses from targets of various size have been made throughout the field of circular sources radiating into water. Calculated results for both uniformly and non-uniformly excited sources (PWO and EWO) were generated by computer using an impulse response approach discussed in chapter 2; the numerical techniques employed are outlined briefly below in section 4.1.

Although transient pressure fields from uniformly excited sources have been thoroughly investigated [13-18, 20-30], they are included here in order to compare their characteristic properties with those of PWO and EWO sources for the purposes of evaluating the usefulness of non-uniformly excited sources in high-resolution NDT.

The effect of target size, material properties and shape on the transmit-receive mode echo responses obtained using uniformly and non-uniformly excited sources, is investigated using the finite-sized target model presented in section 2.6. Furthermore, in order to better understand the echo generating process, an attempt has been made to describe the form of these responses in terms of plane and edge waves. The implications of these results in relation to high resolution testing and current flaw sizing and characterisation techniques employed in NDT will be discussed in chapter 5.

Experimental results from two real sources, a uniformly-excited conventional transducer and a non-uniformly excited prototype EWO transducer, have been compared with calculated results in order to confirm the accuracy of the computer modelling.

Due to the difficulties in fabricating heavily-damped, wideband non-uniformly excited PWO transducers, only theoretical results can at this time be included for such a transducer.

The imaging capabilities of the EWO transducer, along with its ability to locate and characterise targets (flaws), are compared with those of conventional transducers in a number of test applications and in B-scans of various specially constructed phantoms and test blocks containing simulated flaws.

Finally some preliminary results for an EWO transducer propagating into a solid are reported and their relevance to practical pulse-echo testing discussed.

4.1 Numerical Calculations

Pressure waveform calculations were made on a mainframe computer using the impulse response method described in section 2.4. For a uniformly excited source the velocity potential was calculated as a function of time (with a time increment Δt of 10ns) using the analytic expressions given in Appendix 1 and then differentiated numerically to give the pressure impulse response. The pressure waveform for an arbitrary motion of the source could then be obtained by performing a direct time domain convolution of the pressure impulse response with the relevant velocity function.

Transmit-receive mode impulse responses from an idealised point target, interrogated using a uniformly excited source, were calculated by performing a convolution of the pressure impulse response with itself as described earlier in section 2.4.1. The echo waveform was once again found by convolution of this impulse response with the velocity function. Transmit-receive mode beam profiles were generated in a point-by-point fashion by first calculating the transmit-receive echo waveforms and then taking the amplitude of the pulse at each field point as determined by full-wave detection ie. the largest half-cycle of the pulse is detected. It should be noted that with short pulses the method used to detect the amplitude can markedly alter the form of the resulting beam plot; these effects have been thoroughly investigated elsewhere [28].

Pressure waveforms and transmit-receive mode responses for non-uniformly excited sources were obtained by using the extension to the impulse response approach proposed in section 2.5.2. Using this technique the source is treated as a collection of sources of varying radius each weighted by the appropriate velocity amplitude as determined by the weighting profile. This requires the numerical evaluation of the line integral expressions given in eqs. (11) and (12) (section 2.5.2) for the pressure waveform and transmit-receive mode response respectively. The integration with respect to the radial component y was performed using a constant increment Δy of 0.1 mm. For a typical source of radius 9.5 mm this provided a sufficiently smooth approximation to the weighting profile.

For each position of the idealised point target the spectrum of the pulse waveform was also calculated using a Fast Fourier Transform algorithm. The waveforms were sampled at a rate given by the sampling theoreom, ie. $\Delta t = 1/2f_{max.}$. The value for $f_{max.}$ is found from the spectrum of the velocity function (ie. the excitation waveform) and is chosen to be four times the frequency of maximum output since there is negligible usable energy in the pulse spectrum above this frequency.

Echo responses from normally-aligned, flat-ended targets of finite dimensions are calculated by numerical evaluation of the convolutions and the integral in eq. (26) (section 2.6.3). The integration with respect to y was performed using the trapezoidal rule with a constant increment Δy of 0.1 mm which is the optimum for the target sizes studied here. At each value of y on the target surface the velocity potential impulse response was calculated in the same manner as described above.

4.2 Calculated pressure waveforms for uniformly and non-uniformly excited sources in water.

Figs. 4.2.1 - 4.2.4 show pressure waveforms for uniformly and non-uniformly excited circular, piston sources of 9.5 mm radius. In calculating these results, a source velocity function consisting of a single cycle sinusoidal (2 MHz) pulse was chosen. Such a waveform is a reasonable approximation to the shortest pulse that can be obtained from the transducers used. As an aid to presentation each off-axis result is shown horizontally displaced. A direct comparison between computer generated results can be made by taking into account the relative sensitivity figure shown on all plots which has been normalised to 1.00 for the uniformly excited source.

4.2.1 Uniformly excited (conventional) source.

The pressure waveforms from a conventional source, Fig. 4.2.1, are best explained in terms of their plane- and edge-wave structure. Close to the source it can be seen that within the geometrical beam region the plane wave retains its shape and amplitude at all regions where it is not overlapped by an edge wave. On axis the edge-wave contribution is an inverted replica of the earlier arriving plane wave. Off axis the edge wave gives rise to two smaller and distorted pulses which can be considered to arrive from the nearer and further edges of the source. Note that in Fig. 4.2.1 some of the off-axis responses at the shortest range have been truncated in time in order to prevent overlapping with other waveforms. It is not always possible therefore to see the edge-wave component from the further portions of the rim.

Further away from the source the plane- and edge-wave contributions begin to overlap. Initially this gives rise to an increase in amplitude and because the two contributions are of opposite sign produces the effect of differentiation. The shape of the axial far-field pressure waveform is in fact asymptotic to the time differential of the near-field direct plane wave(which is itself identical to the form of the source velocity function). At distances further away from the source than are shown here, the gradual fall off in amplitude with range characteristic of the far field can be observed as the plane and edge waves increasingly overlap. Detailed descriptions of these waveforms and the overall structure of the pulsed beam are available elsewhere [23, 25, 28].

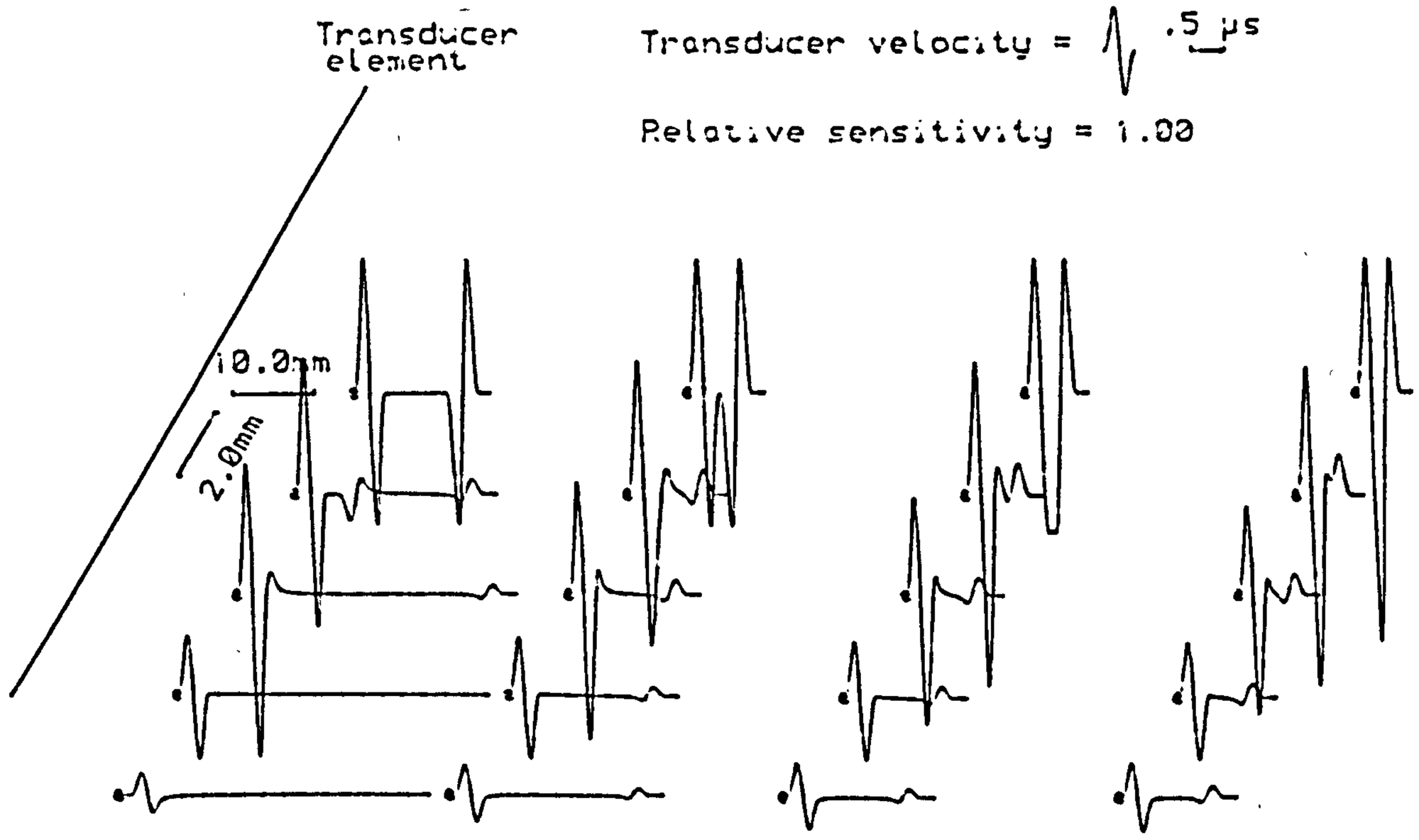

Fig 4.2.1 Computed pressure waveforms at points (•) in the field of a uniformly excited circular source radiating a short pulse into water.

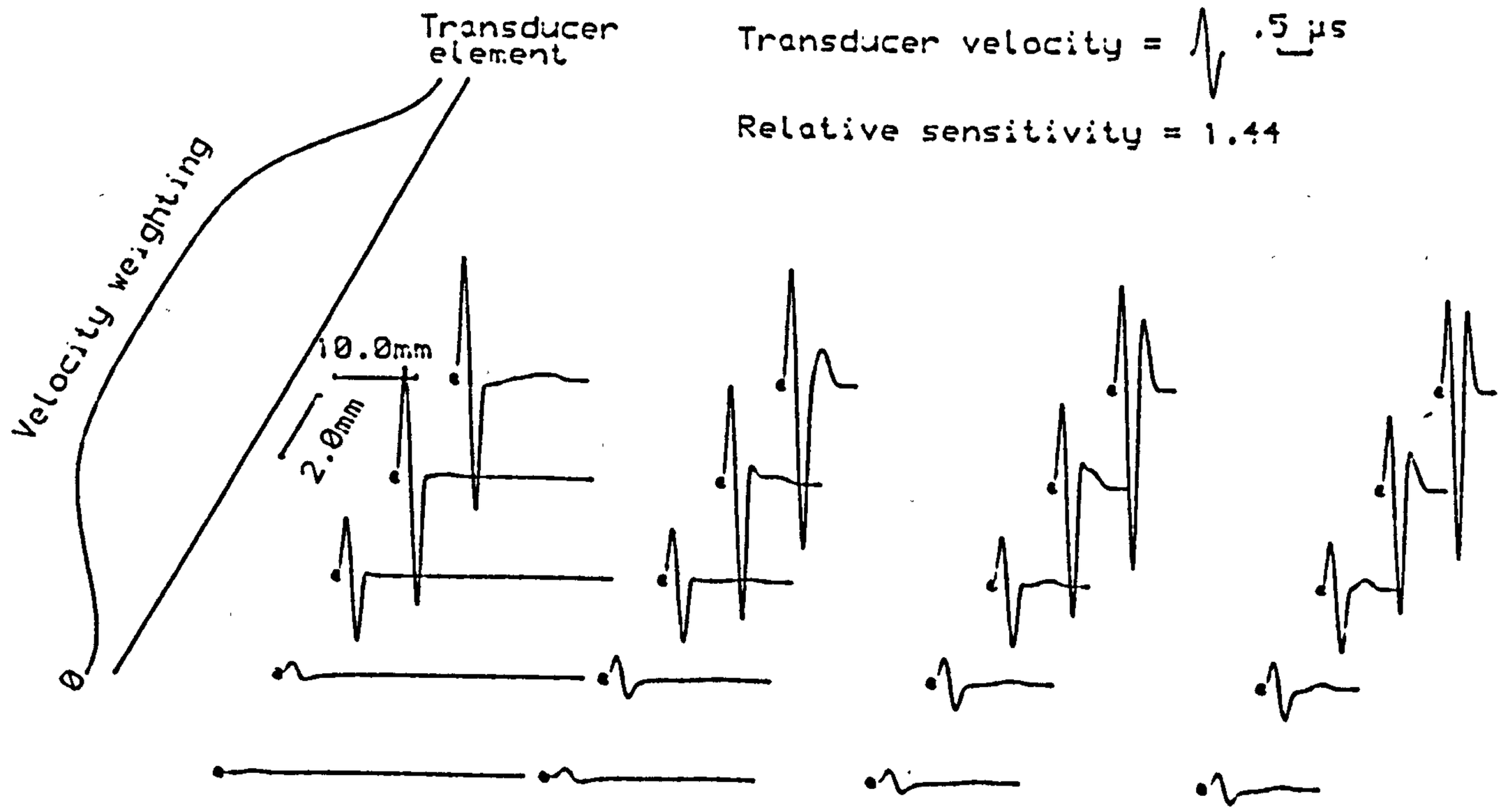

Fig 4.2.2 Computed pressure waveforms at points (•) in the field of a circular PWO source radiating a short pulse into water.

4.2.2 PWO source

Fig. 4.2.2. shows pressure waveforms from a non-uniformly excited PWO source. The weighting profile for the source depicted in Fig. 4.2.2. gives a smooth fall off from maximum excitation in the centre region to zero at the rim; the distance, as measured from the rim, for the amplitude of the profile to fall to half its maximum value is known as the half maximum amplitude width and has chosen to be 3.0 mm in this case. In contrast to pressure waveforms from a conventional source the pulse shapes are much simpler throughout the field, the edge-wave contributions having been smeared out. These results are similar to those published by Harris [54] and Stephanishen [55] for a source with a Gaussian velocity weighting profile which exhibits the same characteristics. Interestingly, at ranges close to the source it is possible to discern a small wave component that Harris terms a "membrane wave" (see section 2.5.2) trailing the direct plane wave. The on-axis amplitude from the PWO source is only 3dB down on that from a conventional source at ranges close to the source and remains fairly constant with range. It is interesting to note that if the transition in the weighting profile is made sharper, so that a larger portion of the source is fully excited, the sensitivity at the further ranges is improved. This improvement is gained at the expense of a loss in pulse shape simplicity and the re-introduction of a multi-pulse structure. The opposite effects to those described above are produced by making the fall-off transition in the weighting profile smoother. The weighting profile used in the calculations is a compromise which maintains a simple pulse shape whilst maximizing far-field sensitivity. Notice that the shape of the axial pressure waveform in the far field is again asymptotic to the time differential of the velocity function.

4.2.3 Ideal EWO source

Fig. 4.2.3 shows pressure waveforms from an "ideal" EWO source. Such a source radiates an edge wave with exactly the same characteristics as that radiated by a conventional source, but as implied does not radiate any plane waves. Although such sources are physically unrealisable for the reasons outlined in section 2.5.2, they are relatively easy to model theoretically [59] and provide a convenient starting point in the study of the characteristics of practical EWO transducers. As can be seen in Fig. 4.2.3. there is a single pulse of

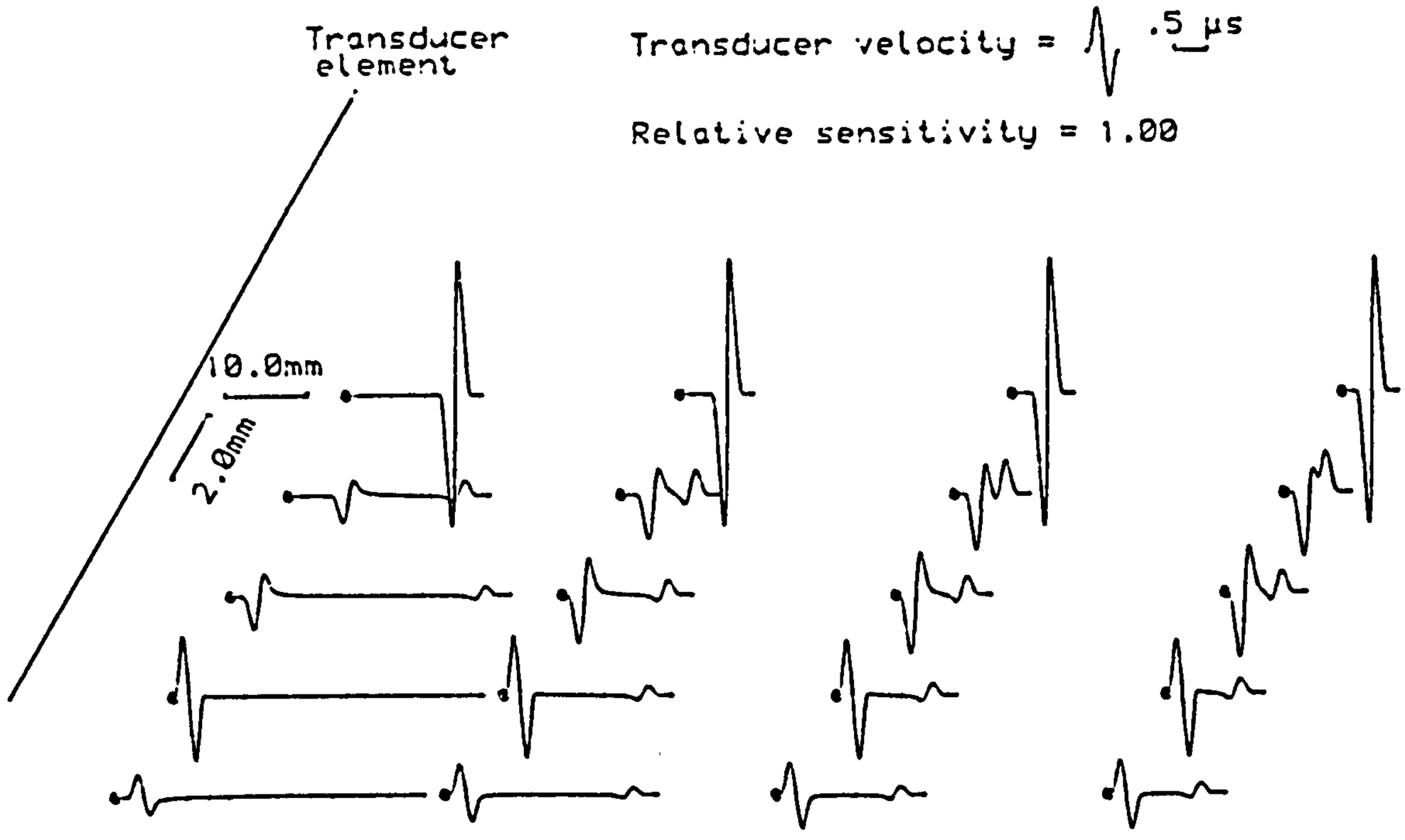

Fig 4.2.3 Computed pressure waveforms at points (·) in the field of an "ideal" circular EWO source radiating a short pulse into water.

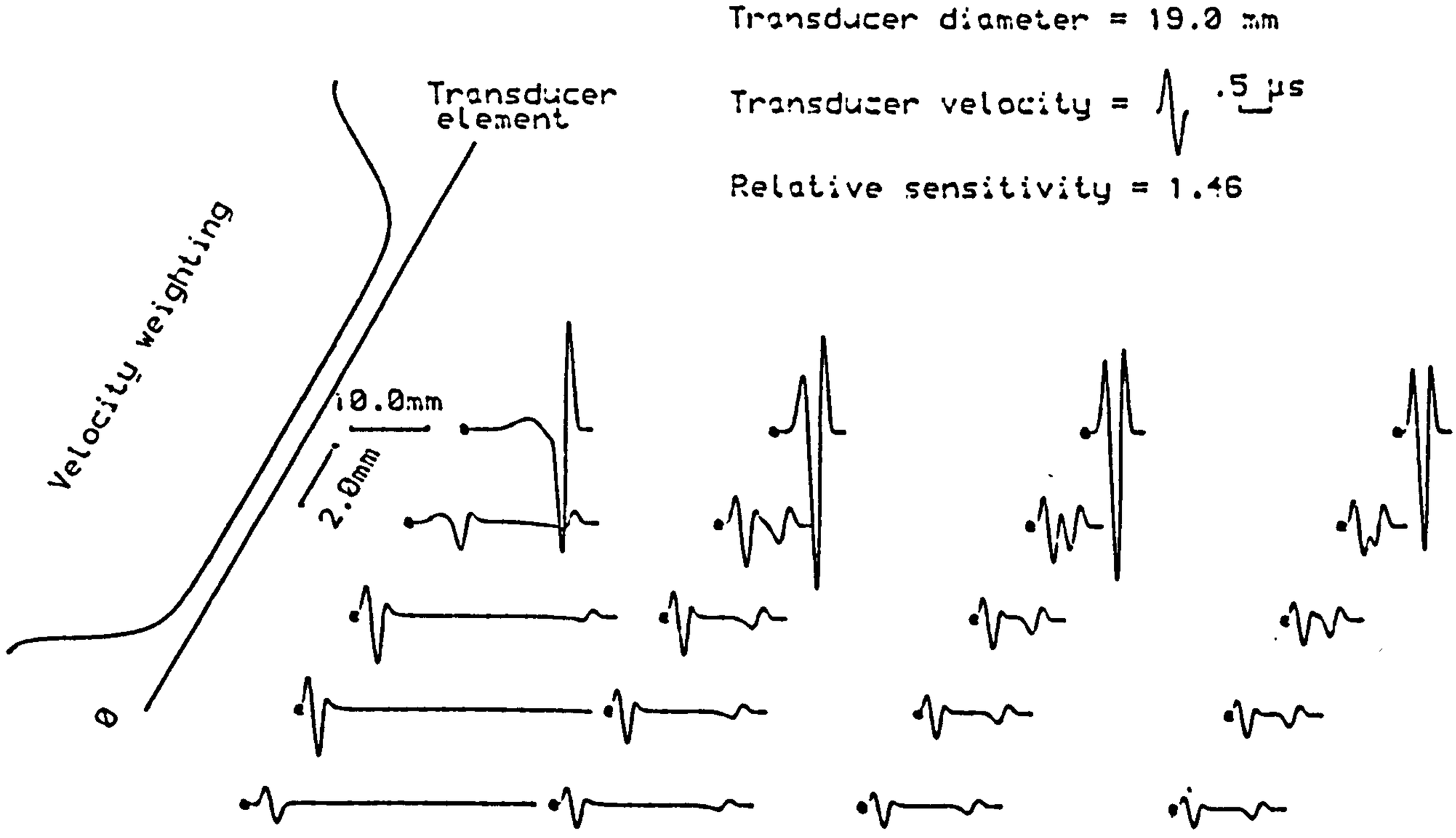

Fig 4.2.4 Computed pressure waveforms at points (·) in the field of a circular EWO source radiating a short pulse into water.

constant amplitude and shape at all points on axis where the contributions from each element of the edge wave arrive simultaneously and in phase. At a given field point off axis the path lengths from all the various portions of the source rim are no longer constant. Thus the edge waves arrive at different times resulting in the net pulse amplitude being much reduced relative to the on-axis value. The constant amplitude with range of the on-axis pulse may at first sight seem surprising since the edge wave has a toroidal wavefront and is thus a spreading wave. However, the edge wave is also very directional being much stronger in the direction straight ahead of the source rim than it is at angles either side. At points along the axis this directivity exactly compensates for the reduction in amplitude with range due to the spreading nature of the wave.

Off axis the edge wave quickly "splits" into two smaller and distorted pulses in the same manner as the edge wave propagating from a conventional source. By following the form of the two edge-wave contributions in Fig.4.2.3 it is possible to observe the way in which the strength of the edge wave varies as a function of direction of propagation. In the direction straight ahead of the rim the amplitude of the edge-wave pulse from the nearer edge is only 6.5dB less than the on-axis pulse value. This relatively large response in the directions straight ahead of the rim would lead to misinterpretations in pulse-echo testing if in fact such a source could be made.

4.2.4 EWO source

The weighting profile for a non-uniformly excited EWO source is in the opposite sense to that of a PWO source, with a smooth fall off from maximum excitation at the rim to zero in the centre. The half maximum amplitude width has been chosen to be 1.5 mm. Hence, as can be seen in the pressure waveforms from such a source (Fig. 4.2.4), it is the direct plane-wave component that is smeared out leaving a single pulse on axis. Although the on-axis pressure waveforms are not so constant in form and amplitude with range as those of the idealised EWO source, they are still much simpler than those of a conventional source. At ranges close to the source the pulse amplitude is only 4dB less than for a conventional source. However, approaching the beginning of the far field, as defined by the centre frequency (2 MHz) of the velocity motion and the whole source aperture, the amplitude begins to decrease.

Note that as for the conventional and PWO sources, the shape of the axial pressure waveform in the far field is again asymptotic to the time differential of the velocity function. For a conventional uniformly excited source the differentiating effect in the far field was explained in terms of the interaction of plane and edge waves (see section 4.2.1). This effect is still observable for PWO and EWO sources because for reasons outlined previously (see section 2.5) "ideal" transducers which radiate just plane waves or just edge waves alone, cannot be realised and in practice both types of wave are present. The weighting function of a practical version of the EWO transducer for example results in there still being a small plane-wave contribution emitted. Although its effect in the near field is not evident, it is more noticeable in the far field as in effect the influence of the weighting function becomes less important. In contrast, the purely theoretical "ideal" EWO transducer exhibits no differentiation effect in the far field.

Off axis the edge wave splits into two smaller, time separated components. However, straight ahead of the source the amplitude of the pulse from the nearer rim is smaller than for the ideal EWO source and falls off with increasing range. For reasons already mentioned, suppression of the response straight ahead of the rim is a desirable characteristic. By making the weighting profile sharper, so that the transition from maximum excitation at the rim to zero excitation occurs in a shorter distance, the straight ahead response is reduced but with consequent loss of far field sensitivity. In a similar manner to the PWO source a compromise weighting profile must be found which optimizes the conflicting characteristics.

4.3 Calculated transmit-receive mode responses from uniformly and non-uniformly excited sources interrogating an idealised point-like target in water

Calculations have been made with the same weighting profiles and velocity functions used in the previous section. Uniformly excited sources are again included so as to illustrate their limitations in high resolution pulse-echo testing and to allow a direct comparison to be made with equivalent PWO and EWO transducers. Comparisons of pulse-echo amplitudes are possible by taking account of the relative sensitivity value on each plot. An understanding of the way in which the propagated ultrasound interacts with an idealised point target gives a valuable insight into the echo generating process that occurs on the reflection/scattering of ultrasound from targets of finite dimensions, which is subsequently considered in section 4.4.

4.3.1. Uniformly excited (conventional) source.

Computed transmit-receive mode responses of a uniformly excited source interrogating an idealised point target are shown in Fig. 4.3.1. These exhibit a more complicated structure than thecorresponding pressure waveforms, especially in the near field. The form of these responses has already been described in previous work[23], but briefly for an axial, idealised point target the plane-and edge-wave reflections are equal in amplitude and each give rise to two output pulses when received back at the source. However, for such a target, the second of the output pulses due to the plane-wave reflection overlaps the first output pulse arising from the edge-wave reflection giving rise to the three pulse structure shown. At sufficiently close range, the three pulses are time separated and the central pulse has twice the amplitude of the other two. At greater ranges into the far field the pulses overlap to produce the effect of double differentiation. As described in section 4.2.1 the pressure incident on the target resembles the differential of the plane-wave pulse and another differentiation takes place on reception of the echo. Off axis the response is more complicated with several pulses being generated, though some of these are of relatively small amplitude.

The spectra of the above waveforms (Fig. 4.3.1.) show strong modulation, particularly in the near field. This modulation corresponds to the reciprocals of the time separation between the plane- and edge-

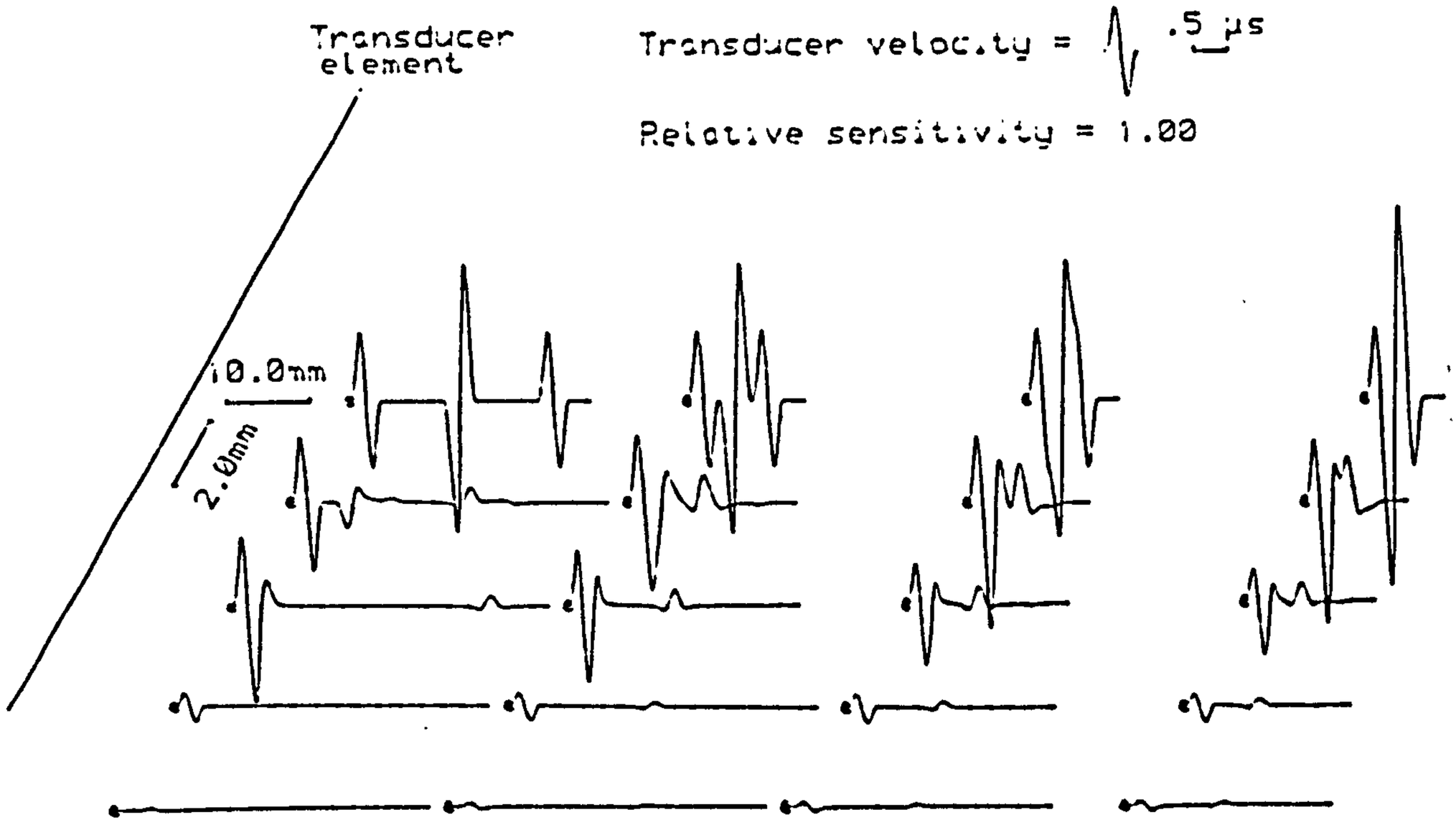

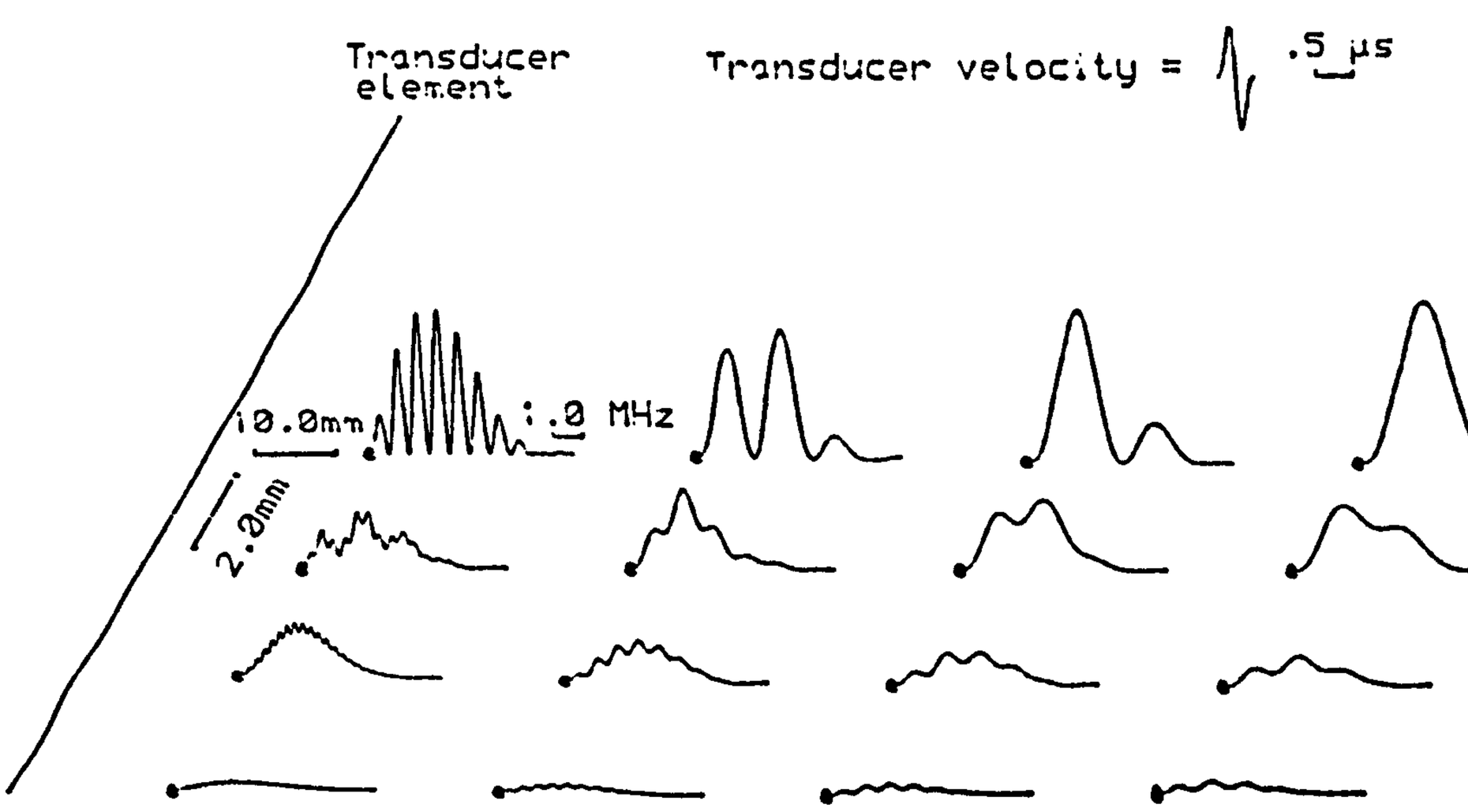

Fig 4.3.1 Computed transmit-receive mode responses and spectra of a uniformly excited circular source interrogating an idealised point reflector in water. (•) indicates the target positions.

wave components [62]. Even off axis, where the amplitude of the edge-wave components are reduced, there is still significant modulation. Further away the axial spectral response is smooth but modulation again appears in the off-axis result. Thus diffraction effects alone, produced by the interaction of plane and edge waves, lead to strong modulation of echo spectra from small targets. This would tend to mask any modulation due to target characteristics and make the application of target characterization techniques which rely on analyzing the frequency content of ultrasonic pulses, very difficult.

Fig. 4.3.2. shows calculated transmit-receive mode beam profiles at various ranges made assuming full-wave detection of the echo pulse amplitude. Close to the source and on-axis, the double-amplitude pulse shown in Fig. 4.3.1 gives rise to a central maximum. Just off axis the various plane-and edge-wave contributions do not overlap and there are no fluctuations in the beam plot, which then falls to half the central maximum. Even further off axis the plane-and edge-wave contributions increasingly overlap. At first the effect is to give an increase in the amplitude of the beam - as the various pulses partially reinforce to give an increase in their peak-to-peak amplitude (see Fig. 4.3.1) - and then a decrease, until at the edge of the geometrical region the beam has one eighth of its on-axis amplitude.

At larger distances from the source, the axial plane-and edge-wave contributions increasingly overlap. At first the affect is to give an increase in the beam amplitude. But at greater ranges, even further into the far field than shown here, the pulses destructively interfere to give the familiar fall off with range. Note that with short pulses, such as those considered here, the off-axis beam amplitude decreases smoothly in the far field, there being no side lobes characteristic of the beam radiated by a source emitting continuous sinusoidal waves.

4.3.2 PWO source.

In contrast to the conventional, uniformly excited source, the echo waveforms from a PWO source interrogating a point-like source shown in Fig. 4.3.3 are much simpler, consisting of a single pulse at all field positions. The axial echo amplitude increases with range reaching a maximum towards the end of the near-field region (as defined in section 4.4.4) before gradually decreasing. This is to be expected since the

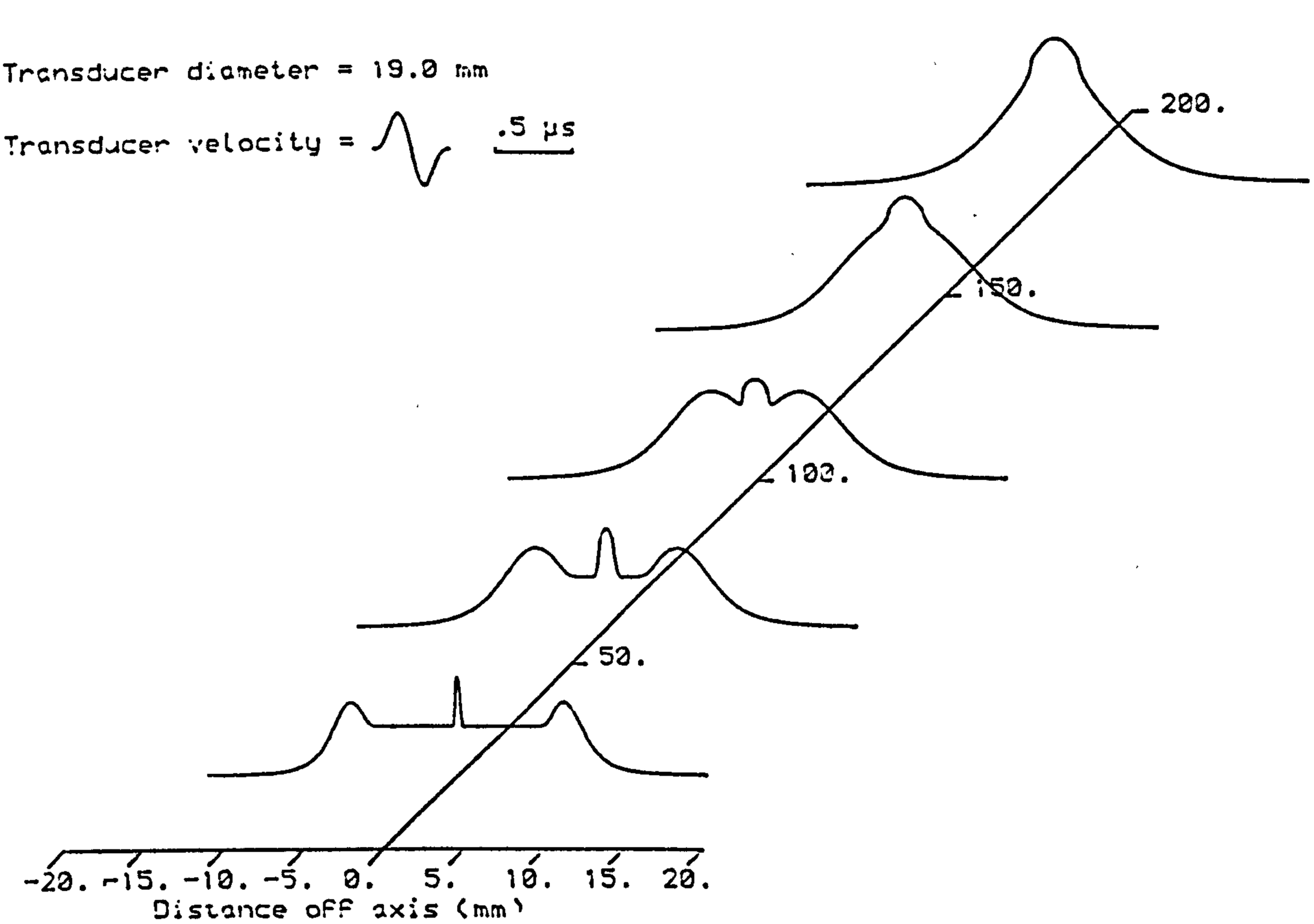

Fig 4.3.2 Computed transmit-receive mode beam plots of a uniformly excited circular source interrogating an idealised point reflector at various ranges in water.

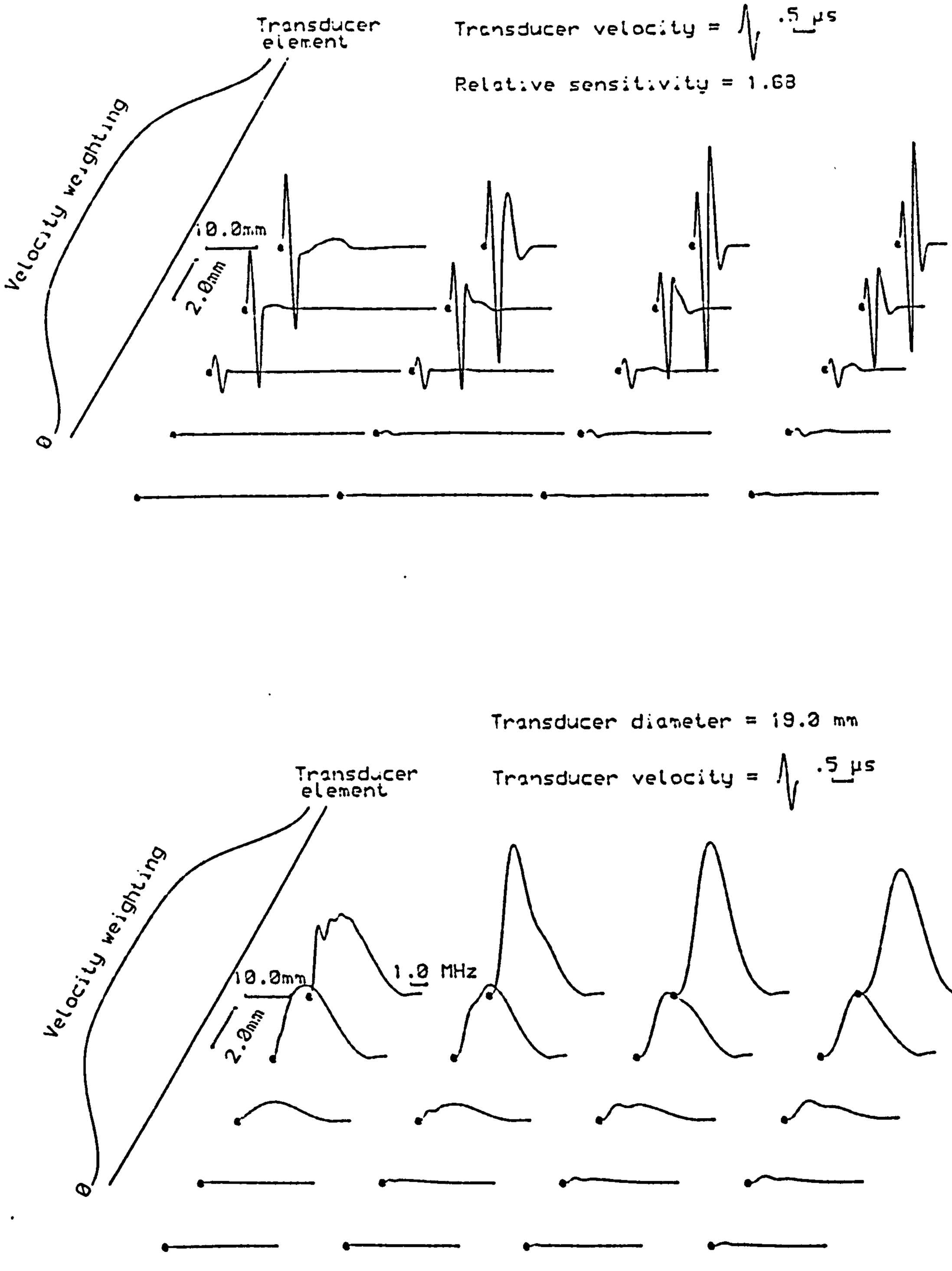

Fig 4.3.3 Computed transmit-receive mode responses and spectra of a circular PWO source interrogating an idealised point reflector in water. (•) indicates the target position.

form of the weighting profile tends to reduce the effective source aperture leading to greater beam spreading in the far field. The shape of the axial response in the far field is, like the conventional source, asymptotic to the second time differential of the velocity function. As discussed before the weighting profile is a trade-off between the minimum of beam spreading together with maximum sensitivity and simple pulse shape.

As Fig. 4.3.3. shows the absence of a multi-pulse structure leads to correspondingly simpler spectra. Therefore any modulation of the spectrum will be characteristic of the target rather than being due to diffraction effects.

At all ranges shown the transmit-receive mode beam profiles (Fig. 4.3.4.) decrease smoothly from a maximum on axis and contain no side lobes. Furthermore, the beam-width is only marginally greater than that from a uniformly excited source of the same aperture.

4.3.3 EWO Source

Calculated transmit-receive mode responses for an EWO source are given in Fig. 4.3.5. On axis everywhere, the response consists of a single pulse which varies in shape and amplitude with range. Close to the source, the axial echo response amplitude is not markedly different from the PWO source and 4-5dB less than a conventional source. However, at greater ranges into the far field the fall off in amplitude is more rapid for the EWO source in comparison with the other two types of source. Once again note that far field transmit-receive mode response asymptotically approaches the second time differential of the velocity function. Off axis the response drops off rapidly with lateral displacement, the on axis edge wave splitting into two miniature edge-wave contributions. This results in sharp lateral resolution. Further off axis, at a range of 20mm, the response straight ahead of the rim is 18dB less than the on- axis response at the same range. The size of this "straight-ahead response" , relative to the corresponding on-axis response, diminishes with increasing range. The consequences of this undesirable response in relation to non-destructive testing is discussed later in section 5.2.3.

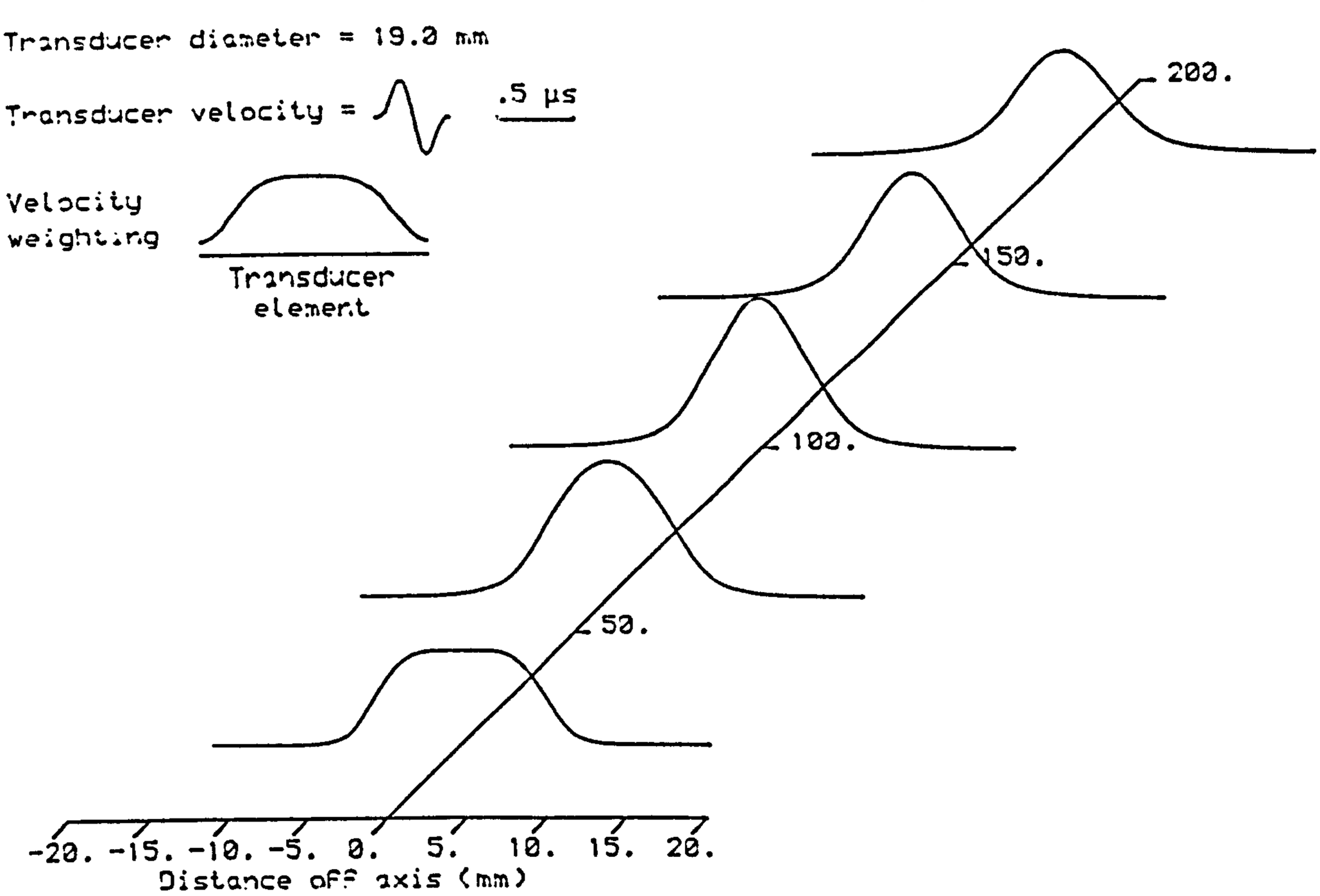

Fig 4.3.4 Computed transmit-receive mode beam plots of a circular PWO source interrogating an idealised point reflector at various ranges in water.

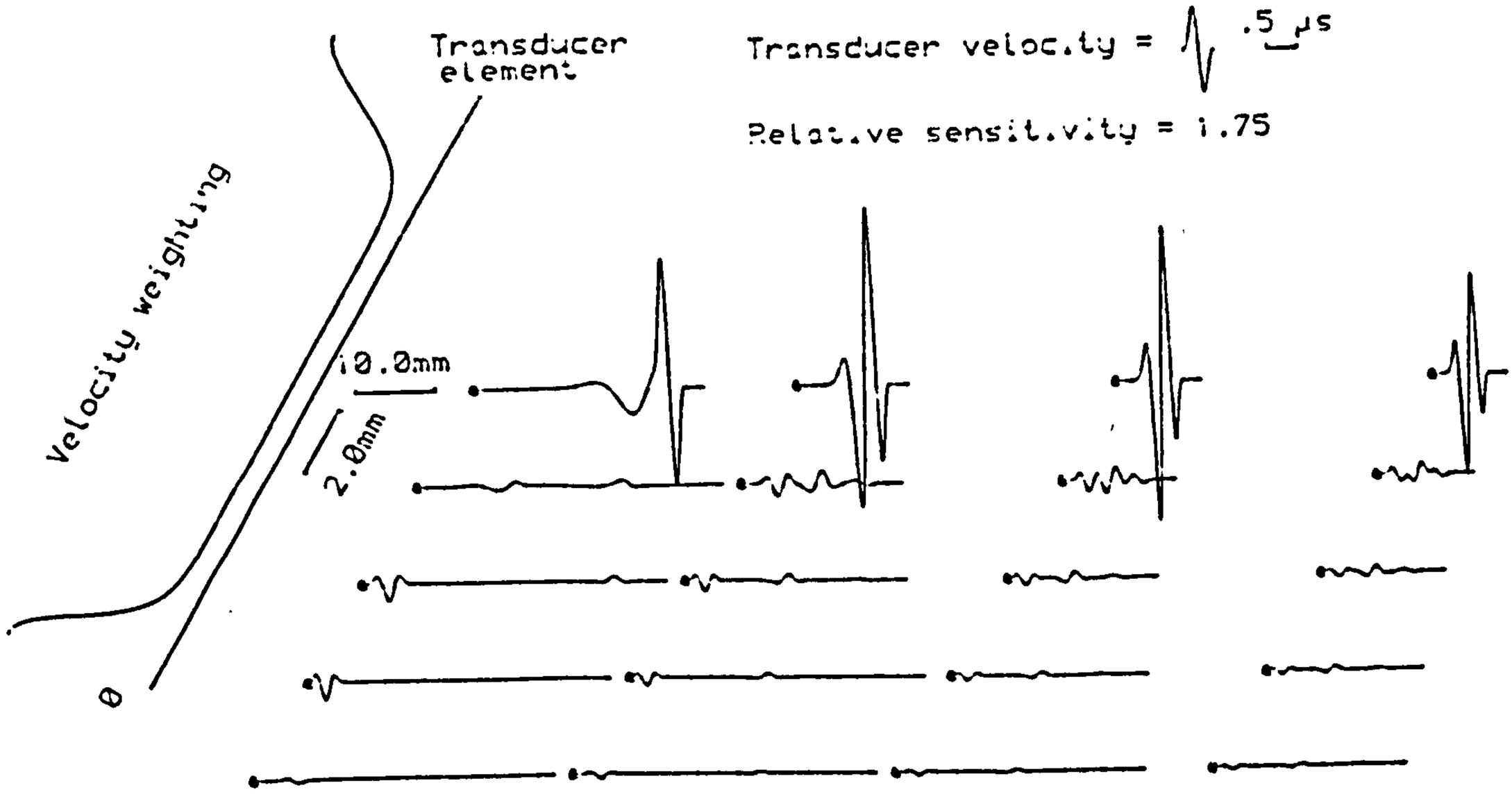

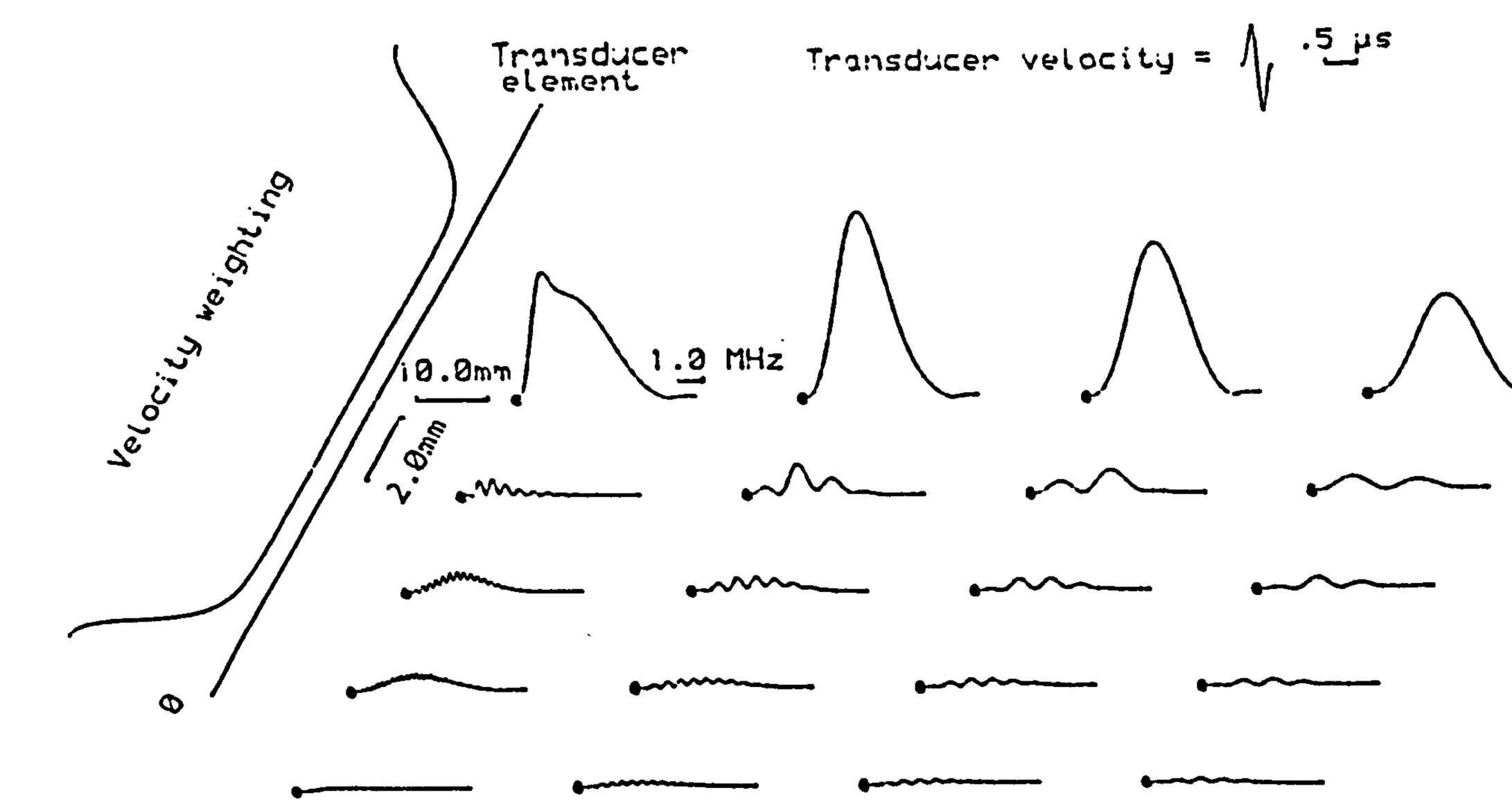

Fig 4.3.5 Computed transmit-receive mode responses and spectra of a circular EWO source interrogating an idealised point reflector in water. (·) indicates the target positions.

The simpler pulse shapes on axis result in correspondingly smoother spectra as shown in Fig. 4.3.5. Off axis the splitting of the edge wave into contributions from the nearer and further rim reintroduces modulation into the spectra.

The beam profile for the EWO source (Fig. 4.3.6) shows how the major response is concentrated on, or close to the axis, and further highlights its excellent lateral resolution. Close to the source the lateral resolution is of order magnitude better than that of a conventional source of the same aperture. Although there is a decrease in lateral resolution with range, a useful improvement in resolution over a conventional source is still achieved even at the furthest range shown here (180 mm). Notice also that the undesirable response straight ahead of the source rim is visible only at the shortest range.

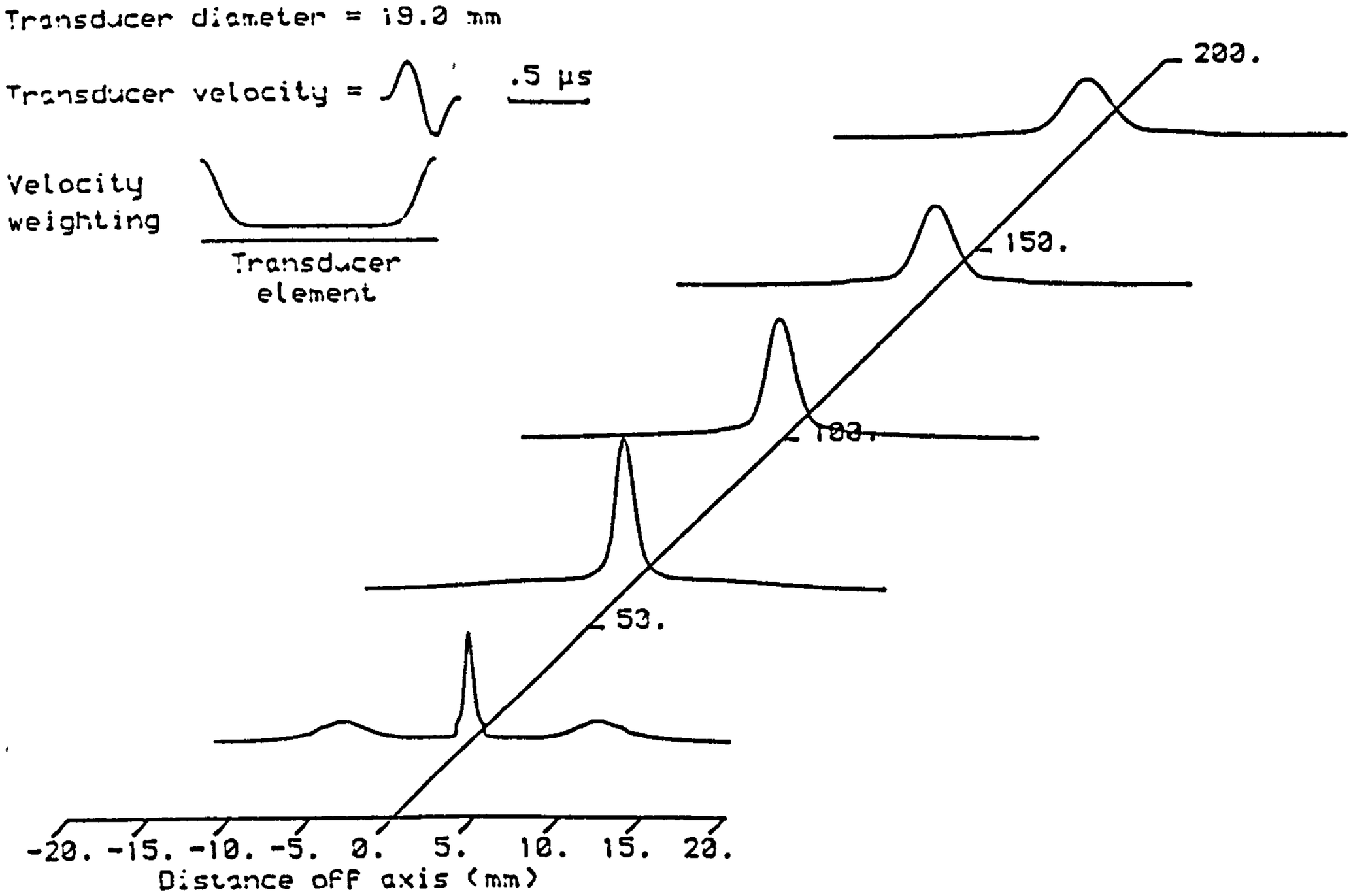

Fig 4.3.6 Computed transmit-receive mode beam plots of a circular EWO source interrogating an idealised point reflector at various ranges in water.

4.4 Calculated transmit-receive mode responses from targets of finite-size.

Using the same source configurations as in section 4.3, equivalent transmit-receive mode calculations were made for uniformly and non-uniformly excited sources interrogating circular, smooth, flat-ended, normally aligned, cylindrical targets of finite dimensions. Echo responses from 4 mm and 19 mm diameter targets were predicted using the mathematical model described in section 2.6.1.

A direct comparison of the various pulse-echo waveform amplitudes given in this section can be made by taking into account the relative sensitivity figure given with each plot. This figure has been normalised to 1.00 for the case of a uniformly excited source interrogating a 19mm diameter target. The dots(.) represent the position of the target centre.

4.4.1 Uniformly excited source

The effect of target size on the transmit-receive mode response for a uniformly excited source can be clearly seen in Fig. 4.4.1 for a target diameter of 4 mm. With this size of target, which is approximately five wavelengths wide at the centre frequency of the velocity function, there is a marked departure from the near field multi-pulse structure obtained from an idealised point target. No longer is there a distinct three pulse structure. For a 4 mm diameter target, the first pulse trailing the plane wave has split into two smaller components which are followed by a fourth pulse. Furthermore, because of the finite dimensions of the target the diffracted edge-wave components are much smaller than the initial plane wave. The edge-wave components are smeared out over the target surface, whereas the plane wave is integrated over the target surface since all plane-wave contributions arrive simultaneously to reinforce. A more detailed physical explanation of the transmit-receive mode pulse structure for finite-sized targets is given in section 4.6.1.1. On axis, approaching the far field, the diffracted edge-wave components are still sufficiently large that for this size of target they overlap with the plane wave to give an increase in amplitude. This effect is clearly evident at a range of 140 mm where the peak-to-peak amplitude is more than twice the amplitude at 30mm. Although not shown here, at ranges further from the source, the amplitude begins to decrease with increasing

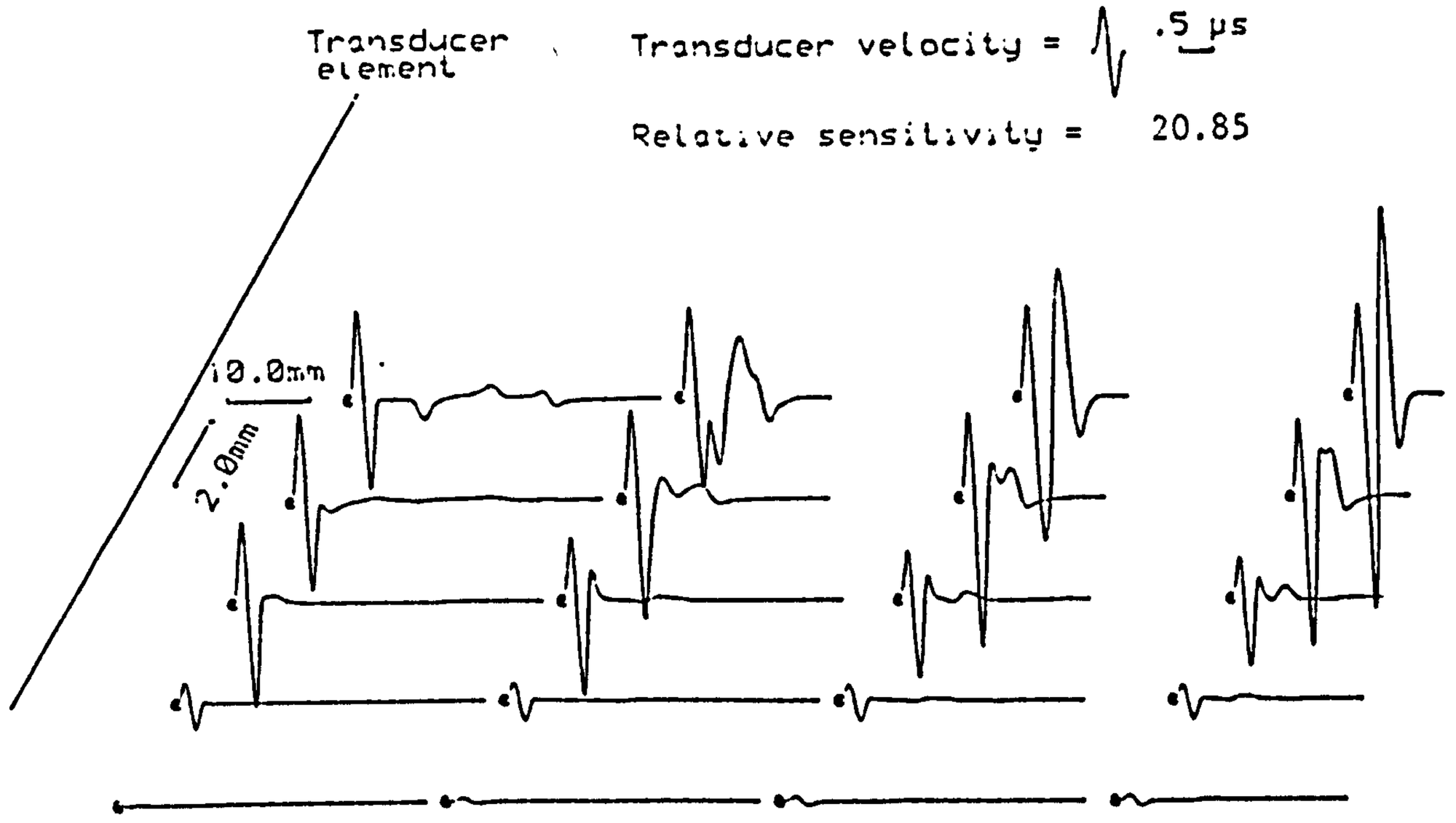

Fig 4.4.1 Computed transmit-receive mode responses of a uniformly excited circular source interrogating a normally-aligned, 4mm diameter circular target in water.

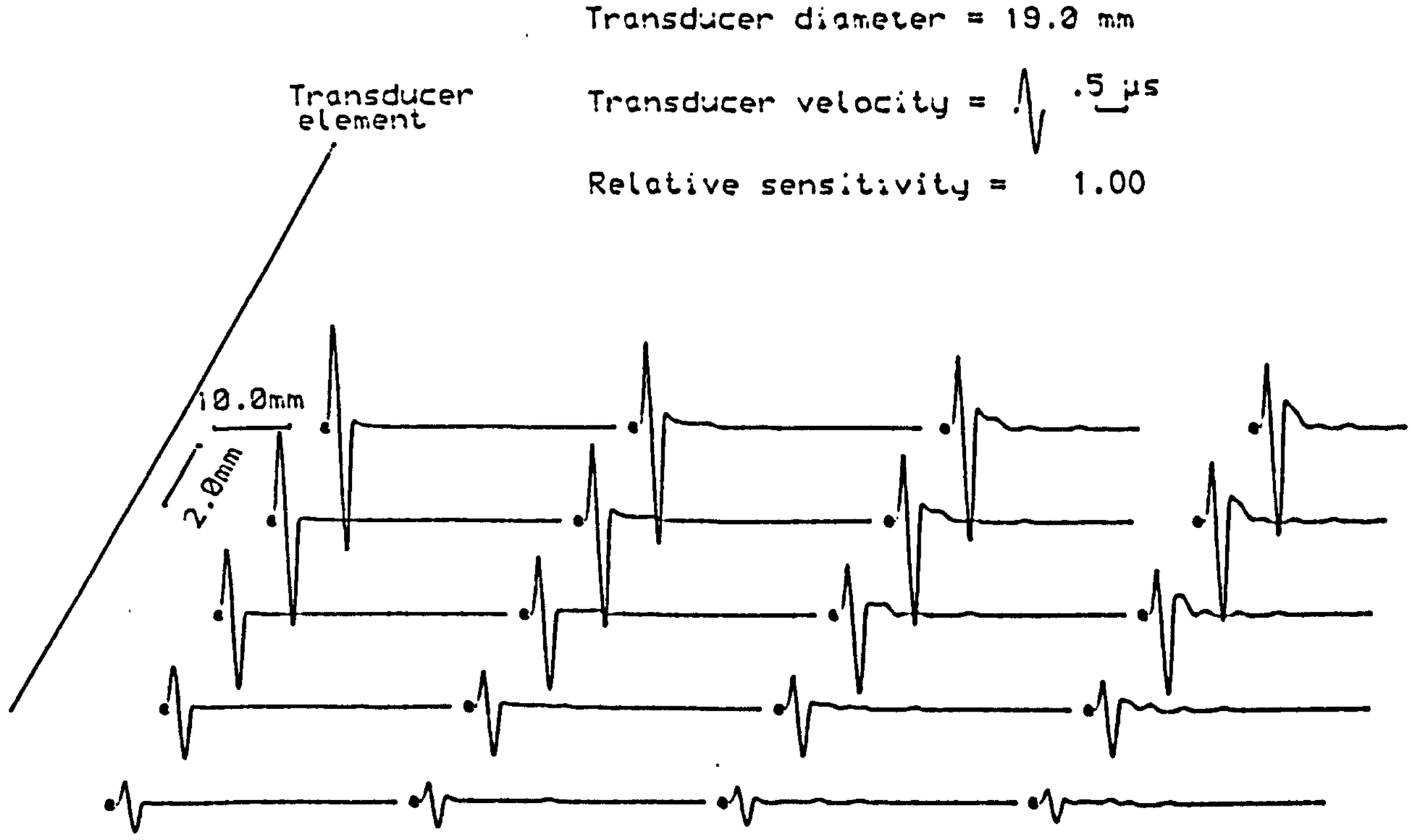

Fig 4.4.2 Computed transmit-receive mode responses of a uniformly excited circular source interrogating a normally-aligned, 19mm diameter circular target in water.

distance in a simil ar manner to a point target. Off axis and in the far field the shape of the pulse waveforms are similar to those from a point target (cf. Fig. 4.3.1.).

For a target of dimensions equivalent to that of the source (ie. 25 wavelengths wide), the echo waveforms (Fig. 4.4.2) are much larger in amplitude than for a 4mm diameter target, as indicated by the relative sensitivity. Because the target now effectively acts as a specular reflector there is no evidence of any multi-pulse structure. The response at all points consists essentially of a single specular reflection of the plane wave. It can be seen that, unlike the smaller point target and 4 mm diameter target, the waveform at the largest range on axis no longer resembles the second time differential of the velocity function. This is because, as explained elsewhere [6], the differentiating effect takes place when the wavefront incident on the target can be assumed to be uniformly plane over the whole of its surface. Obviously the larger the target the greater the range will be before this condition is met. For this size of target the effect of beam spreading taken over the relatively large target surface results in a gradual decrease in echo amplitude as the far field is approached.

4.4.2 PWO Source

The transmit-receive mode response for a PWO source interrogating a 4 mm diameter target are shown in Fig. 4.4.3. The pulse shapes are virtually identical in form to those obtained from a point target (cf. Fig. 4.3.3.) and show no evidence of any complicated multi-pulse structure in either the near or far field. Furthermore, the on-axis echo amplitudes are only 2 or 3dB down on those obtained using a conventional source (cf. Fig. 4.4.1). In contrast to the conventional source, the pulse amplitude remains fairly constant over the ranges shown here, since there are no significant edge-wave components to overlap with the plane wave.

Increasing the target size to 19 mm (see Fig. 4.4.4) in diameter does not significantly alter the shape of the response compared with smaller targets excepting that the echo amplitudes are larger. Only at the furthest axial range is there a noticeable difference in pulse shape compared with a point target (Fig. 4.3.3) and 4 mm diameter target (Fig. 4.4.3), where the far field double differentiation is not achieved for this size of target for the same reasons as discussed in section 4.4.1.

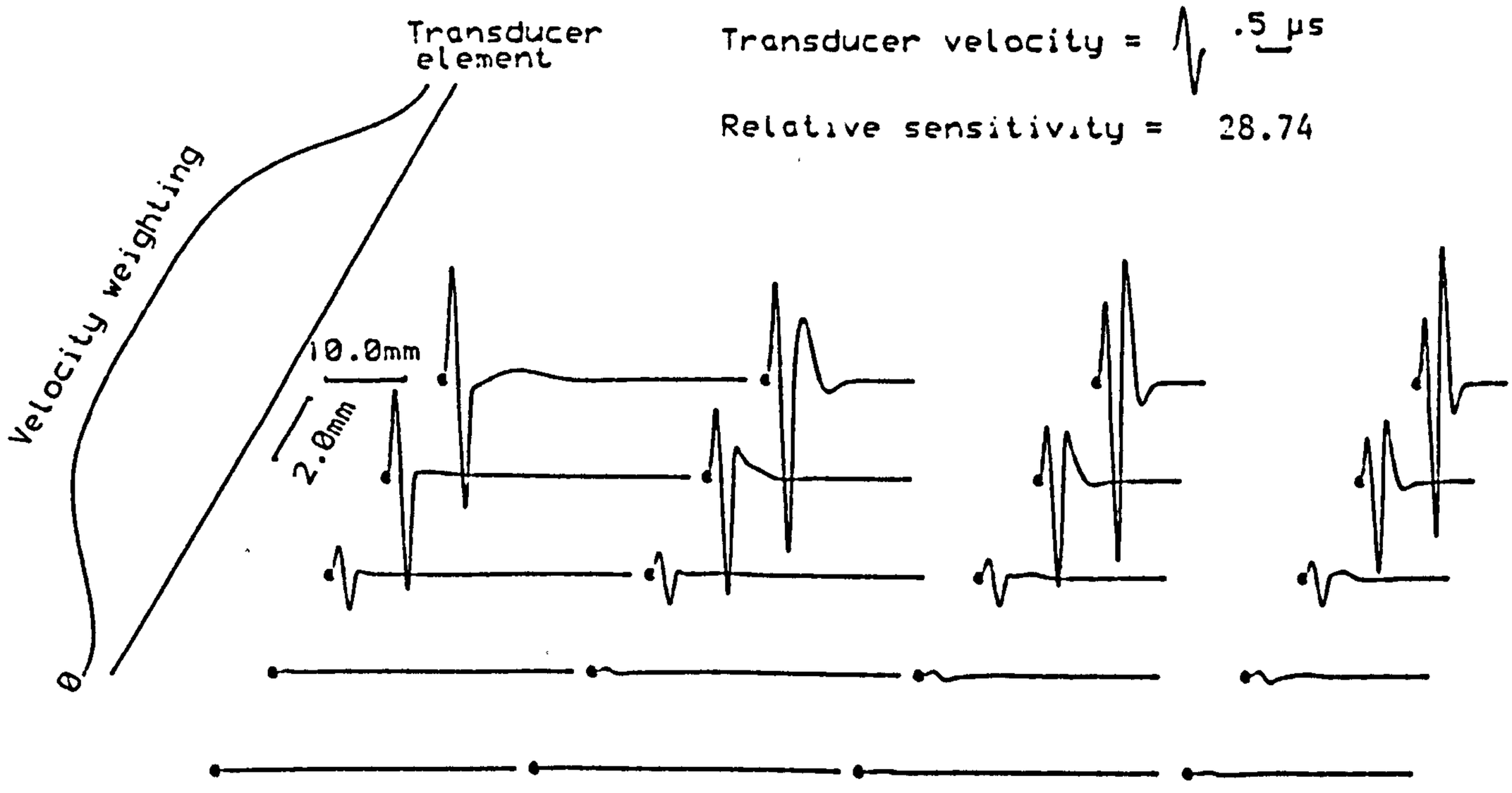

Fig 4.4.3 Computed transmit-receive mode responses of a circular PWO source interrogating a normally-aligned, 4mm diameter circular target in water.

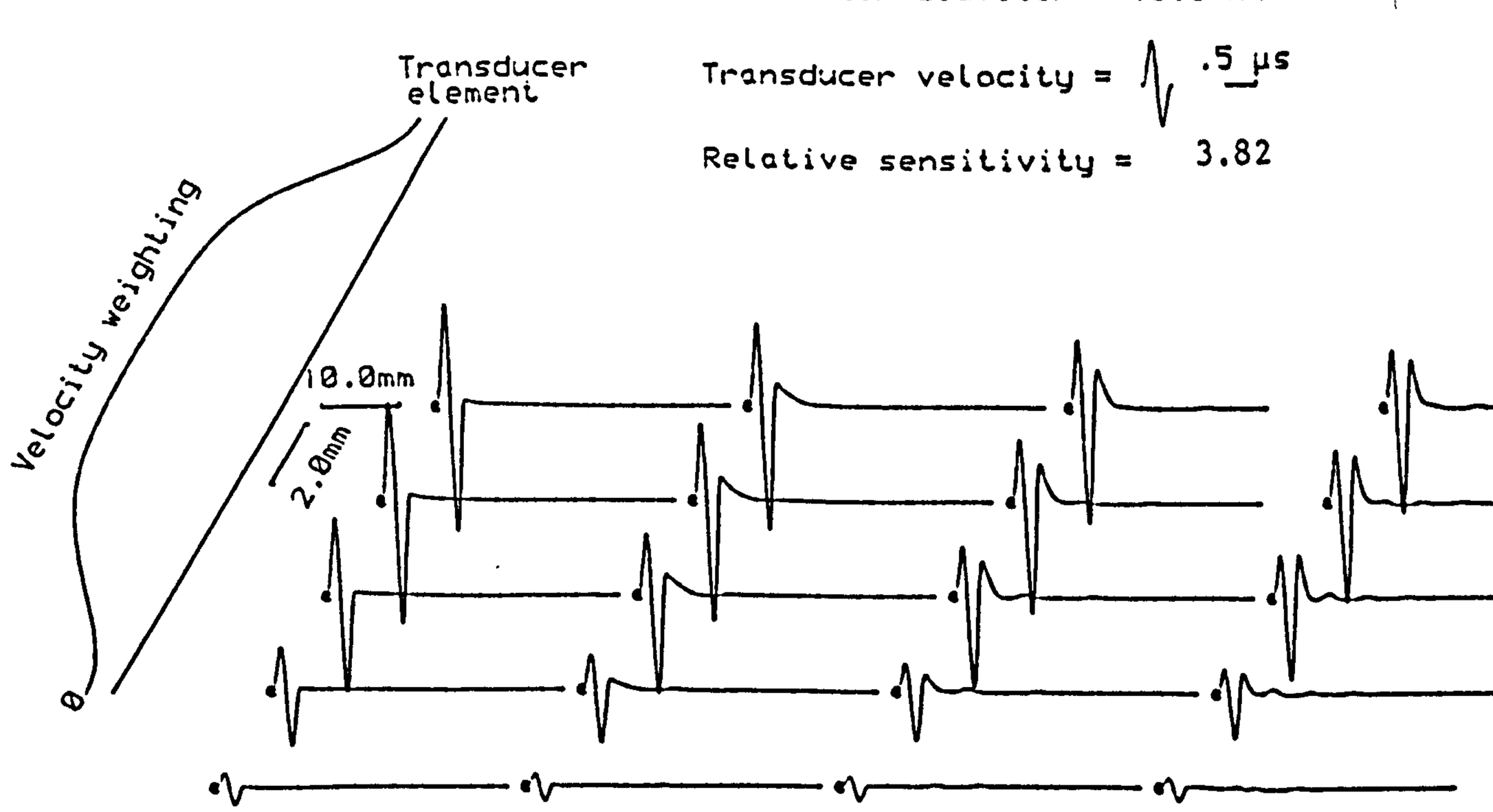

Fig 4.4.4 Computed transmit-receive mode responses of a circular PWO source interrogating a normally-aligned, 19mm diameter circular target in water.

Notice that as for a conventional source the reduction in peak-to-peak amplitude with increasing range is again due to beam spreading.

4.4.3. EWO source.

When using an EWO source to interrogate a 4 mm diameter target (Fig. 4.4.5) the echo response is similiar to that for a point target (Fig. 4.3.5), the major response being concentrated along the axis. However, with the larger 4 mm target the response with the target centered straight ahead of the rim is greater than for a point target.

When the target size reaches the dimensions of the source a marked change to a multi-pulse structure can be observed. The response now consists of a "straight-ahead" response, which arises from portions of the propagating wavefront that travels directly from the source rim to the target edge and back, and a high resolution pulse which travels the longer distance from the source rim to the central portions of the target and back. At ranges close to the source the high resolution pulse is small and well time separated from the initial "straight-ahead" response, but due to the directional nature of edge waves it increases as the target is moved further from the source. At ranges into the far field, the time delay between the two components decreases and they increasingly overlap to produce the effect of differentiation. It should be pointed out that the multi-pulse structure in the near field of an EWO source is only evident for targets of a similar or larger size than that of the source aperture.

Although the amplitude of the echo responses are not nearly as large as those from a conventional or PWO source, there is a smaller disparity in echo amplitudes from targets of differing size. This characteristic of the EWO source can in certain instances be desirable and is discusssed further in section 5.2

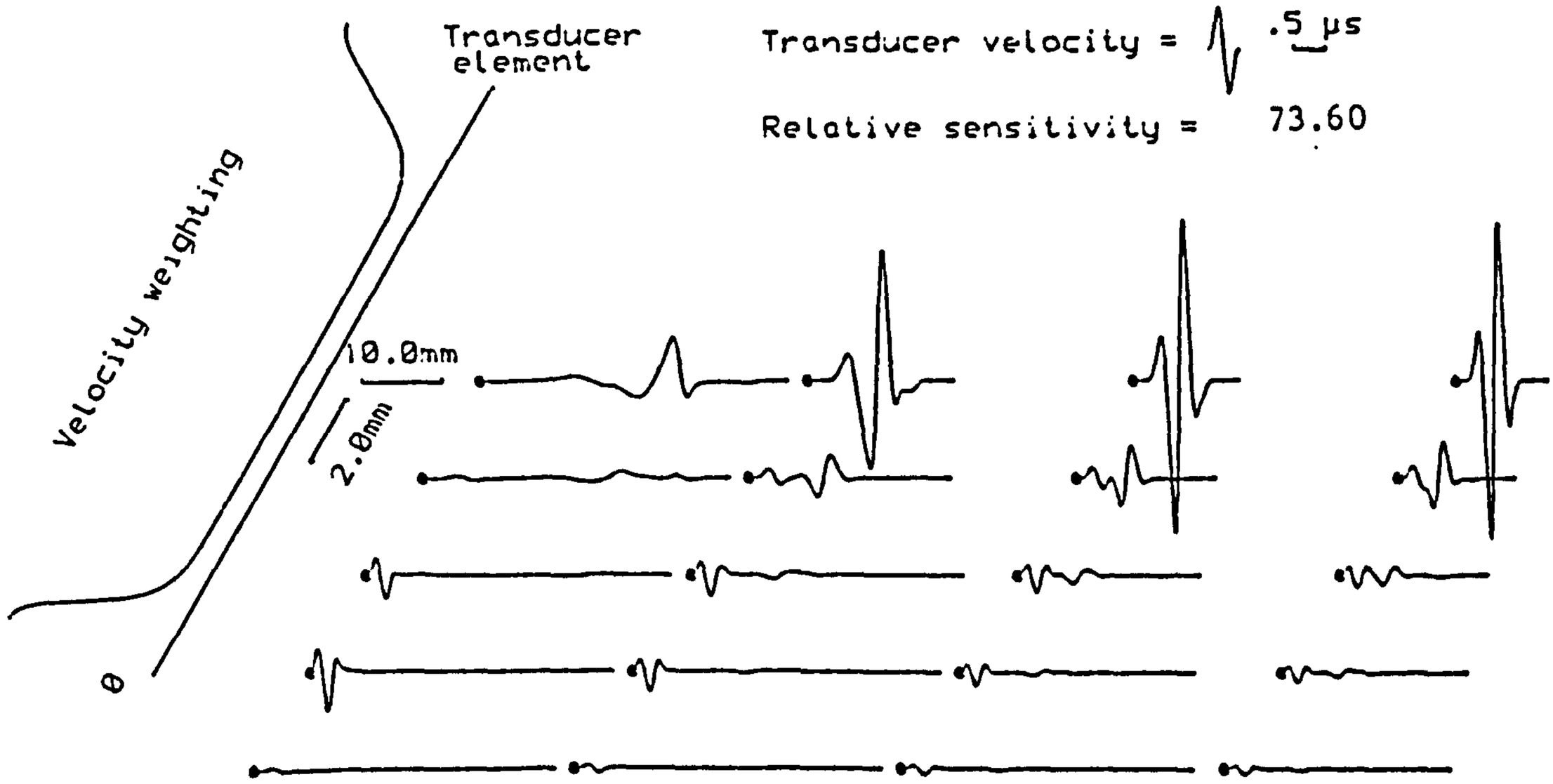

Fig 4.4.5 Computed transmit-receive mode responses of a circular EWO source interrogating a normally-aligned, 4mm diameter circular target in water.

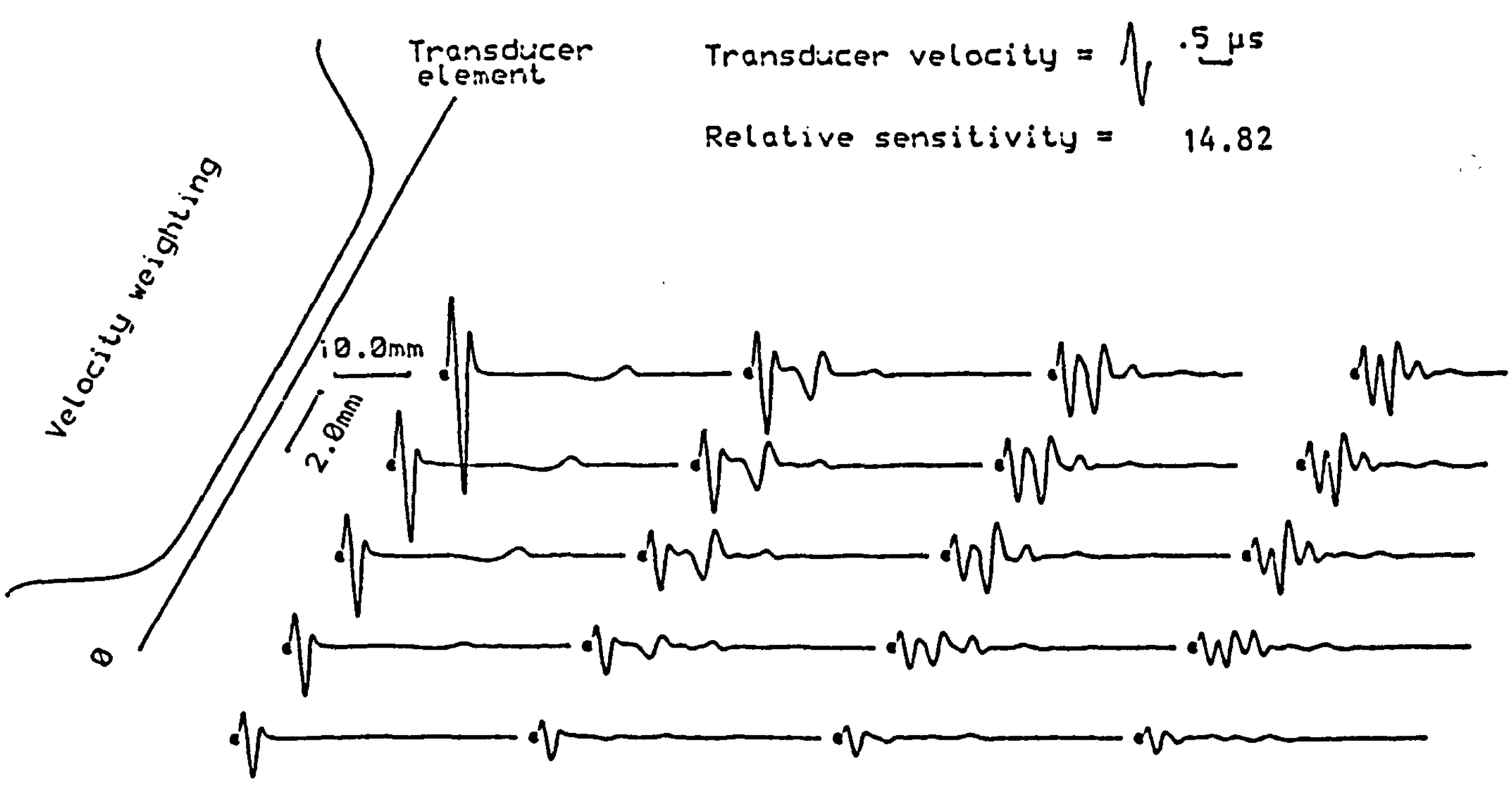

Fig 4.4.6 Computed transmit-receive mode responses of a circular EWO source interrogating a normally-aligned, 19mm diameter circular target in water.

4.5. Measured and calculated field point pressure measurements and transmit-receive mode responses from a small point-like target for a non-uniformly excited source radiating into water.

Detailed experimental measurements of pressure waveforms and transmit-receive mode responses from wideband, uniformly excited transducers have already been reported extensively elsewhere [6, 23-28] and will not therefore be repeated here. These results were shown to be in good agreement with the theory for a piston-like source except in a paraxial region less than three transducer radii from the transducer. Such discrepancies were shown to be caused by an extra ("head") wave which originates from a plate wave propagating laterally across the face of the transducer.

Presented below are experimental measurements for an EWO transducer which are compared with modelled results in order to confirm the accuracy of the extension to the impulse-response method (see section 2.5.2) used in calculating pressure waveforms and transmit-receive mode responses from non-uniformly excited sources.

4.5.1. Field point pressure waveforms.

Measurements of pressure waveforms from a 19 mm diameter prototype EWO transducer were made using a 0.2 mm diameter miniature probe. Figs. 4.5.1. and 4.5.2 show results at various ranges on axis and 2 mm off axis respectively.

In order to give a better comparison between the calculated and measured results it was necessary to determine the velocity weighting function (velocity amplitude distribution) of the transducer along with the velocity function time dependance. The velocity weighting function was obtained by scanning a miniature probe very close to the transducer face and recording the amplitude of the probe output against distance - it has been shown that such a plot is proportional to the spatial variation in the amplitude of the source velocity motion [63]. The actual weighting function of the prototype EWO transducer approximates to a Gaussian fall off, with a half maximum amplitude width of 0.5 mm. The theoretical velocity function of the source was chosen so that the predicted on-axis waveform at 140 mm matches the corresponding measured waveform. Since the shape of the pressure waveform at this range

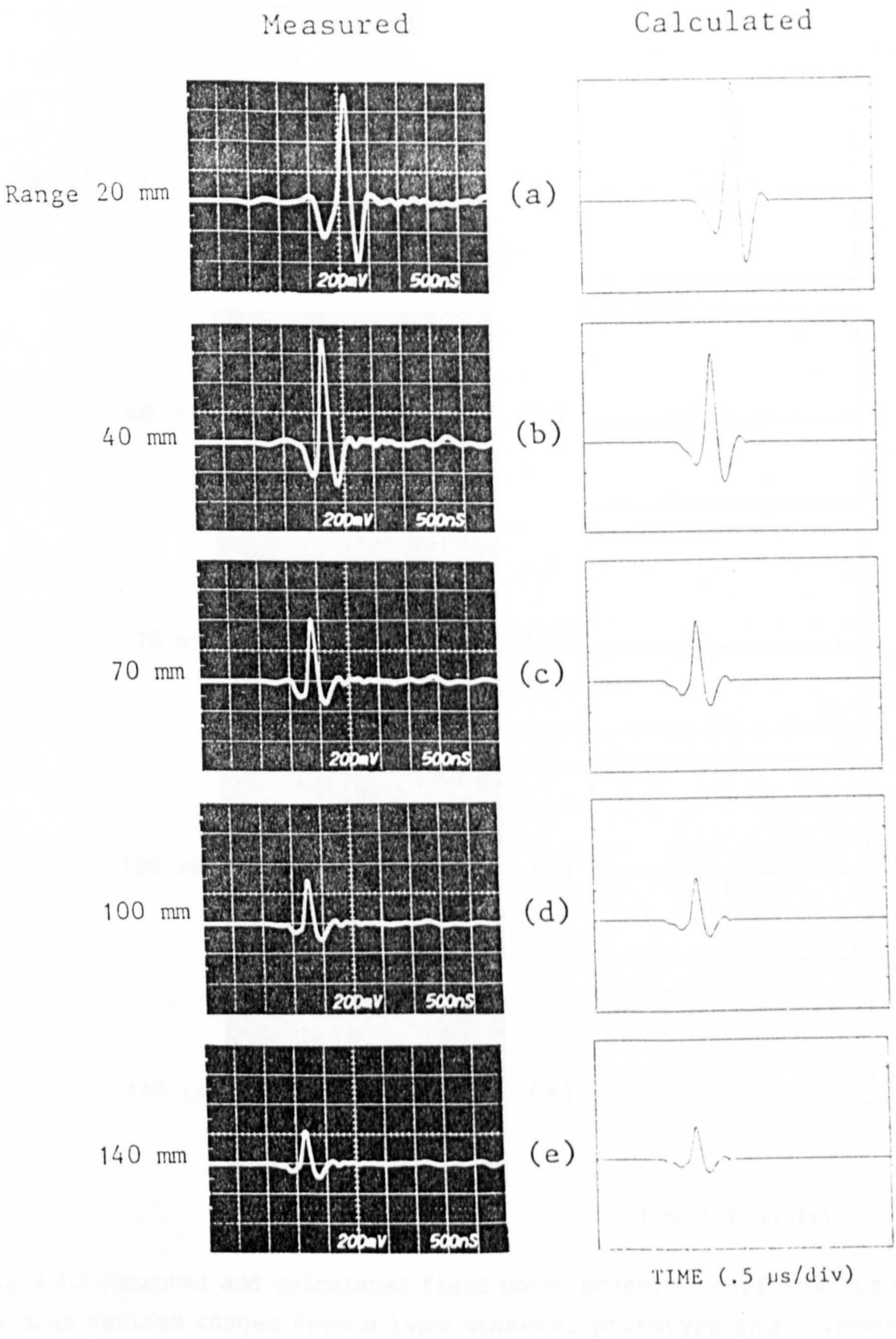

Fig 4.5.1 Measured and calculated field point pressure waveforms on axis, at various ranges from a 19mm diameter prototype EWO transducer radiating into water.

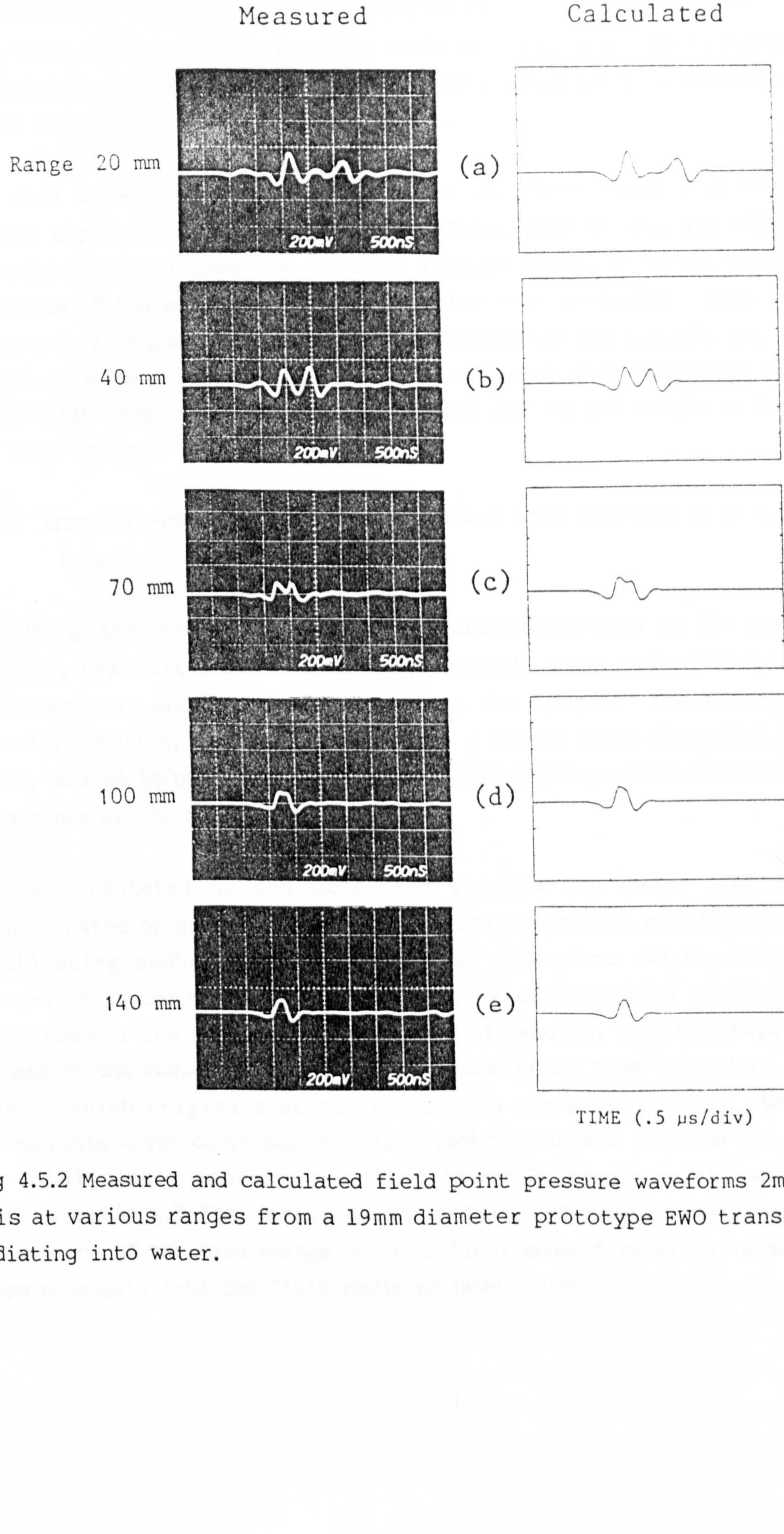

Fig 4.5.2 Measured and calculated field point pressure waveforms 2mm off axis at various ranges from a 19mm diameter prototype EWO transducer radiating into water.

corresponds to the first time differential of the source motion, the time dependance of the velocity function could be obtained by direct numerical integration. The velocity function used here consists of approximately a single cycle sinusoidal (1 MHz) pulse.

Good agreement between measured and calculated results is obtained for the amplitude and shape of the waveforms both on axis and off axis. The only deviation from the modelled results occurs at 40 mm where the amplitude of the measured result is greater than predicted. This slight discrepancy is due to the non-ideal behaviour of the transducer. This effect is more evident in the transmit-receive mode responses from a point target and therefore a fuller description of its origin is left to the next section.

4.5.2 Transmit-receive mode responses and beam profiles from a point target.

Using the same prototype EWO transducer described in the previous section, transmit-receive mode measurements were made with a 0.8 mm diameter flat-ended brass cylinder as the target. The theoretical velocity function, which approximates to a single cycle sinusoidal (3MHz) pulse, was as before chosen so that calculated and measured results match at a range of 140 mm.

As predicted by the modelling results the major response is concentrated on axis (Fig. 4.5.3) with the response 2 mm off axis (Fig. 4.5.4) being much reduced in amplitude. Close to the transducer at ranges of 30 and 50 mm there is poor agreement between the shape and amplitude of the measured and calculated results. This discrepancy is caused by the radiation of head waves which arise from vibrations (plate waves) which originate at the source rim and travel across its face. These plate waves occur because piezoelectric ceramic discs do not behave as ideal piston sources. As implied by Poisson's ratio, which is approximatly 0.3 for ceramics, the lateral as well as the thickness dimensions of the disc change on excitation, generating plate waves which then propagate into the fluid media as head waves.

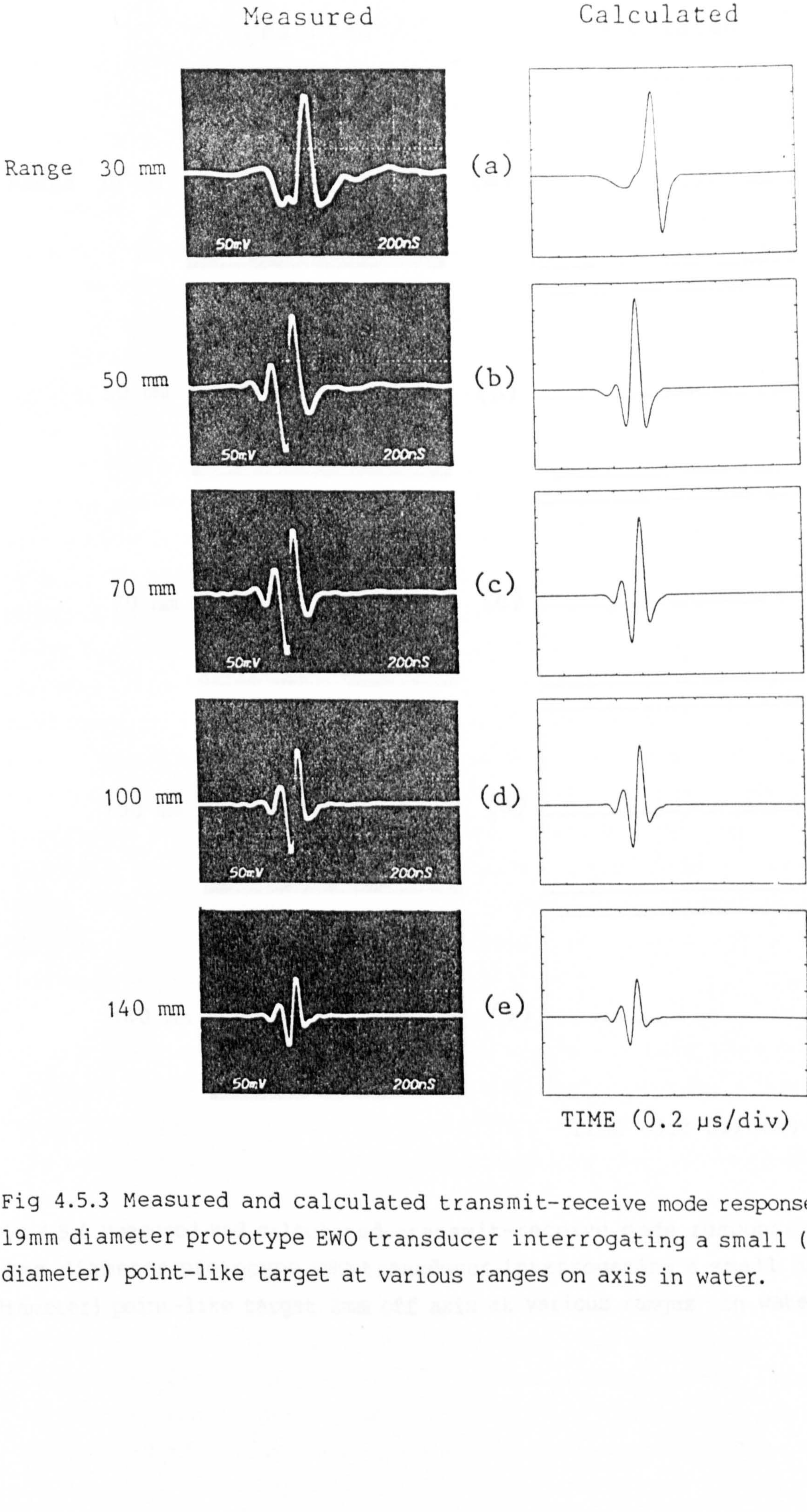

Fig 4.5.3 Measured and calculated transmit-receive mode responses of a 19mm diameter prototype EWO transducer interrogating a small (0.8 mm diameter) point-like target at various ranges on axis in water.

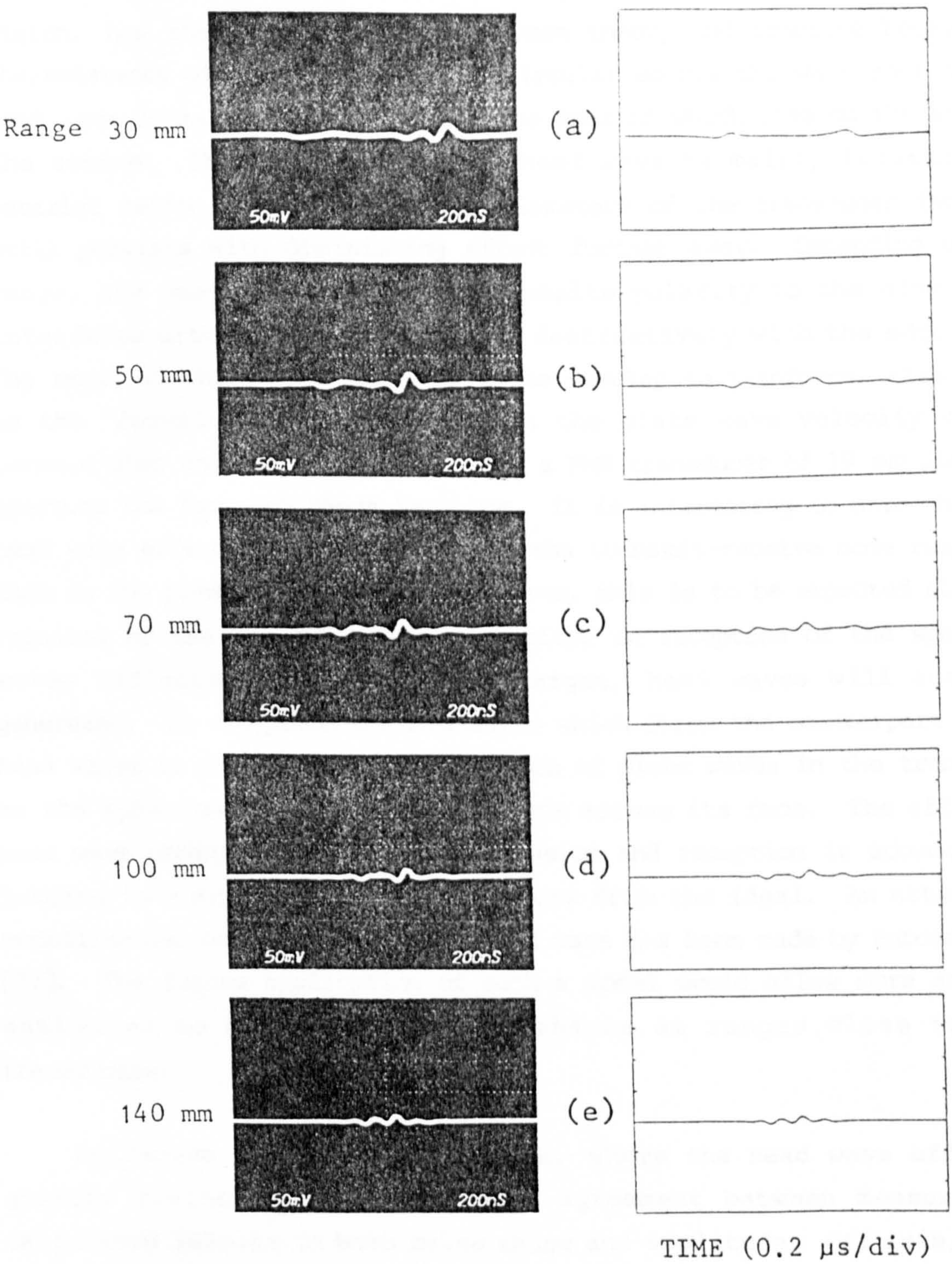

Fig 4.5.4 Measured and calculated transmit-receive mode responses of a 19mm diameter prototype EWO transducer interrogating a small (0.8 mm diameter) point-like target 2mm off axis at various ranges in water.

Previous work [6, 25, 27], associated with the experimental verification of the transient fields predicted by assuming an ideal piston, has shown discrepancies between theory and practice because of the existence of head waves. For a circular source the wavefront of the head wave forms a conical surface, the apex of which lies on the axis of the source. The influence of the head wave is mainly limited to a paraxial region within one to two diameters of the transducer face but still persists with diminishing effect further away. Depending on the range, the head wave (which has opposite polarity to the edge wave) interferes either constructively or destructively with the edge wave. The range at which head and edge waves overlap to reinforce, also known as the "focusing range", depends on the plate wave velocity of the ceramic disc and its dimensions. For a PMN transducer of 19 mm diameter aperture the focusing range is 26 mm. It is interesting to note that the head wave effect is more dramatic in the transmit-receive mode responses than in the pressure waveforms. However, this is to be expected since as required by the principle of reciprocity, on reception of the spherical waves reflected by a point-like target, head waves will again be generated. In reception the mechanism which forms the counterpart of the head waves is presumably the excitation of plate waves in the transducer as the spherical incident wave sweeps across its face. The effect of head wave production on both transmission and reception is accumulative leading to a more noticeable departure from the ideal. An attempt at modelling the contribution of the head wave has been made by Baboux et al [77]. The future application of such a model would allow more accurate estimates to be made of pulse shapes at ranges close to real transducers.

At ranges of 70,100 and 140 mm, where the head wave effect is greatly diminished, there is good agreement between measured and calculated results in both pulse shape and amplitude. Off axis, where the head wave effect is again minimal, there is also good agreement with theory at all ranges.

Transverse transmit-receive mode beam plots were made in the usual way by recording the detected output voltage waveforms from a prototype EWO transducer interrogating a small target (0.8 mm diameter flat-ended brass cylinder) as the Y co-ordinate on an XY plotter, while the X coordinate denotes the lateral position of the target. The amplitude of the pulsed waveforms was detected with a Metrotek MD702 gated peak

detector using full-wave detection which gave a dynamic range of 40 dB. Shown in Fig. 4.5.5 are the transmit-receive mode beam profiles for an EWO tranducer interrogating a point target. Beam plots from a range of 30 mm to 170 mm are given at intervals of 20 mm.

There is reasonable agreement between measured and calculated results at all ranges and demonstrates the excellent lateral resolving power of EWO transducers. At a range of 30 mm it is just possible to observe the response straight ahead of the rim. At a range of 50 mm this response is much reduced in size and further away still is less than the minimum detectable signal.

The consequences of all the results presented in this section in relation to high-resolution pulse-echo testing is discussed at length in chapter 5.

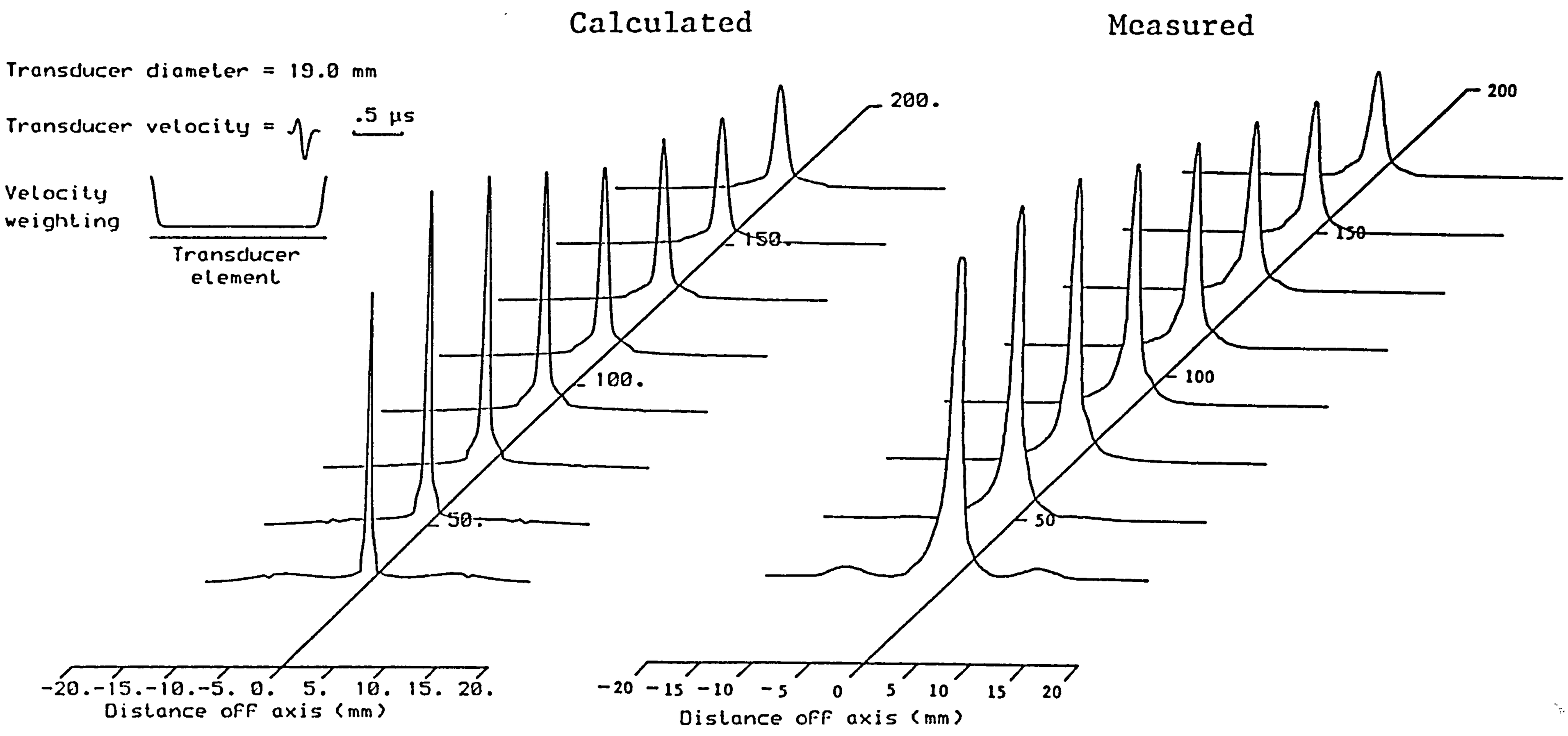

Fig 4.5.5 Measured and calculated transmit-receive mode beam plots at various ranges from a prototype EWO transducer interrogating a small (0.8 mm diameter) point-like target in water.

4.6 Measured and calculated transmit-receive mode responses from solid, finite-sized targets in water for a uniformly excited transducer.

All experimental measurements reported in this section were made using a conventional 19 mm diameter PMN transducer and include transmit-receive mode responses from targets of various size, material properties and shape. These measurements are compared with theoretical predictions calculated using the finite-sized target model described in section 2.6 in order to evaluate the usefulness and accuracy of the model. Some of the general observations and ideas gained from these results are also useful in obtaining an understanding of the way in which the ultrasound from a non-uniformly excited transducer interacts with targets of various dimensions and material properties. Furthermore, the uniformly excited transducer employed here is representative of the best quality wideband conventional transducers currently available and as such provides a good reference with which to compare the performance of the non-uniformly excited transducers. In section 4.7 similar sets of experimental results are reported for a practical prototype version of an EWO transducer.

4.6.1 Echo responses from circular metal targets.

Figs. 4.6.1 and 4.6.2 show measured and calculated transmit-receive mode waveforms at a range of 30 mm for a series of cylindrical brass targets of increasing diameter, the flat circular ends of which are normally aligned to the transducer axis. Targets made from brass were used so as demonstrate the accuracy of the finite-sized target model (section 2.6) in predicting echo responses from strongly reflecting targets. In order to give a better comparison between calculated and measured echo waveforms, the shape of the theoretical source velocity function has been chosen to match the shape of the measured time-separated plane wave from an axial 0.8 mm diameter target. The amplitudes of the calculated echo waveforms have been scaled so that the amplitude of the first received pulse matches the amplitude of the corresponding pulse in the measured waveform. The emitted plane-wave pulse has a simple shape approximating to a single cycle sinusoid (2MHz). The theoretical waveforms have been obtained by convolving this pulse with the appropriate impulse response which has also been included for completeness. The relative sensitivities in the experimental results are given by the scale factors in decibels (dB) in the left hand corners of the figures. Note that the scale factor is an attenuation setting.

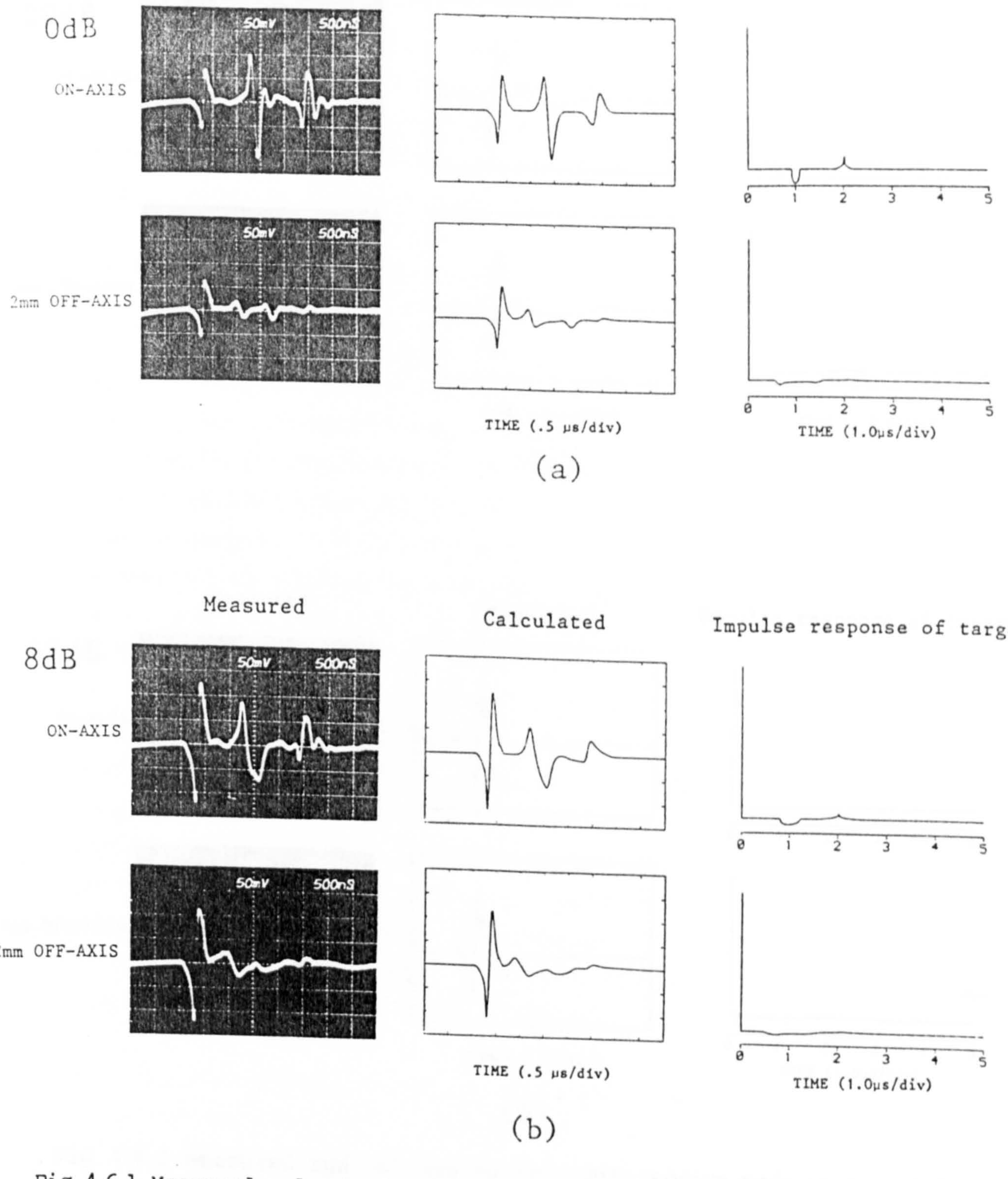

Fig 4.6.1 Measured and calculated transmit-receive mode responses from (a) a 0.8mm diameter, and (b) a 2mm diameter normally-aligned, flat-ended cylindrical brass target at a range of 30mm in water, both on and 2mm off the axis of a 19mm diameter conventional PMN transducer. The corresponding impulsive transmit-receive mode responses are also included.

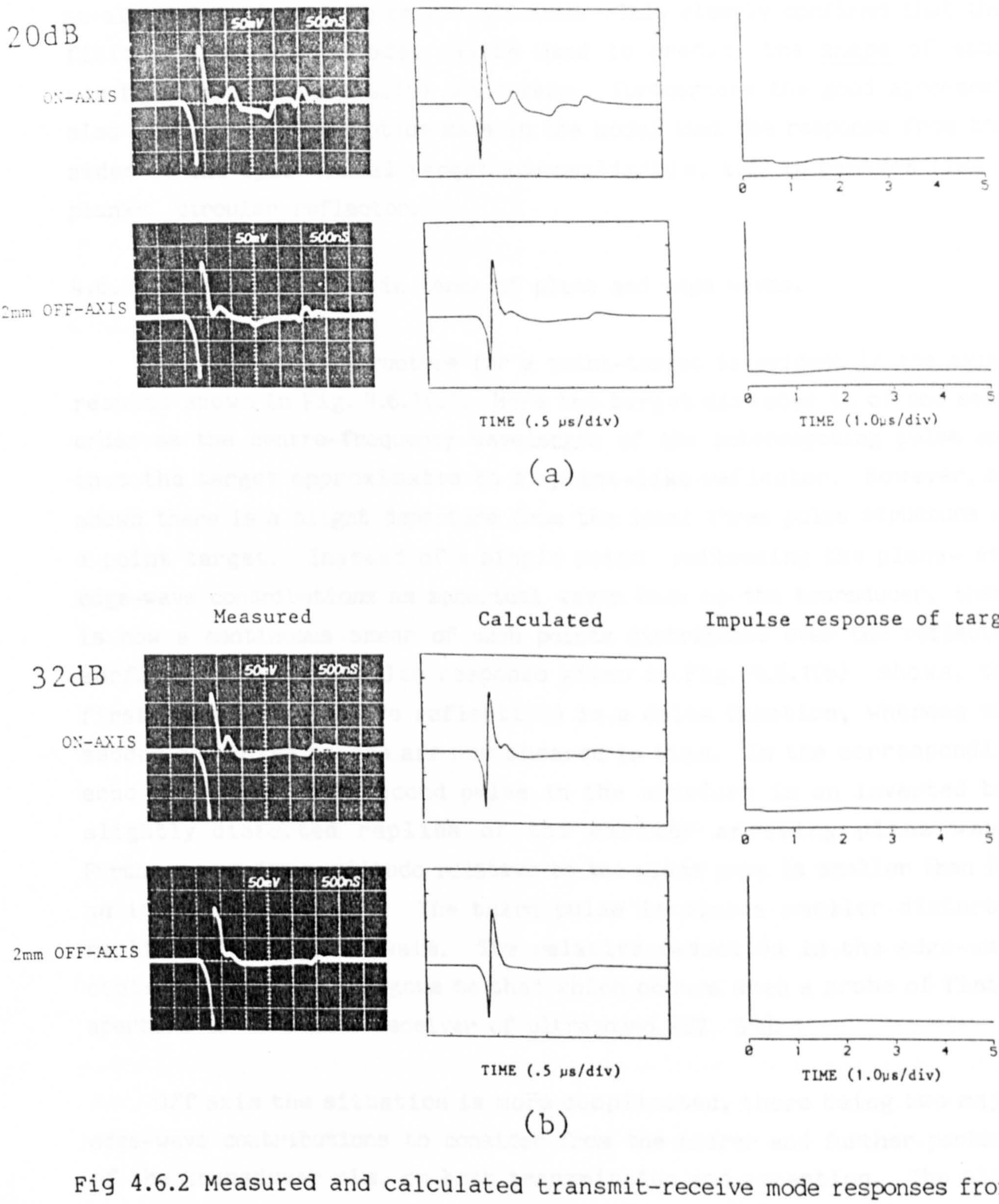

Fig 4.6.2 Measured and calculated transmit-receive mode responses from (a) a 4mm diameter, and (b) an 8mm diameter normally-aligned, flat-ended cylindrical brass target at a range of 30mm in water, both on and 2mm off the axis of a 19mm diameter conventional PMN transducer. The corresponding impulsive transmit-receive mode responses are also included.

The agreement between experiment and theory is found to be excellent at all target sizes both on and off axis. This clearly confirms that the finite-sized target model can be used to predict the shape of echo waveforms from strong solid scatterers. Furthermore the good agreement also confirms the assumption made in the model that the response from the sides of the cylindrical target are negligible, i.e. it behaves like a planar, circular reflector.

4.6.1.1 Echo responses in terms of plane and edge waves.

The three pulse structure for a point-target is evident in the axial results shown in Fig. 4.6.1(a). Here the target diameter is of the same order as the centre-frequency wavelength of the interrogating pulse and thus the target approximates to a point-like reflector. However, as shown there is a slight departure from the ideal three pulse structure of a point target. Instead of a single point reflecting the plane- and edge-wave contributions as spherical waves back to the transducer, there is now a continuous smear of such points distributed over the reflector surface. As the impulse response given in Fig. 4.6.1(b) shows, the first pulse (plane-wave reflection) is a delta function, whereas the second and third pulses are now smeared in time. In the corresponding echo responses, the second pulse in the waveform is an inverted but slightly distorted replica of the earlier arriving plane wave. Furthermore, its amplitude relative to the plane wave is smaller than for an ideal point target. The third pulse is also a smaller distorted replica of the plane wave. The relative reduction in the edge-wave contributions is analagous to that which occurs when a probe of finite aperture is used as a receiver of ultrasound [27, 54].

Off axis the situation is more complicated, there being two major edge-wave contributions to consider from the nearer and further portions of the transducer rim, on both transmission and reception. The plane wave remains the same, but the second and third pulses have split producing the more complicated response consisting of several pulses of smaller amplitude trailing the initial plane-wave pulse.

For a larger axial target of 2 mm diameter (Fig. 4.6.1(b)), it is

still possible to identify a three pulse structure, both in the experimental and calculated results. The plane wave, although retaining the same shape as in Fig. 4.6.1(a), is now larger in amplitude; the increase is approximately proportional to the ratio of target areas. Relative to the plane wave, the second and third pulses are now even smaller and more smeared out in time. Again, the smearing of the edge-wave components is clearly shown in the on-axis impulse response included in Fig. 4.6.1(b). Off axis the response is again complicated, consisting of a number of edge-wave components of smaller amplitude trailing behind the directly transmitted plane wave which retains the same shape and amplitude as on axis.

The responses from a 4 mm diameter target are given in Fig. 4.6.2(a). On axis the response consists of a relatively large, almost specular reflection of the plane wave followed by edge-wave contributions which have been smeared out over the area of the target. A distinct three pulse structure is no longer visible, the second pulse appearing to have split into two separate pulses of opposite polarity. A following fourth pulse is still visible. The edge-wave components are even further reduced in amplitude relative to the plane wave. Off axis the response consists essentially of just the plane wave, the edge-wave components having been almost totally smeared out.

The 8 mm diameter target, being ten wavelengths wide at the centre frequency of the excitation pulse, results in an essentially specular reflection of the direct plane wave as illustrated in Fig. 4.6.2(b). In the on-axis result the edge-wave contributions are now quite small. Note however that for even this relatively large target, the edge-wave contributions would still be of sufficient amplitude to give rise to significant modulation in the spectrum of the echo response. Such modulation could easily be mistaken as being due to target features rather than an effect of diffraction. Off axis, the edge wave components are hardly visible at this sensitivity.

4.6.1.2 Variation of echo response with target range.

The way in which the axial response from a 4 mm diameter, flat-ended, cylindrical brass target varies with range is illustrated in Fig. 4.6.3. The theoretical source velocity motion has been chosen to match the measured plane-wave pulse at 30 mm range (Fig. 4.6.1 (a)) and all

Measured

Calculated

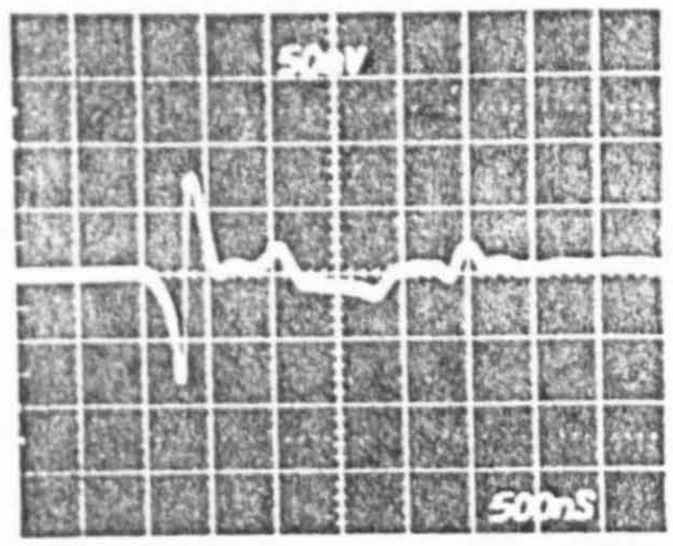

(a)

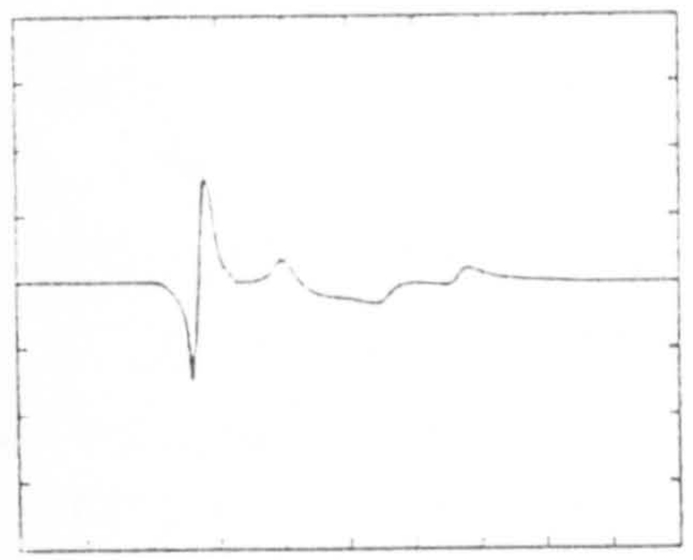

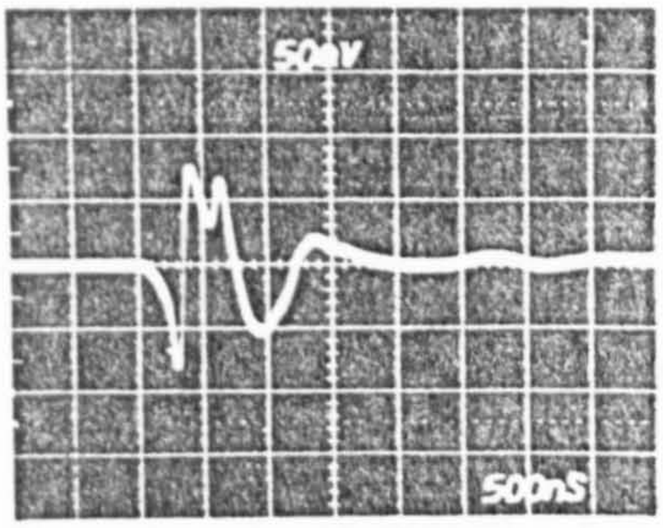

(b)

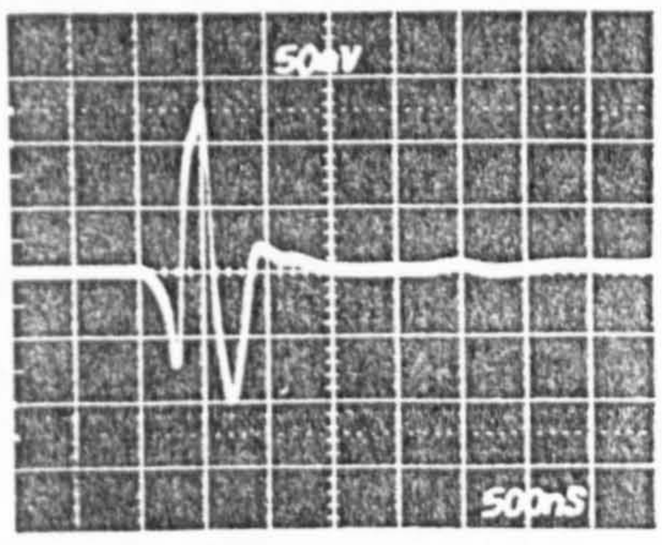

(c)

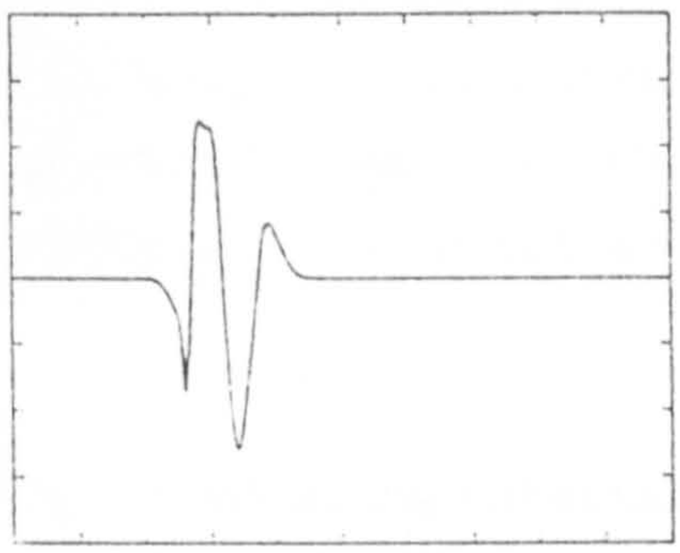

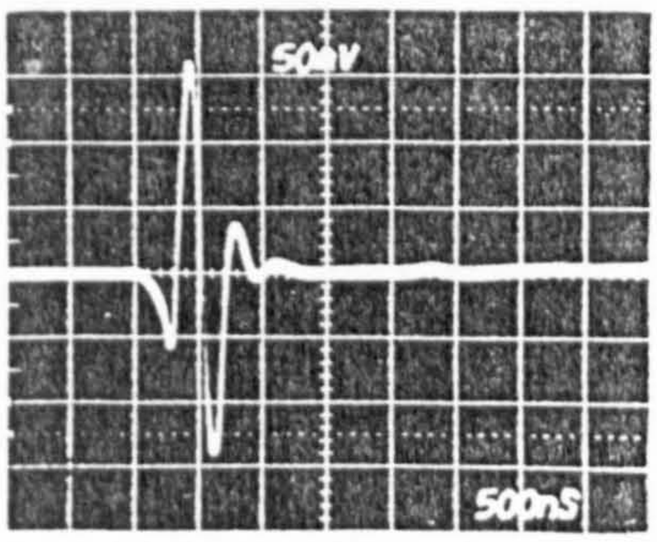

(d)

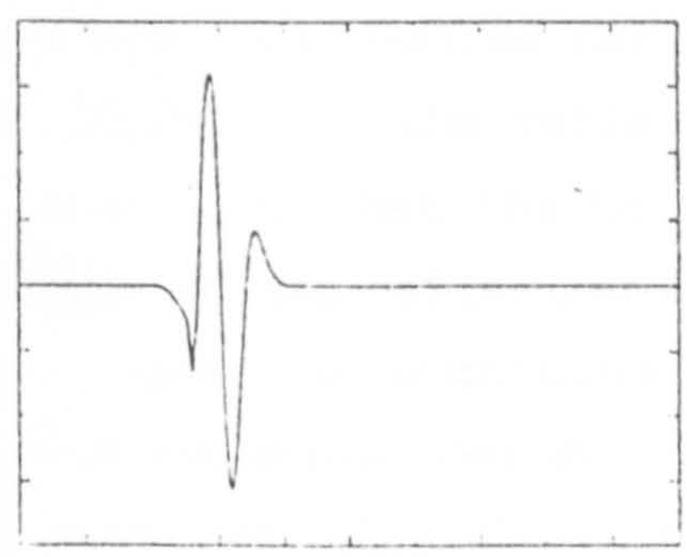

TIME (.5 μs/div)

Fig 4.6.3 Measured and calculated transmit-receive mode responses for an axial, 4mm diameter flat-ended cylindrical target at a range of (a) 30mm, (b) 70mm, (c) 120mm and (d) 180mm in water, using a 19mm diameter conventional PMN transducer.

subsequent results are plotted to the same scale. Close to the transducer at a range of 30 mm (Fig. 4.6.3 (a)), the echo response is the same as that described in Fig. 4.6.2.(a), the multi-pulse structure due to diffraction effects being clearly evident. At a larger range the time separation between the plane- and diffracted edge-wave contributions becomes smaller causing them to overlap as can be seen in Fig. 4.6.3(c). At an even greater range (180 mm, Fig. 4.6.3(d)), the pulses overlap to produce the effect of a double differentiation. As described previously the pressure incident on the target resembles the differential of the plane-wave pulse and another differentiation takes place on reception of the echo. Thus for this target size and range, the echo received has a similar form to the second time differential of the plane-wave, an effect that can be observed in both the theoretical and experimental results.

Note that in all the measured results presented so far there is no evidence of any significant contribution due to the existence of head waves. Since such contributions are only of appreciable size in a paraxial region close to the transducer, their affect taken over the surface of a target of finite dimensions is comparatively small and can be ignored.

4.6.2 Echo responses from circular targets of differing materials.

Implicit in the original derivation of the finite-sized target model (section 2.6) is the requirement that the strength of the reflected wave be much less than that of the incident wave, i.e. that the target be a weak scatterer of ultrasound. The strength of the reflected wave is a function of both its overall dimensions and the magnitude of its acoustic impedance relative to that of the propagating medium. However, as predicted in section 2.6 and confirmed experimentally above, the model can accurately predict the shape of the echo waveform from strongly scattering targets. In order to investigate the affect of different target materials on both the shape and relative amplitude of echo responses, flat-ended, cylindrical targets of various size were machined from Teflon, Perspex (both relatively weak reflecting media with reflection coefficients in water of 0.34 and 0.37 respectively and brass (a strongly reflecting medium with a reflection coefficient of 0.92 in water).

Fig. 4.6.4 shows echo responses from Teflon (on the left) and

brass (right) targets on axis at a range of 30 mm. The corresponding results for targets lying 2 mm off axis are given in Fig. 4.6.5. Excitation and reception conditions are identical in all measurements except for the overall sensitivity which as before is given by the scale factors in the left hand corner of each Figure. Note that the scale factor is an attenuation setting, i.e. the brass signals are larger than the corresponding Teflon ones. Notice that the waveforms from brass and Teflon versions of a particular target size possess an identical shape and structure (but are of course of differing overall amplitude). This is found to be the case for all target sizes, both on and off axis. Even for the largest brass target of 8 mm diameter there is little discernable difference in waveform structure when compared with the weaker scattering target made from Teflon. Since, as explained here, the interrogating waves have a plane- and edge-wave structure, the fact that echo pulse shapes do not vary with target material may at first sight be considered somewhat surprising. Even for normally-aligned targets the incident edge waves will undergo mode conversion at the target surface by an amount which will differ from material to material. Hence it might be anticipated that the angular dependence of the amplitudes of the reflected edge waves will also vary from material to material. However, in practice such variations in the edge-wave components of the reflected waves do not markedly affect the overall echo pulse shape arising from targets of differing materials. This last observation is consistent with the good agreement found between measured results and calculated results obtained using an approach which does not take account of mode conversion at the target surface.

Figs. 4.6.4 and 4.6.5 clearly show that the acoustic properties of a target of given geometry do not affect the shape of the echo waveform, a result which is in agreement with theory. The material properties of the target do however affect the echo amplitude. As previously discussed in section 2.4, there are three proposed methods by which the value of the ratio of echo amplitudes from targets of different acoustic properties but identical size may be calculated. Theory also predicts that this ratio is independent of target size and field position.

In order to confirm these predictions and to assess the accuracy with which the different methods can estimate waveform amplitude ratios, experimental measurements of echo amplitudes have been made using Teflon, brass and Perspex targets of various size. Table 1 shows three sets of

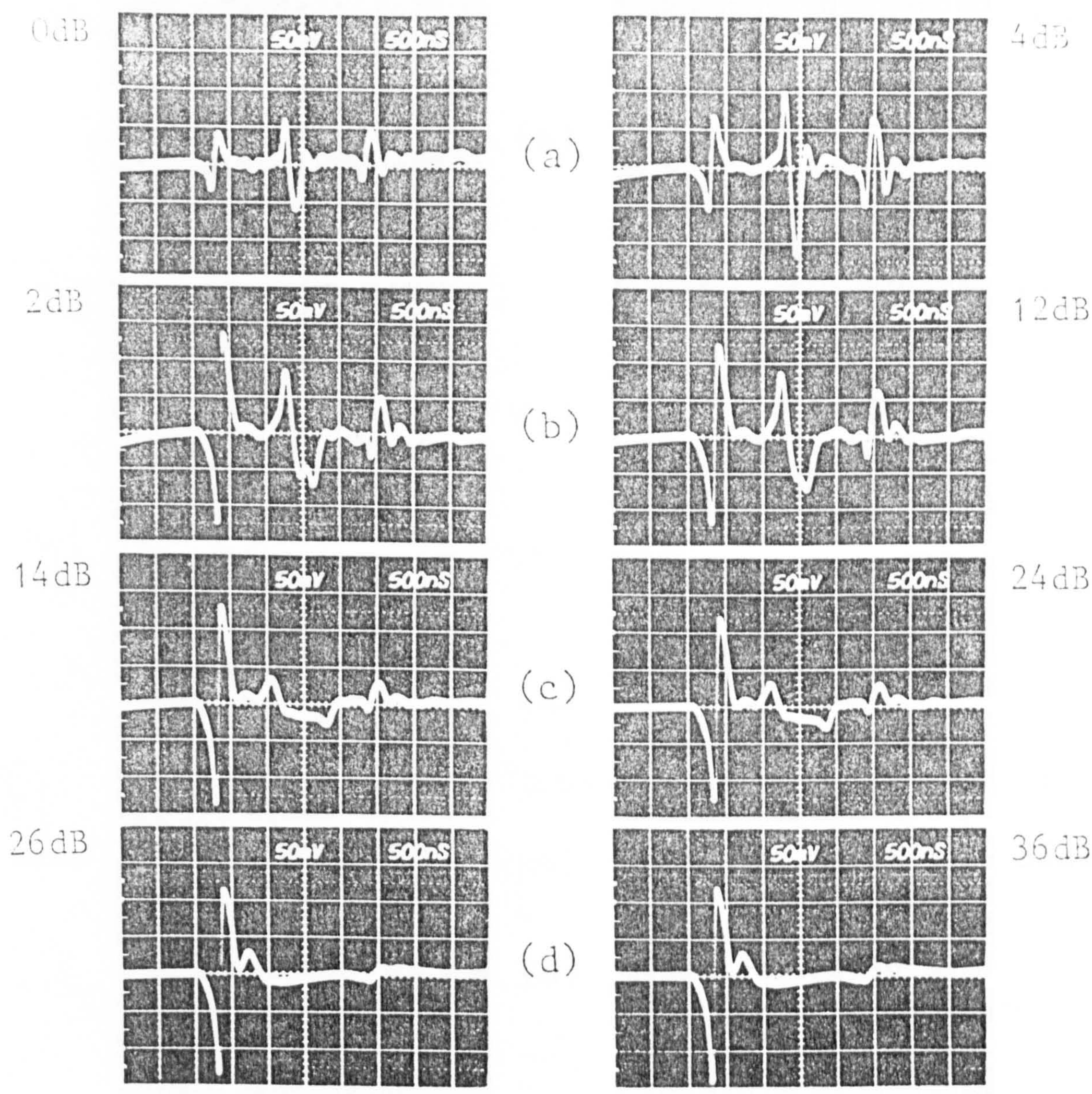

Fig 4.6.4 Measured transmit-receive mode responses from four pairs of axial, flat-ended, cylindrical targets with diameters of (a) 0.8mm, (b) 2mm, (c) 4mm and (d) 8mm. Each pair consists of a Teflon and a brass target of identical geometry. These results were obtained using a 19mm diameter conventional PMN transducer at a range of 30mm in water.

Teflon

Brass

0dB

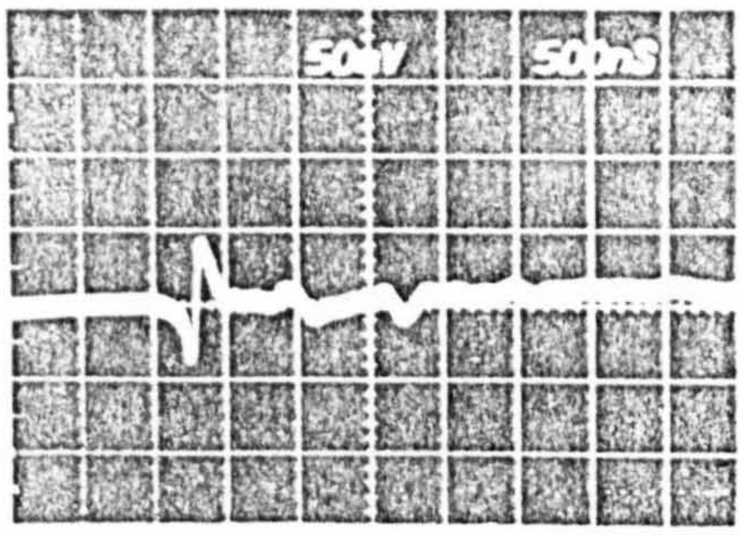

(a)

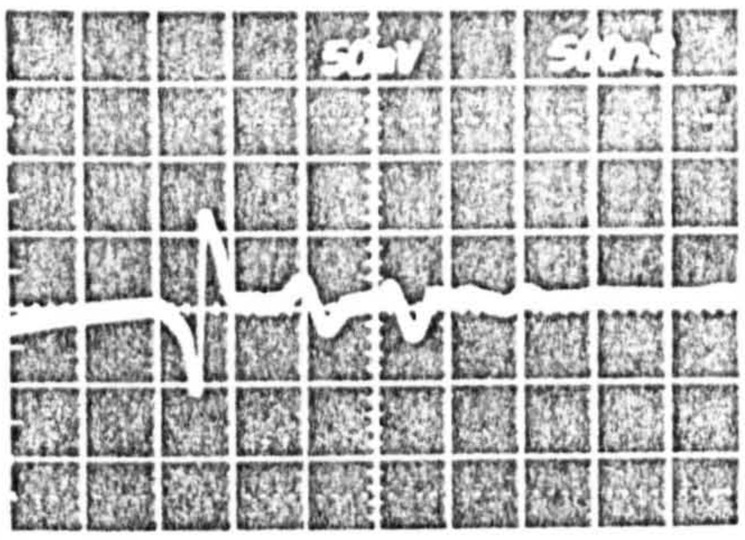

4dB

2dB

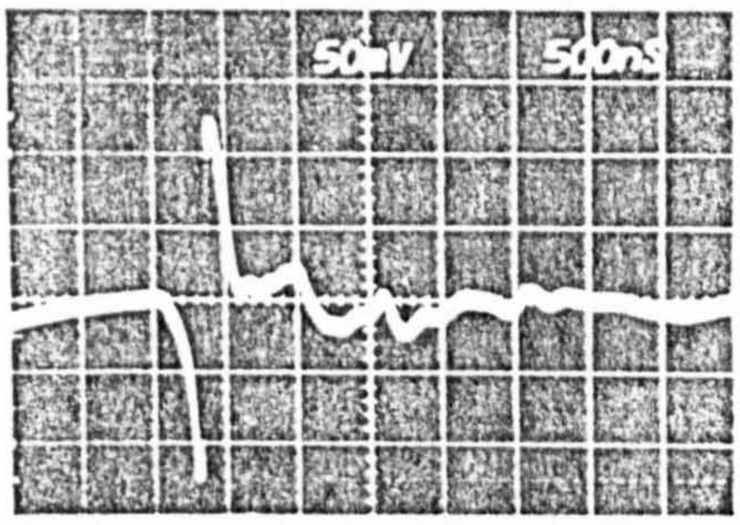

(b)

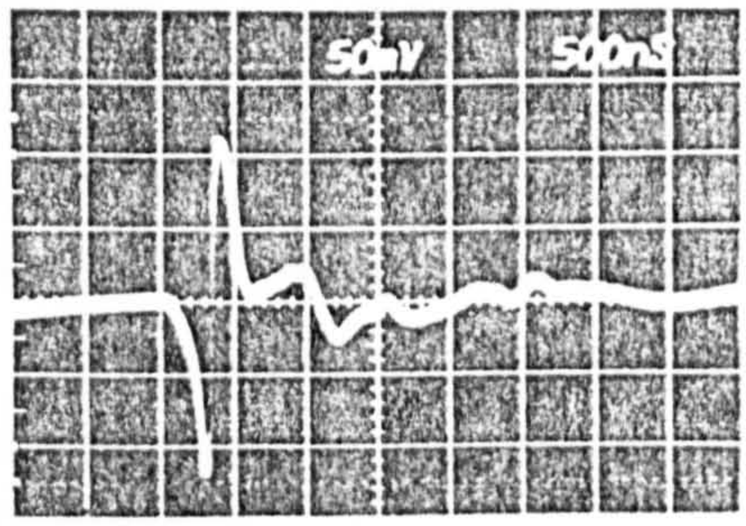

12dB

14dB

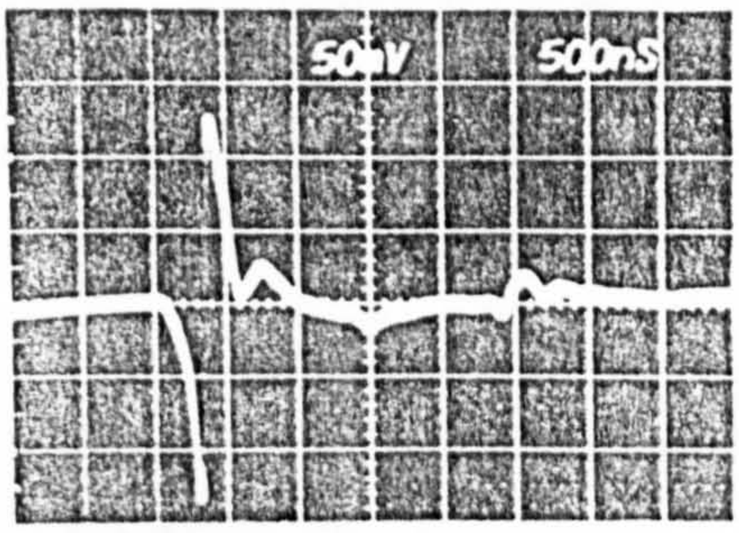

(c)

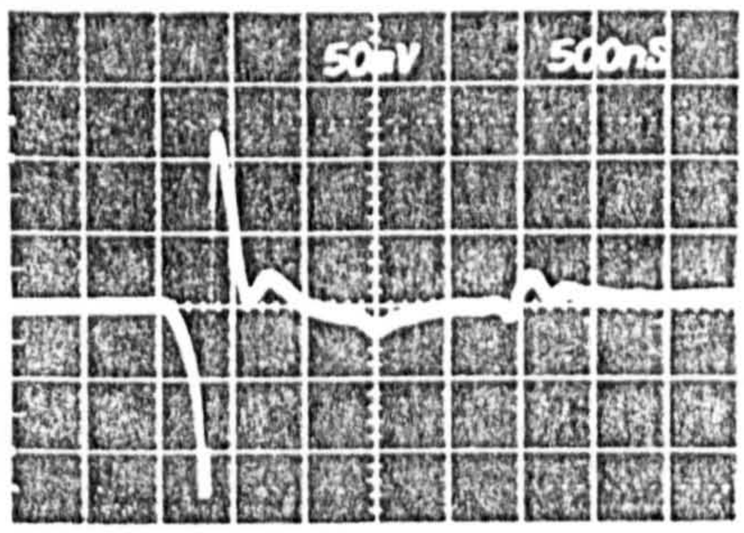

24dB

26dB

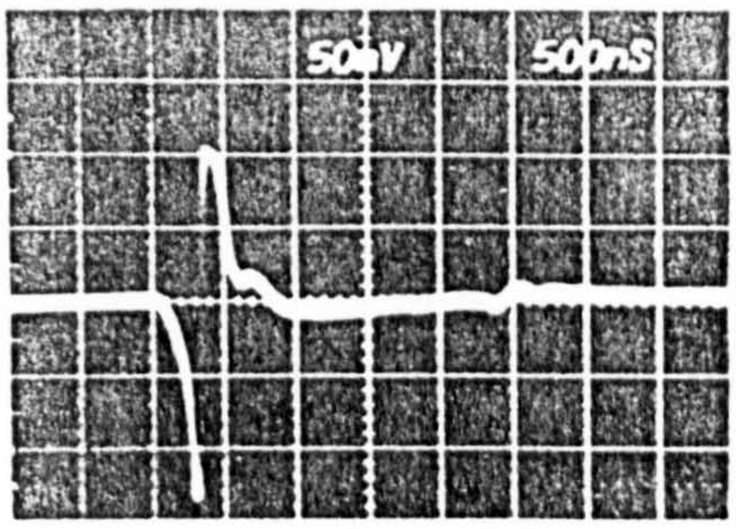

(d)

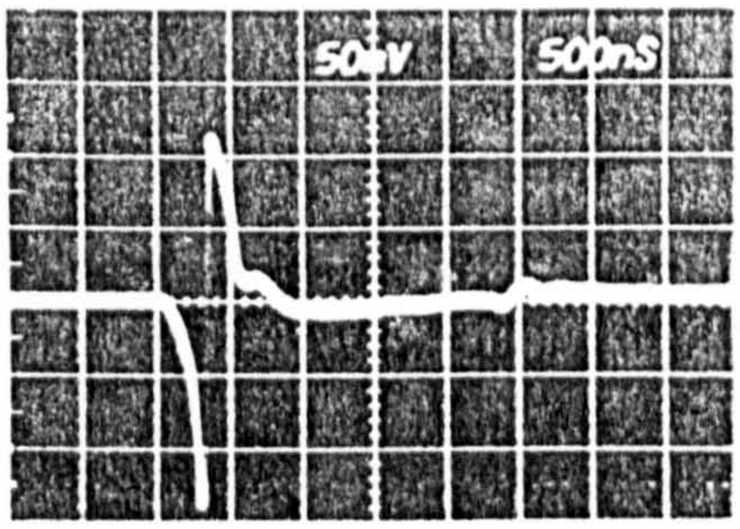

36dB

Fig 4.6.5 Measured transmit-receive mode responses as shown in Fig 4.6.4 but with all targets 2mm off axis.

measured and calculated ratios for various target combinations i.e. brass/Teflon, brass/Perspex and Perspex/Teflon. The measured results were obtained using flat-ended, cylindrical targets machined from these materials in four different sizes.

All measurements were carried out several times in order to obtain an average value. In each case the target was placed on axis at a range of 30 mm and the peak-to-peak amplitude of the waveform measured. Almost identical results were obtained when all the measurements were carried out on axis at a range of 140 mm. This agrees with the theoretical prediction mentioned above that echo amplitude ratios are independent of target position. Also confirmed by the measured results in Table 1 is the fact that echo amplitude ratios are independent of target size. The small variations in the measured results can be attributed to experimental errors, which are discussed below.

Table 1. Calculated and measured ratios of echo pulse amplitudes for brass, Teflon and Perspex targets.

Target diameter (mm)	Target materials	Calculated ratios			Measured ratios
		Ueda & Ichikawa [72]	Stacey [73]	Reflection coefficient	
1	Brass/Teflon	8.63	3.71	2.75	2.96
2		8.63	3.71	2.75	3.05
4		8.63	3.71	2.75	2.96
8		8.63	3.71	2.75	3.14
1	Brass/Perspex	9.11	4.89	2.47	2.25
2		9.11	4.89	2.47	2.37
4		9.11	4.89	2.47	2.39
8		9.11	4.89	2.47	2.64
1	Perspex/Teflon	0.95	0.76	1.11	1.31
2		0.95	0.76	1.11	1.29
4		0.95	0.76	1.11	1.24
8		0.95	0.76	1.11	1.19

In comparison with the measured results, the ratios predicted using weak scattering assumptions [72] (eq.(21)) are quite inaccurate. This is especially true when one of the targets is made from the strong scattering medium brass,and in this case the improved method of Stacey [73] (eqs. (22) and (23)) gives better accuracy. However, as shown by the set of results for Perspex/Teflon, when both targets are made from weaker scattering media, the inaccuracy incurred by using eq. (21) is not so large. The most consistently accurate estimates of the echo amplitude ratios are clearly seen to be provided by the empirical use of the reflection coefficients for normally-incident plane waves, which in all cases agree with the measured results within the limits of experimental error. These include uncertainties in amplification factors, errors in reading waveform amplitudes, variations in the nominal target dimensions, irregularities in target flatness, transducer misalignments and variations in the uniformity of target properties such as density and velocity (a polymer compound such as Teflon for example can exhibit large variations in density and acoustic velocity [78]). The total estimated error due to these uncertainties is $\pm$ 15%. Also note that uncertainties in the exact values of the various material densities and velocities (estimated at $\pm$ 5%) result in errors in the calculated values of the various echo amplitude ratios shown in Table 1.

4.6.3 Variation of echo amplitude with target size.

Fig. 4.6.6 shows theoretical and experimentally-measured relative echo amplitudes versus target area for various sizes of normally-aligned, axial, circular reflectors in water. The measured results were obtained at two ranges (30 mm and 120 mm) in the field of a 9.5 mm radius transducer using a number of flat-ended, cylindrical targets machined from brass. The source driving function has been chosen to match that obtained when making the experimental measurements. The theoretical amplitudes (continuous line) have been normalised so that measured and calculated results are coincident for a target of area 11.3 mm^2. Full-wave detection, i.e. the largest half-cycle, has been used in detecting all echo amplitudes. Target sizes range from 1 mm diameter up to a target with dimensions slightly larger than the source aperture. As can be seen there is a fairly good match between experimental and calculated curves. Deviations from the calculated curves are caused by the same kind of experimental errors as the quantitative measurements associated with the results in Table 1. (section 4.6.2)

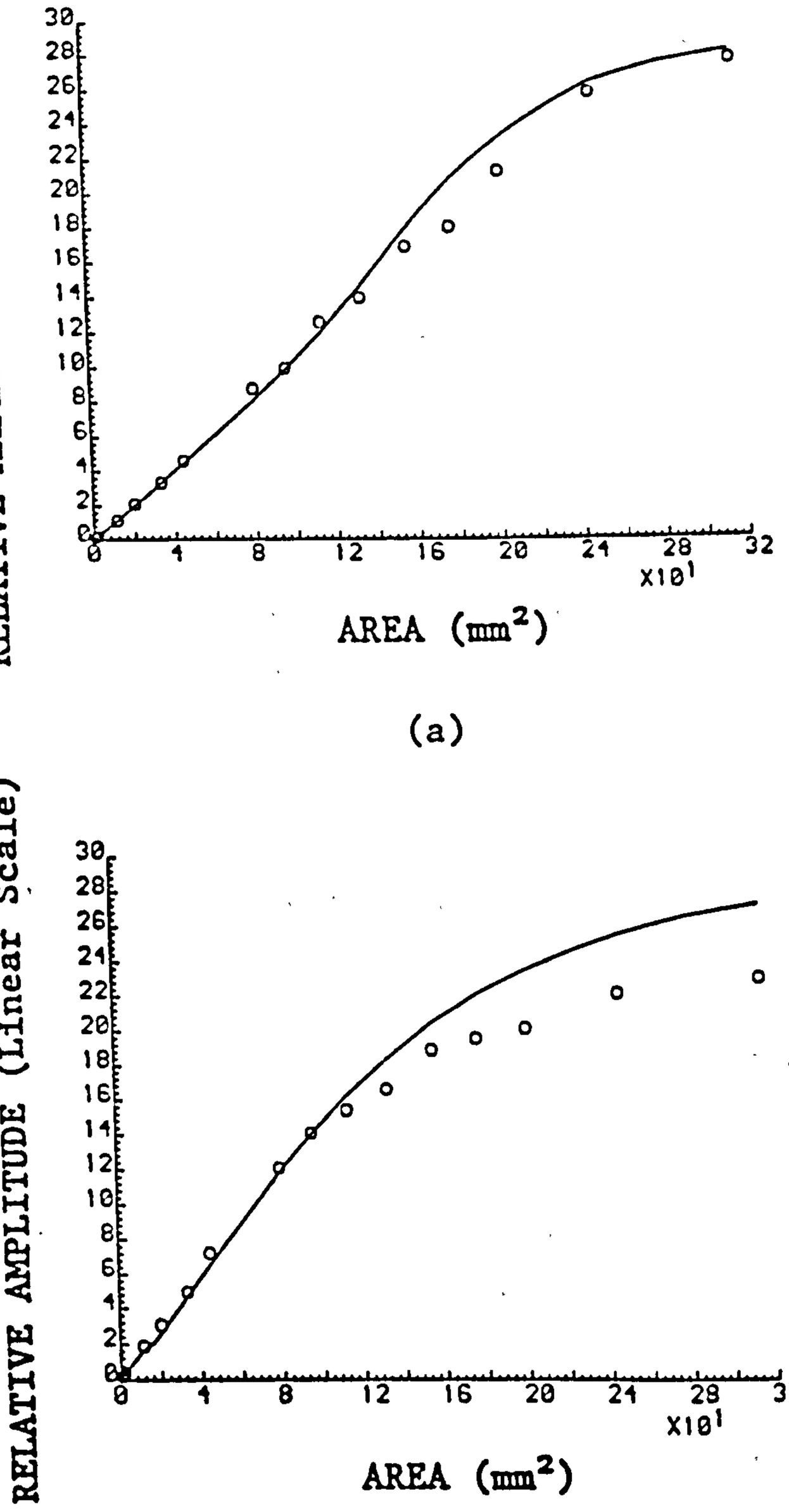

Fig 4.6.6 Calculated (solid line) and experimentally determined (circles) echo amplitudes versus target area, for various sizes of axial, normally-aligned, flat-ended cylindrical targets in water. These were obtained at two ranges: (a) 30mm and (b) 120 mm, using a 19 mm diameter conventional PMN transducer.

As shown in Fig. 4.6.6 (a), at ranges close to the transducer the echo amplitude is proportional to target area for all targets with a diameter less than approximately half the source aperture. Above this size there is a departure from linearity, the echo amplitude becoming greater than would be expected if the amplitude remained linear with area. Eventually, as the target area approaches that of the transducer the rate of increase in the echo amplitude decreases. The reason for this can be understood by considering the form of the transmit-receive mode beam profile (obtained using a point target to probe the field) of a circular transducer emitting a short pulse (see Fig. 4.3.2). In Fig. 4.3.2 it can be seen that at ranges close to the source, apart from a sharp maximum on axis, there are no fluctuations in the beam plot in a central region concentric with the transducer axis. Further off axis there is an initial increase from the central plateau level, which reaches a maximum value and then decreases, until at the edge of the geometric region the beam has an amplitude equal to one half its central plateau level. At a range of 30 mm and for the short pulse emitted, all points on the surface of targets of size less than half the source aperture contribute the same peak pulse amplitude to the overall echo waveform. As a consequence reflected pulse amplitude is proportional to area. For larger targets, as a result of the form of the radiated beam, the contributions from points slightly further off axis are greater than those from the central plateau region causing the departure from linearity.

At a distance of 120 mm, which corresponds to the last axial maximum in the CW field at 2 MHz, the overall shape of the calculated curve is shown in Fig. 4.6.6 (b). Notice that the echo amplitude is not linear with target area over any portion of the graph and the slope of the curve smoothly decreases with increasing area. Again the form of the curve can be understood in terms of the beam profile from a point-like target. At 120 mm there is no central plateau region. From a maximum on axis the transmit-receive mode beam profile falls off smoothly with lateral displacement. Although there is good agreement between calculated and measured results over the early section of the graph there is a slight deviation from the theoretical results at the largest target sizes. This departure from theory is most probably due to alignment errors which are more significant at the larger target sizes.

4.6.4 Echo responses from targets of different shape.

Transmit-receive mode echo waveforms from circular, square and triangular planar targets are shown in Fig. 4.6.7. All three targets, of equal cross-sectional area and machined from brass, have been normally aligned to a conventional transducer at a range of 30 mm on axis.

The form of the echo waveforms from all three targets is almost identical, there being only small differences in the shape of the pulses trailing the plane wave. Because all target areas are equal so too are the plane wave amplitudes. These observations are confirmed by the calculated results which are in good agreement. The structure of the echo responses from these different shapes of target are so similar that even the spectra provide no clear information that would allow them to be individually identified.

Characterising the shape of simple planar targets in this manner is likely to be difficult. Theoretical modelling also shows that this is the case at all field positions and for all target sizes. If the different shaped targets are smaller they all tend to behave as point-like scatterers again generating almost identical echo waveforms. If their dimensions are much larger, they all tend to act as specular reflectors again resulting in similar responses. It may however be possible to extract shape information if the targets are at non-normal orientation relative to the transducer. Using further extensions to the finite-sized target model already outlined in section 4.6 this possibility could be investigated more fully at a later date.

Theoretical modelling and experimental mesurements also show that virtually identical waveforms from targets of different shape, but identical cross sectional area, are also obtained with non-uniformly excited sources.

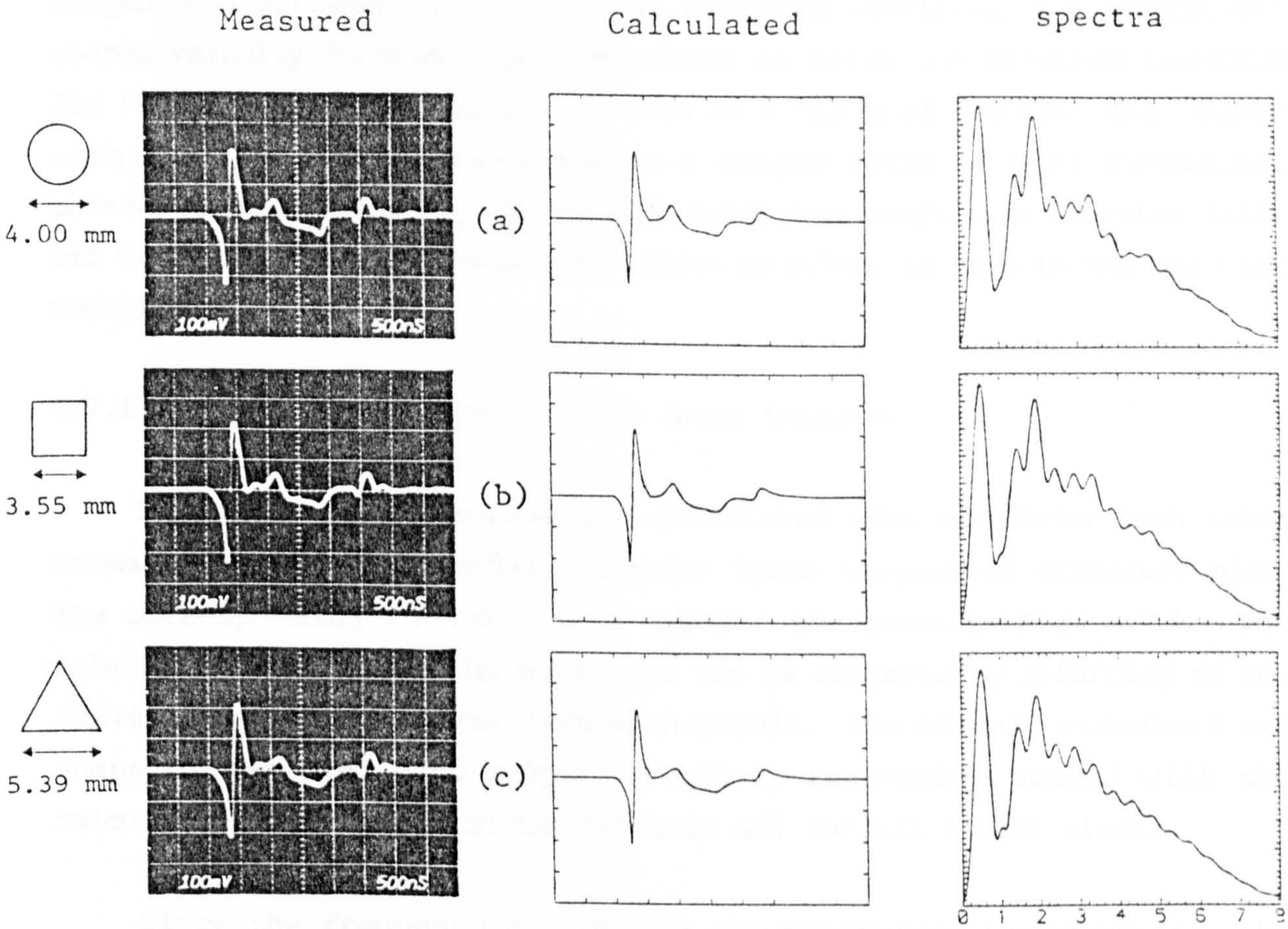

Fig 4.6.7 Measured and calculated transmit-receive mode responses from axial, normally-aligned targets of various shape (of identical cross-sectional area) at a range of 30mm in water, interrogated using a 19mm diameter conventional PMN transducer.

4.7 Measured and calculated transmit-receive mode responses from solid finite-sized targets in water using an EWO transducer.

Experimental measurements reported in this section were made using a 19 mm diameter prototype EWO transducer. In order to obtain a better comparison between calculated and measured waveforms, the theoretical source velocity function has been chosen to match the measured waveform for the 1 mm diameter target on axis at a range of 100 mm. The source velocity function approximates to a single cycle (3 MHz) sinusoidal pulse. An experimentally determined weighting profile, a Gaussian fall-off with a half maximum amplitude width of 0.5mm, is used in the computer modelling.

4.7.1 Echo responses from circular metal targets.

Fig. 4.7.1 shows measured and calculated echo waveforms from axial normally-aligned, flat-ended, circular brass targets of different size. The corresponding 2 mm off-axis results are given in Fig. 4.7.2. The relative amplitudes of the waveforms can be compared by referring to the scale factor (in dB) given with each result. The overall structure and shape of measured echo responses are in reasonable accord with the calculated results both on and off axis and for all target sizes.

Since the frequency content of the excitation waveform (ie. the source velocity function) is such that the wavelengths radiated are of millimetre order, the pulse shapes in Figs. 4.7.1(a) and 4.7.2(a) for a 1 mm diameter target are similar in form to those that would be obtained from an ideal point target. On axis the contributions from each element of the edge wave arrive simultaneously thereby superimposing to give a single pulse which is time differentiated. As commented on previously [6], the axial far-field echo waveform from a point target interrogated by an EWO source is asymptotic to the second time differential of the source velocity function. Even at a range of 100 mm the form of the pulse in figure 4.7.1(a) resembles the second time differential of a sine wave. When the target is moved 2 mm off axis (Fig. 4.7.2 (a)) the situation is more complicated with the edge-wave pulse beginning to split into much smaller, distorted pulses. It is of course this rapid reduction in pulse amplitude with distance off axis that gives the excellent lateral resolution of the EWO source.

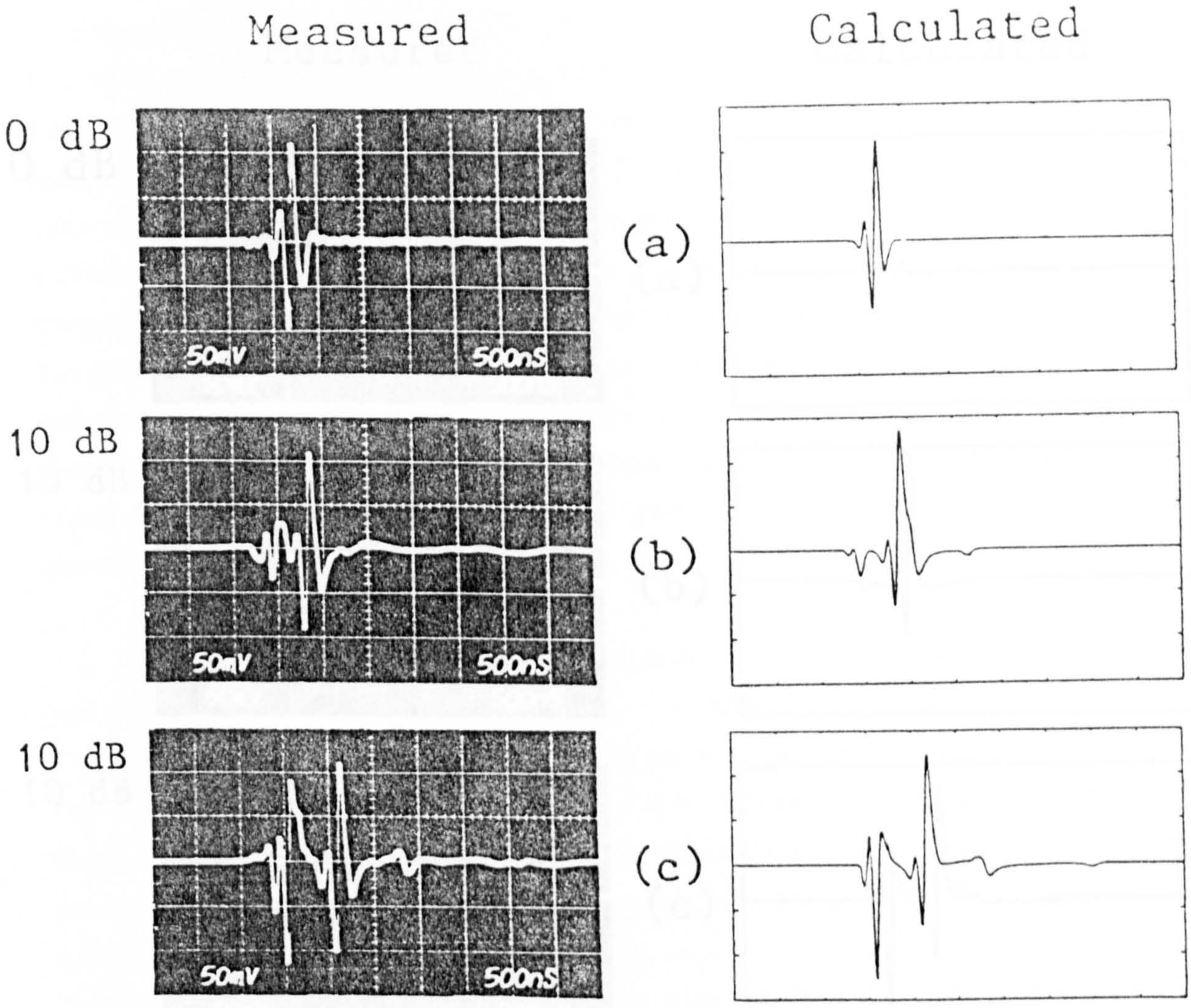

Fig 4.7.1 Measured and calculated transmit-receive mode responses of a 19mm diameter prototype EWO transducer interrogating axial, flat-ended cylindrical brass targets with diameters of (a) 1mm, (b) 10mm and (c) 20mm, at a range of 100mm in water.

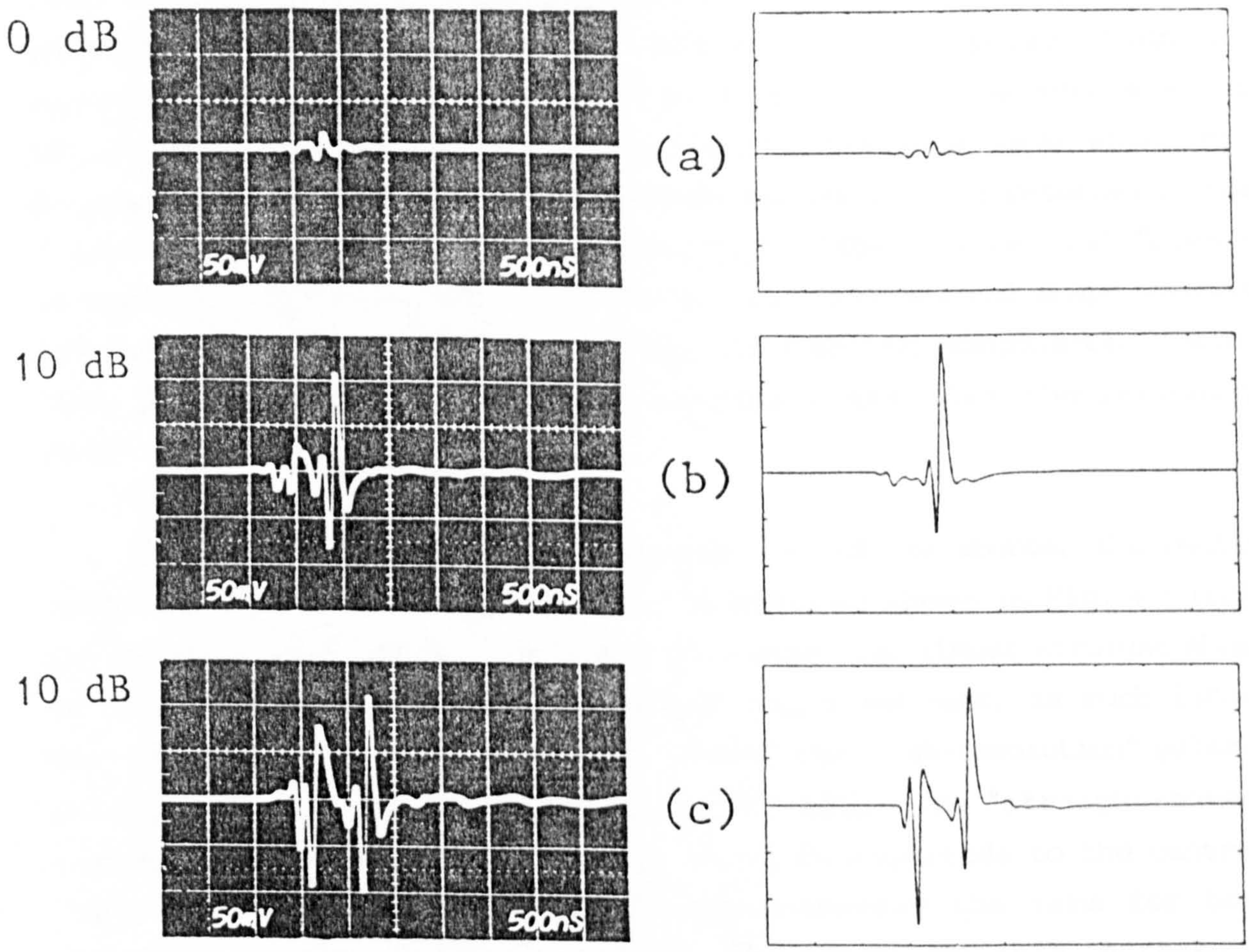

Fig 4.7.2 Measured and calculated transmit-receive responses as in Fig 4.7.1 with the targets 2mm off axis.

As shown in Fig. 4.7.1(b), with a 10 mm diameter target there no longer exists a single pulse on axis. The transmit-receive mode response now consists of three distinct pulses. The central pulse which corresponds to the on-axis "high-resolution" pulse of Fig. 4.7.1(a) is preceded in time by a smaller pulse. This first pulse mostly originates from the portion of the edge wave incident on the target edge and has a shorter time-of-flight than the "high-resolution" pulse which has travelled to the target centre (on axis) and back. The even smaller third pulse corresponds to the portion of the edge wave which has propagated in the direction of the further target rim and returned to the further transducer rim. Off axis (Fig. 4.7.2(b)) the central "high - resolution" pulse remains fairly constant in amplitude and shape whereas the two other pulses have begun to split into smaller components. Notice that all three pulses seen experimentally are also theoretically predicted.

When the target dimensions approach that of the source, the multi-pulse structure is more developed. On axis, as shown in Fig. 4.7.1(c), the first pulse which has propagated in a direction almost straight ahead of the transducer rim to the edge of the target and back, is much larger than for the 10 mm diameter target, whilst the "high-resolution" pulse is only fractionally larger than in Fig. 4.7.1(b). The "straight-ahead" response at this target size is now equal in magnitude to the central "high resolution" pulse, which is approximately the same for both the 10mm and 20mm diameter targets. The reason for this increase in amplitude is due to the fact that the edge wave does not have a uniform amplitude with direction of propagation, being stronger in the direction straight ahead of the rim than at angles either side. The third pulse shown in Fig. 4.7.1(c) is larger in amplitude than the corresponding pulse for a 10 mm diameter target and can be clearly resolved in time from the central pulse. As well as this three pulse structure, theory also predicts a much smaller trailing pulse (see the calculated result of Fig. 4.7.1(c)) which is confirmed experimentally. The relative time of arrival of this fourth pulse corresponds to components of the edge wave which have travelled from the transducer rim to the furthest edge of the target and back. Notice also that as might be anticipated, with larger target dimensions the pulses are more spaced out in time. When the target is moved off axis the "high-resolution" central pulse remains constant and there is a slight reduction in the amplitude of the "straight-ahead" response. Furthermore the third and fourth pulses are now no longer

distinctly visible having split into smaller components which are smeared out in time (Fig. 4.7.2).

The effect of range on echo response is illustrated in Fig. 4.7.3 for a normally-aligned, 10 mm diameter, circular, flat-ended brass target on axis. The result at 100 mm is identical to that shown in Fig. 4.7.1 (b). At the shortest range of 30 mm, the time separation between the various pulse components are larger and because of the geometry and the directional nature of edge waves, the amplitudes are smaller. At a distance of 200 mm from the source the various components overlap to form a single pulse on axis. It should be noted that, although the main features of the echo structure along with the echo amplitudes are predicted by theory, the agreement between measured and calculated results is not as good as for a uniformly excited transducer (see section 4.6). Since most of the results were taken at a range of 100 mm these discrepancies cannot be attributed to head waves. More likely reasons are the difficulties in accurately determining the actual weighting profiles of the transducer and mode conversion at the fluid/solid interface at the target surface. As explained in section 4.6.2 the finite-sized target model takes no account of mode conversion of the non-normal edge waves at the target surface which effects the amplitude of the reflected wave. This effect is possibly more noticeable here because unlike a uniformly excited source the edge-wave contributions are seen in isolation and not swamped by the larger plane-wave reflections. Nevertheless the experimental and calculated results are in reasonable accord, confirming the validity of the finite-sized target model in predicting echo waveforms from targets of finite dimensions interrogated by non-uniformly excited transducers.

Although not shown here, experimental results with the EWO transducer have also shown that the pulse shape from a target of a given geometry is uneffected by that target's material properties. This is consistent with the finding made for a uniformly excited transducer in section 4.6.2. The relative amplitudes of echo waveforms from identical targets of different acoustic impedance was again found to be given (within the limits of experimental uncertainty) by the ratio of their reflection coefficients for a normally-incident plane wave.

Measured

Calculated

Range 30 mm

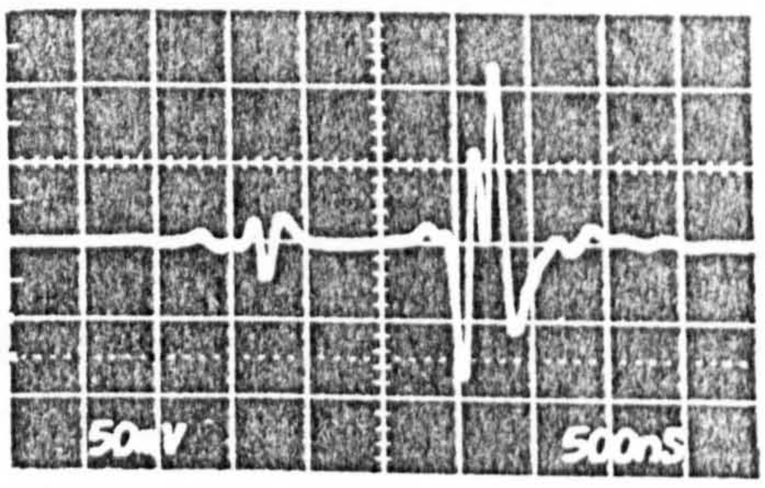

(a)

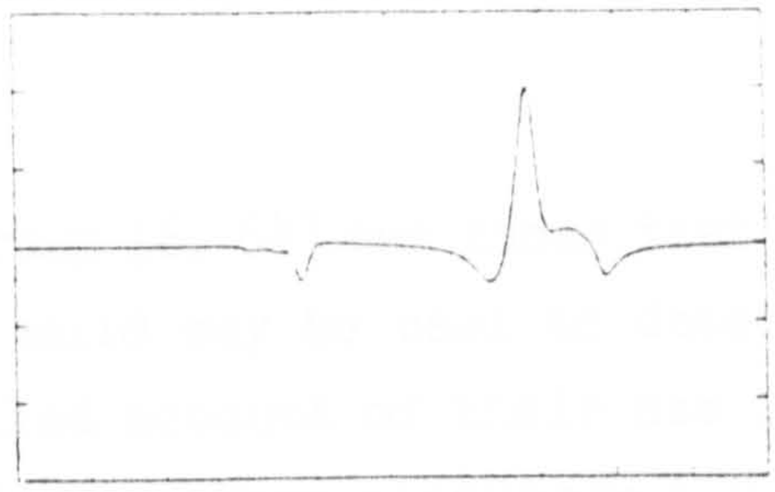

70 mm

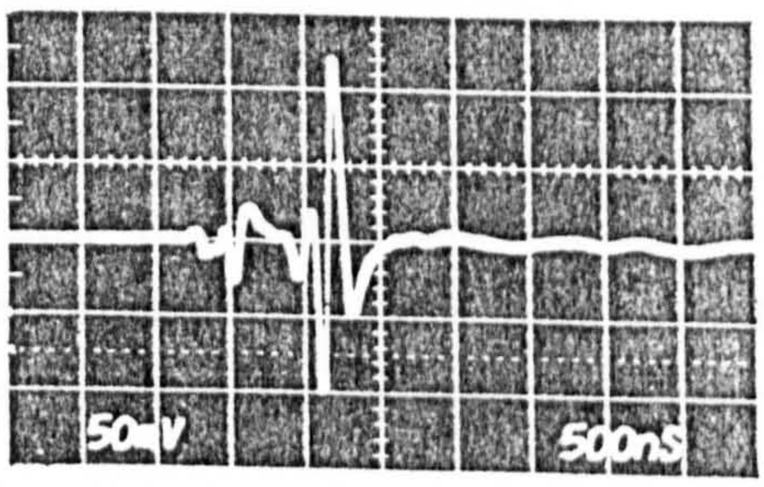

(b)

100 mm

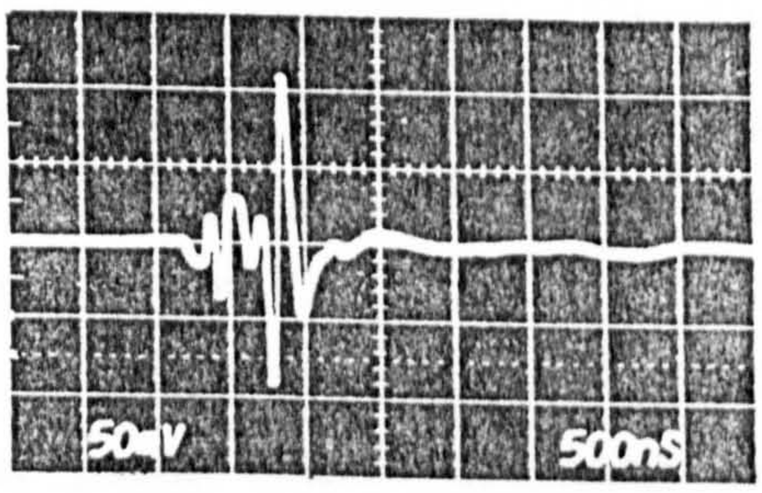

(c)

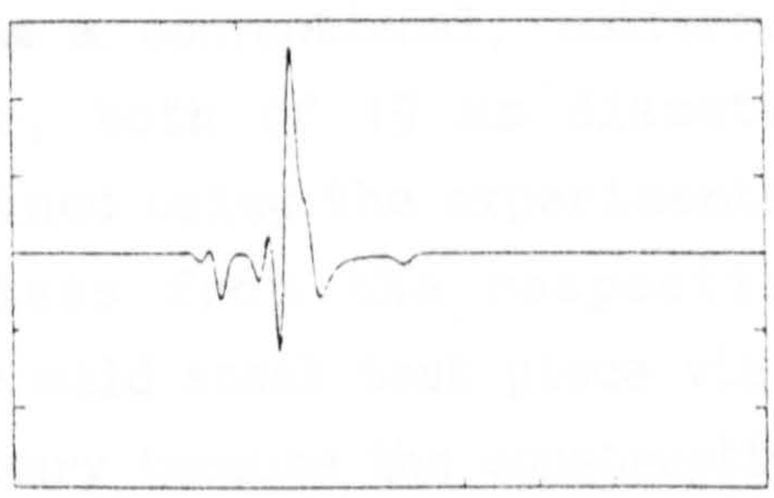

200 mm

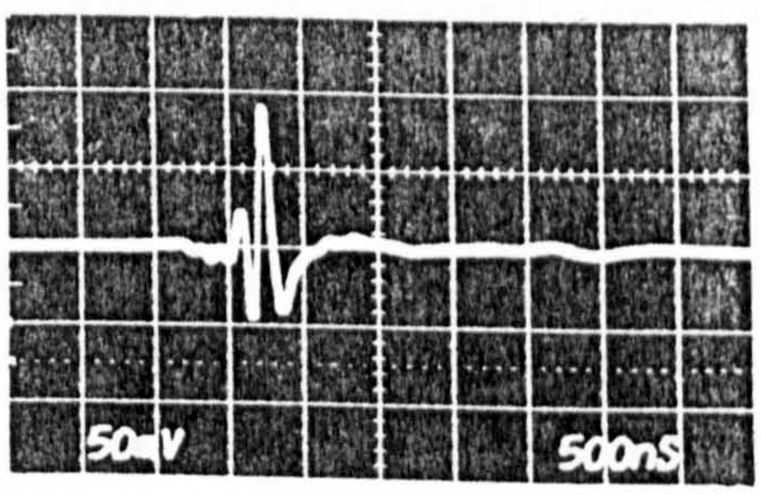

(d)

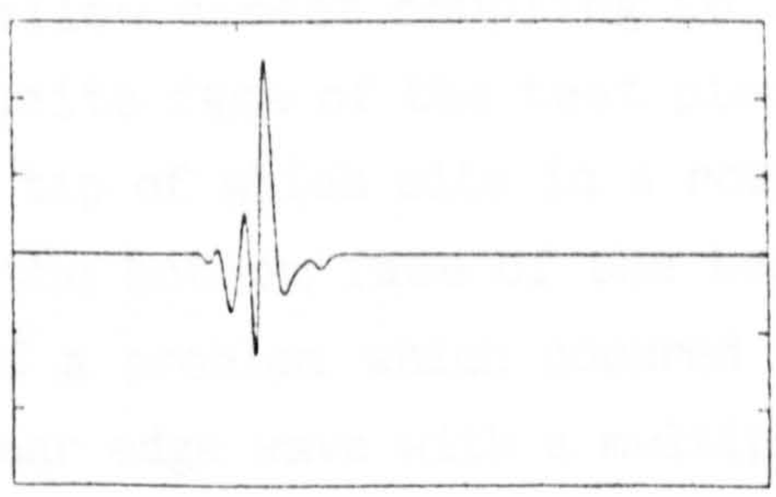

TIME (.5 μs/div)

Fig 4.7.3 Measured and calculated transmit-receive mode responses for an axial, 10mm diameter, flat-ended cylindrical target at a range of (a) 30mm, (b) 70mm, (c) 100mm and (d) 200 mm in water, interrogated using a 19mm diameter prototype EWO transducer.

4.8 Field mesurements in solids.

Preliminary experimental results only are included here and more detailed measurements along with computer modelling is left to future work.

Previous work within the Ultrasonics Group [6, 64] has shown that a miniature probe coupled to the surface of a solid may be used to detect both compression and shear waves. A detailed account of their use in measuring short pulses propagating in a solid is given elsewhere [79]. Essentially the action of the probes is such that they respond to the normal component of the surface velocity motion, which is assumed to be locally plane and unperturbed by the presence of the probe. Since the diameter of the probe (0.4 mm) is smaller than the wavelengths of the propagating pulses it can be considered to act as a point receiver.

Field point measurements of pulses from a conventional, uniformly excited transducer and an EWO transducer, both of 19 mm diameter aperture, propagating in a solid were obtained using the experimental set-up shown in Fig. 4.8.1. Short pulses from the respective transmitting transducers were coupled to the mild steel test piece via a 10 mm water path. Water coupling was necessary because the construction of the prototype EWO transducer does not allow direct coupling to be made. The waveforms appearing at the opposite face of the test piece were measured using the miniature probe, the tip of which sits in a round bottomed hole of 10 mm radius bored into the bottom face of the test piece. The function of the hole was to avoid a problem which occured at some ranges due to the overlapping of the shear edge wave with a multiple reflection of the faster compression wave. In order to avoid problems due to variations in coupling, the probe tip was held into position using a specially constructed jig. A number of steel test pieces of various thickness were used so as to place the probe at different ranges from the source.

Fig. 4.8.2 shows on-axis waveforms at four ranges in steel for a conventional and an EWO transducer. In both cases the transducers are normally aligned to the top surface of the test piece at a coupling distance of 10 mm in water. In both sets of measurements the excitation and receiving systems were kept constant in order to allow a direct comparison of sensitivities.

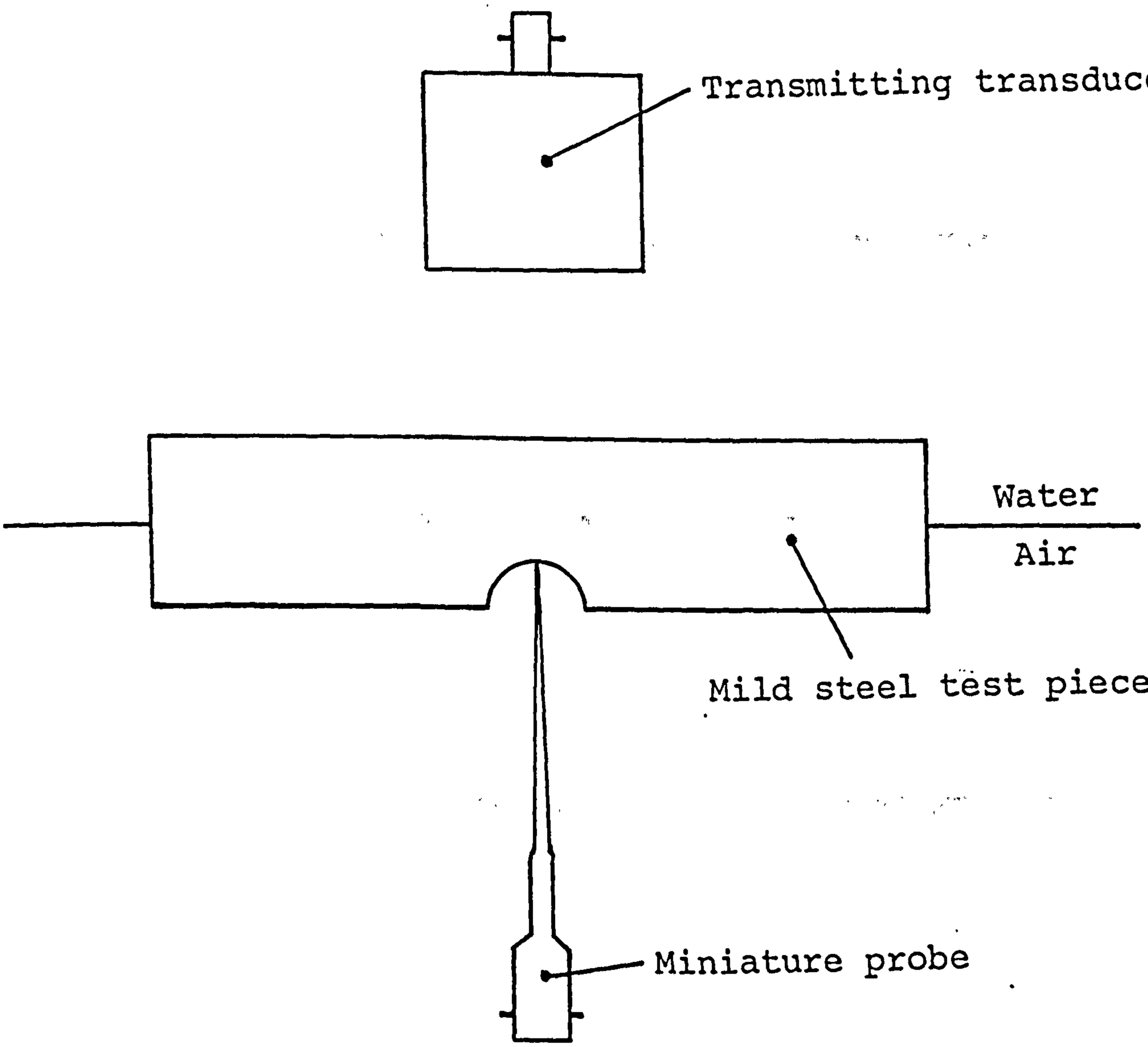

Fig 4.8.1 Measurement of particle velocity waveforms using a miniature probe.

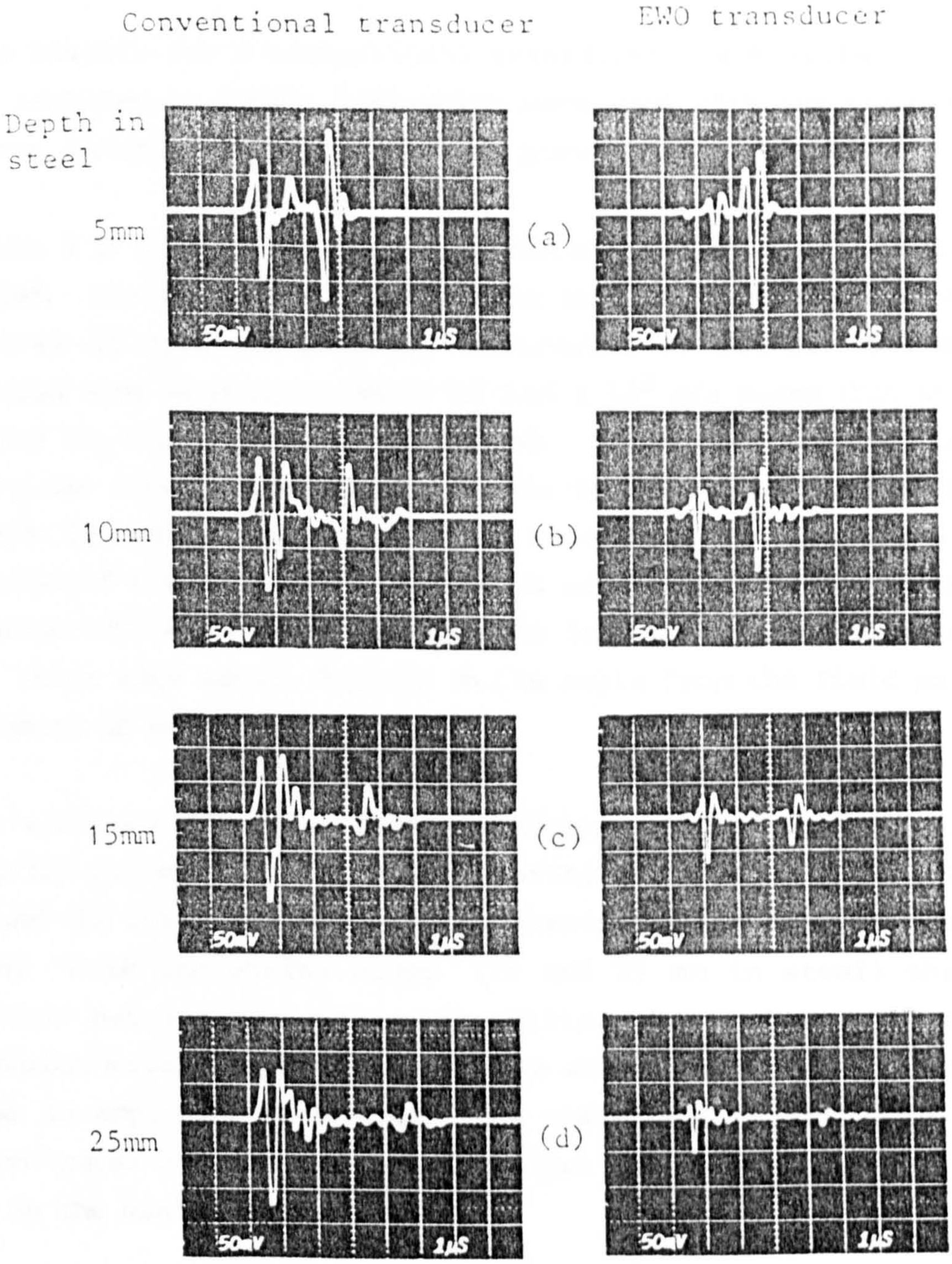

Fig 4.8.2 Measured waveforms at points on the surface of steel test pieces of various thickness. Transmitted pulses were launched from conventional and prototype EWO transducers of 19mm diameter into the opposite surface of each test piece by means of a 10mm water coupling path.

4.8.1 Uniformly excited transducer.

The results for a conventional transducer are similiar to those already published by Weight [64] which were made with the transmitting transducer directly coupled to the test piece.

With a 5 mm thick test piece three distinct pulses can be identified. The first two pulses are the familiar compression plane and edge waves of opposite polarity observable in fluids; the higher compression wave velocity in steel of 5.85 x 10^3 m/s means that at this range they can only just be time resolved. Trailing these two pulses is a third pulse travelling at the shear wave velocity in mild steel of 3.23 x 10^3 m/s. The existence of this shear wave can be attributed to mode conversion of the incident compression edge wave. The proportion of compression edge wave which mode converts into what is termed by Weight [64] a "shear edge wave", depends on the angle from the field point to each element of the transducer rim.

At a range of 10 mm in steel the compression edge wave begins to overlap the plane wave. The time separation between the compression waves and the shear edge wave has increased and its amplitude is much reduced. With increasing range (15 and 25 mm in steel) the time separation between the slower travelling shear edge wave and the compression waves lengthens, while the shear edge wave continues to decrease in amplitude with range. The small ripples observable in the waveform traces are unwanted acoustic noise caused by waves that bounce around in the miniature probe tip.

4.8.2 High-Resolution EWO transducer.

Field point measurements using the EWO transducer as transmitter are also shown in Fig. 4.8.2 to the same scale as the previous results for a conventional transducer. As to be expected there is no direct plane-wave component present and the waveform consists of a compression edge wave followed by a shear edge wave. At the shortest range in steel the trailing shear edge wave is very much larger in amplitude than its compression counterpart. However, with increasing range the amplitude of the shear edge wave diminishes whilst the compression edge wave amplitude increases. At a range of 15 mm in steel the compression edge wave is larger than the shear-wave component which has now become well

time separated. Still further from the transducer the amplitude of the shear edge wave continues to fall off and the large time separation means that in practice it could be conveniently gated out.

The existence of a multi-pulse structure in solids for the high-resolution EWO transducer is undesirable since it can lead to extra spurious target indications especially at short ranges from the transducer. This problem is only likely to affect the EWO transducer when using direct coupling or a very short water coupling path and can be easily overcome by using a larger water coupling distance which tends to minimize the shear edge-wave contribution. Furthermore, when using water coupling in transmit-receive mode shear wave reflections will only be detected via mode conversion at the solid/liquid boundary. Such mode conversion will be weak if the angle of inclination is small. Fig. 4.8.3 shows results for an EWO tranducer made with a coupling path of 60 mm instead of 10 mm; 40-60 mm was a typical path length used in the immersion B-scan testing of solid test pieces shown in section 4.9. Using this technique the response is simpler at all ranges, consisting of a single compression edge wave. The small amplitude of the shear edge wave results in it being lost in the acoustic noise produced in the probe tip. Further note that the extra path length in water causes only a slight reduction in the amplitude of the compression edge wave.

Depth in steel

5mm

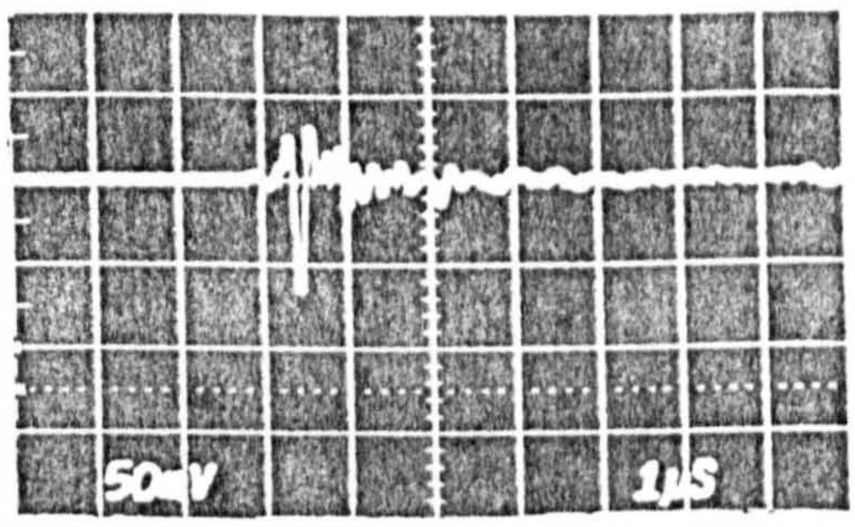

(a)

10mm

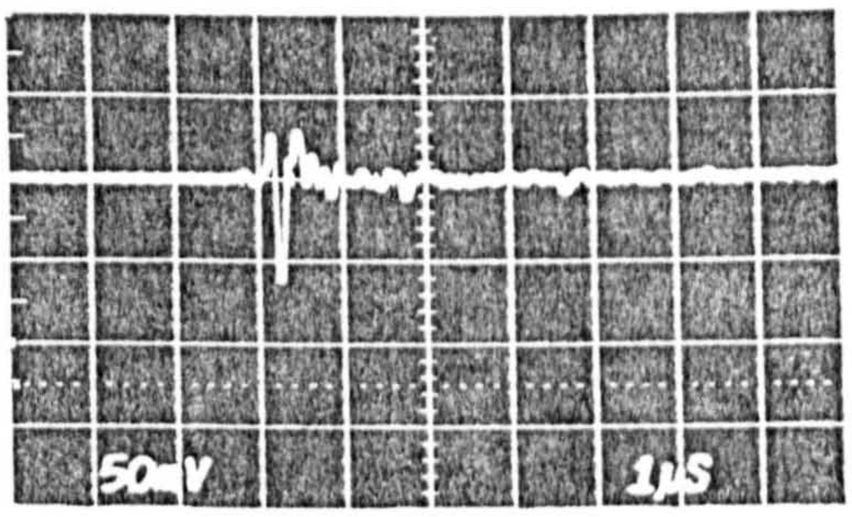

(b)

15mm

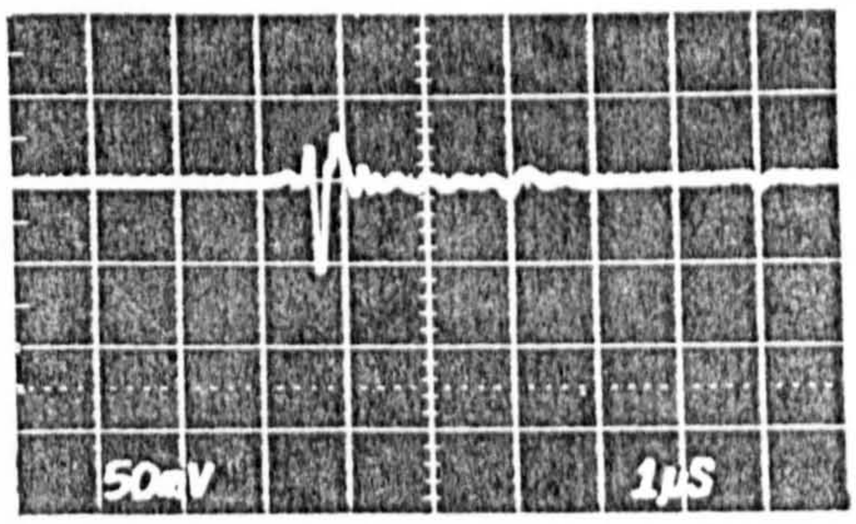

(c)

25mm

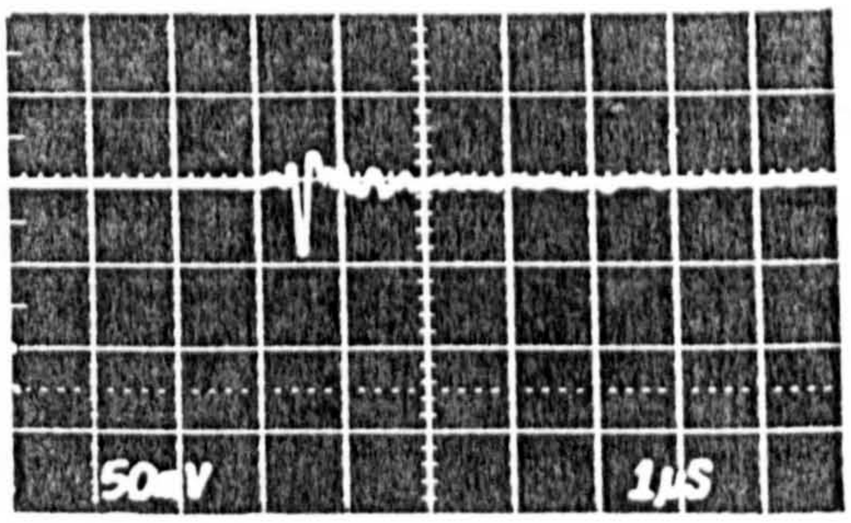

(d)

Fig 4.8.3 Measured waveforms as shown in Fig 4.8.2 for a prototype EWO transducer but with a water coupling path of 60mm.

4.9 Ultrasonic B-scan imaging.

In this section the ability of the prototype EWO transducer to accurately locate and size flaws and defects is examined and compared with an equivalent conventional transducer. This evaluation is made using various specially constructed phantoms (similar to those used in evaluating medical ultrasonic equipment) and solid test blocks containing simulated defects, in conjunction with the imaging system outlined in section 3.4. Scanning of solid test pieces was made using water coupling.

4.9.1 B-scan images of targets in a fluid medium.

Fig. 4.9.1 shows B-scans of a test specimen consisting of an array of lengths of 0.2 mm diameter nylon monofilament thread (a weak scatterer) in water. The specimen consists of three vertically-spaced grids of threads, the second grid lying 40 mm and the third grid 70 mm below the top grid. Each grid consists of four groups of three threads. The spacings of the threads within the groups are 10 mm,6 mm,3 mm and 1.5 mm. The upper B-scan (Fig. 4.9.1 (a)) was obtained using a 19 mm diameter conventional transducer. The poor lateral resolution means that none of the threads within the groupings can be resolved. The lower image was made under identical conditions except with a EWO transducer of 19 mm diameter aperture. In marked contrast to the image above, all threads can be resolved - even those at the closest spacing. This is true for all three grid levels highlighting the EWO transducer's ability to obtain sharp focus over a large depth of field.

A similar test specimen to that above, consisting of an array of 0.2 mm diameter nylon threads, spells out the word TCU and below PHYSICS. Fig. 4.9.2(a) shows that at the coupling range used 60 mm, the range resolution of the conventional transducer is good enough to resolve the threads at each depth. However, the poor lateral resolution makes the word PHYSICS impossible to read. The B-scan in Fig. 4.9.2(b) on the other hand allows both words to be easily read, again demonstrating the excellent lateral and axial resolution of the EWO transducer.

4.9.2 B-scan images of targets in a solid test block.

The aluminium test piece shown in Fig. 4.9.3 contains a row of nine

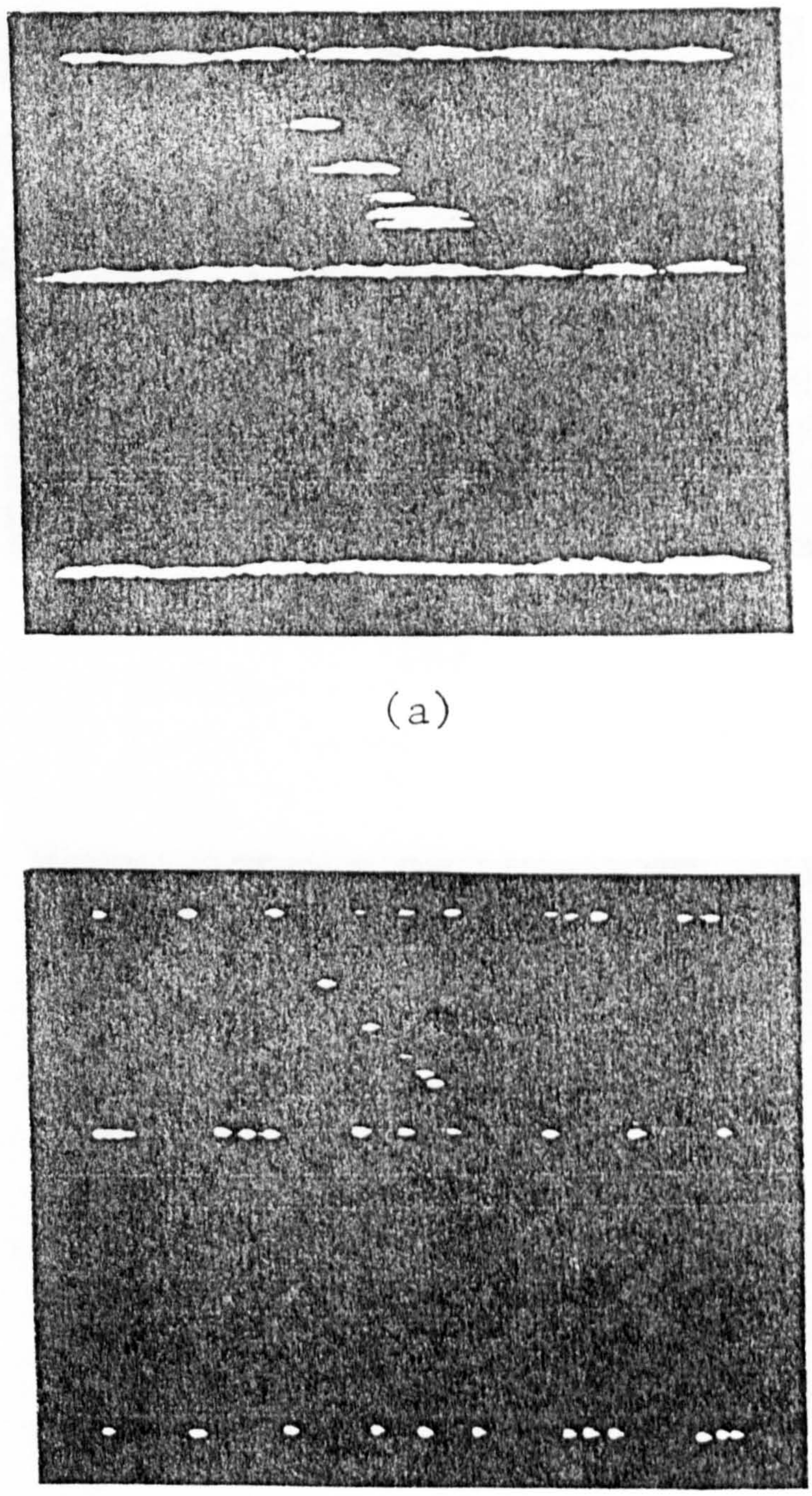

(a)

(b)

Fig 4.9.1 B-scan images of an array of nylon threads consisting of three vertically spaced grids of threads (diameter 0.2mm) suspended in water. These were obtained using (a) a conventional uniformly excited transducer and (b) a prototype EWO transducer, both of 19mm diameter. The closest spaced threads are 1.5mm apart (centre-to-centre).

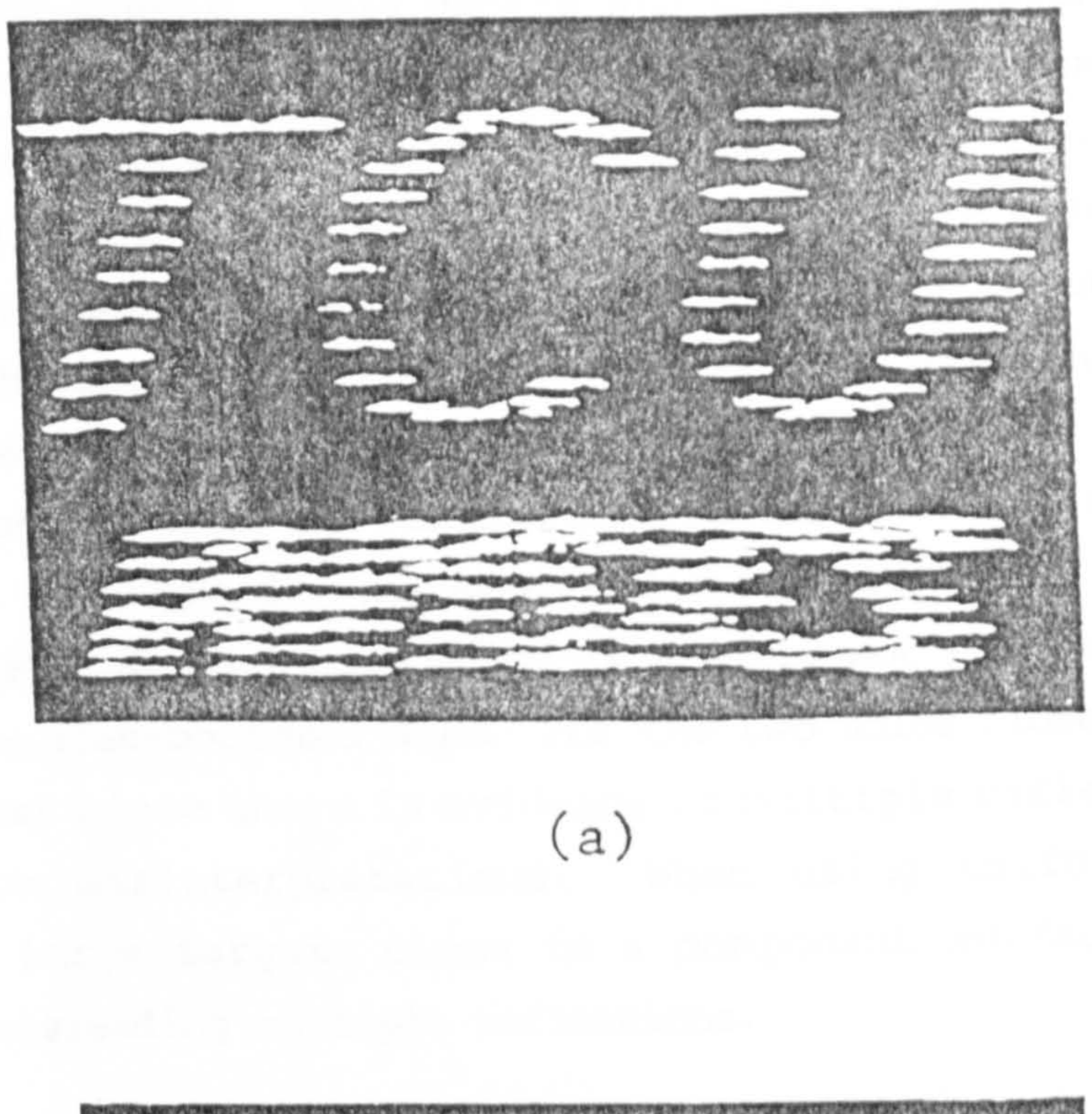

(a)

(b)

Fig 4.9.2 B-scan images of an array of 0.2mm diameter nylon threads, which spell out the words TCU and below PHYSICS, suspended in water. These were obtained using (a) a conventional transducer and (b) a prototype EWO transducer of the same aperture (19mm).

5 mm diameter flat-bottomed holes drilled into the bottom face of the block to various depths. Hole depths and block dimensions are shown schematically in Fig. 4.9.3(a). Fig. 4.9.3(b) was produced using a uniformly excited transducer of aperture 19 mm, whilst Fig. 4.9.3(c) was obtained using an EWO transducer of the same aperture under identical conditions. The coupling distance in water was 40 mm in both cases. In Fig. 4.9.3(b) the bottoms of the holes are all resolved in relation to depth, but the inherent poor lateral resolution of the conventional transducer is of the order of its aperture so that the hole diameters are not accurately represented. The B-scan also indicates that the back face of the test piece is continuous which is clearly not the case due to the presence of the flat-bottomed hole. For the two holes closest to the top face of the test piece there is evidence of multiple reflections which could lead to misinterpretations. When using uniformly excited transducers, large targets close to a component surface inevitably produce such misleading multiple reflections.

In Fig. 4.9.3(c), using an EWO transducer, the diameter of the holes can be ascertained to an accuracy of better than a millimetre at all depths. This highlights the ability of the EWO transducer to accurately size simple defects over a large depth of field in both fluids and solids. It is interesting to note that no multiple reflections are present and that shadows on the back wall of the test block, corresponding to the position of the drilled holes are present as in fact they should be. Note however, that the non-linear relationship between time and range for an EWO transducer leads to errors in the indicated depths of the holes. This non-linear relationship has been modelled for the case of an "ideal" EWO transducer interrogating a solid test piece (containing defects) using water coupling, as well as for the simpler case of direct coupling to a single medium containing scatterers/reflectors. The computer model predicts that for the coupling distance and size of test block used, the maximum error in the measured depth of any internal target as measured by a 19 mm aperture EWO transducer will be 2 mm.

Fig. 4.9.4 also shows B-scan images made of an aluminium test piece with a conventional transducer Fig. 4.9.4(b) and an EWO transducer 4.8.4(c), under the same experimental conditions as in Fig. 4.9.3. The test block contains a row of six flat-bottomed holes which vary both in diameter and depth and is shown schematically in Fig. 4.9.4(a). In Fig.

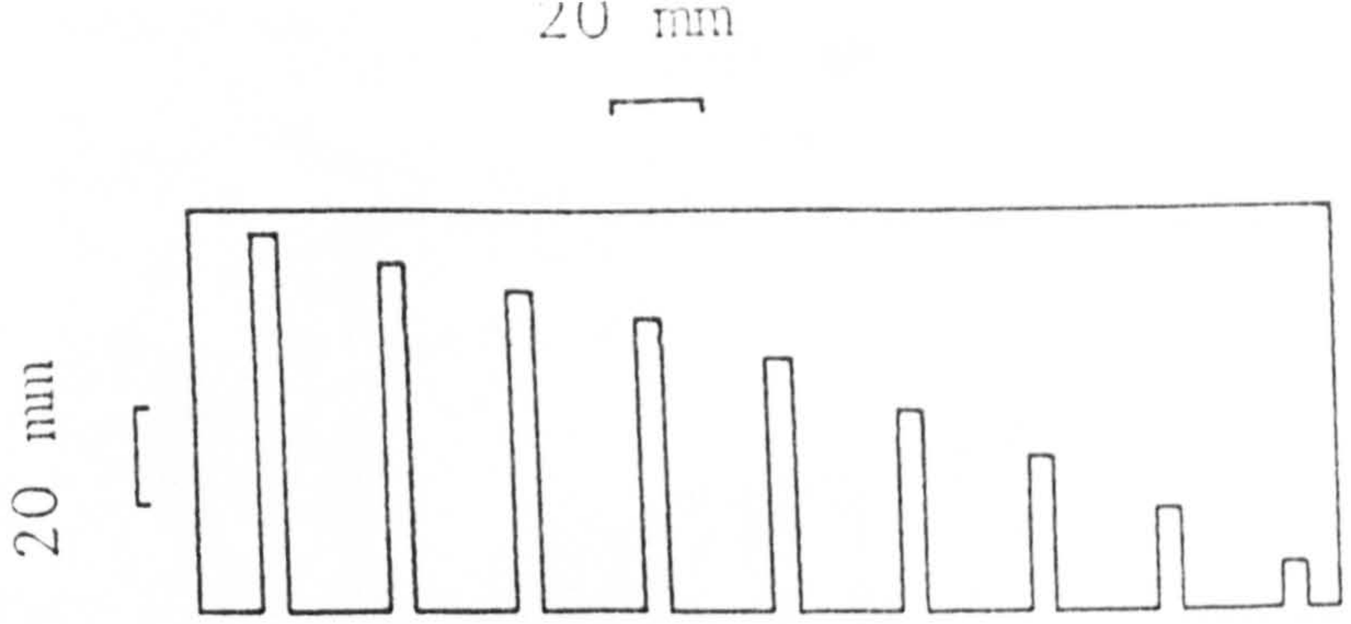

(a)

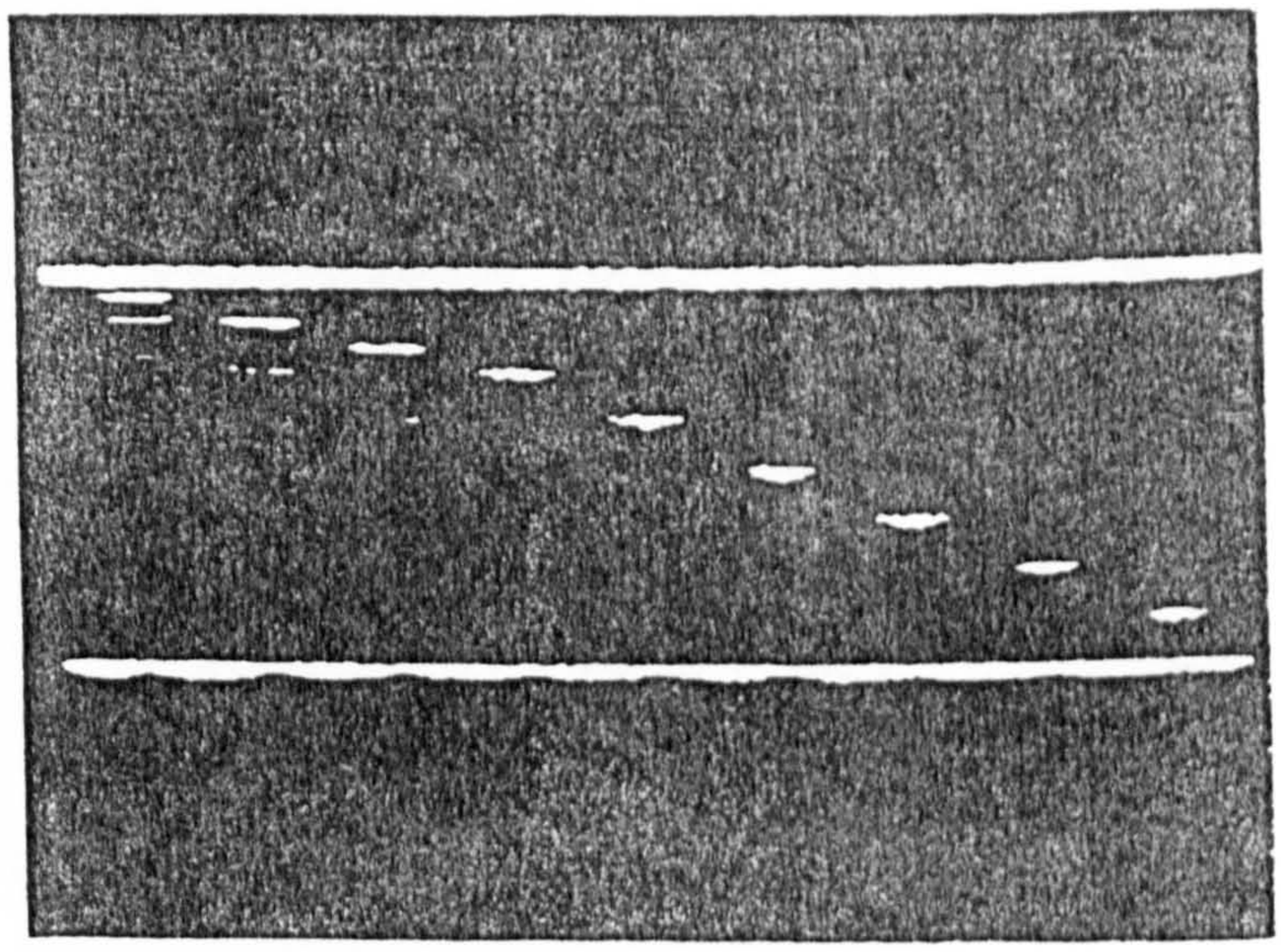

(b)

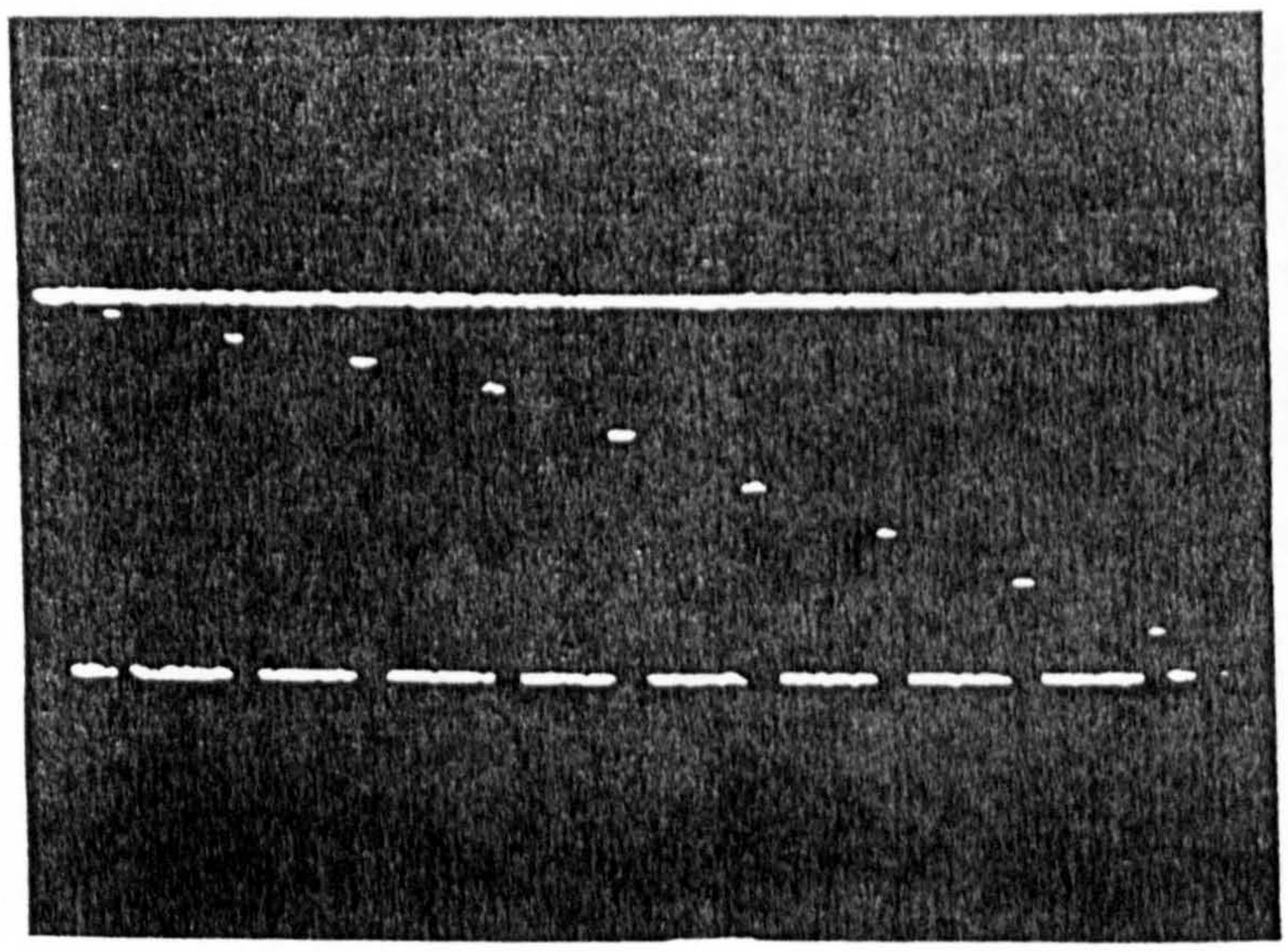

(c)

Fig 4.9.3 B-scan images of an aluminium test piece (shown schematically in (a)) containing nine 5mm diameter flat-bottomed holes at various depths, obtained with (b) a conventional and (c) a prototype EWO transducer, both of 19mm diameter. In both results a 40mm water-coupling path was used.

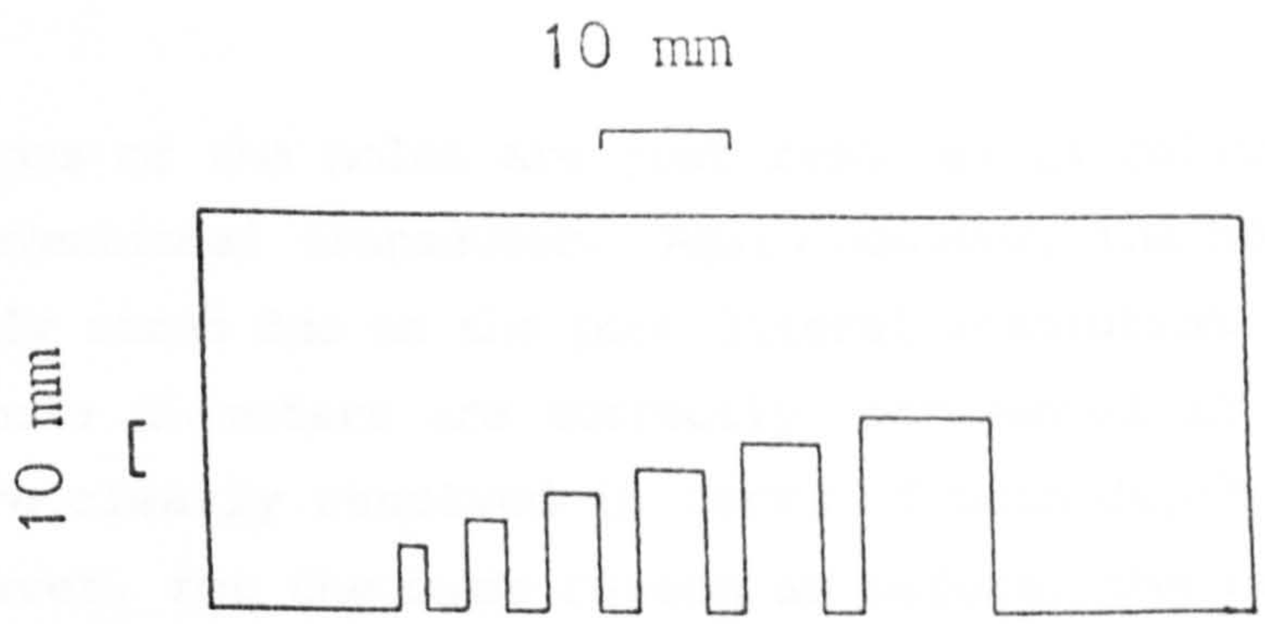

(a)

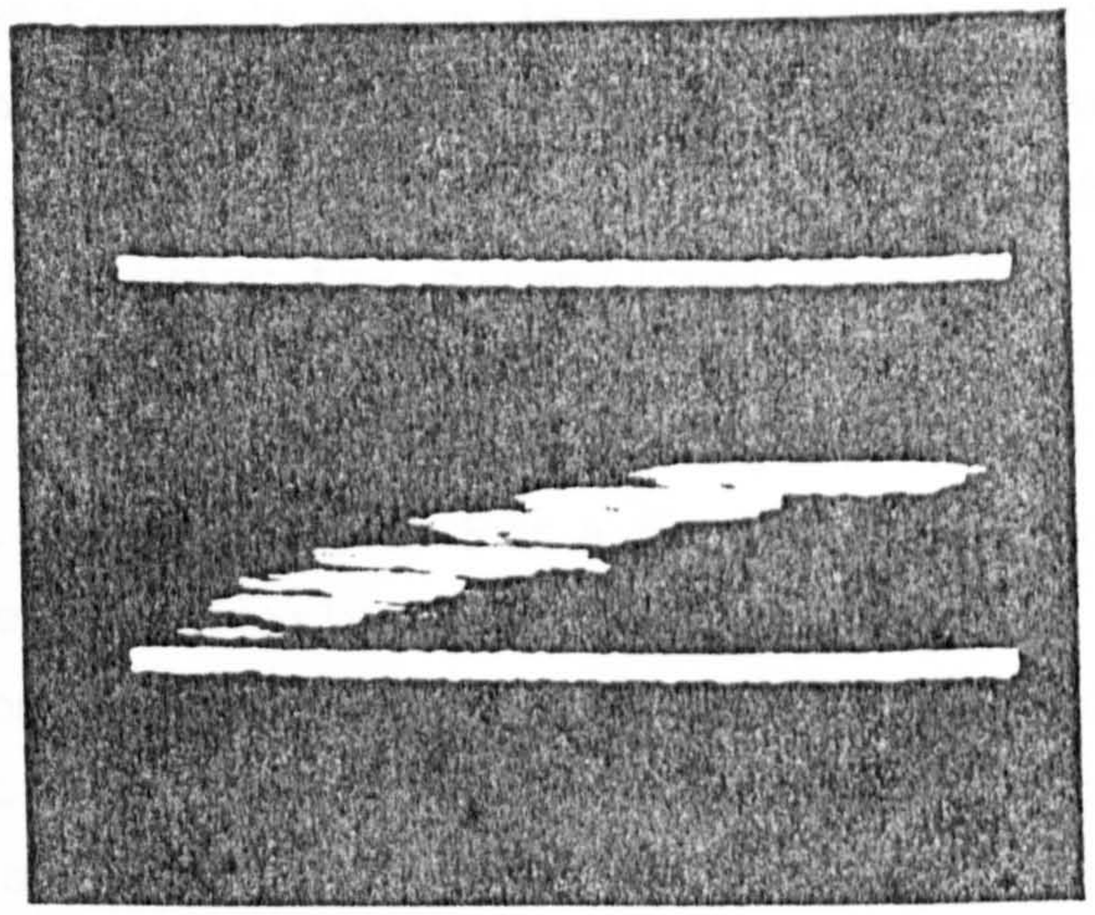

(b)

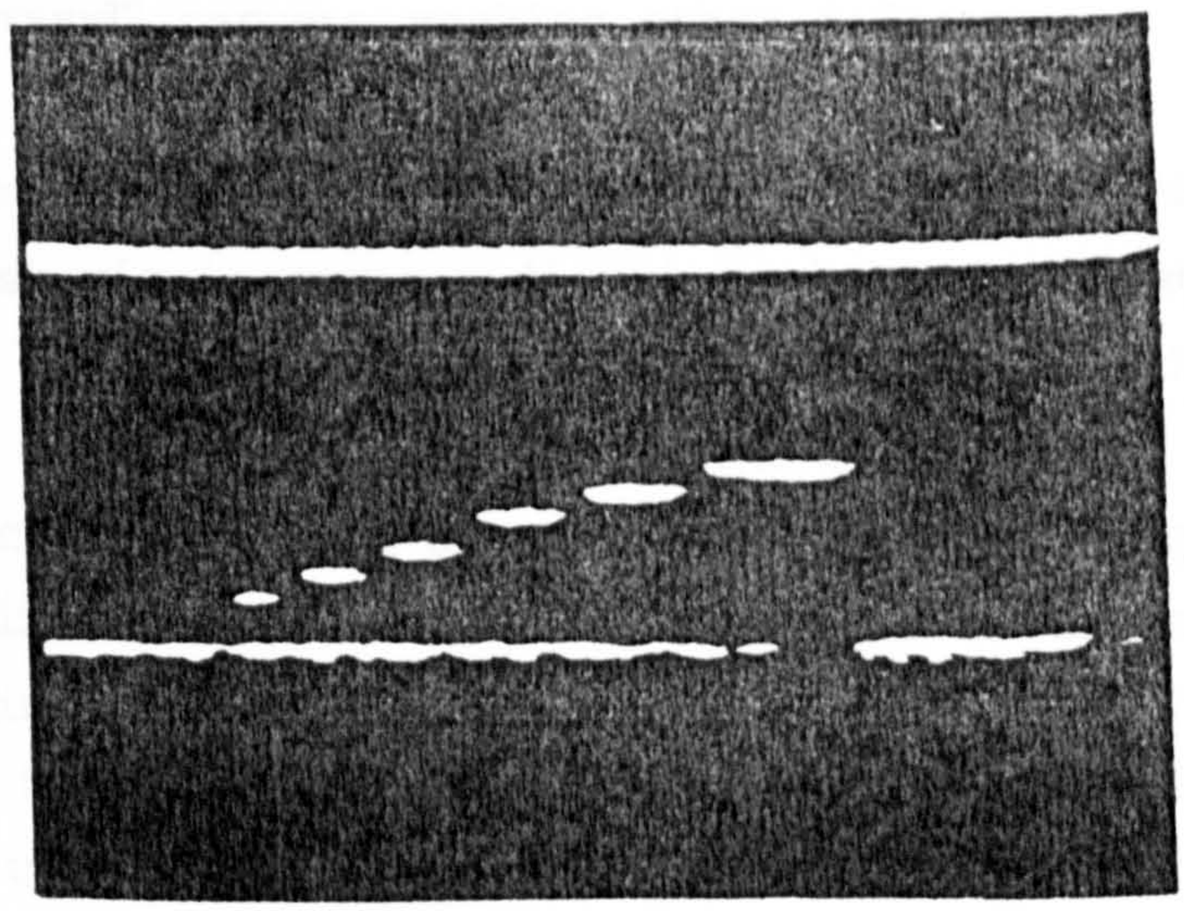

(c)

Fig 4.9.4 B-scan images of an aluminium test piece (shown schematically in (a)) containing six flat-bottomed holes of various size. These were obtained with (b) a conventional and (c) a prototype EWO transducer, both of 19mm diameter, using a 40mm water-coupling path.

4.9.4(b) the bottoms of the holes are just resolved in relation to depth when using a conventional transducer. Again however, the hole diameters are not accurately sized due to the poor lateral resolution. With an EWO transducer the hole diameters are correctly represented in size and the hole bottoms are clearly resolved in terms of both depth and lateral position. However, for the same reason as before, the recorded hole depths are slightly in error.

The schematic diagram of an aluminium block containing a number of circular, side-drilled holes is shown in Fig. 4.9.5(a). This test block has been imaged using a conventional 19 mm diameter transducer (Fig. 4.9.5(b)), an EWO transducer (Fig. 4.9.5 (c)) and a focused transducer f=30 mm (Fig. 4.9.5(d)). Using the conventional transducer the holes in the diagonal can be clearly seen although they are not correctly sized due to poor lateral resolution. The holes lying behind the diagonal cannot however be properly imaged. For a focussed transducer, the hole nearest to the surface is clearly resolved. But because the focussing is maintained over only a small depth the rest of the holes cannot be clearly imaged, especially those at the greatest depths. In contrast the image obtained with an EWO transducer shows all holes clearly resolved, even those lying behind ones above. This illustrates the ability of the EWO transducer (because of the geometry of the radiated waves) to effectively "see around" targets masking other defects.

It should be noted that there is no evidence of any shear edge-wave components causing spurious target indications in either images obtained with a conventional or an EWO transducer. This is because the knowledge gained of the shear edge wave obtained from the experimental mesurements in the previous section allowed a suitable water coupling path to be chosen which minimized its effect. It should however be borne in mind that when inspecting for defects close to a component surface that complications due to the shear edge wave might arise, especially if direct coupling is used.

4.9.3 Target range and echo go-and-return times for EWO transducers.

As mentioned earlier when measuring the range of targets using an EWO transducer, errors are incurred due to the inherent non-linear time/range relationship of this type of source. This error has been modelled for the case of an "ideal" EWO transducer interrogating a solid

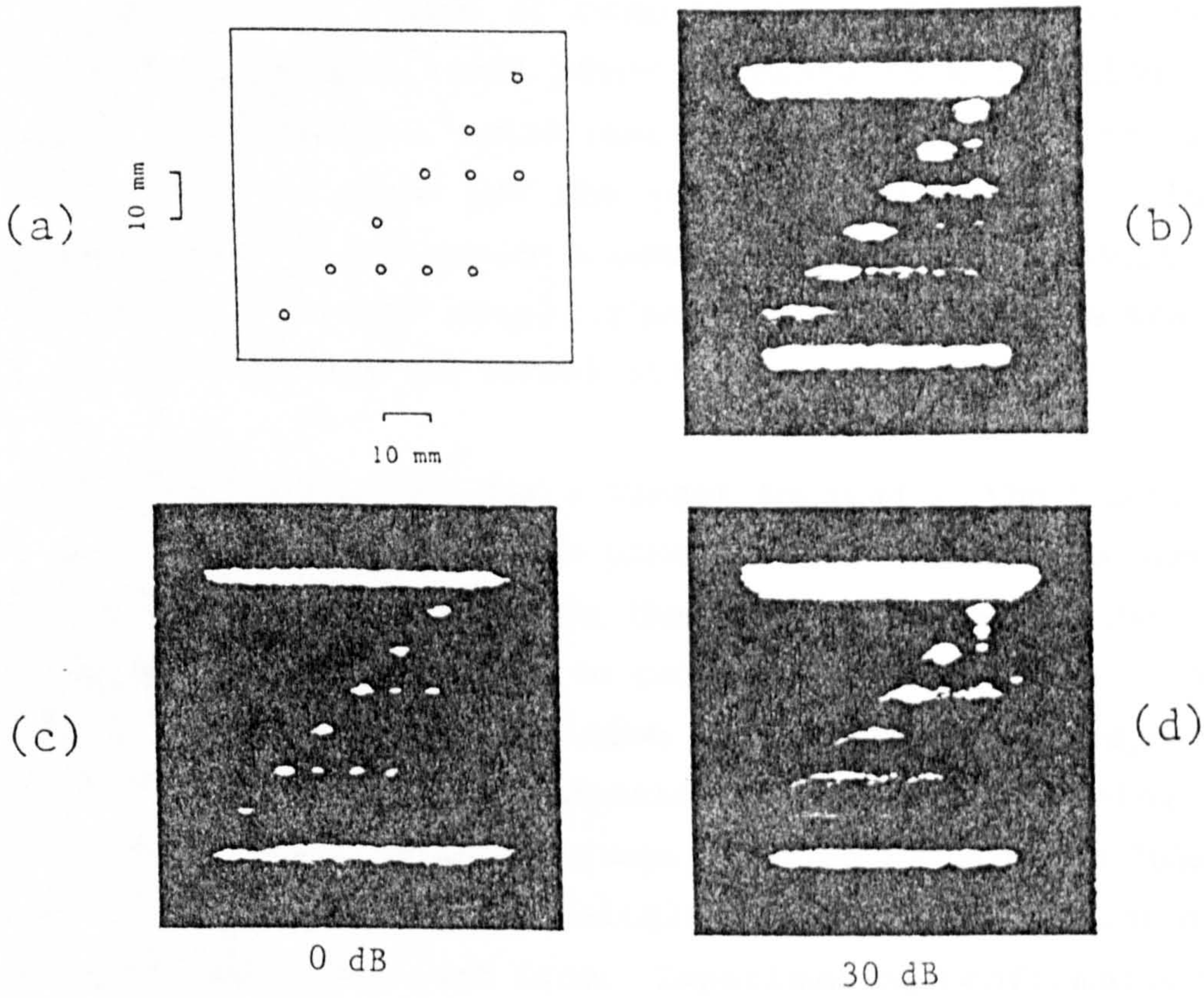

Fig 4.9.5 B-scan images of an aluminium test piece containing a number of 2mm diameter side-drilled holes (shown schematically in (a)). These were obtained with water-coupling using (b) a 19mm diameter conventional transducer, (c) a 19mm diameter prototype EWO transducer and (d) a focused transducer (f=30mm).

test block with water coupling. Using an iterative technique in order to take account of refraction at the liquid/solid boundary the time-of-flight to a target at a given depth can be predicted. By also calculating the relative times of arrival of the echoes from the top and bottom surfaces of the block (the dimensions of which are assumed to be known) the depth of the target as would be measured by an EWO source can be determined. The positional error in range as a function of real target depth is shown as a solid line in Fig. 4.9.3. This theoretical calculation has been made for the experimental set-up employed in obtaining figure 4.9.3, assuming a **compressional** wave velocity in the solid (aluminium), a water coupling path of 40 mm from the transducer face to the block surface and normal alignment of the transducer.

As Fig. 4.9.6 indicates, for a target located at the top or bottom surface of the block the positional error is zero. This is because it is assumed that in actual measurements the slope and delay of the timebase used to display the echoes would be chosen so that the front- and back-wall echoes lie in the same position on the display irrespective of whether an EWO transducer or a conventional transducer was being used. It is found that the error in target range incurred by using an "ideal" EWO transducer shows a well defined single maximum (2.2 mm) for a target located 20 mm below the front face. Experimental confirmation of the calculated results was made using a prototype EWO transducer along with the aluminium test block shown in Figs. 4.9.3. The experimental measurements plotted on Fig. 4.9.6 closely match the theoretical curve, confirming the accuracy of the technique.

Fig. 4.9.7 shows positional error versus target depth for the same test block as in Fig. 4.9.3 but at three different coupling distances in water of 20, 40 and 100 mm. As expected from the geometry of the situation the largest errors occur at the shortest coupling distances. At 20 mm this can be as much as 5.5 mm. At 100 mm however the largest error is less than 0.5 mm. It can also be seen that the maximum positional error occurs at slightly different target depths for the various coupling distances.

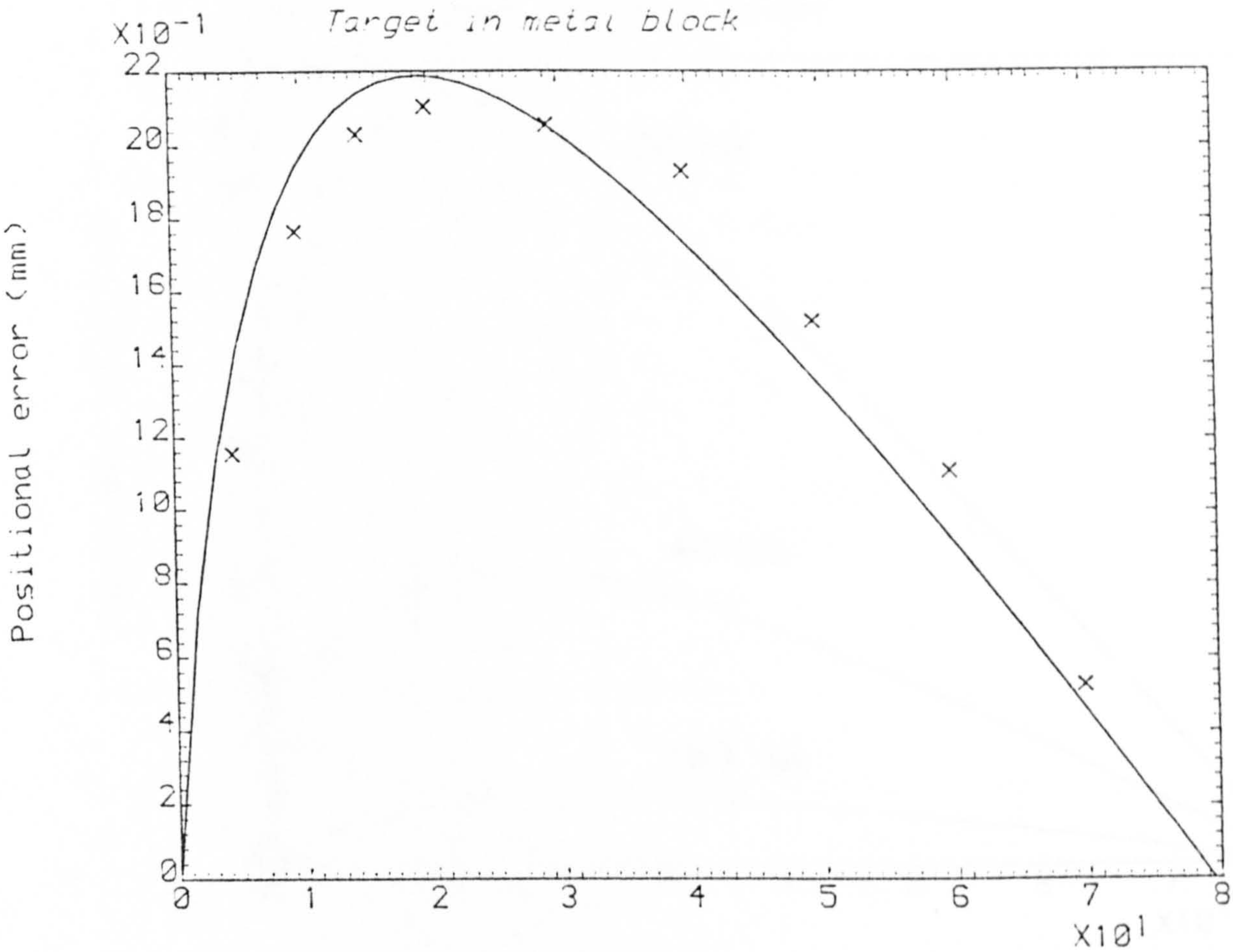

Fig 4.9.6 Calculated (solid line) and measured (crosses) errors in indicated target range for the aluminium test piece shown in Fig 4.9.3, using a 40mm water-coupling path.

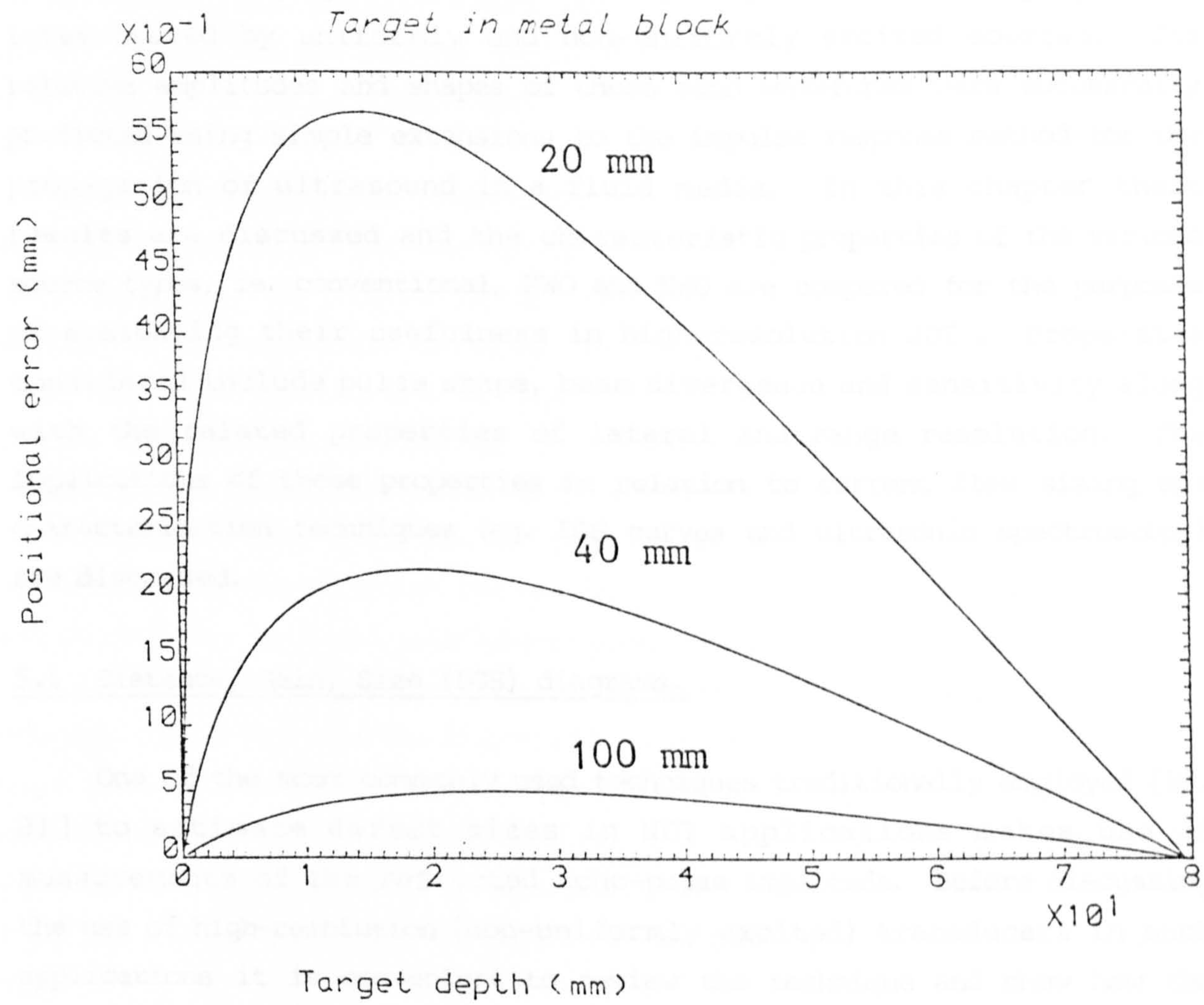

Fig 4.9.7 Theoretically calculated error in target depth as in Fig 4.9.6 for various water-coupling paths.

5. DISCUSSION.

In chapter 4 theoretical results were given which showed the echo responses from targets of various size, shape and material properties interrogated by uniformly and non-uniformly excited sources. The relative amplitudes and shapes of these echo waveforms were sucessfully predicted using simple extensions to the impulse response method for the propagation of ultrasound in a fluid media. In this chapter these results are discussed and the characteristic properties of the various source types, ie. conventional, PWO and EWO are compared for the purposes of evaluating their usefulness in high-resolution NDT . Properties considered include pulse shape, beam divergence and sensitivity along with the related properties of lateral and range resolution. The implications of these properties in relation to current flaw sizing and characterisation techniques (eg. DGS curves and ultrasonic spectroscopy) are discussed.

5.1 Distance, Gain, Size (DGS) diagrams.

One of the most commonly used techniques traditionally employed [80, 81] to estimate defect sizes in NDT applications makes use of measurements of the reflected echo-pulse amplitude. Before discussing the use of high-resolution (non-uniformly excited) transducers in such applications it is convenient to review the technique and show how the theory developed in section 2.6 can be used to improve its accuracy.

5.1.1 Uniformly excited (conventional) source.

The DGS method, whereby the maximum reflection from a defect interrogated by a uniformly excited source is sought and evaluated, was originally proposed by Krautkramer [65]. This technique makes use of the now familiar DGS curves which describe the echo amplitude as a function of gain, distance and target size. These curves have been derived for flaws of various size having the form of a completely reflecting circular disc at right angles to the axis of the radiated field. Using the curves it is possible to determine the size of the equivalent normally-aligned, planar, circular reflector that would produce an echo amplitude equal to that from a natural defect at the same distance. As Krautkramer has pointed out, the size determined can only correspond to the actual flaw size under certain conditions. The limitations and drawbacks associated

with the use of DGS curves have been thoroughly investigated elsewhere [82, 83]. It is well known that the echo amplitude is dependent on many factors other than simply target size including shape, orientation, material properties and surface conditions. Nevertheless, this technique can be useful and is in common use.

Existing theoretically derived DGS curves are valid only in the far field and are based on the assumption that steady-state continuous-wave conditions apply. Very close to the transducer, at a range equivalent to one tenth of the near-field distance, the echo amplitude is assumed to be proportional to the square of the defect diameter (i.e. the area), provided that the flaw is smaller than the source. A substantial part of the ultrasonic field lies between these two regions and the curve for this portion of the field was originally determined experimentally. Furthermore, as Krautkramer points out, for the case of pulses which consist of a few cycles (quasi-continuous waves) there is a deviation from the theoretical predictions which becomes larger the closer the reflector is to the source. For short wideband pulses the deviations become even greater. In a manner similar to that used in obtaining the plots of section 4.6.3 showing the variation of echo amplitude with target size, it is possible to calculate DGS curves which are valid at all points in the field and for any form of excitation from short pulse to CW.

For instance, shown in Fig. 5.1.1. are theoretical DGS curves which have been generated for a 24 mm diameter, circular conventional source. The curves are presented in terms of the usual dimensionless parameters G and A so as to make them more generally applicable. G is the ratio of flaw diameter to the source diameter and A is a CW parameter which represents the usual near-field length given by a^2/λ. Peak-to-peak echo amplitudes have been used in calculating the curves. It was found that other forms of amplitude detection, i.e. half-wave and full-wave detection made little or no difference to the form of the curves. The range of flaw distances given in Fig. 5.1.1. are those over which the theoretical solutions used by Krautkramer [65] are invalid and it is necessary to resort to experimental measurements. When using DGS curves in practice it is necessary to calibrate equipment gain settings in terms of a reference echo from a feature on a standard block so as to allow experimental amplitudes to be normalized to those on the DGS diagram.

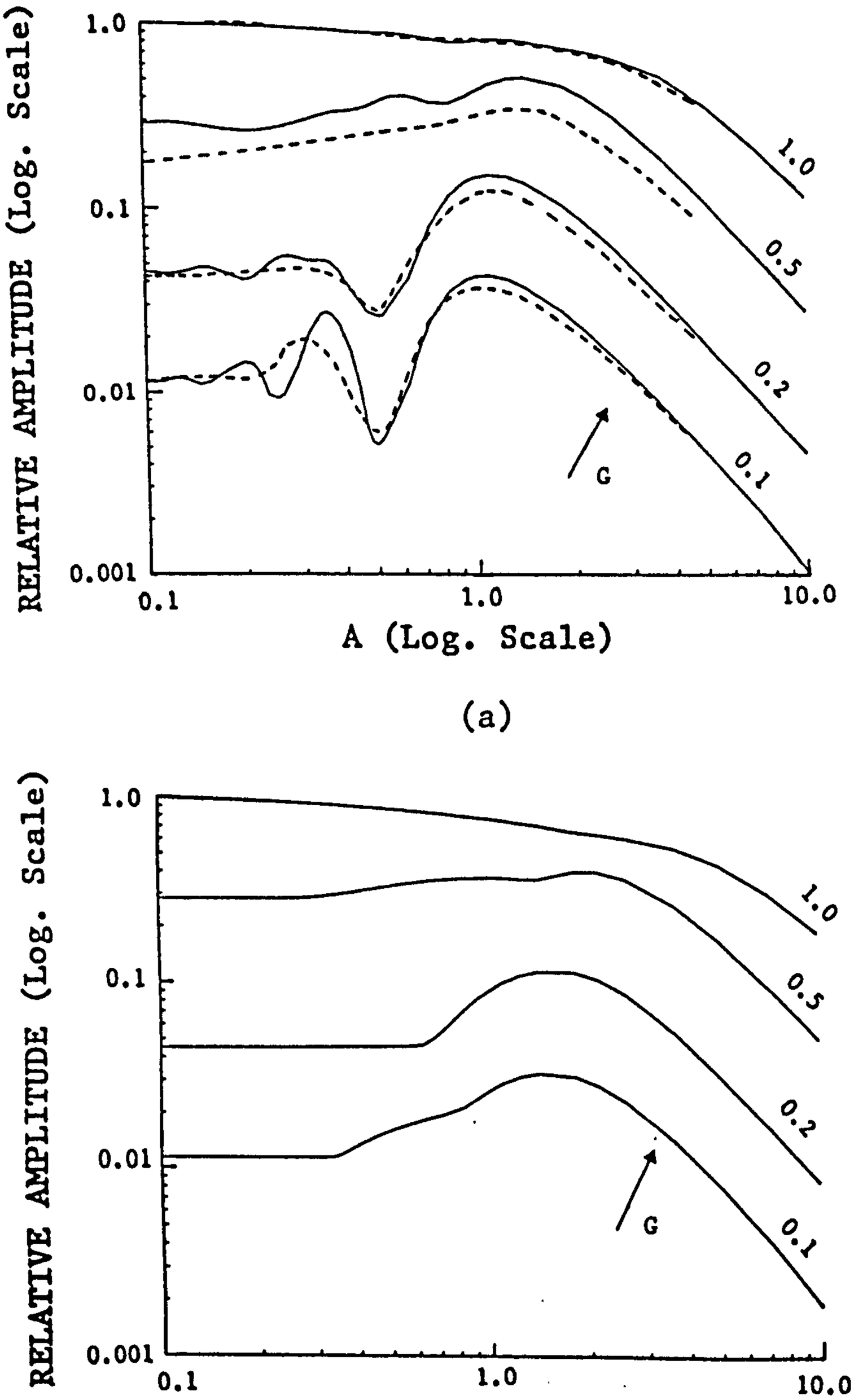

(a)

(b)

Fig 5.1.1 DGS curves calculated for a source excitation consisting of (a) six cycles of a 2MHz, sinusoidal pulse within a half sine-wave envelope and (b) a 2MHz, single-cycle sinusoidal pulse. The original DGS curves given in reference [65] are plotted as a broken line on (a).

The calculated DGS diagram in Fig. 5.1.1.(a) has been derived for a source driving function consisting of six cycles of a 2 MHz, sinusoidal pulse within a half sine-wave envelope. The equivalent experimentally measured DGS curves given in reference [65], which were also obtained using pulses consisting of several cycles at 2 MHz, have been plotted on Fig. 5.1.1.(a) as a broken line. Measured and calculated results are in good agreement except for a target size giving G equal to 0.5, where the measured amplitudes given in reference 65 are lower than predicted. [Interestingly, for this size of target there is a similar discrepancy between the experimental mesurements and theoretical solutions given in reference [65], there being a discontinuity where the experimental and theoretical results link up. Although not shown here, the theoretical solutions of Krautkramer's for ranges greater than about three near-field lengths are in perfect agreement with the calculated results obtained using the present model. This suggests that for G equal to 0.5, the experimentally measured curve given in reference [65] is in error and that the correct curve is in fact given by the calculated solid line in Fig. 5.1.1.(a).]

There is a striking difference in the form of the curves for a small target (G = 0.1) and a large target (G = 1.0). For the former the near field is characterized by large fluctuations (of order magnitude) in amplitude with range. These maxima and minima are equivalent to those found on axis in CW transmit-receive mode beam profiles for a point-like target [28] and are due to interference effects caused by the interaction of plane and edge waves. These fluctuations could lead to large errors in estimates of flaw size if, for example, the target range is not determined accurately. As explained earlier, echo waveforms from larger targets (with dimensions an order of magnitude larger than the wavelength) consist essentially of a specular plane-wave reflection and in this case the interaction of the much smaller edge-wave components make relatively little impression. The curve for G = 1.0 therefore shows a gradual decrease in amplitude with range due to the effects of beam spreading.

Fig. 5.1.1.(b) shows the corresponding DGS diagram calculated for a source driving function consisting of a 2 MHz, single cycle, sinusoidal pulse. The curves clearly demonstrate the marked effect that the form of the radiated pulse has on a DGS diagram. The effect is particularly noticeable within one near-field length (at 2MHz), where the maxima and

minima obtained in Fig. 5.1.1.(a) for smaller targets are completely flattened out when a short pulse is radiated. At ranges greater than one or two near-field lengths both diagrams confirm the well known results that at sufficiently large distances from the source the echo amplitude is inversely proportional to distance (for a given defect size), and that at a given range the echo amplitude is proportional to target area. Furthermore, it has been found that the model is in agreement with Krautkramer's theoretical solutions concerning circular reflectors at ranges of no more than a tenth of the near-field length, namely that echo amplitude is independent of range and proportional to target area. For a small target (G = 0.1) in the near field the time separation between the plane and edge waves in short pulse operation is such that interference does not occur. Hence the echo amplitude is constant with range until further from the source, approaching one near-field length, the plane and edge-wave components gradually overlap producing a maximum. Further away still, the plane and edge waves begin to overlap causing destructive interference and a consequent reduction of amplitude with increasing range. This effect can be clearly seen in the calculated, axial transmit-receive mode responses from a 4 mm diameter target (which for a 19 mm diameter source approximately corresponds to G = 0.2) shown in Fig. 4.4.1. Similarly the form of the curve G = 1.0 can be understood by examination of Fig. 4.4.2 which shows how the echo amplitude from a target of the same dimensions as the source, i.e. G = 1.0, varies with range.

The marked difference between the two sets of DGS curves shown in Fig. 5.1.1. clearly illustrate the error that can be incurred in using the original DGS curve for sizing flaws with short pulse wideband transducers. The introduction of this unnecessary error can be eliminated by use of the finite-sized target model which can produce theoretical DGS diagrams to suit the emitted (plane-wave) pulse in any given application. This model can also be used to calculate the corresponding curves for a PWO transducer.

5.1.2 Non-uniformly excited PWO source.

Fig. 5.1.2 shows two sets of curves equivalent to those given in Fig. 5.1.1 for a PWO source. The results have been calculated for a 24 mm diameter transducer assuming a weighting profile with a half maximum amplitude width of 3mm and again presented in terms of the

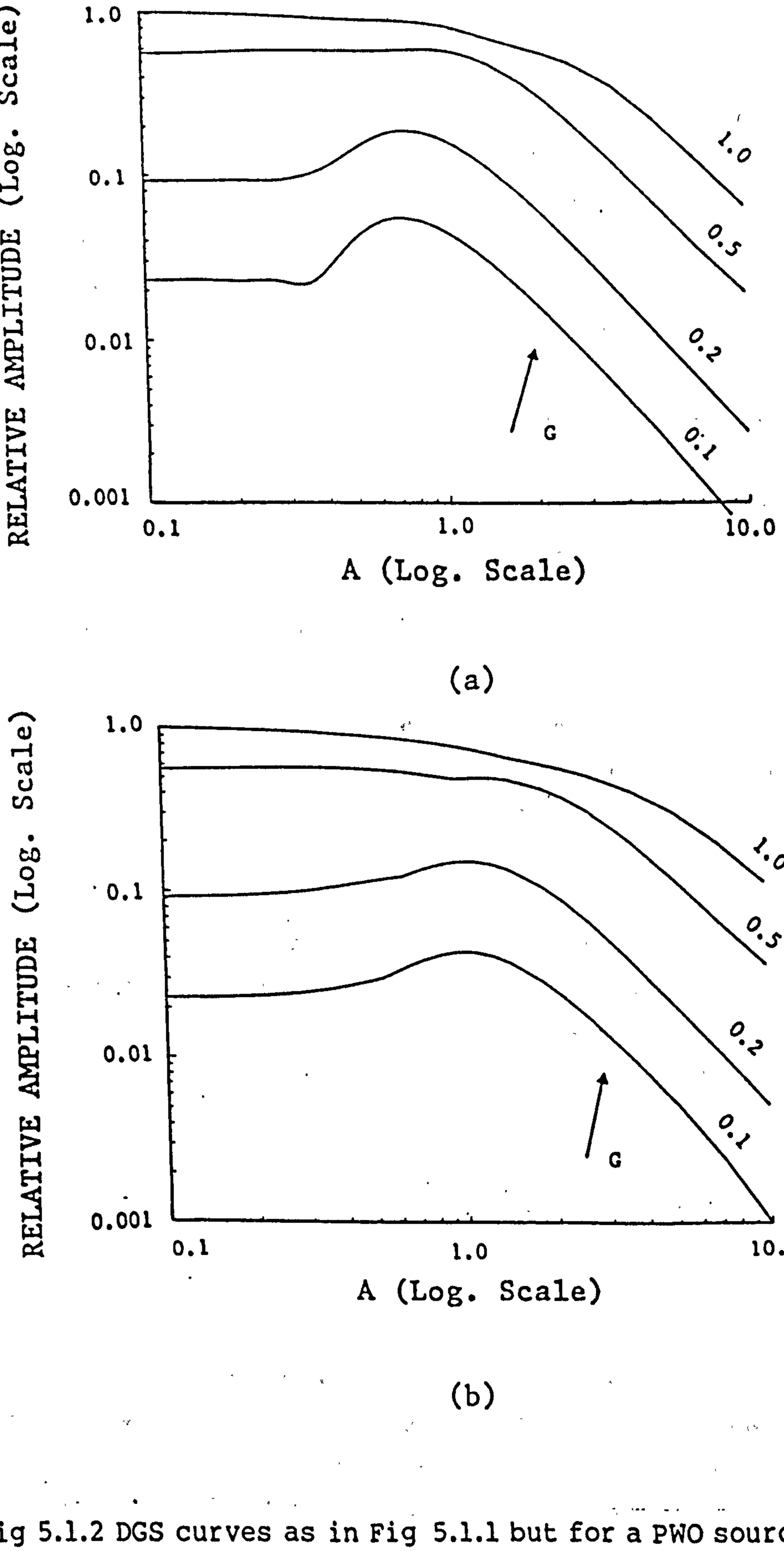

Fig 5.1.2 DGS curves as in Fig 5.1.1 but for a PWO source.

normalised parameters G and A. In Fig. 5.1.2.(a) there is no evidence of any near-field fluctuations for any target size. It should be noted however, that if as discussed earlier (section 4.2.2.) the weighting profile were to be made sharper so that more of the source is fully excited, edge-wave contributions would be reintroduced, resulting in the reintroduction of large amplitude fluctuations in the near field of the DGS curves. The set of DGS curves for short pulse operation see Fig. 5.1.2(b) are similar in form to those in Fig. 5.1.2(a).

For a PWO transducer the form of the DGS curves are not as dependent as a conventional source on the type of excitation used. Furthermore, with relatively much smaller variations in echo amplitude with range in the near field compared with a conventional transducer, the PWO transducer offers advantages of simpler and more reliable flaw sizing based on echo amplitudes and DGS diagrams.

It is also theoretically possible to determine DGS curves for an EWO transducer. However, as the calculated and experimental results for an EWO transducer given in chapter 4 show, the range of echo amplitudes from targets of various size is small in comparison to the variation in amplitude that is obtained with a conventional or PWO source of the same aperture. The EWO is therefore not as suitable as the two other types of source in flaw sizing techniques which make use of echo amplitudes. The smaller disparity in echo amplitude with target size can however be useful in imaging techniques or in applications where there is limited dynamic range (e.g. in a B-scan, see later discussion in section 5.2).

5.1.3 Limitations on the use of DGS diagrams to size defects which lie in a solid media.

DGS curves were originally produced making use of theory which describes ultrasonic propagation in fluid media as well as experimental measurements in water. The calculated results presented here also make this assumption. Care must therefore be taken when extending these curves to the sizing of defects in solids since even a normally-coupled compression wave transducer gives rise to mode-converted shear edge waves by an amount which varies with the angle from the target to the rim of the source. As a result of this the relative amplitudes of the compression plane and edge waves at a (normalised) field point in a fluid and a solid are not the same. This variation in edge-wave amplitude can

in certain circumstances effect the pulse amplitude. As already shown however, the edge-wave components are relatively small for large targets in comparison with the plane wave. Therefore any modifications to the DGS curves due to mode conversion are likely to be confined to the smaller target sizes of wavelength order. Mode conversion of edge waves on propagation and reception will not however cause any complications for a normally-aligned PWO transducer since it does not of course generate any edge waves.

5.2 Ultrasonic imaging techniques

Ultrasonic imaging techniques (such as the B-scans in Section 4.9) which seek to provide a picture in which defects can be identified and characterized are also commonly used in NDT. An essential requirement of such techniques is high lateral and range resolution. Range resolution is typically defined as the ability to discriminate between two or more targets having closely spaced ranges. Lateral resolution on the other hand is the ability to clearly resolve adjacent, closely spaced targets at a given range. The performance of the various source configurations (conventional, PWO, EWO) in imaging applications can be partly assessed in terms of these two commonly used criteria. There are however other important properties that must be considered. For example, these include the ability to identify small targets in the presence of larger ones and detect targets which are poorly orientated relative to the source. Although much of the discussion of the above mentioned criteria in this section will be made with regard to ultrasonic imaging, ie. B- and C-scans, it is often equally relevant to conventional A-scan pulse-echo testing.

5.2.1 Range and Lateral resolution.

In order to completely resolve two targets closely spaced in range the pulse length must be short enough that the echoes from such targets do not overlap on reception back at the transducer. Due to diffraction effects there is a limitation on the range resolution that is achievable when interrogating small targets in the near field of a conventional transducer. The reason for this limitation can be seen in the transmit-receive mode responses from a small target given in Fig. 4.3.1. The on axis multi-pulse structure means that the overall effective pulse length is greater than that of the emitted (plane wave) pulse by an amount equal to twice the extra time it takes the edge-wave component to reach the target - the closer the target is to the transducer the longer the effective pulse length. Range resolution for such small targets cannot therefore be improved by simply using a shorter excitation pulse. As shown in section 4.6 echo waveforms from near field, axial targets of finite-size still exhibit a multi-pulse structure even for a target ten wavelengths wide (centre frequency), see Fig. 4.6.2(b). However, with increasing target size the specular plane wave reflection increasingly swamps the edge-wave components until eventually, as shown in Fig. 4.4.2,

for a target twenty-six wavelengths wide the range resolution at all points in the field is determined solely by the duration of the excitation pulse.

Off axis the output pulse length for the smaller targets is increased further, but the edge-wave components are reduced in amplitude. By moving off axis it may be possible to resolve closely spaced targets if they are of similar size. With targets of very different size, the off-axis edge-wave pulses from the larger targets could be confused with plane-wave echo pulses from the smaller targets. This is obvious from Fig. 4.6.1 and 4.6.2 when taking into account the scale factors and the limitation on range resolution again applies.

As well as reducing the range resolution that can be achieved, the complicated multi-pulse structure most evident on axis could lead to misinterpretations and spurious targets being registered.

As the smaller axial targets are moved further away from the transducer the effective pulse length shortens until well into the far field the plane- and edge-wave components overlap and the range resolution approaches that of the emitted pulse. Overcoming the problem of range resolution by working in the far field is not however always possible or convenient. Inevitably much NDT takes place in the near field for various practical reasons, e.g. poor lateral resolution in the far field due to beam spreading and poor signal to noise ratio because of highly attenuating materials.

In contrast to the above results,the calculated results for the PWO transducer in section 4.3 and 4.4 show that it exhibits good range resolution throughout the field and for all target sizes since the response consists of essentially a single plane-wave pulse. The PWO transducer therefore affords a considerable improvement in range resolution over a conventional transducer in the near field and is limited only by the duration of the excitation pulse. Similarly the EWO transducer shows good range resolution on axis (there being little response off axis) both in the near and far field for all but the largest target sizes. Only when the target reaches the dimensions of the source itself does a multi-pulse structure develop (see Fig. 4.4.6). However, as will be demonstrated later, this drawback will rarely in practice pose a problem and can be easily overcome.

Diffraction limitations also govern the lateral resolution which is related to beam width and beam divergence. At points in the near field of a conventional transducer the plane- and edge-wave components can be time separated and the lateral resolution is determined by the size of the transducer aperture. This can be seen in the transmit-receive mode beam profile for a point target (Fig. 4.3.2). With increasing range into the far field the plane and edge waves overlap and the opposite phase relationship between them is such that they interfere to reduce the amplitude of the wave in the geometric region which increasingly becomes of similar amplitude to the wave in the shadow region. Thus the lateral resolution decreases with range in the far field.

Lateral resolution for a PWO source is similar to that for a conventional source as illustrated by the calculated result in Fig. 4.3.4. In comparison, the EWO exhibits high lateral resolution, the major response being centred on axis in a narrow collimated beam. The high resolution is maintained over a considerable depth of field unlike traditionally-used focussed transducers which can attain such resolution only over a relatively small range of distances. The calculated beam profiles in section 4.3 for a conventional and EWO source both of 19mm diameter and excited with a 2MHz single cycle sinusoid, clearly demonstrate the improvement in lateral resolution offered by the latter. For the conventional source at a range of 20mm the beam-width as defined by a Full Width Half Maximum (FWHM) criteria is 17mm compared with 0.5mm for the EWO source, more than an order of magnitude better. Even at a range of 180mm the lateral resolution is twice as good as that of the conventional source.

The effect of range and lateral resolution on imaging are illustrated in Fig. 5.2.1 which shows B-scan images from normally-aligned, flat-ended brass targets of various size in water. Depicted schematically in Fig. 5.2.1 (a), these targets have been imaged at a range of 25 mm and 100mm using firstly a conventional transducer, Fig. 5.2.1(b), and then an EWO transducer Fig. 5.2.1(c). For the conventional transducer at a range of 25 mm poor lateral resolution causes all target diameters to be oversized. This is particularly evident for the small target (far right) which appears as a straight line of approximately the same length as the transducer aperture. Clearly it would have been impossible to resolve these targets if they had not all been separated by

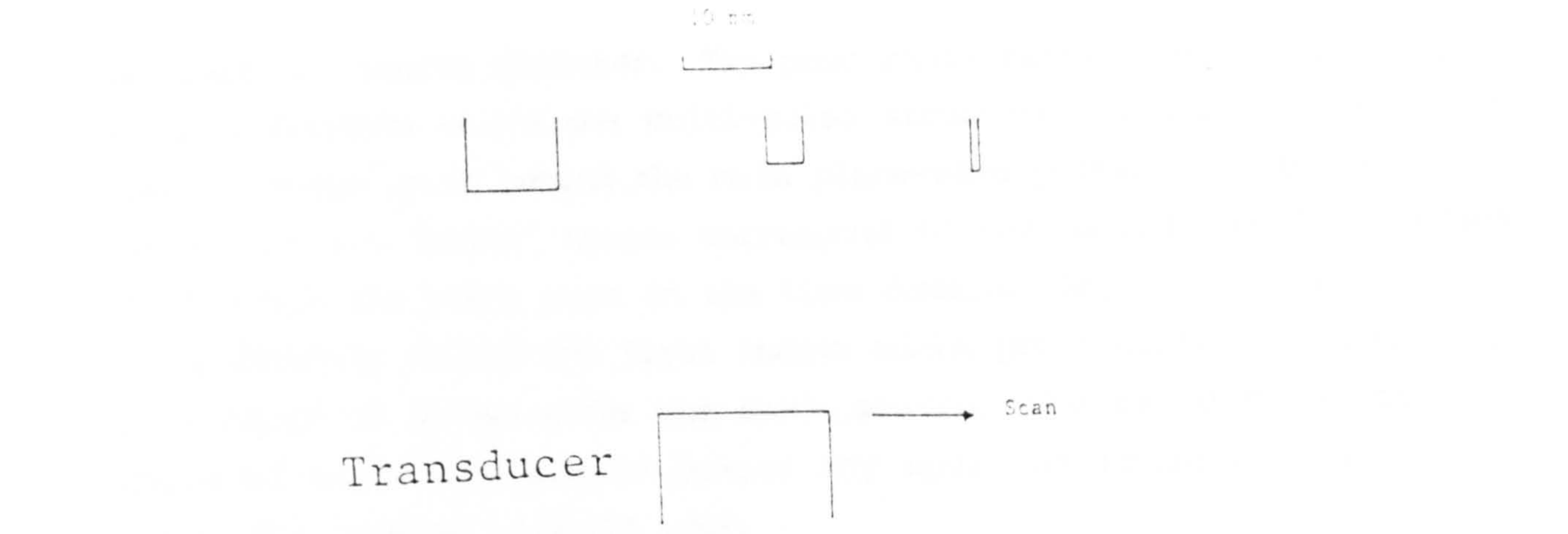

Fig 5.2.1 B-scan images of three axial, normally-aligned, flat-ended cylindrical brass targets of various size in water depicted schematically in (a). The images were obtained using (b) a 19mm diameter conventional transducer and (c) a 19mm diameter prototype EWO transducer at ranges of 25mm and 100mm in water.

at least one source diameter. The poor range resolution is also obvious at this distance where the multi-pulse structure gives rise to spurious target images lying behind the main plane-wave pulse. For the smallest target the two "point" images correspond to the second and third pulses which trail the plane wave in the time domain. Any other small targets lying directly behind the first target might prove difficult to resolve. At a range of 100mm with the same source, the range resolution is improved and there are no longer any spurious images. The lateral resolution however is still poor.

By replacing the conventional transducer with an EWO transducer (Fig. 5.2.1(c)), whilst keeping excitation and reception conditions identical, excellent lateral resolution is achieved and the targets are correctly represented as single straight lines, the length of which accurately corresponds to their diameter and in the case of the small target appearing as a dot. Furthermore with the absence of a multi-pulse structure there are no confusing spurious indications. These improvements in range and lateral resolution are obtained at 25 and 100mm.

Further evidence of the ability of the EWO transducer to accurately identify and size simple defects over a large depth of field in solids as well as fluids is to be found in section 4.8. Potentially the existence of shear edge waves in a solid can cause complications in the interpretation of B-scan images. In practice however, they rarely cause any further problems as demonstrated in the B-scan images shown in section 4.9.

5.2.2 The effect of pulse-echo amplitude variation with target size in ultrasonic imaging.

As well as offering better target resolution the range of peak signal amplitudes from targets of different size interrogated by an EWO transducer is smaller than for a conventional source of the same aperture. This is clearly demonstrated in the results in Figs. 4.7.1 - 4.7.3 which shows echo responses from various finite-sized targets interrogated using an EWO transducer. As indicated by the scale factors, the magnitude of the peak signal from a 1mm target on axis is only 10dB less than the response from a 20mm diameter target. This range of peak signal amplitudes is small in comparison to the range of signal sizes

obtained with an equivalent uniformly excited transducer, where in the near field the amplitude is approximately proportional to the target area for all targets which completely lie within the geometric region of the transducer. Therefore for a conventional transducer the amplitude of the response from a 1mm diameter target will be more than 50dB less than that from a 20mm diameter target. The large disparity between targets of largely differing size can be a disadvantage in imaging systems where there is a limited dynamic range. This mismatch in echo amplitudes can also make it difficult to identify small crack-like targets close to larger perhaps innocuous targets, for example slag inclusions or component surfaces, as the small signal can be difficult to "pick-out" from the much larger reflections nearby. In particular if the large target is a component surface it may be impossible to detect a defect lying close by if it lies within the amplifier dead time following the reception of the large specular reflection. In detecting small defects close to large ones and more specifically sub-surface flaws, the highly collimated beam of the EWO transducer results in there being no large specular reflection from the plane component surface. This allows any small sub-surface defects to be detected by the receiver and hence identified.

5.2.3 Variation in echo response with target orientation

The effect of target orientation relative to the transducer is important to conventional A-scan testing techniques as well as ultrasonic imaging. Fig. 5.2.2 shows echo responses from four sizes of flat-ended brass target at various angles to a 19mm diameter conventional transducer. In each case the centre of the circular reflecting surface was positioned ("centered") on the extended axis of the transducer at a range of 30 mm. Again a single cycle (2MHz) sinusoid was used as the velocity driving function. For a 0.8mm diameter target (approximately one wavelength wide at the centre frequency of excitation) there is no significant change in either pulse shape or amplitude at either 2^{o} or 5^{o}. With targets of 2 mm and 4 mm diameter there is again little change in amplitude and shape at 2^{o}. At an angle of 5^{o} however, a marked distortion and smearing out of the diffracted edge-wave components, together with a reduction in the overall amplitude relative to normal incidence is observable. The relative amplitudes of the echo waveforms can be assessed by reference to the scale factors. For the largest target (ten wavelengths wide), at an angle of 2^{o} the specular plane-wave reflection

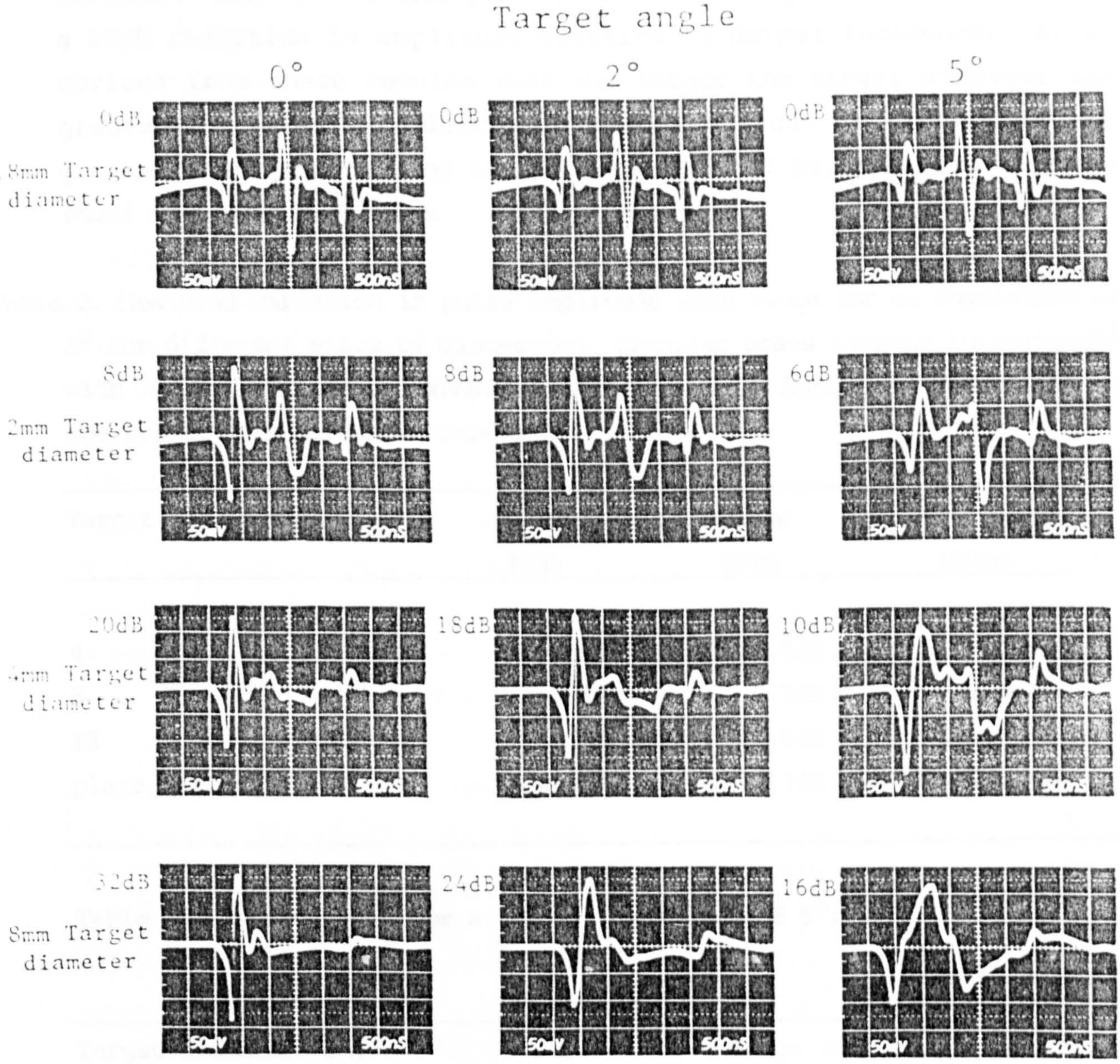

Fig 5.2.2 Measured transmit-receive mode responses of a 19mm diameter conventional transducer interrogating various sizes of axial, flat-ended, cylindrical brass targets at various angles.

has started to become smeared out in time and the amplitude has fallen by 9dB. At 5° the plane wave is increasingly smeared out due to the path difference from the various parts of the reflecting surface, resulting in a 18dB reduction in amplitude relative to normal incidence. It is obvious from these results that the larger the target diameter the greater the relative reduction in echo amplitude with angle and the greater the distortion of the pulse shape will be, relative to those found at normal incidence.

Table 2. Measured variation in pulse amplitude with range for an angulation of 2° for different sizes of flat-ended, circular brass targets interrogated with a 19 mm diameter conventional transducer. Amplitude figures in dB are relative to normal incidence.

Target diameter (mm)	Range		
	30mm	60mm	150mm
4	- 5.7dB	- 1.0dB	- 0.63dB
8	-11.3dB	- 6.7dB	- 6.0 dB
12	-14.0dB	-11.9dB	-11.0 dB
plane reflector	-20.7dB	-18.7dB	-19.5 dB

Table 3. As above but for a target angulation of 5°.

Target diameter (mm)	Range		
	30mm	60mm	150mm
4	-12.2dB	- 5.2dB	-14.0dB
8	-20.3dB	-12.1dB	-24.3dB
12	-22.4dB	-20.6dB	-30.6dB
Plane reflector	-30.5dB	-24.9dB	-32.7dB

As well as being a function of angle and the target size the variation in echo amplitude and shape is also dependent on range. This can be seen in Tables 2 and 3 which show peak-to-peak echo amplitudes versus range for different sizes of target at angles of 2° and 5° respectively. As these results indicate, there is a complicated

relationship between echo amplitude, target size and target range. Interestingly, for both 2^{o} and 5^{o} of angulation the fall in amplitude relative to normal incidence is smaller at 60 mm than at 30 mm range, for the particular transducer size and emitted pulse used here. This is an unexpected result since from simple geometric considerations it might be anticipated that the further the target is from the transducer the smaller the echo response would be for a given orientation and target size, since a larger proportion of the reflected beam will miss the transducer. It is difficult to attribute a simple physical explanation to this result and a more detailed study of the interaction of ultrasonic fields with angled targets (especially in the near field) is left to future work. At a range of 150 mm for an angle of 2^{o} the reduction in amplitude is similar to that at 60mm, but for a 5^{o} tilt in angle the reduction is greater than at the two previous ranges (30 and 60mm), as would be expected. These experimental results are by no means intended to fully describe the effect of target angulation on pulse shape and amplitude but instead are meant merely to illustrate the complicated relationships that exist between echo amplitude/shape and target size/range/angle for a conventional transducer.

In contrast, the effects of target angulation are much less pronounced for an EWO transducer. This is illustrated in Fig. 5.2.3 which shows three sizes of flat-ended brass target at normal incidence and at 2^{o}, centered on axis at a range of 60 mm. These results were made with the EWO transducer previously used and with an excitation waveform approximating to a single cycle sinusoid at 3MHz. For both the 0.8 and 8mm diameter targets there is no change in shape or amplitude with angulation. In comparison, for a conventional transducer interrogating an 8mm diameter target at the same range (see Table 2) the amplitude at 2^{o} is less than half that at normal incidence. It is interesting to notice that with the larger 20 mm diameter target the multi-pulse structure previously discussed in sections 4.4.3 and 4.7 can only be obtained with perfect alignment. A relatively small misorientation and the "straight-ahead" response is lost altogether, having split into smaller components, whilst the high-resolution pulse changes little in shape or amplitude. This means that the multi-pulse structure with its attendant drawbacks i.e. spurious indications etc, is not likely in practice to be a problem for an EWO transducer interrogating targets larger than its own aperture because they will rarely if ever be perfectly aligned.

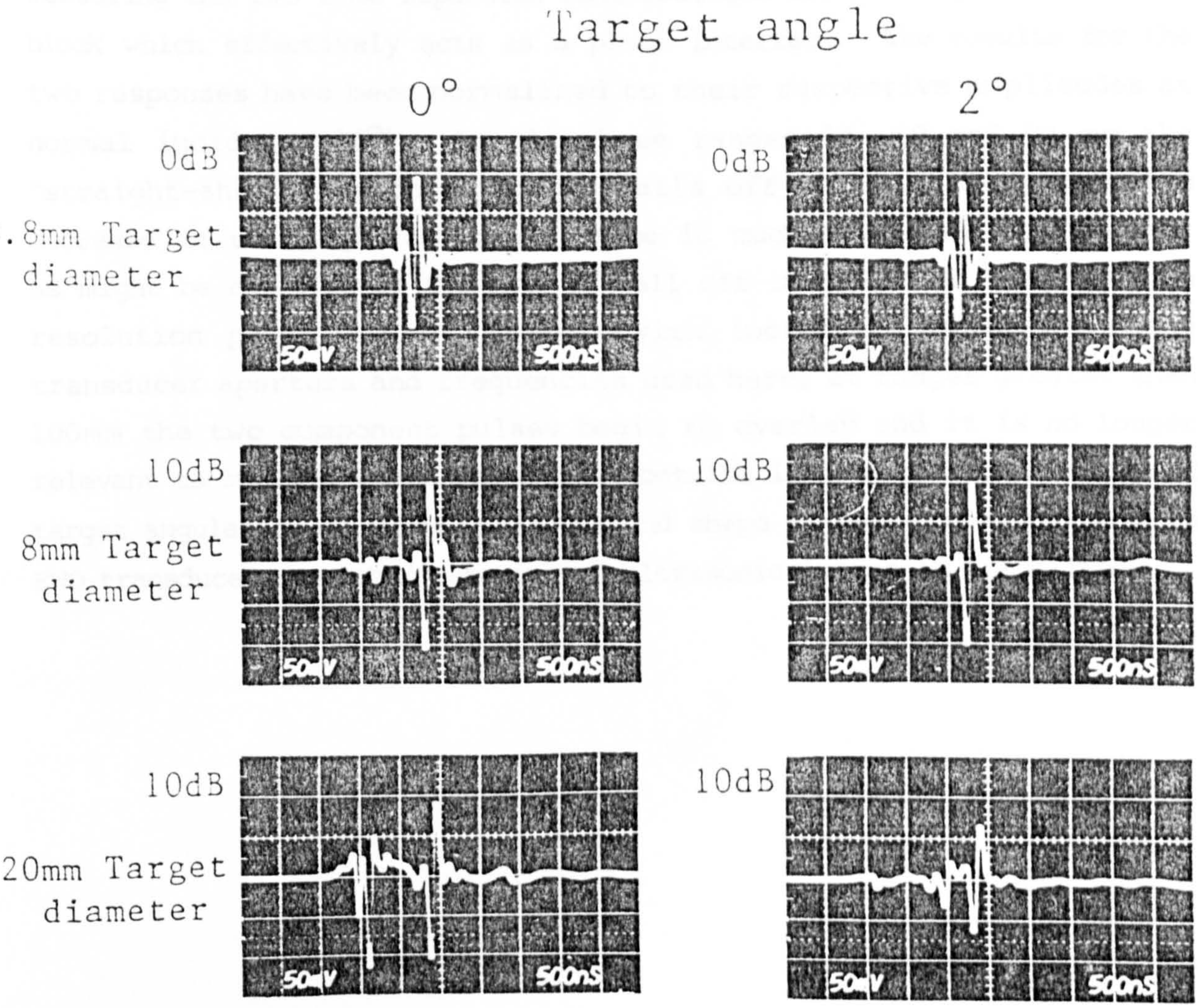

Fig 5.2.3 Measured transmit-receive mode responses for a 19mm diameter prototype EWO transducer interrogating various sizes of axial, flat-ended, cylindrical brass targets at various angles.

The variation in amplitude of the "high-resolution" and the "straight-ahead" responses with angle is given in Fig. 5.2.4 at three different ranges. These graphs were determined experimentally by measuring the two time separated contributions from a large smooth brass block which effectively acts as a plane interface. The results for the two responses have been normalized to their respective amplitudes at normal incidence (0^{o}). At all three ranges 30, 60 and 90 mm the "straight-ahead" response rapidly falls off with angle whereas the decrease in the "high-resolution" probe is much more gradual. However, as might be anticipated the rate of fall off in amplitude for the high resolution pulse becomes greater with increasing range. For the transducer aperture and frequencies used here, at ranges greater than 100mm the two component pulses begin to overlap and it is no longer relevant to measure their individual contributions. Because the effect of target angulation on pulse amplitude and shape is less pronounced with an EWO transducer the interpretation of ultrasonic images is simplified.

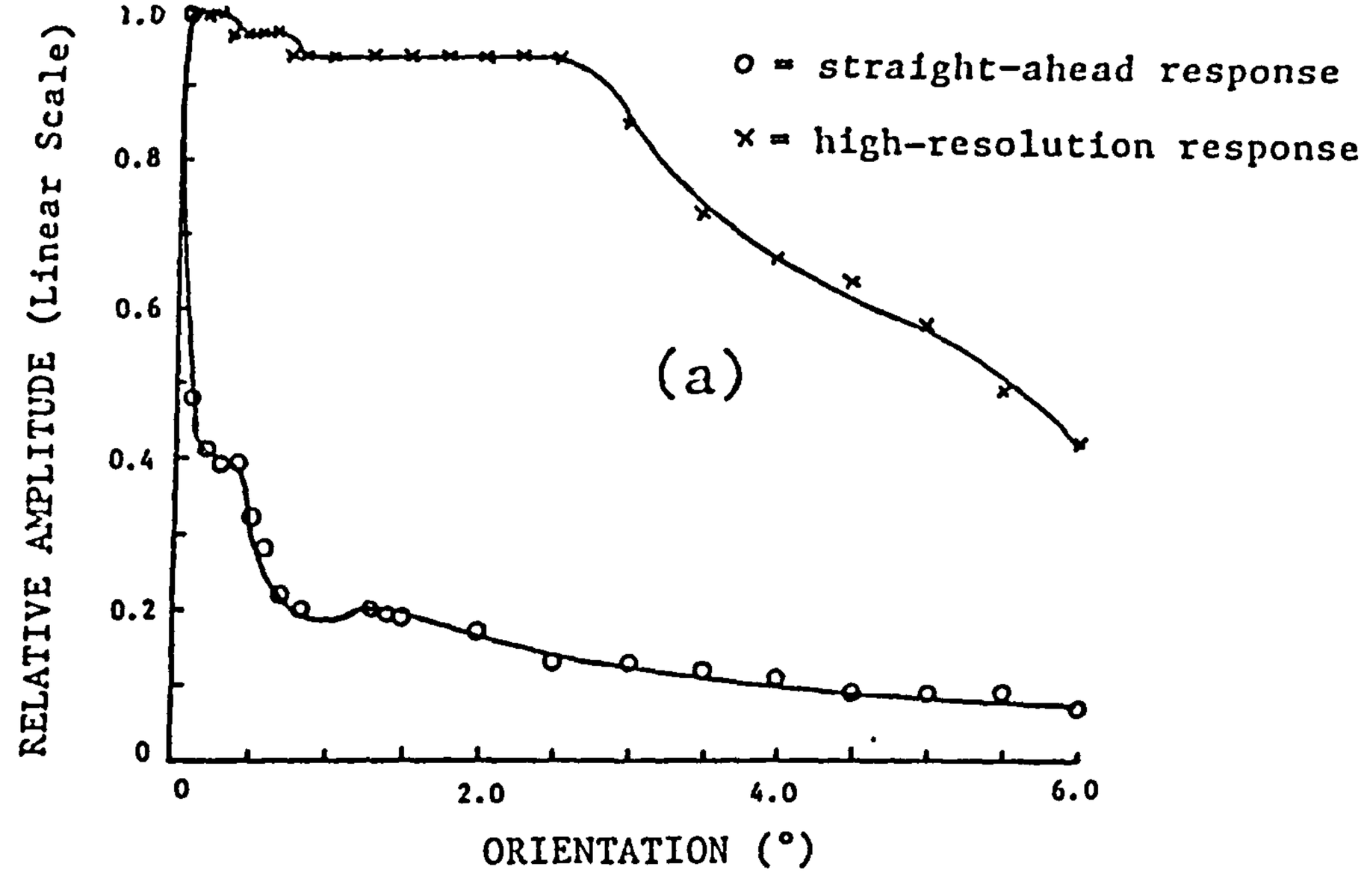

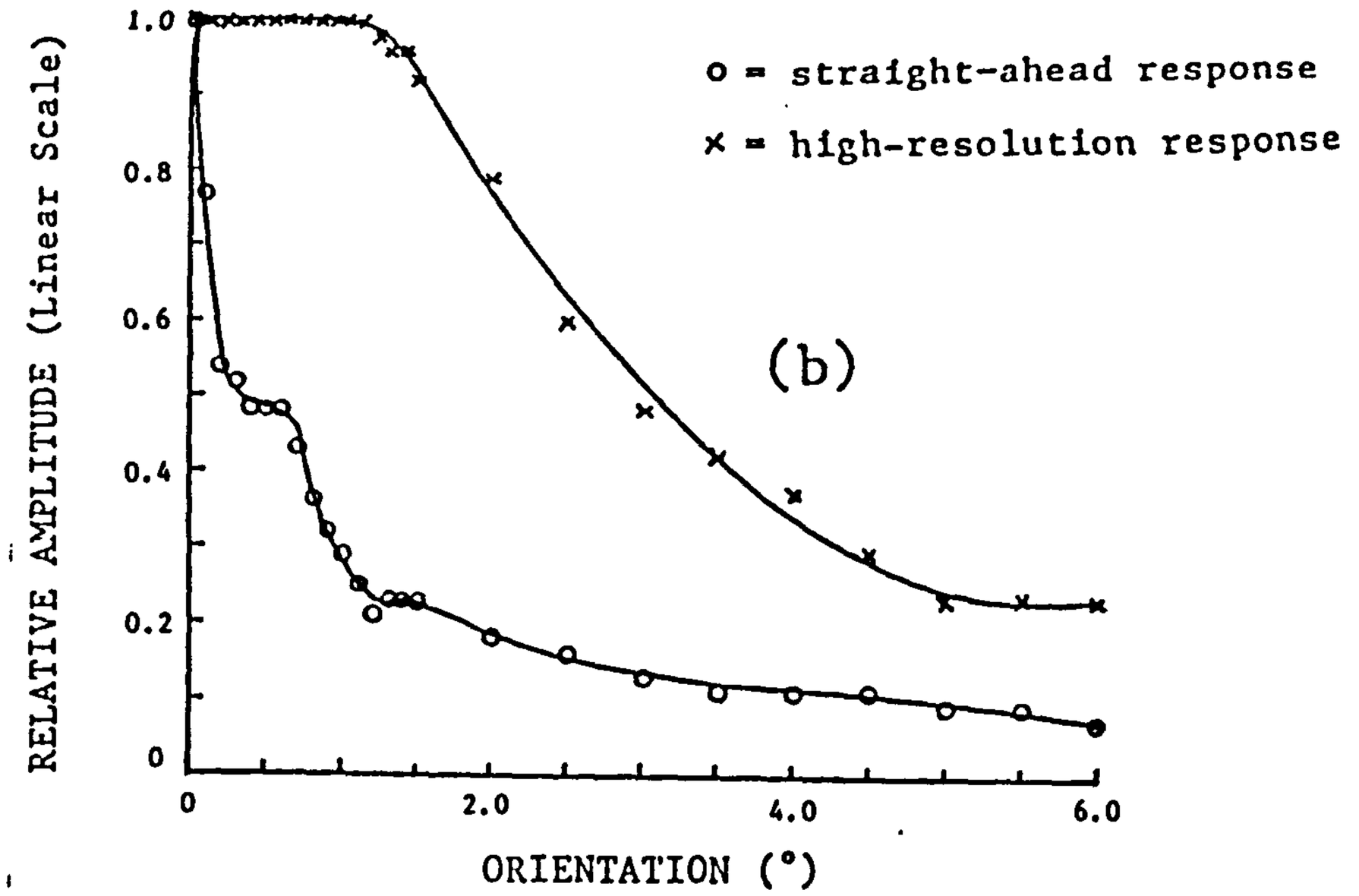

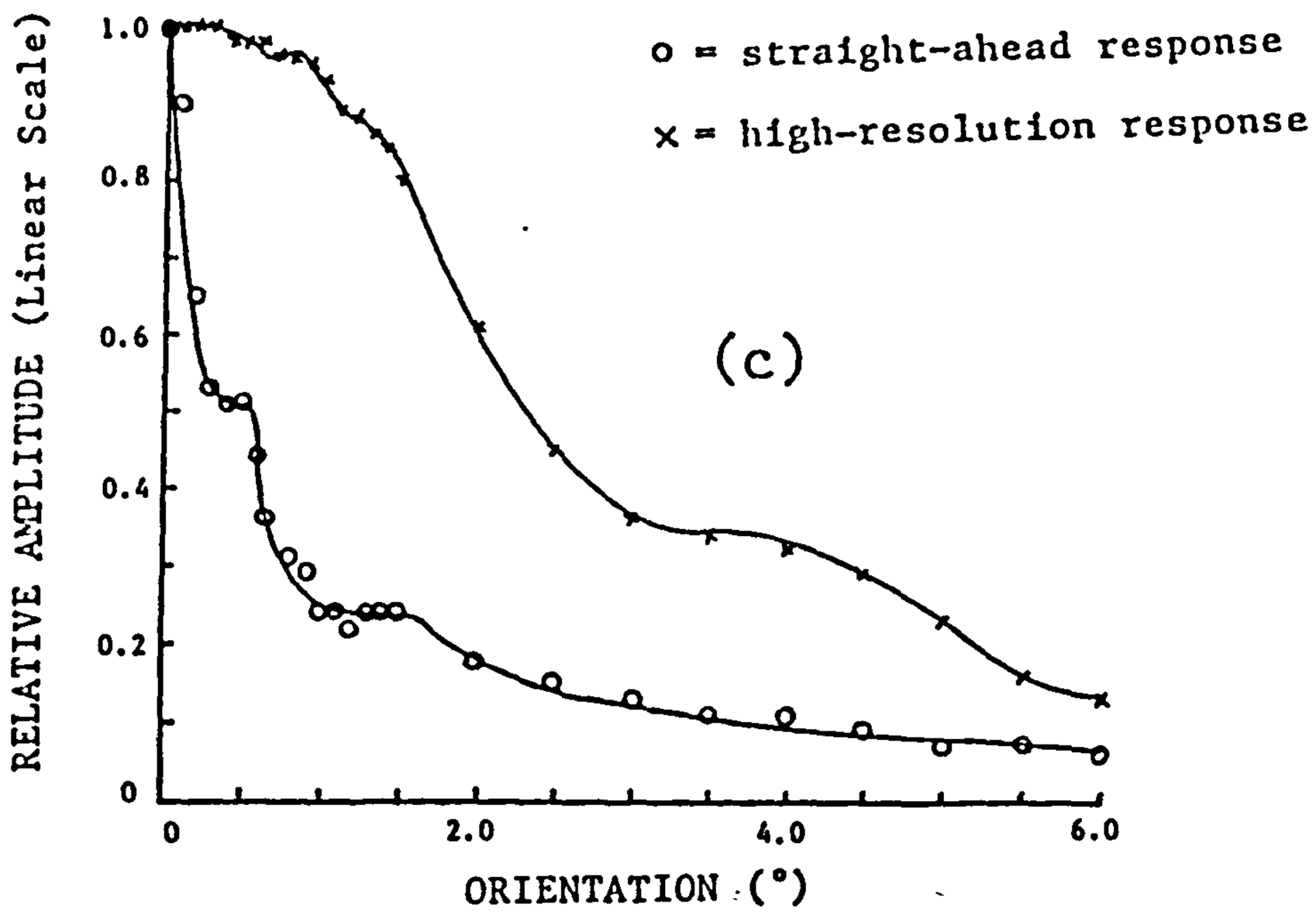

Fig 5.2.4 Measured echo amplitudes of the straight-ahead response and the high-resolution response from a 19mm diameter EWO transducer versus transducer angulation relative to a plane reflector at a range of (a) 30mm, (b) 60mm and (c) 100mm in water.

5.3 Ultrasonic Spectroscopy

Traditional ultrasonic testing has tended to concentrate on correlating the amplitude of received signals to the size of the discontinuities giving rise to those signals. This correlation has been made using techniques such as DGS curves. However, as previously mentioned there are drawbacks to such techniques and amplitude information alone is incapable of providing information about flaw shape and character. This information is very important since a knowledge of the type of discontinuity or flaw that is present allows a better assessment to be made (with the use of fracture mechanics) of the threat it poses to a component. For example, cracks are usually considered more serious than spherical voids (e.g. slag inclusions or porosity) because high stresses at cracks may cause them to propagate. One common technique is to use wideband short pulse transducers in an attempt to relate target characteristics to the shape or frequency content of the ultrasonic pulses arising from them. It has been shown that ultrasonic waves interacting with a target generate so called "diffracted" or scattered echo-wave pulses which originate at discontinuities on the target surface. Such discontinuities include features such as crack edges or the near point and equatorial plane of a sphere for example. The interference of these diffracted echoes back at the transducer results in modulation of the echo spectrum at frequencies which are multiples of $1/\Delta t$ where Δt is the time for the ultrasonic waves to go between two important scattering features. It is this type of modulation that can provide information on defect characteristics.

The measured and calculated results given in chapter 4 have shown that wideband conventional transducers interrogating simple, planar circular targets lead to complicated multi-pulse structures especially in the near field. As explained already these are due to diffraction effects and result in strong modulation in the frequency domain. Even for such simple target geometries the shape of echo spectra can change dramatically with field position and target size. The variation in echo spectra with range for a small target can be seen in Fig. 4.3.1, whilst the effect of target size at a given range is illustrated in Fig. 5.3.1. Fig. 5.3.1 shows echo spectra from four different sizes of circular, planar brass targets at a range of 30 mm. For the smallest target (0.8mm diameter) strong modulation is observable. With increasing target size the edge-wave components become smaller relative to the initial plane

0dB

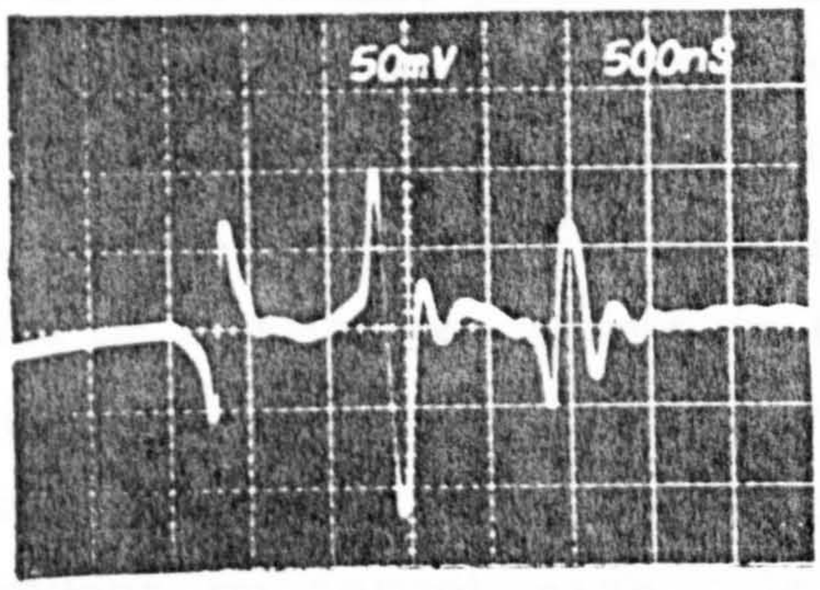

(a)

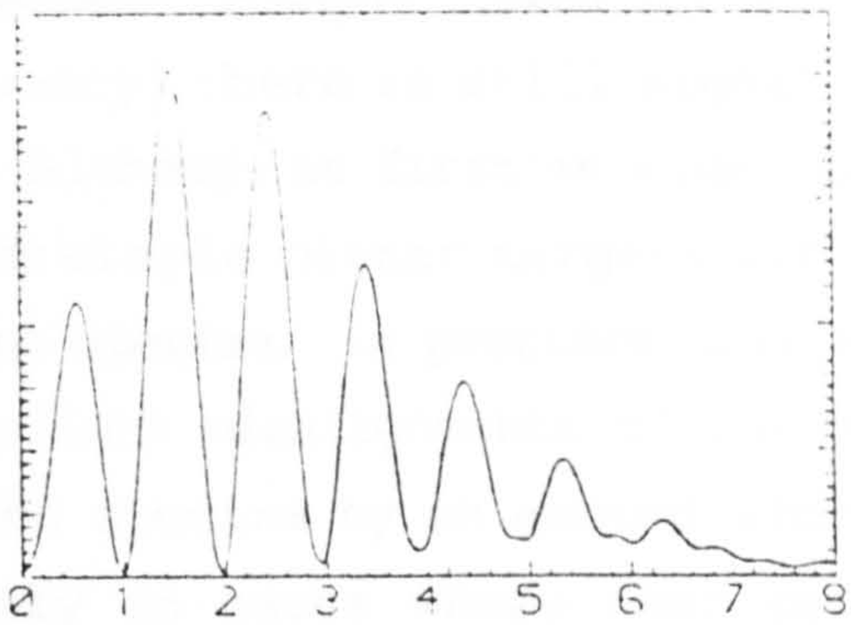

8dB

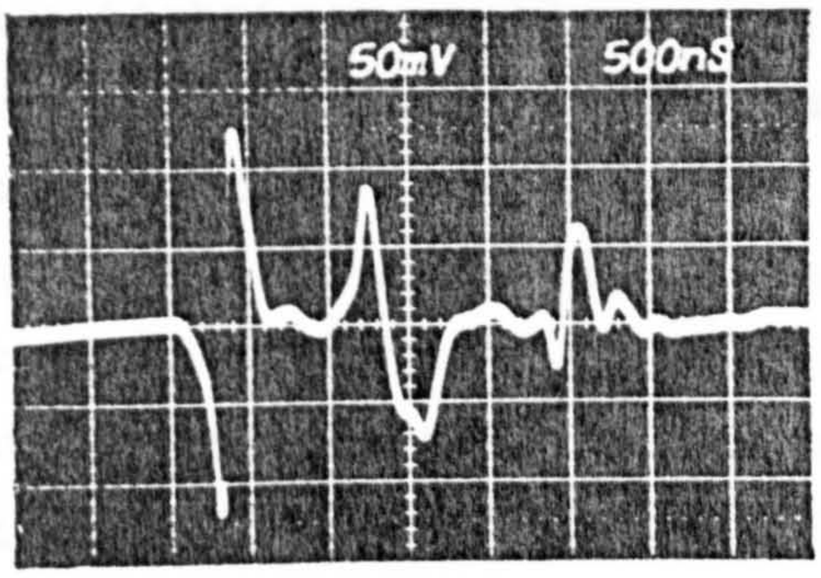

(b)

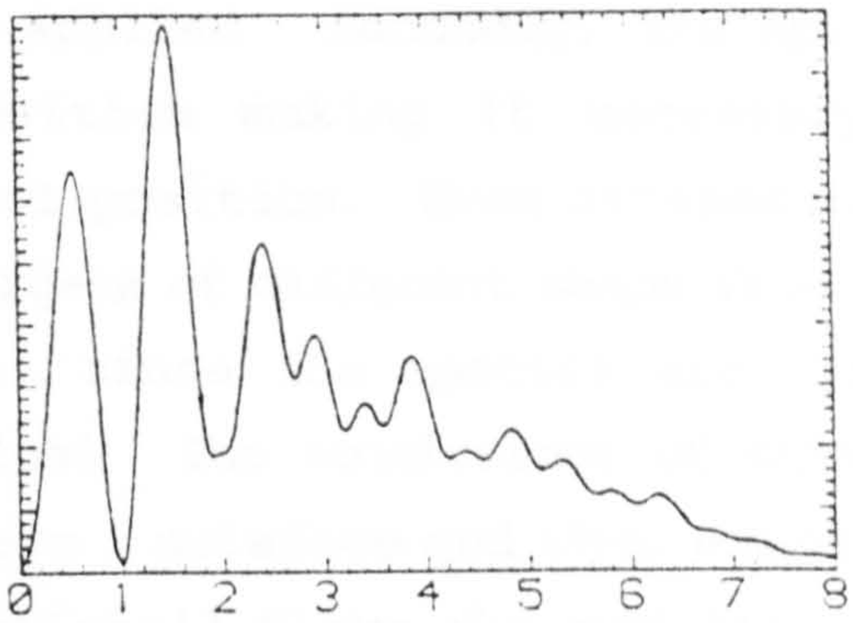

20dB

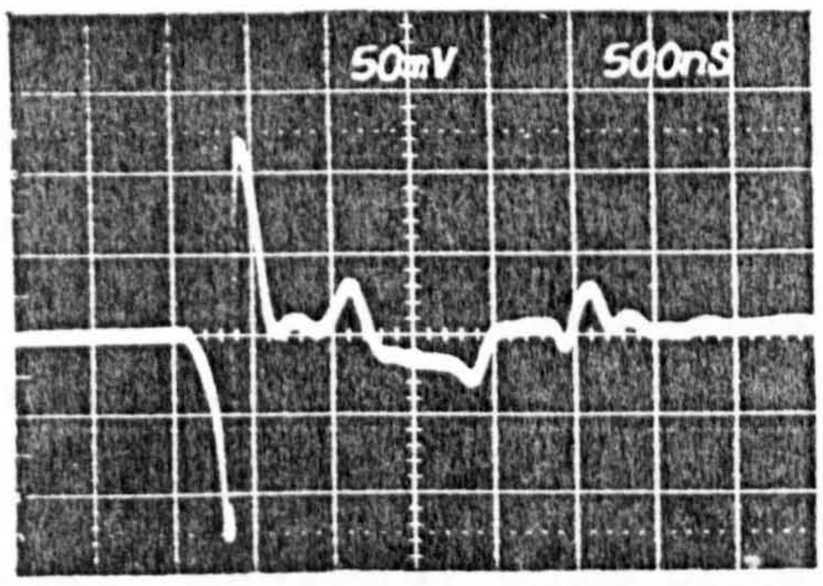

(c)

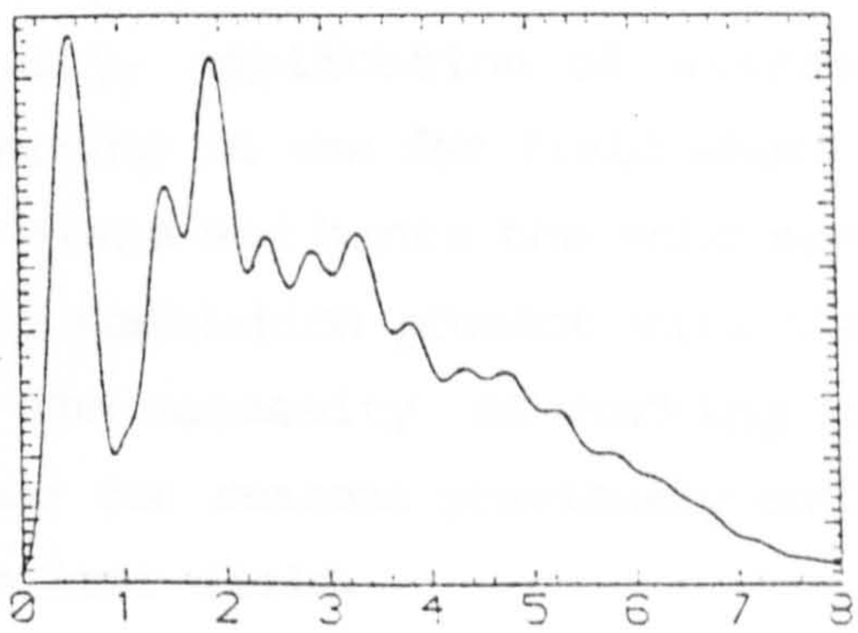

32dB

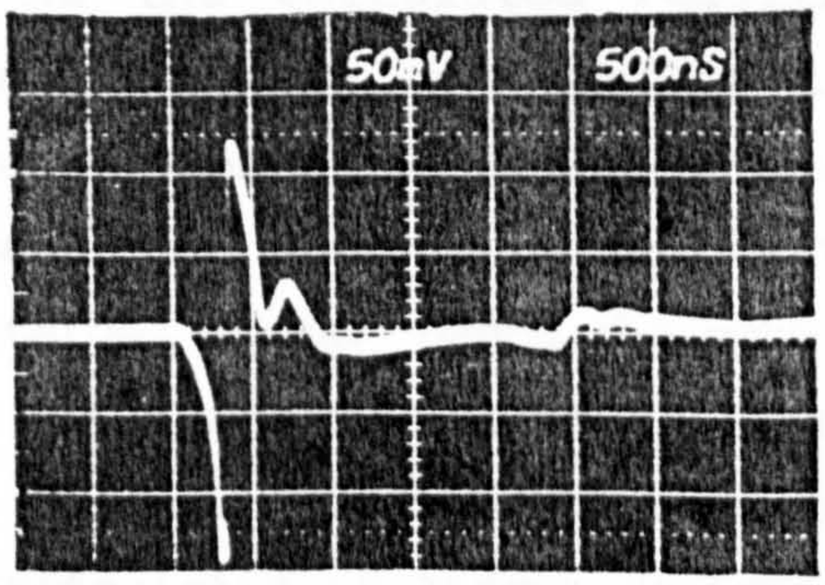

(d)

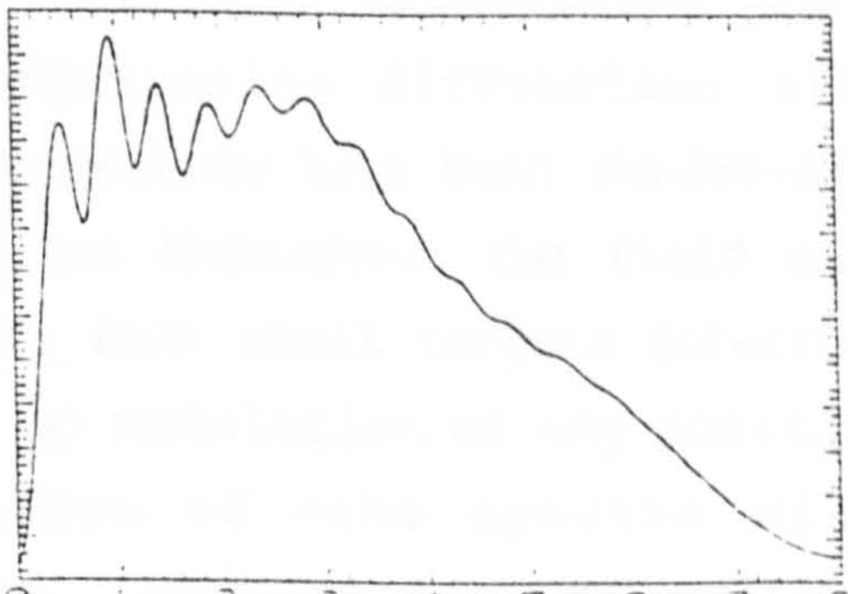

Fig 5.3.1 Measured transmit-receive mode responses along with corresponding spectra for a 19mm diameter conventional PMN transducer interrogating axial, flat-ended cylindrical brass targets with diameters of (a) 0.8mm, (b) 2mm, (c) 4mm and (d) 8mm, at a range of 30mm in water.

wave and the amount of modulation decreases. However, even for a target ten wavelengths wide (at centre frequency) there is still significant modulation due to diffraction effects. Although at first it might appear possible to estimate the flaw size of simple planar targets from the amount of modulation present in the echo spectra, in practice this would prove to be impractical. Firstly, any slight misalignments of the target cause variations in echo waveforms and spectra by an amount which is dependent on target size. It is only in cases where near perfect alignment of the transducer relative to the target can be achieved that such a technique could be accurately applied. Secondly, the spectra varies significantly with field position making it necessary to accurately determine range and lateral position. Even attempting to characterise normally-aligned planar targets of different shape from echo spectra (see Fig. 4.6.7) is difficult since the spectra are almost identical and the shape cannot be deduced. The conclusions of this are that near-field diffraction effects are a nuisance and when examining real planar and non-planar (three-dimensional) flaws the modulation it introduces into the echo spectra is likely to mask the modulation due to the target characteristics. Previously, application of ultrasonic spectroscopy techniques has required working in the far field where the wave can be assumed to be essentially plane and hence the echo spectra free from diffraction modulation. Any modulation present will then be due to target characteristics alone. The necessity of working in the far field is a distinct limitation since for reasons previously outlined much NDT inevitably takes place in the near field.

As the calculated results in section 4 illustrated the PWO transducer does not exhibit the complicating diffraction effects discussed above. Since the edge-wave components have been shaded-out the pulse shapes are simpler and more constant throughout the field and for all target sizes. Hence the echo spectra from small targets interrogated by a PWO transducer contain little or no modulation at any position in the field. Therefore any modulation of echo spectra will be characteristic of target features alone, allowing spectral analysis to be more easily carried out both in the near and far field.

5.4 Target sizing using ultrasonic diffraction analysis.

Another technique which relies on the wavefront being essentially plane and therefore free from diffraction effects is time domain diffraction analysis. Originally proposed by Silk [84], the time domain analysis of "diffracted" signals from the edges of defects is a technique which attempts to improve the accuracy of defect sizing by making use of pulse transit times rather than echo amplitudes. In the near field the multi-pulse structure of echoes from small sharp target features could cause misleading interpretations to be made. For the same reasons as above the use of a PWO transducer would simplify the extraction and interpretation of information on target characteristics using this technique.

6. FUTURE WORK

One main area of future interest is the experimental evaluation of a practical PWO transducer. At the time of writing further development in the non-uniform poling of ceramic discs is still required to realize a working PWO transducer. This work forms part of an on-going research programme in the Ultrasonics Group at the City University and the successful construction of such transducers is anticipated shortly.

As the measured waveforms in chapter 4 have shown, the non-ideal behaviour of ceramic discs results in the radiation of an additional head wave not predicted by the theory. This wave can cause a departure of actual measured responses from those theoretically predicted, an effect which can be particularly marked in the near field of an EWO transducer. Further mathematical modelling which takes account of the head wave effect, based on the work of Baboux et al [77] for example, would enable more accurate predictions to be made of the pressure and echo waveforms from real ceramic transducers. The construction of transducers from polyvinylidene flouride (PVDF) film which exhibits almost ideal piston behaviour and therefore a much reduced head wave effect, should also be investigated.

It is also proposed that the modelling of echo responses from finite-sized targets in fluids be extended in the manner outlined at the end of section 2.6.3, to include target orientations at any arbitrary angle to the source and even more complicated non-planar reflectors. By making use of the simplified impulse response model for solids formulated by Weight [64], it is also recommended that the work on targets of finite-size be extented to make calculations of echo responses from such targets in solid media.

7. CONCLUSIONS

Non-uniform excitation of ultrasonic transducers has been investigated in an attempt to overcome the limitations associated with the diffraction effects found in the field of a conventional uniformly excited source, which are caused by the interaction of the radiated plane and diffracted edge wave. Computer modelling of field point pressure waveforms and transmit-receive mode echo responses from point reflectors in a fluid media has been carried out for two types of such non-uniformly excited source using an extension to the impulse response method. It has been shown that the first type, a PWO source, which has a velocity weighting distribution with a smooth decrease from maximum excitation in the central region to zero at the rim. Such a source tends to "shade out" the diffracted edge-wave component thereby achieving a good range resolution and a reasonably uniform pulse shape throughout the field. The second type, an EWO source with a weighting distribution in the opposite sense to the PWO source above, tends to "shade out" the plane wave and radiates only edge waves. Field-point pressure measurements using specially-constructed miniature probes and transmit-receive mode response measurements from a small target made with a prototype EWO transducer have been compared with the theoretical predictions and found to be in good agreement.

Calculations were also made of transmit-receive mode echo responses arising from solid, planar targets of finite dimensions in a fluid medium, interrogated by short ultrasonic pulses from uniformly and non-uniformly excited sources. These theoretical predictions were based on a weak scattering model first introduced by Ueda and Ichikawa [72]. Originally derived for the specific case of an axial, circular target normally aligned to the source it has been extended and developed into a more generalized version that allows calculations to be made for targets lying at a general field point both on and off axis and for the case of other regular planar target geometries such as rectangles or triangles. Echo responses from both uniformly and non-uniformly excited sources have been calculated using this model.

Detailed experimental measurements have shown that the shape of echo waveforms from a given target was the same whether it was made from a weakly or a strongly reflecting medium. The shape of calculated echo waveforms were found to be in good accord with measured results at all

field positions and for all sizes of target thus verifying that the model is in fact valid for all strengths of scatterer. The good agreement between measured and calculated results were obtained with both a conventional and an EWO source. It was discovered that the acoustic properties of targets effect only the amplitude of echo pulses, the shape being dependent only on its geometry (ie. size). Experiment has shown that the ratio of echo amplitudes from identical finite-sized targets made from different material properties is given by the ratio of the reflection coefficients for a normally-incident plane wave.

Theoretical curves have been obtained which should be a valuable addition to current NDT techniques that make use of DGS diagrams and reflected pulse amplitude in flaw-size estimation. Such diagrams can be determined for all portions of the field and for any radiated pulse. For a conventional source the pulse length was shown to dramatically affect the form of the curves. In contrast to a conventional source, the form of the curves for a PWO source was shown to be fairly independent of pulse length and to be simpler and smoother in shape.

It is clear that all pulse-echo observations in the near field of a conventional source, in particular those involving small targets, must be interpreted with caution because of the multiplicity of echoes which can arise from diffraction effects. Even relatively large targets of simple geometry still give rise to multiple echo waveforms. The PWO source with simpler pulse shapes and spectra throughout the field than a conventional source, offers the possibility of improved target characterisation using ultrasonic spectroscopy. At present the diffraction effects associated with uniformly excited sources often complicates the application of such techniques.

As indicated by calculated and measured results reported here, the EWO source exhibits better lateral resolution (defined by FWHM criteria) and range resolution (defined by the pulse length) than an equivalent conventional source. Experimental results show that a prototype version of the EWO transducer has an optimum lateral resolution about the same as its range resolution, that is about one wavelength at its centre frequency (typically 3-4 MHz). The lateral (and range) resolution is relatively constant over a large 'focal' range, being better than three wavelengths over a range extending from one to twenty transducer radii. B-scan images further highlight the improvement such a source offers over

conventional and focused transducers in their ability to resolve very closely spaced targets over a large depth of field. Furthermore the ability of the EWO transducer to detect small targets close to large specular reflectors and its relative insensitivity to small changes in target angulation make such sources particularly useful in high-resolution NDT.

Appendix 1. Expressions for the angle of equidistant arc on the surface of a circular source.

Region	Time limit	$\Omega(ct)$
Inside geometrical beam $y<a$	$t_0 \leq t \leq t_1$ $t_1 \leq t \leq t_2$	2π $2\cos^{-1}\left(\frac{c^2t^2 - Z^2 + y^2 - a^2}{2y(c^2t^2 - Z^2)^{\frac{1}{2}}}\right)$
On edge, $y = a$	$t=t_0=t_1$ $t_1<t\leq t_2$	π $2\cos^{-1}\left(\frac{(c^2t^2 - Z^2)^{\frac{1}{2}}}{2a}\right)$
Outside geometrical beam, $y>a$	$t_0<t\leq t_1$ $t_1 \leq t \leq t_2$	0 $2\cos^{-1}\left(\frac{c^2t^2 - Z^2 + y^2 - a^2}{2y(c^2t^2 - Z^2)^{\frac{1}{2}}}\right)$

where $t_0 = Z/c$,

$t_1 = 1/c\ [(a - y)^2 + Z^2]^{\frac{1}{2}}$

$t_2 = 1/c\ [(a + y)^2 + Z^2]^{\frac{1}{2}}$

REFERENCES

1. Strutt, J.W.,(Lord Rayleigh), Theory of Sound (Dover, New York, 1945) Vol. 2, chaps. 11-14.

2. Hunter, J.L., Acoustics (Prentice-Hall, Inc., New Jersey 1957).

3. Carter, A.H. and Williams, A.O., "A new expansion for the velocity potential of a piston source", J. Acoust. Soc. Am. 23, 179-184 (1981).

4. Stenzel, H., Leitfaden zur Berechnung von Schallvorgangen (Springer-Verlag ,Berlin ,1958).

5. Zemanek, J., "Beam behaviour within the near field of a vibrating piston", J. Acoust. Soc. Am. 49, 181-191 (1971).

6. Weight, J.P., "The propagation and reception of wide-band ultrasonic pulses", Ph.D. Thesis, The City University, London (1982).

7. Christie, D.G., "The distribution of pressure in the sound beams from probes used with ultrasonic flaw detectors", Mater. Res. 1, 86-97 (1962).

8. Freedman, A., "Transient fields of acoustic radiators", J. Acoust. Soc. Am. 48, 135-138 (1970).

9. Papadakis, E.P. and Fowler, K.A., "Broad-band transducers :Radiation field and selected applications", J. Acoust. Soc. Am. 50, 729-745 (1971).

10. Harris, G.R., "Review of transient field theory for a baffled planar piston", J. Acoust. Soc. Am. 70, 10-20 (1981).

11. King, L.V., "Acoustic radiation field of piezoelastic oscillation and effect of viscosity on transmission", Can. J. Res. 11, 135-146 (1934).

12. Schoch, A., "Considerations in regard to the sound field of a piston diaphragm", Akust. Zh. 6, 318-326 (1941).

13. Fischer, F.A., "Die abstrahlung von impulsen durch ebene kolbenmembranen in starrer wand", Acustica 1, 35-39 (1951).

14. Miles, J.W., "Transient loading of a baffled piston", J. Acoust. Soc. Am. 25, 200-203 (1953).

15. Freedman, A., "Sound field of plane or gently curved pulsed radiators", J. Acoust. Soc. Am. 48, 221-227 (1970).

16. Beaver, W.L., "Sonic near fields of a pulsed piston radiator", J. Acoust. Am. 56, 1043-1048 (1974).

17. Robinson, D.E., Lees. S., and Bess. L., "Near field transient radiation patterns for circular pistons", IEEE Trans. Acoust Speech Signal Processing ASSP-22, 395-403 (1974).

18. Stepanishen, P.R., "Transient radiation from pistons in an infinite planar baffle", J. Acoust. Soc. Am. 49, 1629-1638 (1971).

19. Morton, N., "Thomas Young and the theory of diffraction", Phys. Educ. 14, 450-453, (1979).

20. Kaspar'yants, A.A., "Non-stationary radiation of a sound by a piston", Akust. Zh. 6, 52-56 (1960).

21. Kozina, O.G. and Makarov, G.I., "Transient processes in the acoustic fields generated by a piston membrane of arbitrary shape", Akust. Zh. 7, 53-58 (1961).

22. Tupholme, G.E., "Generation of acoustic pulses by baffled plane pistons", Mathematika 16, 396-404 (1978).

23. Weight, J.P., and Hayman, A.J., "Observations of the propagation of very short ultrasonic pulses and their reflection by small targets", J. Acoust. Soc. Am. 63, 396-404 (1978).

24. Layton, M.R., Carome, E.F., Hardy, H.D., and Bucaro, J.A., "Effects of diffraction on stress pulse propagation ", J. Acoust. Soc. Am. 64, 250-256 (1979).

25. Hayman, A.J., and Weight, J.P., "Transmission and reception of short ultrasonic pulses by circular and square transducers", J. Acoust. Soc. Am. 66, 945-951 (1979).

26. Stephanishen, P.R. and Fisher G., "Experimental verification of the impulse response method to evaluate transient acoustic fields", J. Acoust. Soc. Am 69, 1610-1617 (1981).

27. Harris G.R., Carome, E.F. and Hardy H.D., "An analysis of pulsed ultrasonic fields as measured by PVDF spot-poled membrane hydrophones", IEEE Trans. Son. and Ultrason. SU-30, 295-303 (1983).

28. Weight, J.P., "Ultrasonic beam structures in fluid media", J. Acoust. Soc. Am. 76, 1184-1193 (1984).

29. Hayman, A.J., "Schlieren visualization of focussed ultrasonic images", Ph.D. thesis, The City University, London (1982).

30. Weight, J.P., and Restori, M., "Diffraction effects in the pulsed and continuous wave fields", In: Proceedings of the Institute of Acoustics - Ultrasound in Medicine 8. Institute of Acoustics, Bath U.K., 103-111 (1986).

31. Oberhettinger, F., "On transient solutions of the baffled piston problem", J. Res. Nat. Bur. Stand (U.S.) 65 (b), 1-6 (1961).

32. Jones, R.C., "On the theory of the directional patterns of continuous source distributions on a plane surface", J. Acoust Soc. Am. 16, 147-171 (1945).

33. Pachner, J., "Pressure distribution in the acoustical field excited by a vibrating plate", J. Acoust. Soc. Am. 21, 617-625 (1949).

34. Martin, G.E., and Hickman, J.S., "Directional properties of continuous plane radiators with bizonal amplitude shading", J. Acoust. Soc. Am. 27, 1120-1127 (1955).

35. Miner, G.W., and Laura, P.A. "Calculation of the near field pressure induced by vibrating circular plates", J. Acoust. Soc. Am. 42, 1025-1033 (1967).

36. Papadakis, E.P., "Effects of input amplitude profile upon diffraction loss and phase change in a pulse-echo system", J. Acoust. Soc. Am. 49, 166-168 (1971).

37. Dekker, D.L., Piziali, R.L. and Dong, F., "Effect of boundary conditions on the ultrasonic beam characteristics of circular discs", J. Acoust. Soc. Am. 56, 87-93 (1974).

38. Greenspan, M., "Piston radiator : some extensions of the theory", J. Acoust. Soc. Am. 65, 608-621 (1979).

39. Archer-Hall, J.A., and Gee, D., "A single integral computer method for axisymmeteric transducers with various boundary conditions", NDT Int. 13, 95-101 (1980).

40. Hutchins, D.A., and Archer-Hall, J.A., " Particle velocity near fields of disc radiators with variable drive", Acustica 53, 123-131 (1983).

41. Hutchins, D.A., Mair, H.D., Puhach, P.A., and Osei,J.A., "Continuous wave pressure fields of ultrasonic transducers", J. Acoust. Soc. Am. 80, 1-12 (1986).

42. Haselberg, K. von, and Krautkramer, J., "Ein ultraschallstrahler fur die Werkstoffprufing mit verbesserten Nahfeld", Acustica 9, 359-364 (1959).

43. Martin, F.D., and Breazeale, M.A., "A simple way to eliminate diffraction lobes emitted by ultrasonic transducers", J. Acoust. Soc. Am 49, 1668-9 (1971).

44. Zerwekh, P.S., and Claus, R.O., "An ultrasonic transducer with Gaussian radial velocity distribution", Proc. IEEE Ultrasonics Symposium, 974-976 (1981).

45. Harrison, G.H., and Baker-Kubiczek, E.K., "Single-transducer electrode design for beam shaping in bio-medical ultrasound ", Trans. IEEE Ultrasonics, Ferroelectrics and Frequency Control UFFC-33, 265-272 (1986).

46. Hayward, G., and Kanai, B., "A novel method for improving the spatial field characteristic of piezoelectric transducers", IEEE Ultrasonics Symposium, (1986).

47. Jacquinot, P. and Roizen-Dossier, B., Progress in Optics, Vol. 3 (ed. (ed. E.Wolf, J.Wiley and Sons, 1964).

48. Szabo, T.L., "Acoustic beamshaping and diffraction from tapered amplitude distributions", Proc. IEEE Ultrasonics Symposium, 116-119 (1975).

49. Pohlman, R., Davidts, D. and Semieneu, L., "A novel ultrasonic radiator with interference-suppressed near field", Arch Eisenhuttenwes 48, 185-190 (1977).

50. Bradfield, G., "The use of radially graded ultrasonic radiators to improve the uniformity of the near field", Proc. 2nd Int. Conf. Med. Electro. (ed. C.N. Smyth, Iliffe & Sons Ltd., London 1960).

51. Kossoff, G., "A transducer with uniform intensity distribution", Ultrasonics 9, 196-200 (1971).

52. Kondrat'ev, Yu A., and Karpel'son, A.E., "Formation of narrow slightly diverging ultrasonic beams", translated from Defektoskopiya 10, 95-102 (1978).

53. Burckhardt, C.B., Grandchamp, P.A., and Hoffmann, H., "Focussing ultrasound over a large depth with an annular transducer - an alternative method", IEEE. Trans. Son. Ultrason. 22, 11-15 (1975).

54. Harris G.R. "Transient field of a baffled planar piston having an arbitrary vibration amplitude distribution", J. Acoust. Soc. Am. 70, 186-204 (1981).

55. Stepanishen, P.R., "Acoustic transients from planar axisymmetric vibrators using the impulse response approach", J. Acoust. Soc. Am. 70, 1176-1181 (1981).

56. Tjotta, J.N., and Tjotta, S., "Near field and far field of pulsed acoustic radiators", J. Acoust. Soc. Am.71, 824-834 (1982).

57. Verhoef, W.A., Cloostermans, M.H., and Thijssen, J.M., "The impulse response of a focussed source with an arbitrary axisymmetric surface velocity distribution", J. Acoust. Soc. Am. 75, 1716-1721 (1984).

58. Salmonsson, G. and Mandersson, B., "On ultrasound transducers with curved surface for improvement of lateral resolution", IEEE Trans. Ultrasonics,Ferroelectrics,and Frequency Control UFFC-33, 740-746 (1986)

59. Weight, J.P., "New transducers for high-resolution ultrasonic testing", NDT International 17, 3-8 (1984).

60. Gatcombe, C.P., "Computer modelling of high-resolution ultrasonic transducers", Ph.D. thesis , The City University, London (1987).

61. Fitting, D.W., and Adler, L., Ultrasonic spectral analysis for nondestructive evaluation, (Plenum press , New York, 1981).

62. Brown, A.F., "Materials testing by ultrasonic spectroscopy", Ultrasonics, 202-210 (1973).

63. Brittain, R., and Weight, J.P., "Fabrication of high-resolution ultrasonic transducers", Ultrasonics 25, 100-106 (1987).

64. Weight, J.P., "A model for the propagation of ultrasonic pulses in a solid medium", J. Acoust. Soc. Am. 81, 815-827 (1987).

65. Krautkramer, J., "Determination of the size of defects by the ultrasonic impulse response method", Br. J. Appl. Phys. 10, 240-245 (1959).

66. Freedman, A., "A mechanism of acoustic echo formation", Acustica 12, 10-21 (1962).

67. Neubauer, W.G., "A summation formula for use in determinig the reflection from irregular bodies", J. Acoust. Soc. Am. 35, 279-385 (1963).

68. Johnson, D.M., "A model for predicting the reflection of ultrasonic pulses from a body of known shape", J.Acoust. Soc. Am. 59, 1319-1323 (1976).

69. Haines, N.F., and Langston, D.B., "The reflection of ultrasonic pulses from surfaces ", J. Acoust. Soc. Am. 67, 1443-1453 (1980).

70. Chernow, L.A., Wave propagation in a random medium (Dover, New York, 1960).

71. Chivers, R.C., "The scattering of ultrasound by human tissues - some theoretical models", Ultrasound in med. Biol. 3, 1-13 (1977).

72. Ueda, M. and Ichikawa, H., "Analysis of an echo signal reflected from a weakly scattering volume by a discrete model of the medium", J. Acoust. Soc. Am. 70, 1768-1775 (1981).

73. Stacey, R., "Analysis of echo signals from weak or uniform impurities", submitted for publication in J. Acoust. Soc. Am. (1986).

74. McLaren, S. and Weight, J.P., "Echo responses from finite-sized targets in a fluid media ", To be published in the J. Acoust. Soc. Am., December (1987).

75. Weight, J.P., "Instrumentation associated with the development of wide-band ultrasonic techniques", Masters thesis, The City University, London (1975).

76. Weight, J.P., "Improved resolution transducers and systems for the transmission and/or reception of waves propagated by vibration", U.K. Patent No. GB 2094100B (1982).

77. Baboux, J.C., Lakestani F. and Perdrix M., "Theoretical and experimental study of the contribution of radial modes to the pulsed ultrasonic field radiated by a thick piezoelectric disk", J. Acoust. Soc. Am. 75, 1722-1731 (1984).

78. Brandrup, J., and Immergut, E.H., Polymer Handbook (J.Wiley and Sons,1975).

79. Weight, J.P., "Measurement of longitudinal and transverse waves of pulsed ultrasound in a solid media", To be published in Ultrasonics (1988).

80. Whittaker, V.N., "A review of non-destructive measurement of materials", Non-destructive Testing, 92-100 (1972).

81. Krautkramer, J., and Krautkramer, H., Ultrasonic testing of materials, (Springer-Verlag, Berlin,1977).

82. McNab, A. and Muir, G., "Flaw sizing of real defects", Br. J. NDT 20, 130-134 (1978).

83. Rogerson, A. and Murgatroyd, R.A., "Defect characterization using ultrasonic techniques", Research techniques in NDT Vol.4, (ed. R.S.Sharpe, Academic Press, 1980).

84. Silk, M., "Sizing crack-like defects by ultrasonic waves", Research techniques in NDT Vol.3, (ed. R.S. Sharpe, Academic Press, 1977).

83. Rogerson, A. and Murgatroyd, R.A., "Defect characterization using ultrasonic techniques", Research techniques in NDT Vol.4, (ed. R.S.Sharpe, Academic Press, 1980).

84. Silk, M., "Sizing crack-like defects by ultrasonic waves", Research techniques in NDT Vol.3, (ed. R.S. Sharpe, Academic Press, 1977).